이학박사학위논문

Probing the structure and the disorder of multi-component silicate glasses and melts: Insights from high-resolution solid-state NMR

다성분계 비정질 규산염의 원자구조 및 무질서도 규명: 고상 핵자기공명 분광분석 연구

A dissertation in partial fulfillment of the requirements for the degree of Doctor of Philosophy

2016 년 8 월

서울대학교 대학원

자연과학대학 지구환경과학부

박 선 영

Probing the structure and the disorder of multi-component silicate glasses and melts: Insights from high-resolution solid-state NMR

지도교수 이성근

이 논문을 이학박사 학위논문으로 제출함
2016 년 4 월

서울대학교 대학원
자연과학대학 지구환경과학부
박 선 영

박선영의 이학박사 학위논문을 인준함
2016 년 6 월

위 원 장	이 인 성	(인)
부위원장	이 성 근	(인)
위 원	허 영 숙	(인)
위 원	한 옥 희	(인)
위 원	김 영 규	(인)

Abstract

Probing the structure and the disorder of multi-component silicate glasses and melts: Insights from high-resolution solid-state NMR

Park, Sun Young

School of Earth and Environmental Sciences

The Graduate School

Seoul National University

The structures and the extent of chemical and topological disorder in multi-component silicate glasses and melts provide insight into the macroscopic properties of natural silicate melts. Despite the importance and implications, the detailed structures and disorder in multi-component silicate glasses and melts including basaltic and andesitic glasses and melts are not fully understood.

This dissertation is for a systematic exploration of the atomic structure in multi-component silicate glasses and melts with varying composition–a model system for natural melts- using high-resolution multi-nuclear (^{29}Si, ^{27}Al, ^{17}O and ^{7}Li) solid-state nuclear magnetic resonance (NMR) that can provide detailed coordination environments of framework cations as well as the degree of network polymerization in silicate glasses. The main objective of this thesis is probing the effect of composition on the atomic structures and their effect on macroscopic properties in multi-component silicate glasses including basaltic and andesitic glasses and melts.

The effects of composition on the structure of quaternary CaO-MgO-Al_2O_3-SiO_2 (CMAS) glasses in diopside ($CaMgSi_2O_6$) and Ca-tschermakite ($CaAl_2SiO_6$) join and glass in the diopside-anorthite ($CaAl_2Si_2O_8$) eutectic composition ($Di_{64}An_{36}$)-model systems for basaltic melts- was explored using multi-nuclear solid-state NMR. The predominance of $^{[4]}Al$ and its extensive mixing with $^{[4]}Si$ is consistent with the negative enthalpy of mixing for CMAS glasses obtained by solution calorimetry. The observed increase in non-bridging oxygen (NBO) fraction with increasing mole fraction of diopside ($X_{Diopside}$) indicates an obvious decrease in melt viscosity toward a diopside endmember. The partitioning of Ca^{2+} and Mg^{2+} and/or unmixing of these cations between NBOs and bridging oxygens (BOs) may result in variations in the activity coefficients of CaO and MgO, thus the compositions of melts.

The structural details of model andesitic glasses [CaO-MgO-Na_2O-Al_2O_3-SiO_2 (CMNAS)] in the diopside and jadeite ($NaAlSi_2O_6$) join were investigated using high-resolution solid-state ^{27}Al, ^{17}O MAS and triple-quantum (3Q) MAS NMR and ^{29}Si MAS NMR spectroscopies. The presence of Al-O-Al in jadeite glass implies a violation of the Al-avoidance rule in the glasses and the decrease in the fraction of NBOs with increasing $X_{Diopside}$ is consistent with a decrease in their viscosity. Considering all the experimental Al coordination environments available in the literature, together with the current experimental studies, we attempt to establish the relationship between the fractions of highly coordinated Al and composition, particularly average cationic potential of non-network forming cations ($<c/r>_{ave}$, defined as cationic potential normalized by the mole fraction of each non-network cation). The fraction of highly coordinated Al increases nonlinearly with increasing $<c/r>_{ave}$.

The detailed atomic environments and the extent of cation mixing in Li-Ba silicate glasses with varying X_{BaO} [$BaO/(Li_2O+BaO)$] using high-resolution solid-state NMR spectroscopy were explored. Considering the previously reported experimental results on chemical ordering in mixed-cation silicate glasses, the current results reveal the effect of difference in ionic radius of the cation on a hierarchy in the degree of chemical order for various network modifying cations in the glasses.

The extent of chemical and topological disorder in multi-component Na_2O-MgO-Al_2O_3-SiO_2 (NMAS) glasses in nepheline-forsterite-quartz eutectic composition and KLB-1 basaltic glasses were investigated using high-resolution solid-state ^{27}Al and ^{17}O NMR. The fraction of $^{[5]}Al$ in KLB-1 basaltic glasses increases upto ~2.6% with increasing X_{MgO} [$MgO/(MgO+Al_2O_3)$]. The ^{17}O 3QMAS NMR spectra for the KLB-1 basaltic glasses studied here confirm that the degree of polymerization (BO content) decreases with increasing X_{MgO}. Based on the analysis of the peak position of {Ca, Mg}-mixed NBOs, non-random distributions of Na^+, Ca^{2+}, and Mg^{2+} around both NBOs and BOs are manifested by a moderate degree of partitioning of Ca^{2+} and Mg^{2+} into NBOs and by the spatial proximity between Na^+ and BOs (Al-O-Al and Al-O-Si) in the KLB-1 basaltic glasses studied here.

Keywords: multi-component silicate glasses and melts, basaltic and andesitic melts, solid-state nuclear magnetic resonance, structure and disorder

Student Number: 2010-30103

Table of Contents

Abstract i

List of Figures viii

List of Tables xvii

Chapter 1. Introduction 1

1.1. Introduction 1

1.2. Background of NMR spectroscopy 2

Chapter 2. Structure and disorder in basaltic glasses and melts: Insights from high-resolution solid-state NMR study of glasses in diopside–Ca-tschermakite join and diopside–anorthite eutectic composition 6

Abstract 6

2.1. Introduction 7

2.2. Experimental methods 10

2.2.1. Sample preparation 10

2.2.2. High-resolution NMR spectroscopy of quaternary silicate glasses 12

2.2.3. Spectrometer 16

2.3. Results and discussion 18

2.3.1. Effects of composition on Al coordination environments in basaltic glasses and melts in diopside–Ca-tschermakite join: ^{27}Al 3QMAS NMR results 18

2.3.2. Effects of composition on network connectivity and disorder in the glasses and melts in diopside–Ca-tschermakite join: Insights from ^{17}O MAS and 3QMAS NMR results 24

2.3.3. The extent of Ca-Mg disorder in the glasses in diopside–Ca-tschermakite join: A view from ^{17}O NMR 27

2.3.4. Effect of composition on Si environment in glasses in diopside–Ca-tschermakite join: ^{29}Si MAS NMR results 32

2.3.5. Structure and disorder in $Di_{64}An_{36}$ glass: insights from high-resolution solid-state NMR 36

2.3.6. Implications for macroscopic thermodynamic and transport properties and geochemical processes 40

2.4. Conclusions 43

Chapter 3. High-resolution solid-state NMR study of the effect of composition on network connectivity and structural disorder in multi-component glasses in the diopside and jadeite join: implications for structure of andesitic melts 58

Abstract 58

3.1. Introduction 59

3.2. Experimental methods 65

3.2.1. Sample preparation 65

3.2.2. NMR spectroscopy 67

3.2.3. Previous studies on the fraction of highly coordinated Al in aluminosilicate glasses using high-resolution solid-state NMR 68

3.3. Results and discussion 71

3.3.1. Al coordination environments in model andesitic glasses in the diopside–jadeite join: ^{27}Al MAS and 3QMAS NMR results 71

3.3.2. Probing the extent of network connectivity and configurational disorder in the model andesitic glasses and melts in the diopside–jadeite joins ^{17}O MAS and 3QMAS NMR results. 78

3.3.3. Preferential partitioning between NBO and non-network cations and the degree of Si/Al disorder. 83

3.3.4. Si environment in the multi-component aluminosilicate glasses in the diopside–jadeite join: ^{29}Si MAS NMR results 87

3.3.5. Effects of average cationic potential on Al coordination environments in multi-component aluminosilicate glasses 91

3.3.6. Implications for macroscopic thermodynamic and transport properties and geochemical processes 99

3.4. Conclusions 103

Chapter 4. Effects of difference in ionic radii on chemical ordering in mixed-cation silicate glasses: insights from solid-state ^{17}O and ^{7}Li NMR of Li-Ba silicate glasses 117

Abstract 117

4.1. Introduction 118
4.2. Experimental methods 124
4.2.1. Sample preparation 124
4.2.2. NMR spectroscopy 124
4.3. Results and discussion 126
4.3.1. The NBO and BO environments in Li-Ba silicate glasses: ^{17}O MAS and 3QMAS NMR results 126
4.3.2. Li environments in Li-Ba silicate glasses: ^{7}Li MAS NMR results 141
4.3.3. The extent of cation order, difference in cation radii, and transport properties 143
4.4. Conclusions 146
Chapter 5. Probing the structural disorder of natural basaltic glasses and melts: high-resolution solid-state ^{27}Al and ^{17}O NMR study of glasses in nepheline-forsterite-quartz eutectic composition and KLB-1 basaltic glasses 159
Abstract 159
5.1. Introduction 160
5.2. Experimental methods 165
5.2.1. Sample preparation 165
5.2.2. NMR spectroscopy 166
5.3. Results and discussion 171
5.3.1. Al environments of NMAS glasses in nepheline-forsterite-quartz eutectic composition and KLB-1 basaltic glasses: ^{27}Al MAS and 3QMAS NMR results 171
5.3.2. Variation in NMR parameters in NMAS glasses in nepheline-forsterite-quartz eutectic composition and KLB-1 basaltic glasses 179
5.3.3. Probing the extent of network connectivity and configurational disorder: ^{17}O 3QMAS NMR results of Na-Mg silicate glasses 181
5.3.4. Probing the extent of network connectivity and configurational disorder in NMAS glasses and melts in nepheline-forsterite-quartz eutectic composition: ^{17}O MAS and 3QMAS NMR results 185

5.3.5. Preferential partitioning between NBO and non-network cations and the degree of Si/Al disorder. 190
5.3.6. Implications for macroscopic thermodynamic and transport properties and geochemical processes 194
5.4. Conclusions 199
Appendix 223
A1. Abstracts published in Korean journal 223
A1.1. A solid-state ^{27}Al MAS and 3QMAS NMR study of basaltic and phonolitic silicate glasses 223
A2. Publication list 224
요약 (국문초록) 229

List of Figures

Chapter 2

Figure 2.1. Quadrupolar coupling constant (C_q) of $^{[4]}$Al in CaO–MgO–Al_2O_3–SiO_2 glasses in diopside–Ca-tschermakite pseudobinary join with varying $X_{Diopside}$. The asymmetry parameter is assumed to be 0.5. The estimated error bar of ±0.4 MHz for $^{[4]}$Al and ±0.5 MHz for $^{[5]}$Al are determined on the basis of uncertainty in position of center of gravity of each peak.

Figure 2.2. ^{29}Si MAS NMR spectra for CaO–MgO–Al_2O_3–SiO_2 glasses in diopside–Ca-tschermakite join at 9.4 T with varying mole fraction of diopside ($X_{Diopside}$).

Figure 2.3. Peak widths (full-width at half-maximum) of $^{[4]}$Si in ^{29}Si MAS NMR spectra for CaO-MgO–Al_2O_3–SiO_2 glasses in diopside–Ca-tschermakite pseudobinary join at 9.4 T. $X_{Diopside}$ is the mole fraction of diopside. Diamonds indicate the results in this study and circles denote the results for previous study (Kirkpatrick et al., 1986). Error bar of ±0.5 ppm was estimated from the uncertainty in sample composition, phasing of NMR spectrum, and NMR processing conditions.

Figure 2.4. ^{27}Al 3QMAS NMR spectrum for glass in diopside–anorthite eutectic composition ($Di_{64}An_{36}$) at 9.4 T. Contour lines is drawn at 5% intervals from relative intensities of 12% to 87% with added lines at 2%, 3.5%, 6%, and 8%.

Figure 2.5. ^{17}O 3QMAS NMR spectrum for glass in diopside–anorthite eutectic composition ($Di_{64}An_{36}$) at 9.4 T. Contour lines is drawn at 5%

intervals from relative intensities of 3% to 88% with added lines at 4.5, 6 and 37%.

Figure 2.A1. The isotropic projections of ^{27}Al 3QMAS NMR spectra for CaO–MgO–Al_2O_3–SiO_2 glasses in diopside-Ca-tschermakite join and diopside-anorthite eutectic composition (red) with the simulated peaks of $^{[4]}$Al (~-40 and ~-52 ppm) and $^{[5]}$Al (-25 ppm). Note that $^{[5]}$Al fraction can be calculated from the ratio of -25 ppm peak fraction/total area. $X_{Diopside}$ is the mole fraction of diopside.

Chapter 3

Figure 3.1. ^{27}Al MAS NMR spectra for CaO–MgO–Na_2O–Al_2O_3–SiO_2 glasses in the diopside–jadeite join at 9.4 T with varying mole fractions of diopside ($X_{Diopside}$).

Figure 3.2. (A) ^{27}Al 3QMAS NMR spectra for CaO–MgO–Na_2O–Al_2O_3–SiO_2 glasses in the diopside–jadeite join at 9.4 T with varying mole fractions of diopside ($X_{Diopside}$).Contour lines are drawn at 5% intervals from relative intensities of 12% to 97% with added lines at 2%, 4%, 6%, and 8%. The total NMR collection time for single spectrum is approximately 16~18 h. (B) Total isotropic projection of ^{27}Al 3QMAS NMR spectra.

Figure 3.3. Quadrupolar coupling constant (C_q) of $^{[4]}$Al in glasses in the diopside–jadeite pseudobinary join with varying $X_{Diopside}$. The asymmetry parameter is assumed to be 0.5. The estimated error bar of ±0.4 MHz for $^{[4]}$Al was determined based on the uncertainty in the position of the center of gravity of each peak.

Figure 3.4. ^{17}O MAS NMR spectra for $CaO–MgO–Na_2O–Al_2O_3–SiO_2$ glasses in the diopside–jadeite join at 9.4 T with varying mole fractions of diopside ($X_{Diopside}$).

Figure 3.5. ^{17}O 3QMAS NMR spectra for $CaO–MgO–Na_2O–Al_2O_3–SiO_2$ glasses in the diopside–jadeite join at 9.4 T with varying mole fractions of diopside ($X_{Diopside}$). Open square refers the predicted peak position of Na-O-Si. Contour lines are drawn at 5% intervals from relative intensities of 7% to 92% with added lines at 2.5% and 5%. The total NMR collection time for single spectrum is approximately 3~4 days.

Figure 3.6. Total isotropic projection of ^{17}O 3QMAS NMR spectra for $CaO–MgO–Na_2O–Al_2O_3–SiO_2$ glasses in the diopside–jadeite join at 9.4 T with varying mole fractions of diopside ($X_{Diopside}$).

Figure 3.7. ^{29}Si MAS NMR spectra for $CaO–MgO–Na_2O–Al_2O_3–SiO_2$ glasses in the diopside–jadeite join at 9.4 T with varying mole fractions of diopside ($X_{Diopside}$).

Figure 3.8. (A) Peak widths (FWHM) of $^{[4]}Si$ in ^{29}Si MAS NMR spectra for $CaO–MgO–Na_2O–Al_2O_3–SiO_2$ glasses in the diopside–jadeite pseudobinary join and $CaO–MgO–Al_2O_3–SiO_2$ glasses in the diopside–Ca–tschermakite pseudobinary join at 9.4 T. $X_{Diopside}$ is the mole fraction of diopside. Error bar of ±0.5 ppm was estimated from the uncertainty in the sample composition, phasing of the NMR spectrum, and the NMR processing conditions. (B) Center of gravity of ^{29}Si MAS NMR spectra for $CaO–MgO–Na_2O–Al_2O_3–SiO_2$ glasses in the diopside–jadeite pseudobinary join and $CaO–MgO–Al_2O_3–SiO_2$ glasses in the diopside–Ca–tschermakite pseudobinary join at 9.4 T. $X_{Diopside}$ is the mole fraction of diopside.

Figure 3.9. (A) Population of $^{[5]}$Al for $CaO–MgO–Al_2O_3–SiO_2$ glasses in the diopside–Ca–tschermakite pseudobinary join, diopside–anorthite eutectic glass, and $CaO–MgO–Na_2O–Al_2O_3–SiO_2$ glasses in the diopside–jadeite pseudobinary join with varying mole fractions of diopside ($X_{Diopside}$). (B) Population of $^{[5]}$Al for the glasses with $<c/r>_{ave}$ (average cationic potential). The error bar of ±0.5% was estimated based on estimated uncertainty in the peak area and the quadrupolar coupling constant (C_q) that affects peak intensity.

Figure 3.10. Ternary phase diagram showing the glass compositions of the current and previous studies of the Al coordination environments in the diverse ternary and multi-component silicate glasses. M refers to non-framework cation (Ca^{2+}, Mg^{2+}, Na^+, K^+, Ba^{2+}). Each symbol shows the composition of the glasses (as labeled with references) plotted in the ternary diagram.

Figure 3.11. The population of $^{[5,6]}$Al in the diverse ternary and multi-component aluminosilicate glasses with varying average cationic potential, $<c/r>_{ave}$.

Figure 3.12. (A) The population of $^{[5,6]}$Al in peraluminous aluminosilicate glasses with varying $<c/r>_{ave}$. The blue dotted line is for $M^{n+}O_{n/2}/Al_2O_3$ of ~0.3. The red dotted line is for $M^{n+}O_{n/2}/Al_2O_3$ of ~0.6. (B) The population of $^{[5,6]}$Al of charge-balanced glasses ($M^{n+}O_{n/2}/Al_2O_3 = 1$) with varying Si/Al ratio. (C) The population of $^{[5,6]}$Al of peralkaline aluminosilicate glass with varying $<c/r>_{ave}$.

Figure 3.13. The predicted population of $^{[5]}$Al in natural volcanic glass that includes basalt, rhyolite, andesite, phonolite, and trachyte with varying $<c/r>_{ave}$.

Chapter 4

Figure 4.1. Variations in the isotropic chemical shift (δ_{iso}) and quadrupolar coupling constant (C_q) of NBOs in the ^{17}O 3QMAS NMR spectra of silicate glasses (Angeli et al., 2011; Lee, 2004b; Lee et al., 2003; Lee and Stebbins, 2000b, 2003; Maekawa et al., 1996; Timken et al., 1987; Xue et al., 1994).

Figure 4.2. ^{17}O MAS NMR spectra of Li-Ba silicate glasses with varying X_{BaO} [BaO/(Li_2O+BaO)] at 9.4 T.

Figure 4.3. ^{17}O 3QMAS NMR spectra of Li-Ba silicate glasses with varying X_{BaO} [BaO/(Li_2O+BaO)] at 9.4 T. The contour lines are drawn at 5% intervals for relative intensities of 7–97%, with added lines at 5%.

Figure 4.4. Total isotropic projection of the ^{17}O 3QMAS NMR spectra for Li-Ba silicate glasses with varying X_{BaO} [BaO/(Li_2O+BaO)] at 9.4 T.

Figure 4.5. (A) ^{17}O 3QMAS NMR spectra of Li-Ba silicate glass at X_{BaO} = 0.25 with varying *rf* field strength (B_1 strength). (B) Total isotropic projection of the ^{17}O 3QMAS NMR spectra for Li-Ba silicate glass at X_{BaO} = 0.25 with varying *rf* field strength. The green area shows Li-O-Si, the red area shows Si-O-Si, and the blue area shows {Li, Ba}-O-Si.

Figure 4.6. Simulation results of the ^{17}O MAS NMR spectra of Li-Ba silicate glasses with varying X_{BaO} [BaO/(Li_2O+BaO)]. The red and black lines represent the experimental and simulation results, respectively.

Figure 4.7. Fraction of *N*-O-Si (N = Li^+, Na^+, and Mg^+) as determined from the simulation results by varying X_M [X_M=M/(M+N), M = Ba^{2+} and Ca^{2+}]. The black diamonds indicate the Na-O-Si fractions for Na-Ca silicate glasses (Lee and Stebbins, 2003); the open circles present the

fractions of Na-O-Si for Ba-Na silicate glasses; the black triangle indicates the Mg-O-Si fraction for a Ba-Mg silicate glass (Lee et al., 2003); and the blue squares indicate the Li-O-Si fractions for Li-Ba silicate glasses (current study).

Figure 4.8. (A) ^{7}Li MAS NMR spectra for of Li-Ba silicate glasses with varying X_{BaO} [BaO/(Li_2O+BaO)] at 9.4 T. (B) Variation of the peak maximums and peak widths of the ^{7}Li MAS NMR spectra of Li-Ba silicate glasses (X_{BaO} = 0 and 0.75). (C) ^{7}Li MAS NMR spectra for $Li_2Si_2O_5$ glasses with varying spinning speed (12, 15, and 18 kHz).

Figure 4.9. Full-width at half-maximum of the ^{7}Li MAS NMR spectra of Li-Ba silicate glasses with varying X_{BaO} [BaO/(Li_2O+BaO)] at 9.4 T. The error bars of ±0.3 ppm were estimated from the uncertainty in the sample composition, phasing of the NMR spectrum, and NMR processing conditions.

Figure 4.A1. ^{29}Si MAS NMR spectra and simulation results for Li-Ba silicate glasses with varying X_{BaO} [BaO/(Li_2O+BaO)] at 9.4 T.

Figure 4.A2. Q^n distribution in Li, Na, K, and Li-Ba silicate glasses with varying M_2O (M refers to non-framework cation, Li^+, Na^+, K^+, and Li^++Ba^{2+}). Diamonds indicate the results in this study (black one is Q^3, blue one is Q^2 and red one is Q^4) and circles, squares, and triangles denote the results for previous study (Maekawa et al., 1991).

Chapter 5

Figure 5.1. (A) ^{27}Al MAS NMR spectra for Na_2O–MgO–Al_2O_3–SiO_2 glasses in nepheline-forsterite-quartz eutectic composition at 9.4 T with varying X_{MgO} [MgO/(MgO+Al_2O_3)]. (B) ^{27}Al 3QMAS NMR spectra for Na_2O–

$MgO–Al_2O_3–SiO_2$ glasses in nepheline-forsterite-quartz eutectic composition with varying X_{MgO}. Contour lines are drawn at 5% intervals from relative intensities of 2% to 97%. (C) Total isotropic projection of ^{27}Al 3QMAS NMR spectra for $Na_2O–MgO–Al_2O_3–SiO_2$ glasses in nepheline-forsterite-quartz eutectic composition with varying X_{MgO}.

Figure 5.2. (A) ^{27}Al MAS NMR spectra for KLB-1 basaltic glasses at 9.4 T with varying X_{MgO} [$MgO/(MgO+Al_2O_3)$]. (B) ^{27}Al 3QMAS NMR spectra for KLB-1 basaltic glasses at 9.4 T with varying X_{MgO} [$MgO/(MgO+Al_2O_3)$].Contour lines are drawn at 5% intervals from relative intensities of 12% to 82% with added lines at 4%, 6% and 8%. (C) Total isotropic projection of ^{27}Al 3QMAS NMR spectra for KLB-1 basaltic glasses with varying X_{MgO}.

Figure 5.3. Population of $^{[5]}Al$ for KLB-1 basaltic glasses with varying X_{MgO}. The error bar of $\pm 0.5\%$ was estimated based on estimated uncertainty in peak area and quadrupolar coupling constant (C_q) that affects peak intensity.

Figure 5.4. Quadrupolar coupling constant (C_q) of $^{[4]}Al$ in $Na_2O–MgO–Al_2O_3–SiO_2$ glasses in nepheline-forsterite-quartz eutectic composition and those of $^{[4]}Al$ and $^{[5]}Al$ in KLB-1 basaltic glasses at 9.4 T with varying X_{MgO} [$MgO/(MgO+Al_2O_3)$]. The asymmetry parameter is assumed to be 0.5. The estimated error bar of ±0.4 MHz for $^{[4]}Al$ and that of ±0.5 MHz for $^{[5]}Al$ were determined based on the uncertainty in the position of the center of gravity of each peak.

Figure 5.5. ^{17}O 3QMAS NMR spectra for Na-Mg silicate glasses with varying X_{MgO} [$MgO/(MgO+Al_2O_3)$]. Contour lines are drawn at 5% intervals from relative intensities of 3% to 98%.

Figure 5.6. Total isotropic projection of ^{17}O 3QMAS NMR spectra for Na-Mg silicate glasses with varying at 9.4 T with varying X_{MgO} [$MgO/(MgO+Al_2O_3)$].

Figure 5.7. ^{17}O 3QMAS NMR spectra for $Na_2O–MgO–Al_2O_3–SiO_2$ glasses in nepheline-forsterite-quartz eutectic composition at 9.4 T with varying X_{MgO} [$MgO/(MgO+Al_2O_3)$]. Contour lines is drawn at 5% intervals from relative intensities of 8% to 98% with added lines at 3% and 5%.

Figure 5.8. Total isotropic projection of ^{17}O 3QMAS NMR spectra for $Na_2O–MgO–Al_2O_3–SiO_2$ glasses in nepheline-forsterite-quartz eutectic composition at 9.4 T with varying X_{MgO} [$MgO/(MgO+Al_2O_3)$].

Figure 5.9. ^{17}O MAS NMR spectra for KLB-1 basaltic glasses at 9.4 T with varying X_{MgO} [$MgO/(MgO+Al_2O_3)$].

Figure 5.10. ^{17}O 3QMAS NMR spectra for KLB-1 basaltic glasses at 9.4 T with varying X_{MgO} [$MgO/(MgO+Al_2O_3)$].Contour lines are drawn at 5% intervals from relative intensities of 8% to 98% with added lines at 4%.

Figure 5.A1. ^{17}O MAS NMR spectra for Na-Mg silicate glasses with varying X_{MgO} [$MgO/(MgO+Al_2O_3)$].

Figure 5.A2. ^{29}Si MAS NMR spectra for Na-Mg silicate glasses with varying X_{MgO} [$MgO/(MgO+Al_2O_3)$] and simulation results of the ^{29}Si MAS NMR spectra for Na-Mg silicate glasses at X_{MgO}=0.025 and 0.05. The red and black lines represent the experimental and simulation results, respectively.

Figure 5.A3. Peak widths (full-width at half-maximum) of $^{[4]}Al$ in ^{27}Al MAS NMR spectra for $Na_2O–MgO–Al_2O_3–SiO_2$ glasses in nepheline-forsterite-quartz eutectic composition with varying X_{MgO} [$MgO/(MgO+Al_2O_3)$] at 9.4 T.

Figure 5.A4. ^{17}O MAS NMR spectra for Na_2O–MgO–Al_2O_3–SiO_2 glasses in nepheline-forsterite-quartz eutectic composition at 9.4 T with varying X_{MgO} [MgO/(MgO+Al_2O_3)].

Figure 5.A5. Total isotropic projection of ^{17}O 3QMAS NMR spectra for KLB-1 basaltic glasses at 9.4 T with varying X_{MgO} [MgO/(MgO+Al_2O_3)].

List of Tables

Chapter 2

Table 2.1. Nominal compositions of $CaO–MgO–Al_2O_3–SiO_2$ silicate glasses in diopside–Ca-tschermakite pseudobinary join and glass in the diopside–anorthite eutectic ($Di_{64}An_{36}$). $X_{Diopside}$ is the mole fraction of diopside.

Table 2.2. Nominal compositions and ICP analyses for $CaO–MgO–Al_2O_3–SiO_2$ glasses in diopside–Ca-tschermakite pseudobinary join and glass in the diopside–anorthite eutectic ($Di_{64}An_{36}$). $X_{Diopside}$ is the mole fraction of diopside.

Chapter 3

Table 3.1. Nominal compositions and ICP analyses for $CaO–MgO–Na_2O–Al_2O_3–SiO_2$ silicate glasses in the diopside–jadeite pseudobinary join. $X_{Diopside}$ is the mole fraction of diopside. NBO/T = $2*\{X_{(CaO+MgO+Na2O)}-X_{Al2O3}\}/[1-\{X_{(CaO+MgO+Na2O)}-X_{Al2O3}\}]$.

Table A1. The center of gravity (obtained from MAS and isotropic dimension) and NMR parameters [the isotropic chemical shift (δ_{iso}^{CS}) and quadrupolar coupling constant (C_q)] for $^{[4]}Al$ in $CaO–MgO–Na_2O–Al_2O_3–SiO_2$ glasses in diopside-jadeite join. $X_{Diopside}$ is the mole fraction of diopside.

Table 4.1. Order/disorder of cation distribution in various mixed-cation silicate glasses.

Table 4.2 Nominal compositions and ICP analysis results for Li-Ba silicate glasses. X_{BaO} is the $BaO/(BaO+Li_2O)$ mole fraction.

Table 4.3. Simulation parameters and results for ^{17}O MAS NMR spectra for Li-Ba silicate glasses.

Table 5.1. Nominal composition and ICP analysis of Na-Mg disilicate glasses.

Table 5.2. Nominal composition and ICP analysis of Na_2O-MgO-Al_2O_3-SiO_2 (NMAS) glasses in nepheline-forsterite-quartz eutectic composition.

Table 5.3. Nominal composition and ICP analysis of KLB-1 basaltic glasse

Chapter 1. Introduction

1.1. Introduction

The structures (e.g., coordination number and network connectivity) and the extent of chemical and topological disorder in multi-component silicate glasses provide insight into the macroscopic properties (e.g., energy, entropy, viscosity, diffusivity, and activity coefficients of silica) (e.g., Giordano et al., 2008; Karki and Stixrude, 2010; Kelsey et al., 2008; Lee, 2005; Navrotsky et al., 1983; Neuville et al., 2004, 2006; Potuzak and Dingwell, 2006 and references therein). Despite the importance and implications, the detailed structures and disorder in multi-component silicate glasses and melts including basaltic and andesitic glasses and melts are not fully understood. Because it is in general challenging to probe the local atomic structures of multi-component silicate glasses beyond ternary, as the number of species (and the types of chemical bonding) in the glasses and thus the overlaps among them increase with increasing number of components.

The composition of melt varies with temperature, pressure, and the melt fraction (e.g., Kushiro, 2001). Crystal fractionation, wall-rock assimilation, and magma differentiation process also affect the composition of melts. Recent study of ocean rise provides that the compositions of natural melts vary with mantle composition, temperature, and focused melting (Dick and Zhou, 2015). This thesis is for an exploration of the atomic structure in multi-component silicate glasses and melts with varying composition using high-resolution multi-nuclear (^{29}Si, ^{27}Al, ^{17}O and ^{7}Li) solid-state Nuclear Magnetic Resonance (NMR) that can provide detailed coordination environments of framework cations as well as the degree of

network polymerization in silicate glasses. The main objective of this thesis is probing the effect of composition on the atomic structures and their effect on macroscopic properties in multi-component silicate glasses including basaltic [diopside ($CaMgSi_2O_6$)-Ca-tschermakite ($CaAl_2SiO_6$) join, diopside-anorthite eutectic, basaltic melts from upper mantle peridotite (KLB-1) and andesitic [diopside-jadeite ($NaAlSi_2O_6$) join] glasses and melts.

This thesis is composed of 5 chapters. In chapter 1, the principle of NMR spectroscopy are briefly demonstrated. In chapter 2, the structure and disorder and their effect on macroscopic properties of basaltic glasses and melts in diopside-Ca-tschermakite join and diopside-anorthite eutectic composition are presented. In chapter 3, the effect of composition on network connectivity and structural disorder in multi-component glasses in the diopside and jadeite join and implications for structure of andesitic melts are presented. In chapter 4, the effects of difference in ionic radii on chemical ordering in mixed-cation silicate glasses are presented. In chapter 5, high-resolution solid-state ^{27}Al and ^{17}O NMR study of NMAS (Na_2O-MgO-Al_2O_3-SiO_2) glasses in nepheline-forsterite-quartz eutectic composition (simplest model basaltic melts) and basaltic glasses generated from upper mantle peridotite (KLB-1). Finally, in the appendix, abstract of paper published in domestic journals and publication list are presented.

1.2. Background of NMR spectroscopy

NMR process occurs when the nuclear magnetic moment associated with a nuclear spin is placed in an external magnetic field. Using this process, NMR spectroscopy measure interaction between *rf* signal and spin relaxation of material. The enhancement of NMR is an element-specific probe for the analysis of molecular structure. Also NMR provides

quantitative information. Solid-state NMR has been particularly effective in unveiling atomic structures of multi-component glasses (e.g., Allwardt et al., 2005; Kelsey et al., 2008; Lee, 2010; Lee et al., 2005; Lee and Sung, 2008; Neuville et al., 2006; Park and Lee, 2012, 2014; Xue and Kanzaki, 2008).

The 'chemical shift' is major important term in NMR spectroscopy. The magnetic fields experienced by nuclei at two sites in the same molecule are different if the electronic environments are different. This effect is called the chemical shift. Though the unit of NMR spectrum is frequency like other spectroscopy, it is expressed dimensionless ppm traditionally, which is divided relative shift to reference compound (usually liquid with same isotope) by Larmor frequency of investigating nuclei.

The detail information of quantitative analysis for the fraction of highly coordinated Al in multi-component silicate glasses using 3QMAS NMR are demonstrated in chapter 2 appendix. The previous studies for the atomic structure of multi-component silicate glasses using multi-nuclear NMR are presented in chapter 2 and the previous studies for the highly coordinate Al in aluminosilicate glasses using high-resolution solid-state NMR are presented chapter 3.

References

Allwardt, J.R., Poe, B.T. and Stebbins, J.F. (2005) The effect of fictive temperature on Al coordination in high-pressure (10 GPa) sodium aluminosilicate glasses. *Am. Miner.* 90, 1453-1457.

Dick, H.J.B. and Zhou, H. (2015) Ocean rises are products of variable mantle composition, temperature and focused melting. *Nature Geosci.* 8, 68-74.

Giordano, D., Potuzak, M., Romano, C., Dingwell, D.B. and Nowak, M. (2008) Viscosity and glass transition temperature of hydrous melts in the system $CaAl_2Si_2O_8$-$CaMgSi_2O_6$. *Chem. Geol.* 256, 203-215.

Karki, B.B. and Stixrude, L.P. (2010) Viscosity of $MgSiO_3$ Liquid at Earth's Mantle Conditions: Implications for an Early Magma Ocean. *Science* 328, 740-742.

Kelsey, K.E., Allwardt, J.R. and Stebbins, J.F. (2008) Ca-Mg mixing in aluminosilicate glasses: An investigation using ^{17}O MAS and 3QMAS and ^{27}Al MAS NMR. *J. Non-Cryst. Solids* 354, 4644-4653.

Kushiro, I. (2001) Partial melting experiments on peridotite and origin of mid-ocean ridge basalt. *Annu. Rev. Earth Planet. Sci.* 29, 71-107.

Lee, S.K. (2005) Microscopic origins of macroscopic properties of silicate melts and glasses at ambient and high pressure: Implications for melt generation and dynamics. *Geochim. Cosmochim. Acta* 69, 3695-3710.

Lee, S.K. (2010) Effect of pressure on structure of oxide glasses at high pressure: Insights from solid-state NMR of quadrupolar nuclides. *Solid State Nucl. Magn. Reson.* 38, 45-57.

Lee, S.K., Cody, G.D. and Mysen, B.O. (2005) Structure and the extent of disorder in quaternary (Ca-Mg and Ca-Na) aluminosilicate glasses and melts. *Am. Miner.* 90, 1393-1401.

Lee, S.K. and Sung, S. (2008) The effect of network-modifying cations on the structure and disorder in peralkaline Ca-Na aluminosilicate glasses: O-17 3QMAS NMR study. *Chem. Geol.* 256, 326-333.

Navrotsky, A., Zimmermann, H.D. and Hervig, R.L. (1983) Thermochemical study of glasses in the system $CaMgSi_2O_6$-$CaAl_2SiO_6$. *Geochim. Cosmochim. Acta* 47, 1535-1538.

Neuville, D.R., Cormier, L. and Massiot, D. (2004) Al environment in tectosilicate and peraluminous glasses: A Al-27 MQ-MAS NMR, Raman, and XANES investigation. *Geochim. Cosmochim. Acta* 68, 5071-5079.

Neuville, D.R., Cormier, L. and Massiot, D. (2006) Al coordination and speciation in calcium aluminosilicate glasses: Effects of composition determined by Al-27 MQ-MAS NMR and Raman spectroscopy. *Chem. Geol.* 229, 173-185.

Park, S.Y. and Lee, S.K. (2012) Structure and disorder in basaltic glasses and melts: Insights from high-resolution solid-state NMR study of glasses in diopside-Ca-tschermakite join and diopside-anorthite eutectic composition. *Geochim. Cosmochim. Acta* 80, 125-142.

Park, S.Y. and Lee, S.K. (2014) High-resolution solid-state NMR study of the effect of composition on network connectivity and structural disorder in multi-component glasses in the diopside and jadeite join: Implications for structure of andesitic melts. *Geochim. Cosmochim. Acta* 147, 26-42.

Potuzak, M. and Dingwell, D.B. (2006) Temperature-dependent thennal. expansivities of multicomponent natural melts between 993 and 1803 K. *Chem. Geol.* 229, 10-27.

Xue, X.Y. and Kanzaki, M. (2008) Structure of hydrous aluminosilicate glasses along the diopside-anorthite join: A comprehensive one- and two-dimensional ^{1}H and ^{27}Al NMR study. *Geochim. Cosmochim. Acta* 72, 2331-2348.

Chapter 2. Structure and disorder in basaltic glasses and melts: Insights from high-resolution solid-state NMR study of glasses in diopside–Ca-tschermakite join and diopside–anorthite eutectic composition

Sun Young Park and Sung Keun Lee

Published in *Geochimica et Cosmochimica Acta*, 2012, v. 80, 125-142

Abstract

Here, we report experimental results on the effects of composition on the structure of quaternary CaO–MgO–Al_2O_3–SiO_2 (CMAS) glasses in diopside ($CaMgSi_2O_6$) and Ca-tschermakite ($CaAl_2SiO_6$) join and glass in the diopside–anorthite eutectic composition ($Di_{64}An_{36}$)-model systems for basaltic melts-using multi-nuclear solid-state nuclear magnetic resonance (NMR). The ^{27}Al 3QMAS NMR spectra of CMAS glasses in diopside–Ca-tschermakite join show predominant $^{[4]}$Al and a non-negligible fraction of $^{[5]}$Al. The fraction of $^{[5]}$Al species increases with increasing mole fraction of diopside ($X_{Diopside}$). The structurally relevant quadrupolar coupling constant of $^{[4]}$Al in the glasses decreases with increasing $X_{Diopside}$, suggesting a decrease in network distortion around $^{[4]}$Al. Approximately 3.3% of $^{[5]}$Al is observed for $Di_{64}An_{36}$ glass, consistent with a previous study (Xue and Kanzaki, 2007). There are also non-negligible fraction of Al–O–Al and significant fractions of Si-O-Al in $Di_{64}An_{36}$ glass, indicating extensive mixing between Si and Al and violation of the Al-avoidance in basaltic glasses. The ^{17}O 3QMAS NMR spectra of CMAS glasses show that three types of bridging oxygens (BO, Si–O–Si, Al–O–Al, and Si–O–Al) and two types of non-bridging oxygens (NBO, Ca-NBO, and mixed {Ca, Mg}-NBO) are partially resolved. The fraction of NBO in the basaltic glasses decreases with

decreasing $X_{Diopside}$. A presence of the prominent ^{3}Ca-NBO peak (NBO surrounded by three Ca^{2+} cations) in the CMAS glass at an intermediate compositions ($X_{Diopside}$ = 0.5) suggests non-random distributions of Ca^{2+} and Mg^{2+} around NBOs and BOs, characterized either by preferential partitioning of Ca^{2+} into NBOs and/or structural arrangement toward unmixing of Ca^{2+} and Mg^{2+} around NBO.

The observed structural changes in the CMAS glasses can provide an improved understanding of their structure–property relationships. The predominance of $^{[4]}$Al and its extensive mixing with $^{[4]}$Si is consistent with the negative enthalpy of mixing for CMAS glasses obtained by solution calorimetry. The observed increase in NBO fraction (as also expected from the chemical composition) with increasing $X_{Diopside}$ indicates an obvious decrease in melt viscosity toward a diopside endmember. The partitioning of Ca^{2+} and Mg^{2+} and/or unmixing of these cations between NBOs and BOs may result in variations in the activity coefficients of CaO and MgO, thus the compositions of melts.

2.1. Introduction

The structures (coordination number and network connectivity) and the extent of chemical and topological disorder in multi-component basaltic glasses and melts provide insights into the macroscopic properties (e.g., energy, entropy, viscosity, diffusivity, crystal-melt partitioning coefficients, and activity coefficients of silica) and the dynamics of magmas in the Earth's crust and interior (e.g., Giordano et al., 2008; Karki and Stixrude, 2010; Kelsey et al., 2008; Lee, 2005, 2011; Lee and Stebbins, 2009; Mysen and Richet, 2005; Navrotsky et al., 1983; Neuville, 2006; Neuville et al., 2004; Potuzak and Dingwell, 2006 and references therein). They also allow us to understand

geochemical processes involving magmas (i.e., melting, migration, and emplacement) and have implications for the chemical differentiation of the early Earth (e.g., Asimow and Ahrens, 2010; Lee et al., 2010; Lee, 2011; Mysen and Richet, 2005; Ohtani, 2009; Ohtani et al., 1986; Stebbins, 1995; Stixrude and Karki, 2005; Tinker et al., 2003 and references therein). The detailed structures of basaltic glasses can also play an important role in dissolution behavior of the glasses in contact with aqueous fluids (Gordon and Brady, 2002), potentially controlling the chemistry of groundwater in basaltic aquifers. Despite the importance and implications, the detailed structures and disorder in key multi-component basaltic glasses and melts are not fully understood. The objective of this study is thus to unveil the detailed atomic configurations and the degree of network connectivity and disorder in the model basaltic glasses and melts with varying composition and provide atomistic links between the structure and properties of corresponding melts.

Quaternary CaO–MgO–Al_2O_3–SiO_2 (CMAS) glasses and melts [particularly, diopside ($CaMgSi_2O_6$)–Ca-tschermakite ($CaAl_2SiO_6$) and diopside–anorthite ($CaAl_2Si_2O_8$) joins], are among the most geologically important model systems for basaltic melts (e.g., Bowen, 1915; Gasparik, 1984; Herzberg and Zhang, 1996; Kushiro, 1998; Lee et al., 2005; Liu and O'Neill, 2004; Neuville and Richet, 1991; Presnall et al., 1979; Walter and Presnall, 1994; Winter, 2009 and references therein). The CMAS glasses also have major applications in the glass-ceramics industry (Khater, 2010; Xiao et al., 2006). The macroscopic properties of CMAS glasses and melts in these joins vary with composition. For example, the enthalpy of mixing for glasses in the diopside–Ca-tschermakite join [$X_{Diopside}$= ($MgO+SiO_2$)/Al_2O_3 ratio] shows negative deviation from ideal mixing, but those for crystalline analogues were reported to be positive (Navrotsky et al., 1983). The

configurational entropy, densities, and bulk modulus of the glasses and melts in the diopside-anorthite join increase with diopside content ($X_{diopside}$= MgO/Al_2O_3 ratio) (Ai and Lange, 2008; Asimow and Ahrens, 2010; Barbieri et al., 2004; Schilling et al., 2001; Taniguchi, 1989). The viscosities of silicate melts in diopside–anorthite join decrease with increasing diopside content (Del Gaudio and Behrens, 2009; Getson and Whittington, 2007; Tauber and Arndt, 1987). A study of the dissolution reactions of natural basaltic glasses showed that the leaching of Mg^{2+} is faster than that of Ca^{2+} (Gordon and Brady, 2002). The concentration of Ca^{2+} in groundwater is lower than predicted from the compositions of basaltic glasses (Hurwitz et al., 2003). As for the CMAS glass in the diopside–anorthite eutectic ($Di_{64}An_{36}$), important model basalts, the density, viscosity, and bulk modulus of the melts have intermediate values between those of diopside and anorthite (Ai and Lange, 2008; Taniguchi, 1989).

The changes in the aforementioned thermodynamics and kinetic properties of CMAS glasses and melts in diopside-Ca-tschermakite and diopside–anorthite joins with composition strongly indicate that the atomic structures (short-range to medium-range scale) of these glasses and melts vary with composition. However, it is in general challenging to probe the local atomic structures of multi-component silicate glasses beyond ternary, both theoretically and experimentally as the number of species (and the types of chemical bonding) in the glasses and thus the overlaps among them increase with increasing number of components. Indeed, whereas earlier pioneering studies of atomic structure of multi-component CMAS glasses provided information on average coordination numbers (see below), the detailed atomic environments such as connectivity and proximity of each atomic species in multi-component silicate glasses have not yet been fully

understood (e.g., Brown et al., 1995; Mysen and Richet, 2005 and references therein). Consequently, little is known about the extent of Al-Si mixing, network polymerization, and topological disorder in glasses with more realistic chemical compositions, comparable to natural basaltic melts. Whereas compositions of basaltic melts vary with temperature, pressure, and melt fraction (Kushiro, 2001), the structural evolution of basaltic melts and glasses with composition is not well-understood.

In this study, we thus explore the structures (coordination number of framework cations and connectivity between them) and the extent of disorder (chemical and topological) in quaternary silicates glasses in the $CaO–MgO–Al_2O_3–SiO_2$ glasses in diopside ($CaMgSi_2O_6$)–Ca-tschermakite ($CaAl_2SiO_6$) join and the diopside–anorthite ($CaAl_2Si_2O_8$) eutectic composition ($Di_{64}An_{36}$) using high-resolution multi-nuclear (^{29}Si, ^{27}Al, and ^{17}O) solid-state NMR that can provide detailed coordination environments of framework cations (Si and Al) as well as the degree of network polymerization in silicate glasses [bridging oxygen (BO) and non-bridging oxygen (NBO) environments] (See 2.2. below for previous studies). While natural basaltic glasses have additional essential components (FeO and Fe_2O_3), NMR has shown limited utility in resolving atomic structures of iron-bearing glasses. Thus the focus of the current study is on the iron-free CMAS glasses.

2.2. Experimental methods

2.2.1. Sample preparation

A series of CMAS glasses in diopside ($CaMgSi_2O_6$) - Ca-tschermakite ($CaAl_2SiO_6$) join containing 0, 25, 50, 75, and 100 mol% $CaMgSi_2O_6$ component were synthesized from carbonate ($CaCO_3$) and

oxides (MgO, Al_2O_3, and SiO_2). The nominal compositions of the glasses are CMAS quaternary with xCaO:yMgO:(x - y)Al_2O_3:(x + y)SiO_2 (x = 4, y = 0, 1, 2, 3, 4) (Table 2.1). The starting Al_2O_3, $CaCO_3$, and SiO_2 powders were dried at 400 °C for 48 h; MgO was dried at 1300 °C for 2 h. The weighed powders were mixed by grinding in an agate mortar, and then decarbonated in a Pt crucible at 800 °C for 1 h. The samples were then melted above their respective melting temperature (1550–1600 °C) for 1 h, and quenched into glasses by plunging the bottom of the Pt crucible into a water bath. Approximately 0.2 wt% of cobalt oxide was added to enhance spin–lattice relaxation. A negligible weight loss (~0.1-1.0 wt%) was observed after considering decarbonation. ^{17}O-enriched glasses in the diopside – Ca-tschermakite join and glass in the diopside ($CaMgSi_2O_6$)–anorthite ($CaAl_2Si_2O_8$) eutectic composition (diopside:anorthite = 64:36 mol%, CaO:MgO:Al_2O_3:SiO_2 = 25:16:9:50 mol%) were synthesized from carbonates ($CaCO_3$) and oxides, including ^{17}O-enriched SiO_2. The ^{17}O-enriched SiO_2 was prepared by hydrolyzing $SiCl_4$ in 20% and 40% ^{17}O-enriched water. Approximately 0.2 wt% of cobalt oxide was added to enhance spin–lattice relaxation. The mixtures were then fused in a Pt crucible for 1 h at 1600 °C in an Ar environment. The melt was quenched by removing the crucible from the furnace and then manually lowering it into water. A negligible weight loss (~1.0 wt%) was observed after considering decarbonation. Table 2.1 shows the nominal compositions of CMAS glasses in diopside–Ca-tschermakite join and glass in the diopside–anorthite eutectic composition. Table 2.2 also shows the chemical compositions of CMAS glasses determined by ICP-AES. The analysis was performed for CaO, MgO, and Al_2O_3 because SiO_2 is volatilized during pretreatment by reacting with hydrofluoric acid at 160–180 °C. While the chemical analysis here assumes that the nominal SiO_2

content is correct, taking into consideration negligible weight loss during synthesis and the consistency with ICP analysis, the compositions of the glasses are likely to be close to the nominal compositions. The predicted NBO fraction [NBO/(NBO + BO)] --the degree of network polymerization-- varies from 0.67 ($X_{Diopside}$ = 1) to 0 ($X_{Diopside}$ = 0) (Eckert, 1994): the NBO/T (the number of non-bridging oxygens per tetrahedral network cation) values for CMAS glasses in the join, predicted from the composition, change from 2 ($X_{Diopside}$ = 1) to 0 ($X_{Diopside}$ = 0) (Table 2.1). We also note that because the structures explored here were those of glasses quenched from melts, the structures studied here represent the atomic configurations of super-cooled liquids and at the glass-transition temperature, below which the melt structure is frozen. Because the glass-transition temperature is lower than the melting temperature of silicate glasses and thus the structures of glasses studied here are expected to be different from the structures of corresponding liquids. The effect of temperature on the glass structure can be probed using NMR by controlling quench rate during synthesis (and thus variation in T_g), which often show minor but detectable structural differences (e.g., Stebbins et al., 2008).

2.2.2. High-resolution NMR spectroscopy of quaternary silicate glasses

Solid-state NMR has been particularly effective in unveiling atomic structures of multi-component glasses (Eckert, 1994; Oestrike and Kirkpatrick, 1988; Stebbins, 1995). Because high-resolution NMR is the main experimental tool here, we briefly summarize the previous experimental efforts to reveal the structures of quaternary CMAS glasses using NMR. 1D

Table 2.1. Nominal compositions of CaO–MgO–Al_2O_3–SiO_2 silicate glasses in diopside–Ca-tschermakite pseudobinary join and glass in the diopside–anorthite eutectic ($Di_{64}An_{36}$). $X_{Diopside}$ is the mole fraction of diopside.

Composition		NBO/T	T_g (°C)	CMAS mol% (nominal composition)			
				CaO	MgO	Al_2O_3	SiO_2
$X_{Diopside}$	0	0	842*	33.3	0.0	33.3	33.3
	0.25	0.4	802§	30.8	7.7	23.1	38.4
	0.5	0.8	769§	28.6	14.3	14.3	42.9
	0.75	1.3	727†	26.7	20.0	6.7	46.6
	1	2	715‡	25.0	25.0	0.0	50.0
$Di_{64}An_{36}$		0.9	730‡	25.0	16.0	9.0	50.0

$NBO/T=2*(X_{(CaO+MgO)}-X_{Al2O3})/(1-(X_{(CaO+MgO)}-X_{Al2O3}))$

*(Neuville et al., 2004a)

†(Goel et al., 2008)

‡(Taniguchi, 1992)

§ The T_g of the glass was calculated assuming a linear increase in T_g with decreasing $X_{Diopside}$.

Table 2.2. Nominal compositions and ICP analyses for CaO–MgO–Al_2O_3–SiO_2 glasses in diopside–Ca-tschermakite pseudobinary join and glass in the diopside–anorthite eutectic ($Di_{64}An_{36}$). $X_{Diopside}$ is the mole fraction of diopside.

Composition		CMAS mol% (nominal composition)			CMAS mol% (ICP analysis)*		
		CaO	MgO	Al_2O_3	CaO	MgO	Al_2O_3
$X_{Diopside}$	0	50.0	0.0	50.0	49.3±1.7	0.1	50.6±1.7
	0.25	50.0	12.5	37.5	49.9±0.5	12.3±0.7	37.8±1.2
	0.50	50.0	25.0	25.0	50.5±0.5	24.8±0.9	24.7±0.9
	0.75	50.0	37.5	12.5	50.3±0.3	37.5±0.2	12.2±0.5
	1	50.0	50.0	0.0	50.0±0.2	49.9±0.1	0.1
$Di_{64}An_{36}$		50.0	32.0	18.0	50.0±0.5	32.0±0.5	18.0±1.1

*The analysis was performed for CaO, MgO, and Al_2O_3 because SiO_2 is volatilized during pretreatment by reacting with hydrofluoric acid. The chemical analysis here assumes that the nominal SiO_2 content is correct.

^{29}Si magic-angle spinning (MAS) NMR study of glasses in diopside–Ca-tschermakite join showed that the coordination number of Si is 4 (Kirkpatrick et al., 1986). ^{27}Al MAS NMR studies of quaternary aluminosilicate glasses showed that the four coordinated Al ($^{[4]}$Al) is dominant (Allwardt et al., 2007; Kelsey et al., 2008; Neuville et al., 2008) and the fraction of highly coordinated Al in glasses in the pyrope ($Mg_3Al_2Si_3O_{12}$)-grossularite ($Ca_3Al_2Si_3O_{12}$) join increases with Mg^{2+} content (Kelsey et al., 2008; Neuville et al., 2008). Detailed Al coordination environments and topological disorder (due to bond length-angle distribution and distortion of glass networks around Al) in multi-component aluminosilicate glasses were also revealed by 2D triple-quantum magic-angle spinning (3QMAS) (e.g., Allwardt et al., 2005; Allwardt et al., 2007; Angeli et al., 2007; Kelsey et al., 2008b; Lee et al., 2005; Lee et al., 2009b; Lee et al., 2010; Lee and Stebbins, 2000; Lee and Sung, 2008; Neuville, 2006; Neuville et al., 2008; Toplis et al., 2000; Xue and Kanzaki, 2007, 2008). The fraction of $^{[5]}$Al and the degree of network distortion around Al in Ca-Mg aluminosilicate glasses are more significant than those in Ca-Na aluminosilicate glasses (Lee et al., 2005). The presence of a few % of $^{[5]}$Al in hydrous glasses in diopside–anorthite join (Xue and Kanzaki, 2007, 2008), in good agreement with the results from molecular dynamics simulations (Vuilleumier et al., 2009).

The degree of polymerization and cation mixing in silicate glasses can be estimated by probing bonding environments around bridging (BO) and non-bridging oxygens (NBOs) using ^{17}O 3QMAS NMR (see Lee et al., 2005; Stebbins et al., 2001a; Stebbins et al., 2001b): these studies showed the evidence of the presence of Al–O–Al in peralkaline aluminosilicates ($CaO:MgO:Al_2O_3$: SiO_2 = 9.3:27.9:12.4:50.4 mol%) (Lee et al., 2005), an increase in the topological disorder in Si–O–Si and Si–O–Al in $CaO–Na_2O–$

Al_2O_3–SiO_2 glasses with Ca^{2+} content (Lee and Sung, 2008), and non-random Ca-Mg mixing around NBO in grossularite-pyrope composition glasses (Kelsey et al., 2008). NBO fraction in CaO–Na_2O–Al_2O_3–SiO_2 glasses is also reported to decrease with pressure (Lee, 2011).

2.2.3. Spectrometer

The ^{27}Al 3QMAS NMR spectra of CMAS glasses in diopside–Ca-tschermakite pseudobinary join and the $Di_{64}An_{36}$ glass were collected using a Varian solid-state NMR 400 system (9.4 T) at 104.229 MHz with a 3.2 mm Varian double-resonance probe (Seoul National University, Korea). A fast amplitude modulation (FAM)-based shifted-echo pulse sequence (consisting of two hard pulses with durations of 3.0 and 0.6 μs and a subsequent soft pulse with a duration of 15 μs) was used in ^{27}Al 3QMAS NMR (Baltisberger et al., 1996; Madhu et al., 1999; Zhao et al., 2001). A relaxation delay of 1 s was used. We have not observed any differential relaxation of Al sites with varying relaxation delays. Approximately 2880 to 6240 scans were averaged to achieve the signal-to-noise ratio shown in the 3QMAS NMR spectra. The ^{17}O MAS and 3QMAS NMR spectra of CMAS glasses and the $Di_{64}An_{36}$ glass composition were collected on a Varian solid-state NMR 400 system (9.4 T), at a Larmor frequency of 54.229 MHz, using a 4 mm Doty double-resonance probe. The relaxation delay for ^{17}O MAS NMR were 1 s and the radio frequency pulse strength was 0.4 μs. Sample spinning speeds of 14 kHz were used. In the 3QMAS NMR experiment at 9.4 T, a FAM-based shifted-echo pulse sequence with a hard pulse of duration 4.5 μs for multiple-quantum excitation and two 1.1 μs pulses for single quantum reconversion, a soft pulse of duration approximately 20 μs, and an echo time of approximately 500 μs (integer multiple of a rotor period) was used with a relaxation delay of 1 s.

While the longer relaxation delays are necessary to fully relax the spectrum for Ca-bearing silicate glasses, previous studies showed that negligible effect on differential relaxation of oxygen sites in the glasses (Allwardt et al., 2003; Lee and Stebbins, 2006). Approximately 12960 to 19296 scans of free-induction decay (FID) were averaged to achieve the signal-to-noise ratio shown in the ^{17}O 3QMAS NMR spectra. Approximately 60–70 FIDs were collected to construct the 2D spectra. The radio frequency (*rf*) field strengths for hard pulses for ^{27}Al 3QMAS and ^{17}O 3QMAS NMR are approximately 125 kHz and 75 kHz, respectively. The spectra were referenced to external tap water. ^{29}Si MAS NMR spectra were collected using a Varian solid 400 system at 9.4 T at 79.495 MHz, with a recycle delay of 3 s, a pulse length of 1.6 μs, and a spinning speed of 12 kHz, providing improved signal-to-noise ratio in the spectrum compared with an earlier pioneering study (Kirkpatrick et al., 1986). Previous studies have not shown any evidence of potential differential relaxations with varying relaxation time from 1s to 60 (Allwardt et al., 2003). All spectra were referenced to tetramethylsilane (TMS) solution. Note that the level of contour line for ^{27}Al 3QMAS NMR spectra presented here is as low as 2%, and that for ^{17}O 3QMAS NMR spectra for CMAS glasses in diopside-Ca-tschermakite join is 4% (that for diopside-anorthite eutectic are 3%), the quality of the spectra are thus much improved from the previous 2D NMR results for multi-component silicate glasses (e.g., Lee et al., 2005 and other ^{17}O and ^{27}Al NMR studies).

2.3. Results and discussion

2.3.1. Effects of composition on Al coordination environments in basaltic glasses and melts in diopside–Ca-tschermakite join: ^{27}Al 3QMAS NMR results

^{27}Al 3QMAS NMR spectra for CMAS glasses in diopside–Ca-tschermakite join with varying mole fractions of diopside ($X_{Diopside}$) show two Al-coordination environments, mostly $^{[4]}$Al and a small fraction of $^{[5]}$Al (as labeled). Note that these peak assignments are based on previous NMR studies on crystalline and glassy aluminosilicates (see Baltisberger et al., 1996 and references therein). The ^{27}Al 3QMAS NMR spectrum of Ca-tschermakite glass shows predominantly $^{[4]}$Al and a non-negligible amount of $^{[5]}$Al. The peak maximum of $^{[4]}$Al moves from -42±1.5 ppm ($X_{Diopside}$ = 0.75) to -46±1.5 ppm ($X_{Diopside}$ = 0) in the isotropic dimension. The peak maximum of $^{[5]}$Al moves from -20±2.5 ppm ($X_{Diopside}$ = 0) to -25±2.5 ppm ($X_{Diopside}$ = 0.75) in the isotropic dimension. The peak width (the width of full spectrum in MAS dimension) of $^{[4]}$Al in the MAS dimension measures the magnitudes of quadrupolar interactions and thus the degree of distortion around the Al coordination environments (chemical shift distribution in each Al species partly contributes to the peak width in the MAS dimension). The measured peak width at half-maximum of $^{[4]}$Al in the MAS dimension decreases from 53.5±1.5 ppm ($X_{Diopside}$ = 0) to 43.9±1.5 ppm ($X_{Diopside}$ = 0.75), suggesting that the degree of network distortion around Al (and thus the bond length and angle distribution) apparently decreases with increasing $X_{Diopside}$. As indicated by an increase in the number of contour lines for $^{[5]}$Al from 1 (for $X_{diopside}$ = 0.25) to 3 (for $X_{diopside}$ = 0.75), the fraction of $^{[5]}$Al tends to increase with increasing $X_{Diopside}$, suggesting a moderate increase in chemical disorder (i.e., configurational disorder due to mixing between $^{[4]}$Al and $^{[5]}$Al that

increases with increasing $^{[5]}$Al fraction) in the glasses with Mg^{2+} content (see further results and discussion below).

The total isotropic projections of the ^{27}Al 3QMAS NMR spectra for CMAS glasses in diopside–Ca-tschermakite pseudobinary join with varying $X_{Diopside}$ confirms that $^{[4]}$Al is dominant and a small, but non-negligible, fraction of $^{[5]}$Al can also be detected. Although $^{[6]}$Al is not clearly shown in the 2D NMR spectra, the total isotropic projection shows an intensity near the expected peak positions for $^{[6]}$Al (~ -5 ppm in MAS and isotropic dimension) in the glasses with $X_{Diopside}$ = 0.75 (Baltisberger et al., 1996). We thus note that there could be a minor fraction of $^{[6]}$Al in glasses in diopside–Ca-tschermakite join, below the current detection limit of ~0.5% in the 2D NMR spectra (considering signal to noise ratio of the spectrum) in particular, for glasses with high Mg^{2+} contents; this may be detected in high-field MAS NMR (> 14.1 T) (Stebbins et al., 2000).

The peak maximum of $^{[4]}$Al in the isotropic projection shifts toward higher frequency with increasing $X_{Diopside}$, accompanied by a shift to higher frequency in the MAS dimension. This is because the fractions of Q^4_{Al}(4Si) (Al^{3+} is surrounded by four $^{[4]}$Si as the next nearest neighbors) and/or Q^4_{Al}(3Si) increase with increasing $X_{Diopside}$ with increasing Si/Al ratio in the glass [here, Q^n_{Al}(mSi) refers to a Al species with n bridging oxygens and m (0-4) Si as the next nearest neighbors]. The similar results were observed for charge-balanced Ca- and Na- aluminosilicate glasses (Lee and Stebbins, 2000). As mentioned above, the measured peak width for $^{[4]}$Al in the isotropic projection slightly decreases with increasing $X_{Diopside}$, partly as a result of a decrease in dispersion in Q^4_{Al}-species distribution: All the Al atoms tend to be fully polymerized-- surrounded by only BOs (i.e., Q^4_{Al}) (Allwardt et al., 2003), and the Al–O–Al fraction in the glass decreases while the Si-O-Al

fraction increase with increasing $X_{Diopside}$. Therefore, the decrease in Al fraction (and Al-O-Al) with increasing $X_{Diopside}$ inevitably results in an increase in the fraction of Q^4_{Al} species with a larger number of Si as next nearest neighbors [i.e., Q^4_{Al}(4Si) and/or Q^4_{Al}(3Si)].

The relative population of $^{[5]}$Al is calibrated taking into consideration the 3QMAS efficiency (excitation of triple-quantum coherence and its reconversion to single-quantum coherence) of each Al site (Lee et al., 2010). Note that the 3QMAS efficiency is affected by quadrupolar interactions between nuclear quadrupole moment and electric field gradient around Al nuclide (Bak et al., 2000; Baltisberger et al., 1996). The calibrated fraction of $^{[5]}$Al slightly decreases with increasing $X_{Diopside}$ from 1.7±0.5% ($X_{Diopside}$ = 0) to 1.2±0.5% ($X_{Diopside}$ = 0.25), while the variation is within error range. It increases with a further increase in $X_{Diopside}$ to 3.0±0.5% ($X_{Diopside}$ = 0.75) (see appendix for detailed procedures for quantitative estimation of Al site fraction). This trend is to some extent consistent with previous NMR studies ternary aluminosilicate glasses where the fraction of $^{[5]}$Al increases with increasing cation field strength (Allwardt et al., 2005; Bunker et al., 1991; Kelsey et al., 2008; Lee et al., 2005).

While more detailed description of quantification of Al site fractions is given in appendix, we note that estimation of the fraction of a small amount of $^{[5]}$Al and $^{[6]}$Al (~1-10%) is intrinsically difficult because the measurement and analysis of 1D ^{27}Al MAS NMR at high (and low) field often depends on the model for the parameter (C_q and isotropic chemical shift) distributions and assumptions used to fit the 1D experimental data and 2D ^{27}Al 3QMAS technique is not quantitative and the larger C_q sites are often underestimated. Recent ^{27}Al 3QMAS and MAS NMR spectra for Ca-tschermakite at 17.6 T indicated that the $^{[5]}$Al fraction ranges ~8 % (Neuville

et al., 2006). The reason for the potential difference in the $^{[5]}$Al fraction is likely due to the different *rf* power levels (150 kHz vs. 125 kHz) and static magnetic fields of the two experiments (17.6 vs. 9.4 T): experiments at higher rf field often lead to more signal intensity from larger C_q sites. It should be noted that the $^{[5]}$Al fraction in the current study may not be regarded as unique value but rather represents one of the possible solutions (potentially minimum values, see appendix for details).

Figure 2.1 shows the effects of composition on the quadrupolar coupling constant [$C_q = P_q/(1 + \eta^2/3)^{1/2}$ where P_q and η are the quadrupolar coupling product and the asymmetry parameter, respectively] of $^{[4]}$Al in CMAS glasses in diopside–Ca-tschermakite join. As P_q (instead of C_q) is obtained from the 2D 3QMAS NMR spectrum, in order to calculate C_q the asymmetry parameter is assumed to be 0.5 here: average η of Al sites in crystalline anorthite is ~0.66 and there is minor difference in P_q and C_q with varying η from 0.4 to 0.7 (5%≤) (Kirkpatrick et al., 1985). The C_q of quadrupolar nuclide is sensitive to variations in local symmetry and thus its value represents the extent of lattice distortion (Baltisberger et al., 1996; Ghose and Tsang, 1973). The average C_q of $^{[4]}$Al in the glasses decreases slightly with increasing $X_{Diopside}$ from 6.6 ± 0.4 MHz ($X_{Diopside}$ = 0) to 6.1 ± 0.4 MHz ($X_{Diopside}$ = 0.75). The current result suggests that the degree of average deviation from perfect tetrahedral symmetry around $^{[4]}$Al (due to bond length and angle distribution and thus network distortion around Al) decreases with increasing $X_{Diopside}$: on the basis of chemical composition of the glasses studied here, the proportion of Q^4(3Si) (Al with 1Al and 3Si next-nearest neighbors), instead of Q^4(4Si) is expected to increase with decreasing $X_{Diopside}$ = 0.75 to 0 and the former is likely to be more distorted because a further deviation from tetrahedral symmetry for the former is obvious from

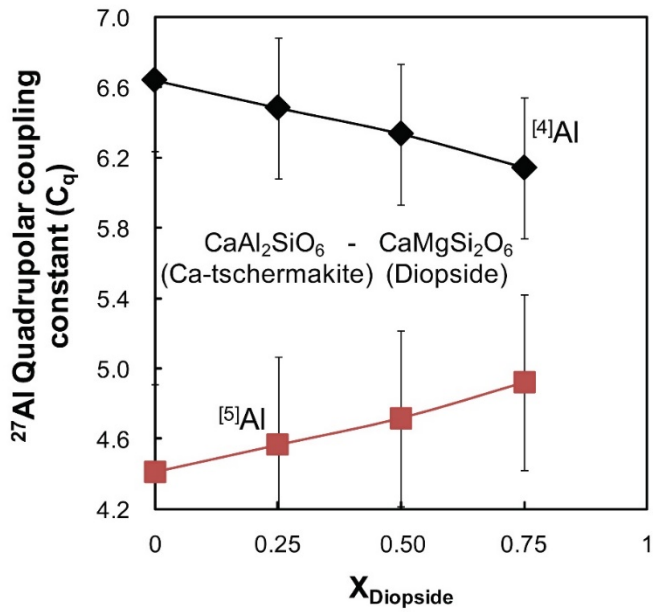

Figure 2.1. Quadrupolar coupling constant (C_q) of [4]Al in CaO–MgO–Al_2O_3–SiO_2 glasses in diopside–Ca-tschermakite pseudobinary join with varying $X_{Diopside}$. The asymmetry parameter is assumed to be 0.5. The estimated error bar of ±0.4 MHz for [4]Al and ±0.5 MHz for [5]Al are determined on the basis of uncertainty in position of center of gravity of each peak.

the composition of the species, and contributes to an increase in the average C_q values. The C_q of $^{[5]}$Al seems to increase slightly from 4.4 ± 0.5 MHz (for $X_{Diopside}$ = 0) to 4.9 ± 0.5 MHz ($X_{Diopside}$ = 0.75) with increasing $X_{Diopside}$. This result demonstrates that the presence of Mg^{2+} leads to the formation of $^{[5]}$Al and increases the degree of network distortion and thus Al-O bond length and angle distribution around $^{[5]}$Al. Note that due to relatively low $^{[5]}$Al intensity there is uncertainty in the absolute C_q value of $^{[5]}$Al. Furthermore, the C_q value for the site can be larger at higher magnetic field. The current results thus show the observed trend for C_q's for both $^{[4,5]}$Al with increasing $X_{Diopside}$ at 9.4 T. The observed effect of composition on Al coordination environments may be partly due to the effect of varying glass transition temperature (T_g) with composition on the glass structures. The T_g of the glasses tends to increase with decreasing $X_{diopside}$ (Goel et al., 2008; Neuville et al., 2004; Taniguchi, 1992) (Table 2). Whereas an increase in T_g would result in an increase in the fraction of highly coordinated Al, the opposite trend (a decrease in $^{[5]}$Al fraction with increasing $X_{diopside}$) is shown from ^{27}Al NMR spectra, indicating that the observed trend is not likely due to T_g effect.

While the Ca K-edge XANES may not be sensitive to changes in local distortion around Ca, network distortion around Ca in crystals and glasses were recently investigated using Ca K-edge XANES (e.g., Cormier and Neuville, 2004). Revealing the detailed structures of multi-component aluminosilicate glasses using x-ray scattering techniques is challenging: one of the best experimental results for ternary calcium aluminosilicate glasses (similar composition to Ca-tschermakite glass) using x-ray scattering successfully reported the structure factor of the glasses with varying scattering vector up to 40 A^{-1}, yet the extracted Si coordination number (3.2) was significantly smaller than 4 (Petkov et al., 2000).

2.3.2. Effects of composition on network connectivity and disorder in the glasses and melts in diopside–Ca-tschermakite join: Insights from ^{17}O MAS and 3QMAS NMR results

The peak assignments for the oxygen clusters in the following ^{17}O MAS and 3QMAS NMR spectra are based on the previous reports on binary, ternary, and quaternary CMAS glasses. Here, the term cluster is defined as a specific structural unit or structural environment that consists of several cations and anions with specific bonding between them in the glass network. Briefly, while NBO and BO peak positions slightly vary with composition (Si/Al, fractions of non-network forming cations, etc.), peaks positions for three types of BOs (Si-O-Si, Al-O-Al, and Si-O-Al) in ^{17}O 3QMAS NMR spectra for oxide glasses at 9.4 T have been well constrained (e.g., Lee and Stebbins, 2002). NMR characteristics (peak positions and structurally relevant NMR parameters) for various NBOs (Ca-O-Si, {Ca, Mg}-O-Si) in the CMAS glass were reported in the previous ^{17}O NMR study for ternary Ca-Mg silicate glasses with varying Ca/Mg ratio, Ca-aluminosilicate glasses, and quaternary Ca-Mg aluminosilicate glasses (e.g., Allwardt et al., 2003; Allwardt and Stebbins, 2004; Kelsey et al., 2008; Lee et al., 2005; Lee and Stebbins, 2000, 2002; Stebbins and Xu, 1997).

The ^{17}O MAS NMR spectra of Ca-tschermakite ($CaAl_2SiO_6$) glasses show the presence of a Ca-NBO (Ca-O-Si) peak at ~99 ppm and overlapping Al–O–Al and Al–O–Si peaks, consistent with an earlier NMR study (Lee and Stebbins, 2002): the presence of NBOs (approximately 4–5%) in nominally *fully polymerized* Ca-aluminosilicate glasses including anorthite composition glass was previously reported (Stebbins and Xu, 1997). Si–O–Si and {Ca, Mg}-mixed NBO are partially resolved in the ^{17}O MAS NMR spectrum for diopside glass (see ^{17}O 3QMAS NMR spectrum below where these peaks are

better resolved). As NBO peak positions move to lower frequency (more negative chemical shift) from Ca-O-Si (~100 ppm) to Mg-O-Si (i.e., Mg-NBO at ~35 ppm) (Allwardt and Stebbins, 2004; Lee et al., 2003), the NBOs in Ca-tschermakite glass are all ^{3}Ca–O–Si (the superscript refers to the number of each cation around NBO: e.g., ^{2}Ca^{1}Mg thus refers to two Ca^{2+} and one Mg^{2+} around NBO). Those in quaternary CMAS glasses at the intermediate composition show varying fractions of ^{3}Ca–O–Si and {Ca, Mg}-O-Si (^{2}Ca^{1}Mg-O-Si and ^{1}Ca^{2}Mg-O-Si) (Allwardt and Stebbins, 2004). ^{3}Mg-O-Si peak overlaps with other NBO and BO peaks in the join. No evidence for the presence of Al-NBO (e.g., Ca-O-Al at ~130-150 ppm in the MAS NMR spectrum at 9.4 T) was found. Whereas considerable overlaps among BO and NBO peaks make it difficult to estimate quantitatively the changes in their fractions with varying X_{Diopside}, qualitatively, the peak shape and width for each oxygen sites change with increasing X_{Diopside}, indicating changes in oxygen cluster populations and thus the connectivity among cations.

^{17}O 3QMAS NMR spectra for CMAS glasses in diopside–Ca-tschermakite join with varying X_{Diopside} provide enhanced resolution among the oxygen peaks compared to that obtained in ^{17}O MAS NMR spectra: because the total projection of the spectra into MAS dimension in the 2D ^{17}O 3QMAS NMR spectrum for the glass yields a spectrum similar to the 1D ^{17}O MAS NMR spectrum, the overlaps among oxygen peak in the ^{17}O MAS NMR spectra can be expected. These spectra show multiple oxygen sites, particularly Si–O–Si, Si–O–Al, and Ca-O-Si peaks. The oxygen peak from 130 ppm to 0 ppm in the MAS dimension stem from different types of NBOs [^{3}Ca-O-Si, ^{3}Mg-O-Si, and mixed-{Ca, Mg}-NBO]: the ^{3}Ca-O-Si peak is well resolved at -64 ppm in the isotropic dimension and the Mg-O-Si and/or mixed-NBO peaks partially overlap with the BO peaks. The chemical

shielding of the mixed-NBO peaks increases with increasing $X_{Diopside}$ (the peak shifts to a higher frequency in the isotropic dimension); the chemical shift dispersion of NBO peak apparently increases with increasing $X_{Diopside}$. The partially resolved ^{3}Ca-O-Si peak is observed for the CMAS glass with varying $X_{Diopside}$ from 0 to 0.5, suggesting prevalence of ^{3}Ca-NBO in the quaternary silicate glasses studied here. The current results also show that peak position of ^{3}Ca-O-Si is rather invariant with composition (see 3.3 below for further discussion).

For BOs, the previous study showed that the peak maxima of Al–O–Al and Al–O–Si in CMAS glasses are at approximately -36 and -40 ppm, respectively, in the isotropic dimension (Lee and Stebbins, 2002). The proportion of each BO and NBO structural environment apparently changes with $X_{Diopside}$. For example, the proportion of each BO was reported to be 38 ± 5% for Al–O–Al and 62 ± 5% for Al–O–Si in Ca-tschermakite ($CaAl_2SiO_6$) glass (Lee and Stebbins, 2002), and the fraction of both species apparently decreases with increasing $X_{Diopside}$. The significant fractions of Al-O-Si in all the CMAS glasses indicates extensive mixing between Al and Si (Lee et al., 2005; Lee and Stebbins, 1999). The spectra at $X_{diopside}$ = 0.5 and 0.75 are different in that the latter shows apparently larger Si-O-Si peak intensity. While Al-O-Al peak overlaps with mixed NBO peak as well as Si-O-Al, the intensity of the feature at -20 ppm in the isotropic dimension (a high frequency tail of Al-O-Al peak) is smaller for the latter, indicating a decrease in Al-O-Al fraction. The intensity of Si–O–Si peak (-50 ppm in the isotropic dimension) and {Ca, Mg}-mixed NBOs peak also increase with increasing $X_{Diopside}$ up to endmember diopside glass, where the Ca/Mg ratio reaches 1. Again due to overlap, quantitative fractions of these sites cannot be obtained. The total isotropic projection (the sum of data along lines parallel to the MAS

axis of the 2D 3QMAS NMR spectrum) of 2D ^{17}O 3QMAS NMR spectra for CMAS glasses in diopside–Ca-tschermakite join show that the Ca-NBO (^{3}Ca-O-Si) peak is partially resolved at approximately -64 ppm for glasses with $X_{Diopside}$ values of 0, 0.25, and 0.5 (For the glasses with $X_{Diopside}$ = 0.75 and 1, ^{3}Ca-O-Si peak overlaps with mixed {Ca, Mg}-NBO peaks).

2.3.3. The extent of Ca-Mg disorder in the glasses in diopside–Ca-tschermakite join: A view from ^{17}O NMR

The degree of Ca-Mg disorder in silicate glasses can be estimated from atomic environments around NBO sand BOs that are resolved in the ^{17}O NMR spectra for the glasses studied here. The ^{17}O 3QMAS NMR spectrum for CMAS glass at an intermediate compositions ($X_{Diopside}$ = 0.5) shows that a partially resolved ^{3}Ca-O-Si peak is observed at approximately -64 ppm. The presence of the observed prevalence of ^{3}Ca-O-Si peak in the intermediate composition glass may have important structural implications, particularly Ca^{2+} and Mg^{2+} distribution around NBOs and BOs. In order to check whether a random distribution of Ca^{2+} and Mg^{2+} around NBOs can account for the observed prevalence of ^{3}Ca-NBO in the CMAS glasses studied here, we attempt to calculate the hypothetical NBO distribution assuming a random distribution of Ca^{2+} and Mg^{2+} around NBOs for CMAS glasses at $X_{Diopside}$ = 0.5. The random distribution model of Ca^{2+} and Mg^{2+} around NBOs in CMAS glasses leads to the formation of four possible NBO configurations, i.e., ^{3}Ca-NBO, ^{2}Ca^{1}M g-NBO, ^{1}Ca^{2}Mg-NBO, and ^{3}Mg-NBO (Allwardt and Stebbins, 2004). On the basis of the peak position and width of Ca-NBO (from Ca-tschermakite) and those of Mg-NBO (from $MgSiO_3$ glass) (Allwardt and Stebbins, 2004; Lee et al., 2003), and the expected trend in the chemical shift in which the peak position of the NBO linearly increases

with the number of Ca^{2+} around the NBO (as is the case for Ca-Mg and Ca-Na silicate and aluminosilicate glasses) (Allwardt and Stebbins, 2004; Lee and Sung, 2008), the predicted peak positions of each NBO are approximately -67 (^{3}Ca-NBO), -56 (^{2}Ca^{1}Mg-NBO), -46 (^{1}Ca^{2}Mg-NBO), and -36 (^{3}Mg-NBO) ppm in the isotropic dimension. Then, the fraction of each NBO environment at Ca/(Ca + Mg) (x = 0.67) can be calculated for the glass: taking into account the number of distinguishable configurations for each NBO environment (i.e., $_{3}C_{0}$, $:_{3}C_{1}$,: $_{3}C_{2}$, $:_{3}C_{3}$ = 1:3:3:1), the predicated fractions assuming its random distribution are 29.5% [^{3}Ca-NBO, x^{3}], 55.5% [^{2}Ca^{1}Mg-NBO, $3x^{2}(1 - x)$], 22.3% [^{1}Ca^{2}Mg-NBO, $3x(1 - x)^{2}$], and 3.7% [^{3}Mg-NBO, $(1 - x)^{3}$] (Kelsey et al., 2008). The expected peak maximum for the total NBOs, based on the random distribution model, is at approximately -54 ppm as shown in a predicted hypothetical isotropic projection of NBO in glasses at X_{Diopside} = 0.5. Therefore, random distribution of Ca-Mg apparently fails to account for an observation of a distinct NBO peak maximum at the ^{3}Ca-NBO peak (around ~-64 ppm) in the 2D ^{17}O 3QMAS NMR spectrum for CMAS glass at X_{Diopside} = 0.5. These results therefore indicate that fraction of ^{3}Ca–O–Si in total NBO is likely to be higher than that predicted from the random distribution of Ca^{2+} and Mg^{2+}.

The observed prevalence of ^{3}Ca–O–Si and the deviation from random Ca-Mg mixing may have following structural origins. First, it may imply the obvious preferential partitioning of Ca^{2+} into NBOs and proximity between Mg^{2+} and BOs, including Si–O–Al and Al-O-Al, at intermediate compositions: Mg^{2+} can thus play a role as a charge-balancing cation, while Ca^{2+} acts as a network-modifying cation in CMAS glasses in diopside–Ca-tschermakite join. The preferential partitioning of Ca^{2+} and Mg^{2+} between NBOs and BOs (Al–O–Al, Al–O–Si) in glasses can be expressed:

$$\text{Ca--- Al–O–Al + Mg-NBO = Mg---Al–O–Al + Ca-NBO} \quad (1)$$

$$\text{Ca--- Al–O–Si + Mg-NBO = Mg--- Al–O–Si + Ca-NBO} \quad (2)$$

$$\text{Ca--- Si–O–Si + Mg-NBO = Mg--- Si–O–Si + Ca-NBO} \quad (3)$$

Note that Ca --- T-O-T indicates the proximity between Ca^{2+} and bridging oxygen T-O-T (T is framework cation including Si and Al). Here, the fractions of Al-O-Al, Al-O-Si, and Si-O-Si in the glasses depend on the Si/Al ratio and the degree of Si/Al disorder. With increasing Si-Al disorder, the Al-O-Al fraction increase at constant Si/Al ratio (see below for the discussion the degree of Al avoidance).

Second, the current result with the prevalence of ^{3}Ca-O-Si peak in the intermediate composition glasses also imply a non-random distribution of Ca-Mg around NBOs toward a slight degree of unmixing between these cations (i.e., clustering of Ca^{2+} and Mg^{2+}). This leads to smaller fractions of mixed NBO peaks (^{2}Ca^{1}Mg-O-Si and ^{1}Ca^{2}Mg-O-Si) than those predicted from random distribution model, which results in partially resolved ^{3}Ca-O-Si peaks observed in the current study. Previous ^{17}O MAS NMR study of glasses in pyrope-grossularite join also showed that Ca-Mg mixing around NBO may not be well-explained with a random mixing of the non-framework cations (Kelsey et al., 2008): the result rather indicated that the ^{3}Ca-NBO intensities were roughly (or slightly larger than) those expected from the random model, but the ^{2}Ca^{1}Mg-NBO was much lower. The authors thus suggested that there is an excess of Mg^{2+} over Ca^{2+} present in the average coordination shell of the NBO (Kelsey et al., 2008). Although the analysis given in the previous study is careful, due to peak overlap among Mg-O-Si peak and BO peaks (a well resolved Mg-NBO peak is necessary to

confirm the asserted conclusion in Mg-NBO preference), an unambiguous conclusion that can be drawn from the previous ^{17}O MAS NMR data is indeed the prevalence of ^{3}Ca-O-Si peak, which is consistent with the current result. Whereas it is not explicitly proposed in the previous study, this implies a structural tendency toward Ca-Mg unmixing in the CMAS glasses rather than Mg-NBO preference because a Mg-NBO preference should lead to a decrease in ^{3}Ca-O-Si peak fraction (i.e., should be less than that predicted from a random distribution model).

We note that the first proposal of preferential partitioning of Ca^{2+} into NBOs may not completely comply with experimental results for the binary alkali silicates and other quaternary glasses. For example, preferential partitioning of network modifying cations into BO has been found for Ca–Na aluminosilicate glasses, where the cation (i.e., Ca^{2+}) with the larger cation field strength prefers to have close proximity to NBOs (Lee and Sung, 2008). This is consistent with the suggestions from earlier Raman and ^{29}Si MAS NMR studies of binary alkali silicate glasses where disproportionation among Q-species [K_n=[Q^{n+1}] [Q^{n-1}]/[[Q^n]^2, here, Q^n refers to a Si species with n bridging oxygens] increases with increasing cation field strength of network modifying cations at constant NBO/T (Maekawa et al., 1991; Mysen, 1988; Mysen et al., 1982). These indirect results imply that cation with a larger field strength may have preferential proximity to NBOs. The proposed Ca-NBO preference (over Mg-NBO) in the CMAS thus indicates that the local arrangement of non-network-forming cations can be more complicated in the composition join studied here, and this cannot simply be predicted from the cation field strength of the network-modifying cations alone. In contrast to the known preference of a high field strength cation to NBO, when a pair of cations with identical charges but different ionic radii are mixed, steric

effects may predominate, favoring the larger cation, with a low cation field strength, for occupation of both BOs and NBOs (Lee et al., 2003): In mixing between Ca^{2+} and Mg^{2+} in CMAS glasses, the difference between the ionic radius of Ca^{2+} (1.14 Å) and that of Mg^{2+} (0.72 Å) may play a major role in the partitioning of Mg^{2+} and Ca^{2+} into both NBOs and BOs. This anomaly may result from a strong affinity between Mg^{2+} and Al–O–Al (e.g., Eq. 1) due to structural preference to have smaller charge-balancing cations (Mg^{2+} instead of Ca^{2+}) near Al-O-Al.

The proposed non-random distribution of Ca-Mg around NBOs toward unmixing between these cations in the CMAS glasses here is not completely consistent with the earlier suggestion of Ca-Mg random mixing in the glasses in the grossularite-pyrope join deduced from the viscosity measurement and estimation of macroscopic configurational entropy (Neuville and Richet, 1991). Ca-Mg mixing in the join (and a slight deviation from random distribution) can only *partly* contribute to the total configurational entropy of the glasses and additional (and often unknown amount of) topological contribution needs to be constrained. Whereas these two possible descriptions of the nature of Ca-Mg mixing in the glasses are consistent with the prevalence of ^{3}Ca-O-Si as shown in 2D ^{17}O NMR spectra, the above analyses based on 3QMAS NMR can be non-unique due to peak overlap for the Mg-NBO and the BO. The data given here thus cannot independently confirm whether the observed prevalence of ^{3}Ca-O-Si is due to unmixing of Ca-Mg or preferential preference of NBO for Ca over Mg or a combination of both. The current discussion of Ca-Mg distribution around NBO (as well as BO) can be more complicated upon formation of $^{[5]}$Al and thus $^{[5]}$Al-O-$^{[4]}$Si. Because the fraction of $^{[5,6]}$Al-O-$^{[4]}$Si is minor, its contribution to the pronounced Ca-Mg distribution in the glasses is not likely

to be significant. Its contribution, however, can be prominent for the aluminosilicate glasses quenched from melts at high pressure where significant fractions of highly coordinated framework cations were observed (see Lee, 2010 and reference therein). Because the information of Q-species distribution of alkaline earth aluminosilicate glasses (beyond ternary) is difficult to obtain using both Raman and ^{29}Si NMR, the current ^{17}O NMR data, though insufficient, provide an opportunity to unveil the nature of cation mixing around NBO in the multi-component quaternary glasses. Future attempt with a complete model of the 2D NMR data may provide better analysis of the Ca-Mg mixing and proposed preferential portioning in the quaternary silicate glasses.

We also note that the trend in composition-induced changes in peak position and width for Si-O-Si in glasses suggests that thus Si-O-Si can have spatial proximity to both Mg^{2+} and Ca^{2+} because both BOs and NBOs are apparently affected by the changes in Ca/Mg in the glasses. The trend suggests a rather homogeneous distribution of Mg^{2+} and Ca^{2+}, without formation of nano-meter scale heterogeneity characterized by segregation of Ca–Mg (Lee and Stebbins, 2003, 2009).

2.3.4. Effect of composition on Si environment in glasses in diopside–Ca-tschermakite join: ^{29}Si MAS NMR results

Figure 2.2 shows the ^{29}Si MAS NMR spectra for CMAS silicate glasses in diopside–Ca-tschermakite join. Note that four distinct Si environments were well-resolved in the ^{29}Si MAS NMR spectra for crystalline diopside–Ca-tschermakite solid solutions (Flemming and Luth, 2002). However, a single broad peak of slightly asymmetric shape is

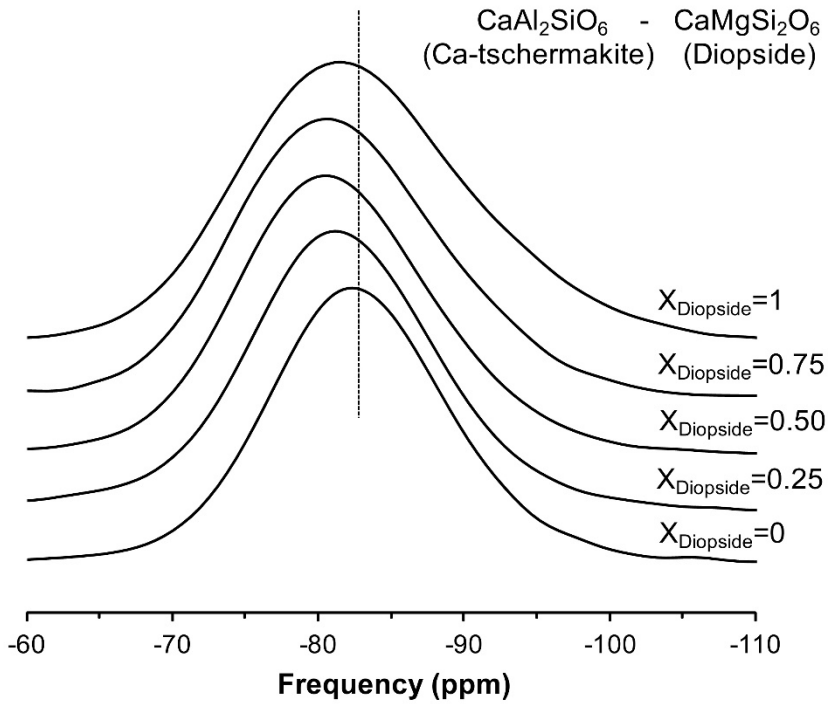

Figure 2.2. ^{29}Si MAS NMR spectra for $CaO–MgO–Al_2O_3–SiO_2$ glasses in diopside–Ca-tschermakite join at 9.4 T with varying mole fraction of diopside ($X_{Diopside}$).

observed in ^{29}Si MAS NMR spectra of the CMAS glasses. These chemical shift ranges for the peak correspond to four-coordinated Si, consistent with earlier ^{29}Si MAS NMR studies (Kirkpatrick et al., 1986). The peak maximum increases with increasing $X_{Diopside}$ from ~-82.3 ppm for $X_{Diopside}$ = 0 to ~-80.5 ppm for $X_{Diopside}$ = 0.5, and then decreases to ~-81.7 ppm for $X_{Diopside}$ = 1. This slight changes in peak maximum and the asymmetry in peak shape are due to complicated variations in the fractions of $Q^n(m\text{Al})$ species (Si species with zero through m Al next nearest neighbors with n bridging oxygen, $n \geq m$) that has distinct ^{29}Si chemical shifts with varying n and m (Kirkpatrick et al., 1986).

Figure 2.3 shows that the peak widths (full-width at half-maximum, FWHM) of the ^{29}Si MAS NMR spectra for the CMAS glasses decrease systematically from approximately 18 ppm for $X_{Diopside}$ = 1 to approximately 14 ppm for $X_{Diopside}$ = 0. The trends (increasing peak width with decreasing diopside content) are consistent with earlier ^{29}Si MAS NMR study (Kirkpatrick et al., 1986). The slight difference in peak width between the previous and current studies is mostly due to a significant increase in signal-to-noise ratio in the current spectrum and/or potential difference in chemical composition and synthesis conditions (e.g., quench rate). The peak shapes of ^{29}Si MAS NMR spectra of glasses in diopside–Ca-tschermakite join also reveal an increased asymmetry at lower frequencies. As the ^{17}O 3QMAS NMR spectra for CMAS glasses showed that the NBO fraction increases with increasing $X_{Diopside}$, and all the NBOs are bound to Si (i.e., Ca–O–Si, Mg–O–Si, and {Ca, Mg}–O–Si), an increase in peak width with diopside content is thus consistent with increasing configurational disorder due to dispersion in Q-species distribution: several Q species including Q^1, Q^2, and Q^3 is also likely to be present with increasing diopside content (Kirkpatrick et al., 1986; Mysen and Richet, 2005). However, predominant Q^4 species (in addition to

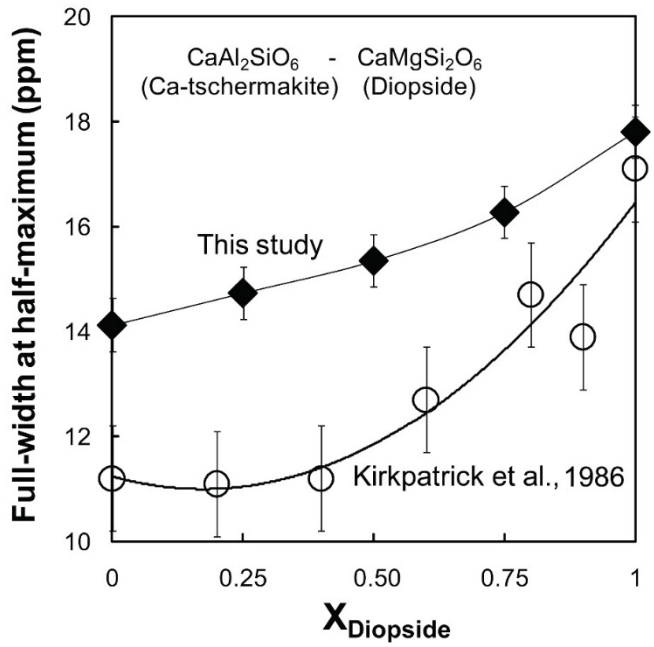

Figure 2.3. Peak widths (full-width at half-maximum) of $^{[4]}$Si in ^{29}Si MAS NMR spectra for CaO-MgO–Al_2O_3–SiO_2 glasses in diopside–Ca-tschermakite pseudobinary join at 9.4 T. $X_{Diopside}$ is the mole fraction of diopside. Diamonds indicate the results in this study and circles denote the results for previous study (Kirkpatrick et al., 1986). Error bar of ±0.5 ppm was estimated from the uncertainty in sample composition, phasing of NMR spectrum, and NMR processing conditions.

a minor fraction of Q^3 species predicted from the presence of Si-NBO) are present for Ca-tschermakite glass with predicted relative fractions of ~60% of Q^4(4Al), ~35% of Q^4(3Al), and ~5% of Q^4(2Al), respectively on the basis of the moderate degree of Al avoidance (Q of ~ 0.85) expected for Ca-aluminosilicate glasses (Lee and Stebbins, 1999); the degree of Al avoidance [Q, varies from 0 (random Si-Al mixing) to 1 (complete Al-avoidance)] decreases with Mg^{2+} content, which leads to a formation of more Al-O-Al and thus broadening of Q^n(mAl) distribution (Lee et al., 2005).

2.3.5. Structure and disorder in $Di_{64}An_{36}$ glass: insights from high-resolution solid-state NMR

The melts in diopside–anorthite eutectic composition have been used to model the first formed basaltic melts (Bowen, 1915). Figure 2.4 shows the ^{27}Al 3QMAS NMR spectrum for $Di_{64}An_{36}$ glass. The peak maximum for $^{[4]}$Al is at -41.3±1.5 ppm and that of $^{[5]}$Al is at -21.8±2.5 ppm in the isotropic dimension. The fraction of $^{[5]}$Al is ~3.3±0.5%, in good agreement with the earlier ^{27}Al NMR study for the $Di_{64}An_{36}$ glass (Xue and Kanzaki, 2007): whereas the percentage of $^{[5]}$Al is from 3.0% (for $X_{Diopside}$ = 0) to 5.1% (for $X_{Diopside}$ = 0.8) in diopside–anorthite join without C_q-3QMAS efficiency calibration (Xue and Kanzaki, 2008), the calibrated $^{[5]}$Al fractions considering 3QMAS efficiency, however, are consistent with the current results.

The C_q of $^{[4]}$Al for glass in $Di_{64}An_{36}$ is 6.0 ± 0.5 MHz and that of $^{[5]}$Al is 4.6 ± 0.5 MHz, which is similar to the values for CMAS glasses in diopside–Ca-tschermakite join (in particular, $X_{Diopside}$ = 0.75). The current C_q values is similar to those from the earlier study (C_q's of $^{[4]}$Al and $^{[5]}$Al in $Di_{64}An_{36}$ glass were 5.5 MHz and 4.3 MHz, respectively) (Xue and Kanzaki, 2007): note that

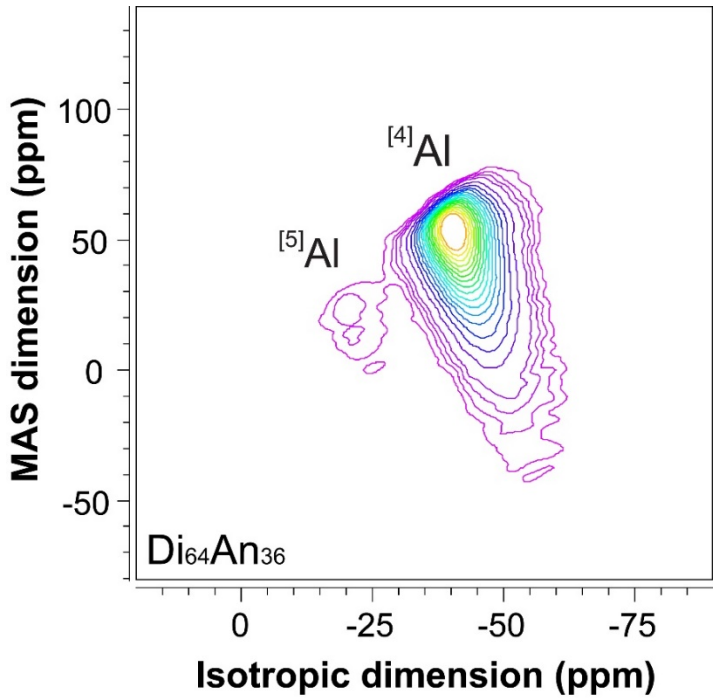

Figure 2.4. ^{27}Al 3QMAS NMR spectrum for glass in diopside–anorthite eutectic composition ($Di_{64}An_{36}$) at 9.4 T. Contour lines is drawn at 5% intervals from relative intensities of 12% to 87% with added lineat 2%, 3.5%, 6%, and 8%.

in the previous study, the P_q values were reported and thus C_q values were estimated from P_q, assuming an asymmetry parameter η of 0.5. The slight difference is due to the fact that in the previous study the peak maximum position is used to get the C_q value while we used the center of gravity of each peak.

Figure 2.5 shows the ^{17}O 3QMAS NMR spectrum for $Di_{64}An_{36}$ glass. This spectrum shows partially resolved multiple oxygen sites such as Si–O–Si, Si–O–Al, Al–O–Al, and Ca-NBO (-62.5 ppm in the isotropic dimension). The NBO peaks from -80 ppm to -25 ppm in the isotropic dimension stem from distinct NBOs (Ca-O-Si, Mg-O-Si, and {Ca, Mg}-O-Si). The Mg-NBO and {Ca, Mg}-NBO peaks partially overlap with the Si–O–Al peak. The Ca-NBO peak in the spectrum for $Di_{64}An_{36}$ glass is also well resolved at -63 ppm in the isotropic dimension as is the case for CMAS glasses in the diopside-Ca-tschermakite join whereas Ca/(Ca + Mg) ratio for $Di_{64}An_{36}$ glass is 0.61. Taking into consideration similar arguments presented in section 3.3, the presence of distinct ^{3}Ca–O–Si peak in the 2D spectrum for $Di_{64}An_{36}$ glass again suggests NBOs preference to Ca^{2+} and/or a tendency toward a slight degree of unmixing between Ca and Mg around NBO. The spectrum also shows a non-negligible fraction of Al–O–Al with Al/Si ratio in the glasses of ~0.36. Here we calculated oxygen cluster populations considering varying degree of Al avoidance (Q) from 0.80 (expected for Mg-end member) to 0.875 (value for charge-balanced aluminosilicate glasses) using the relations (equations) presented in the previous modeling because it has also been shown that the degree of Al avoidance decrease with increasing cation field

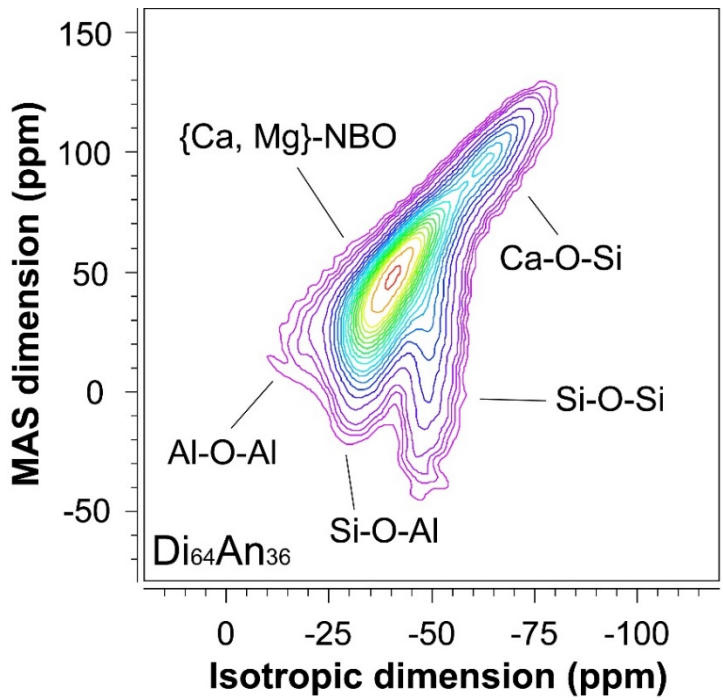

Figure 2.5. ^{17}O 3QMAS NMR spectrum for glass in diopside–anorthite eutectic composition ($Di_{64}An_{36}$) at 9.4 T. Contour lines is drawn at 5% intervals from relative intensities of 3% to 88% with added lines at 4.5, 6 and 37%.

strength of non-framework cations (Mg^{2+} and Ca^{2+}) (Lee et al., 2005; Lee and Stebbins, 1999, 2002): the calculated fractions of total-NBO, Al-O-Al, Al-O-Si, and Si-O-Si in the glass at Q=0.8 are 38.1 %, 6.7 (5.3) %, 29.4 (32.1) %, and 25.8 (24.4) %, respectively [the value in ( ) is fraction of oxygen species calculated at Q=0.875]. The significant fraction of Si-O-Al also suggests the extensive mixing between Al and Si in $Di_{64}An_{36}$ glass (see Lee, 2005 for details).

2.3.6. Implications for macroscopic thermodynamic and transport properties and geochemical processes

While the solid-state NMR techniques provide an improved resolution among atomic sites in geologically relevant, complex multi-component silicate glasses, further efforts should be given to develop methods to yield quantitative information of these partially resolved features in 2D spectrum, which will better constrain the diverse degree of disorder in the glasses. As basaltic glasses certainly have another important components including iron oxides (in addition to non-negligible fractions of MnO, TiO_2, Na_2O, K_2O, and P_2O_5), the application of current results of model basaltic glasses to real natural basaltic glasses thus have obvious limitations. Solid-state NMR has a limited usefulness in resolving atomic configurations in iron-bearing melts and glasses due to interaction between unpaired electrons in *d*-orbitals and nuclear spins of interest. The observed atomic structures of CMAS glasses in diopside–Ca-tschermakite join and $Di_{64}An_{36}$ glass provide atomistic insights into macroscopic properties and relevant geophysical processes. Due to overlap among peaks in the glass system studied here, the information of quantitative fraction of each oxygen cluster is missing. The information is necessary to make a direct-quantitative link between atomic structures and properties: the degree of deviation from

random mixing is necessary to constrain the enthalpy of mixing. The following discussion is thus qualitative and only focuses on the properties that can be consistent with experimental observation revealed from the NMR study here. First, the predominance of $^{[4]}$Al and its extensive mixing with Si, as evidenced by the significant fractions of $^{[4]}$Al–O–$^{[4]}$Si, is consistent with the negative experimental enthalpy of mixing obtained by solution calorimetry for CMAS glasses in diopside–Ca-tschermakite join (Navrotsky et al., 1983). The extensive Si-Al mixing in the glasses studied here is similar to the results from previous studies of ternary and quaternary aluminosilicate glasses where mixing between different framework cations are often preferred (Lee et al., 2005). The presence of Al-O-Al is also apparent for the glasses studied here. While it is difficult to quantify the fractions of those bridging oxygens due to overlap among peaks, as reported for ternary aluminosilicate glasses, it is likely that the degree of intermixing between Al and Si (degree of Al avoidance, Q) may range between a random distribution, (Q=0) and chemical order (Q=1). Upon mixing between Ca-tschermakite and diopside endmember components in the glasses, major contribution to configurational thermodynamic properties (e.g., configurational enthalpy and/or excess Gibbs free energy of mixing) is from the mixing between framework units, namely, $^{[4]}$Al and $^{[4]}$Si in the glasses: mixing between $CaAl_2SiO_6$ – $CaMgSi_2O_6$ can thus be modeled with taking into consideration only a mixing between 2Al and 1Si (with Mg^{2+}). Due to considerable mixing between Si and Al in the melts, activity coefficient of silica is thus expected to be less than 1 (predicted value for a random distribution of Al-Si), increasing the tendency to form a silica-rich melt in contact with mantle rocks (see Ryerson, 1985 and references therein).

Second, as it can also be expected from the composition, the relative NBO fraction increases with increasing X_{Diopside}. The viscosities of silicate melts decrease with decreasing degree of melt polymerization and thus NBO fraction (e.g., $\eta \propto \exp[A/(B + X_{NBO})]$, where A and B are constant) (Giordano and Dingwell, 2003; Lee et al., 2004). The viscosities of silicate melts in diopside–anorthite join decrease with increasing X_{Diopside} (Del Gaudio and Behrens, 2009; Getson and Whittington, 2007).

Third, the chemical shift dispersion of NBO peak increases with X_{Diopside}, implies extensive mixing between Ca^{2+} and Mg^{2+} around the NBOs. However, the Ca-Mg distribution around NBO is more complicated as the prevalence of ^{3}Ca-NBO in intermediate compositions in glasses in diopside–Ca-tschermakite join and $Di_{64}An_{36}$ glass provide evidence for a moderate degree of preferential partitioning of Ca^{2+} into NBOs and/or a non-random Ca-Mg distribution toward a slight degree of unmixing of these cations around NBO. Because major configurational thermodynamic properties of the glasses in the join results from framework mixing, the slight deviation from randomness in Ca-Mg disorder may not contribute much to the total thermodynamic properties in the join. We note that due to overlap among oxygen peaks and thus lack of information of quantitative fractions of oxygen sites, it is difficult to provide the quantitative estimation of configurational entropy using the current results.

Finally, while it is largely speculative and the current data cannot confirm the structural orgins of the prevalence of ^{3}Ca-O-Si , the proposed preferential partitioning of Ca^{2+} and Mg^{2+} between NBOs and BOs and potential deviation from random Ca-Mg mixing may result in variations in diffusivity of theses cations in the melts (Allwardt et al., 2003). Again it is certainly a weak correlation, but the suggested NBO preference also has

implications for dissolution mechanisms of basalts in contact with aqueous fluids. Taking into consideration the stronger bond between network-modifying cations (Ca^{2+}) and NBOs, Mg^{2+} (with proximity to BO) in basalts is likely to be dissolved easily. Thus, this preference could affect the chemical composition of groundwater on volcanic islands where Mg^{2+} concentration is higher than expected from the composition of basalts (Hurwitz et al., 2003).

2.4. Conclusions

The experimental data presented here provide structural details of atomic configurations, cation connectivity, and the extent of disorder in multi-component CMAS glasses in diopside–Ca-tschermakite pseudobinary join and the $Di_{64}An_{36}$ glass. On the basis of variation of peak width in ^{29}Si MAS NMR spectra for the glasses, while it is currently difficult to provide a quantitative description of the extent of topological disorder due to overlap among each Q-species, topological (peak widths) and chemical disorder (dispersion in Q species) around $^{[4]}Si$ apparently increases with Mg^{2+} content. The ^{27}Al 3QMAS NMR spectra for the join clearly show that the fraction of $^{[5]}Al$ increases with $X_{Diopside}$. It is thus evident that the degree of configurational (chemical mixing) disorder around Al due to the formation of $^{[5]}Al$ increases with $X_{Diopside}$: disorder due to chemical mixing increases with increasing $^{[5]}Al$ fraction. The ^{27}Al C_q's for $^{[4,5]}Al$ demonstrate that a topological disorder around $^{[4]}Al$ clearly decreases with $X_{Diopside}$ while that around $^{[5]}Al$ increases with $X_{Diopside}$. We cautiously speculate that the distortion of in the electric field gradient around $^{[4]}Al$ may be less significant with Mg^{2+} near $^{[4]}Al$, leading to a decrease in ^{27}Al C_q.

^{17}O 3QMAS NMR spectra for CMAS glasses studied here show that the degree of polymerization decreases with increasing $X_{Diopside}$, consistent

with a prediction from composition of the glasses: the 2D spectra show that the non-negligible fraction of ^{3}Ca-O-Si in the Ca-tschermakite composition glass ($X_{Diopside}$ =0) and the significant fraction of NBO in the diopside composition glass ($X_{Diopside}$ =1). The intensity for NBO peak apparently increases with $X_{Diopside}$. The significant fraction of Si-O-Al again supports an extensive mixing between $^{[4]}$Al and $^{[4]}$Si. Al-O-Al is also clearly visible in $Di_{64}An_{36}$ glass, highlighted with the presence of Al-O-Al and $^{[5]}$Al. A non-random distribution of Ca^{2+} and Mg^{2+} around both NBO and BO is manifested: on the basis of analysis of ^{3}Ca-O-Si peak position analysis in the 2D 3QMAS NMR spectrum, this could be due to a moderate degree of partitioning of Ca^{2+} into NBO and spatial proximity between Mg^{2+} and Al-O-Al and/or Al-O-Si in the basaltic glasses studied here. Additionally, the prevalence of ^{3}Ca-O-Si peak implies potential tendency toward unmixing of Ca-Mg around NBO. Further theoretical calculations and effort to model 2D spectra with overlapped oxygen peaks are necessary to confirm the current speculations and suggestions.

APPENDIX

Here, we briefly discuss the potential problems in quantification of small fractions of Al sites in the glasses using NMR. First, NMR experiment at 9.4 T, 1 dimensional ^{27}Al MAS NMR for the glasses studied here does not yield any evidence for the presence of highly coordinated Al (data not shown here). However, 2-dimensional ^{27}Al 3QMAS NMR data indeed provide evidence for the presence of non-negligible fractions of $^{[5]}$Al. As this 2D 3QMAS NMR technique is not quantitative in that the species population is dependent on the C_q of the site at a given *rf* field. In most cases, with increasing C_q from 4 to 8 MHz (typical C_q ranges for Al sites), the peak

intensity decreases (Lee et al., 2010). Therefore the fractions of large C_q sites are underestimated. In order to yield quantitative fraction, it is necessary to calibrate the experimental fraction with the C_q-intensity curve. In the current study, we yielded calibrated fraction taking into consideration C_q-peak intensity curve that we have calculated using numerical simulations (Lee et al., 2010). While the above procedures are rigorous, it is also possible that large C_q sites are intrinsically underestimated.

Previous 1D MAS for CAS glass at high field provide careful and quantitative information of small amount of $^{[5]}$Al sites (Neuville et al., 2006). $^{[5]}$Al peak fraction of ~ 8% was reported for $CaAl_2SiO_6$ glass in the ^{27}Al NMR spectra collected at higher magnetic field (Neuville et al., 2006), which is larger than that presented in the earlier ^{27}Al 3QMAS NMR and current study at lower magnetic fields (Lee and Stebbins, 2000, 2006). We also note that the calculated C_q of $^{[5]}$Al site in $CaAl_2SiO_6$ glass is reported to be 7.8 MHz, systematically larger than these reported in the current study as well as those reported by Xue and Kanzaki (Xue and Kanzaki, 2008) at 9.4 T (~4-5 MHz). These results again suggest that the 2D 3QMAS study at 9.4 T may not excite the Al sites with larger C_q effectively and thus the faction of these Al site can be underestimated. Additionally, lineshape analysis of 1D MAS at high field can be model dependent and may systematically overestimate the width of $^{[5]}$Al peak that leads to a larger C_q values.

We also summarized how the C_q and the fraction of Al sites were calculated, along with their uncertainties. Center of gravity for each Al peak was obtained from projections in the MAS and isotropic dimension. The estimated center of gravity for $^{[4]}$Al and $^{[5]}$Al peaks (δ_{3QMAS} is the center of gravity in the isotropic dimension and δ_{MAS} is that in MAS dimension in

3QMAS NMR spectra) are shown in table A1. On the basis of relationship between structurally relevant NMR parameters and δ_{3QMAS} and δ_{MAS}, mean values of P_q and δ_{iso}^{CS} of Al sites were estimated (Lee and Stebbins, 2000). Finally, C_q was calculated by assuming that η is 0.5. The results are also shown in table A1.

The isotropic projection was obtained by integrating NMR data from -120 ppm to 50 parallel to the MAS dimension (spanning the frequency range for [4]Al), which often obscures the presence of peak with low intensity (such as [5,6]Al). This method of projection is necessary to obtain quantitative [4,5]Al fractions. Therefore, we used the information from 2D NMR to constrain the presence of peak in the isotropic projection. Isotropic projection of the ^{27}Al 3QMAS NMR spectra were simulated using multiple Gaussian peaks representing [4]Al and [5]Al. Figure A1 show the results of a simulation with several Gaussian peaks of the total isotropic projection of the ^{27}Al 3QMAS NMR spectra. As mentioned in the text, the NMR signal intensity in the 3QMAS NMR experiment is determined by efficiencies in triple quantum excitation and single quantum reconversion that are dependent on the magnitude of the interactions between the nuclear quadrupolar moment and the electric field gradient (i.e., C_q). The observed NMR signal intensity was, therefore, scaled to take into consideration the magnitude of the quadrupolar interactions characteristic of each Al coordination environment by numerical simulations. The 3QMAS efficiency with quadrupolar coupling constant (C_q) at quadrupolar asymmetry parameter (η) of 0.5 has been calculated in the previous study (Lee et al., 2010). The error bar of 0.5% of Al site fraction stems from a) C_q variation and corresponding changes in 3QMAS efficiency (~0.3%) and b) uncertainty in the [5]Al fraction in peak area estimation

(~0.3%). Taking into consideration of other unknown uncertainties including that of compositions, and the total error bar ±0.5% is estimated.

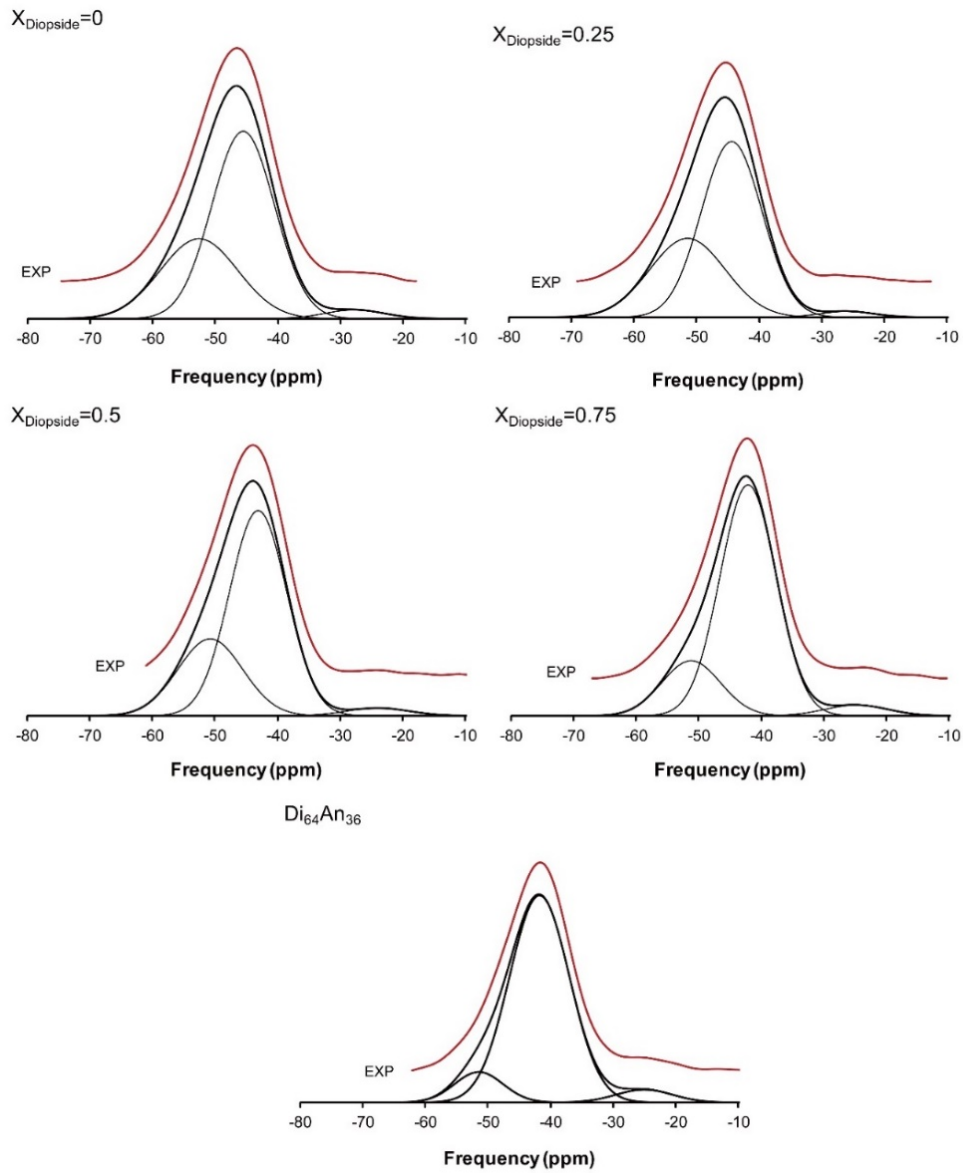

Figure 2.A1. The isotropic projections of ^{27}Al 3QMAS NMR spectra for CaO–MgO–Al_2O_3–SiO_2 glasses in diopside-Ca-tschermakite join and diopside-anorthite eutectic composition (red) with the simulated peaks of $^{[4]}$Al (~-40 and ~-52 ppm) and $^{[5]}$Al (-25 ppm). Note that $^{[5]}$Al fraction can be calculated from the ratio of -25 ppm peak fraction/total area. $X_{Diopside}$ is the mole fraction of diopside.

References

Ai, Y.H., Lange, R.A., 2008. New acoustic velocity measurements on CaO-MgO-Al_2O_3-SiO_2 liquids: Reevaluation of the volume and compressibility of $CaMgSi_2O_6$-$CaAl_2Si_2O_8$ liquids to 25 GPa. *J. Geophys. Res.-Sol. Ea.* 113.

Allwardt, J.R., Lee, S.K., Stebbins, J.F., 2003. Bonding preferences of non-bridging O atoms: Evidence from ^{17}O MAS and 3QMAS NMR on calcium aluminate and low-silica Ca-aluminosilicate glasses. *Am. Miner.* 88, 949-954.

Allwardt, J.R., Stebbins, J.F., 2004. Ca-Mg and K-Mg mixing around non-bridging O atoms in silicate glasses: An investigation using ^{17}O MAS and 3QMAS NMR. *Am. Miner.* 89, 777-784.

Allwardt, J.R., Stebbins, J.F., Schmidt, B.C., Frost, D.J., Withers, A.C., Hirschmann, M.M., 2005. Aluminum coordination and the densification of high-pressure aluminosilicate glasses. *Am. Miner.* 90, 1218-1222.

Allwardt, J.R., Stebbins, J.F., Terasaki, H., Du, L.S., Frost, D.J., Withers, A.C., Hirschmann, M.M., Suzuki, A., Ohtani, E., 2007. Effect of structural transitions on properties of high-pressure silicate melts: ^{27}Al NMR, glass densities, and melt viscosities. *Am. Miner.* 92, 1093-1104.

Angeli, F., Gaillard, M., Jollivet, P., Charpentier, T., 2007. Contribution of ^{43}Ca MAS NMR for probing the structural configuration of calcium in glass. *Chem. Phys. Lett.* 440, 324-328.

Asimow, P.D., Ahrens, T.J., 2010. Shock compression of liquid silicates to 125 GPa: The anorthite-diopside join. *J. Geophys. Res.-Sol. Ea.* 115.

Bak, M., Rasmussen, J.T., Nielsen, N.C., 2000. SIMPSON: A general simulation program for solid-state NMR spectroscopy. *J. Magn. Reson.* 147, 296-330.

Baltisberger, J.H., Xu, Z., Stebbins, J.F., Wang, S.H., Pines, A., 1996. Triple-quantum two-dimensional ^{27}Al magic-angle spinning nuclear magnetic resonance spectroscopic study of aluminosilicate and aluminate crystals and glasses. *J. Am. Chem. Soc.* 118, 7209-7214.

Barbieri, L., Corradi, A.B., Lancellotti, I., Leonelli, C., Montorsi, M., 2004. Experimental and computer simulation study of glasses belonging to diopside-anorthite system. *J. Non.-Cryst. Solids* 345, 724-729.

Bowen, N.L., 1915. The crystallization of haplobasaltic, haplodioritic and related magmas. *Am. J. Sci.* 40, 161-185.

Brown, G.E., Farges, F., Calas, G., 1995. X-ray scattering and x-ray spectroscopy studies of silicate melts, in: Stebbins, J.F., McMillan, P.F., Dingwell, D.B. (Eds.), Structure, Dynamics and Properties of Silicate Melts. Mineralogical Society of America, Washington, DC, pp. 317-410.

Bunker, B.C., Kirkpatrick, R.J., Brow, R.K., Turner, G.L., Nelson, C., 1991. Local-structure of alkaline-earth boroaluminate crystals and glasses: II, ^{11}B and ^{27}Al MAS NMR-spectroscopy of alkaline-earth boroaluminate glasses. *J. Non.-Cryst. Solids* 74, 1430-1438.

Cormier, L., Neuville, D.R., 2004. Ca and Na environments in Na_2O-CaO-Al_2O_3-SiO_2 glasses: influence of cation mixing and cation-network interactions. *Chem. Geol.* 213, 103-113.

Del Gaudio, P., Behrens, H., 2009. An experimental study on the pressure dependence of viscosity in silicate melts. *J. Chem. Phys.* 131.

Eckert, H., 1994. Structural studies of non-crystalline solids using solid state NMR. New experimental approaches and results, in: Blumich, B. (Ed.), Solid-State NMR IV.Methods and Applications of Solid-State NMR. Springer-Verlag, Berlin.

Flemming, R.L., Luth, R.W., 2002. ^{29}Si MAS NMR study of diopside-Ca-Tschermak clinopyroxenes: Detecting both tetrahedral and octahedral Al substitution. *Am. Miner.* 87, 25-36.

Gasparik, T., 1984. Experimentally determined stability of clinopyroxene + garnet + corundum in the system CaO-MgO-Al_2O_3-SiO_2. *Am. Miner.* 69, 1025-1035.

Getson, J.M., Whittington, A.G., 2007. Liquid and magma viscosity in the anorthite-forsterite-diopsidequartz system and implications for the

viscosity-temperature paths of cooling magmas. *J. Geophys. Res.-Sol. Ea.* 112.

Ghose, S., Tsang, T., 1973. Structural dependence of quadrupole coupling-constant E2QQ/H for ^{27}Al and crystal-field parameter D for Fe^{3+} in aluminosilicate. *Am. Miner.* 58, 748-755.

Giordano, D., Dingwell, D.B., 2003. Non-Arrhenian multicomponent melt viscosity: a model. *Earth Planet. Sc. Lett.* 208, 337-349.

Giordano, D., Potuzak, M., Romano, C., Dingwell, D.B., Nowak, M., 2008. Viscosity and glass transition temperature of hydrous melts in the system $CaAl_2Si_2O_8$-$CaMgSi_2O_6$. *Chem. Geol.* 256, 203-215.

Goel, A., Shaaban, E.R., Tulyaganov, D.U., Ferreira, J.M.F., 2008. Study of crystallization kinetics in glasses along the diopside-Ca-Tschermak join. *J Am.Ceram. Soc.* 91, 2690-2697.

Gordon, S.J., Brady, P.V., 2002. In situ determination of long-term basaltic glass dissolution in the unsaturated zone. *Chem. Geol.* 190, 113-122.

Herzberg, C., Zhang, J.Z., 1996. Melting experiments on anhydrous peridotite KLB-1: Compositions of magmas in the upper mantle and transition zone. *J. Geophys. Res.-Sol. Ea.* 101, 8271-8295.

Hurwitz, S., Goff, F., Janik, C.J., Evans, W.C., Counce, D.A., Sorey, M.L., Ingebritsen, S.E., 2003. Mixing of magmatic volatiles with groundwater and interaction with basalt on the summit of Kilauea Volcano, Hawaii. *J. Geophys. Res.-Sol. Ea.* 108.

Karki, B.B., Stixrude, L.P., 2010. Viscosity of MgSiO(3) liquid at Earth's mantle conditions: implications for an early magma ocean. Science 328, 740-742.

Kelsey, K.E., Allwardt, J.R., Stebbins, J.F., 2008a. Ca-Mg mixing in aluminosilicate glasses: An investigation using ^{17}O MAS and 3QMAS and ^{27}Al MAS NMR. *J. Non-Cryst. Solids* 354, 4644-4653.

Kelsey, K.E., Stebbins, J.F., Du, L.S., Mosenfelder, J.L., Asimow, P.D., Geiger, C.A., 2008b. Cation order/disorder behavior and crystal chemistry of

pyrope-grossular garnets: An ^{17}O 3QMAS and ^{27}Al MAS NMR spectroscopic study. *Am. Miner.* 93, 134-143.

Khater, G.A., 2010. Glass-ceramics in the CaO-MgO-Al_2O_3-SiO_2 system based on industrial waste materials. *J. Non-Cryst. Solids* 356, 3066-3070.

Kirkpatrick, R.J., Kinsey, R.A., Smith, K.A., Henderson, D.M., Oldfield, E., 1985. High-resolution solid-state ^{23}Na, ^{27}Al, and ^{29}Si nuclear magnetic-resonance spectroscopic reconnaissance of alkali and plagioclase feldspars. *Am. Miner.* 70, 106-123.

Kirkpatrick, R.J., Oestrike, R., Weiss, C.A., Smith, K.A., Oldfield, E., 1986. High-resolution ^{27}Al and ^{29}Si NMR-spectroscopy of glasses and crystals along the join $CaMgSi_2O_6$-$CaAl_2SiO_6$. *Am. Miner.* 71, 705-711.

Kushiro, I., 1998. Compositions of partial melts formed in mantle peridotites at high pressures and their relation to those of primitive MORB. *Phys. Earth Planet. In.* 107, 103-110.

Kushiro, I., 2001. Partial melting experiments on peridotite and origin of mid-ocean ridge basalt. *Annu. Rev. Earth Pl. Sc.* 29, 71-107.

Lee, C.T.A., Luffi, P., Hoink, T., Li, J., Dasgupta, R., Hernlund, J., 2010a. Upside-down differentiation and generation of a 'primordial' lower mantle. *Nature* 463, 930-U102.

Lee, S.K., 2005. Microscopic origins of macroscopic properties of silicate melts and glasses at ambient and high pressure: Implications for melt generation and dynamics. *Geochim. Cosmochim. Acta* 69, 3695-3710.

Lee, S.K., 2010. Effect of pressure on structure of oxide glasses at high pressure: Insights from solid-state NMR of quadrupolar nuclides. *Solid State Nucl. Magn. Reson.* 38, 45-57.

Lee, S.K., 2011. Simplicity in melt densification in multi-component magmatic reservoirs in earth's interior revealed by multi-nuclear magnetic resonance. *P. Natl. Acad. Sci. USA*. 108, 6847-6852.

Lee, S.K., Cody, G.D., Fei, Y.W., Mysen, B.O., 2004. Nature of polymerization and properties of silicate melts and glasses at high pressure. *Geochim. Cosmochim. Acta* 68, 4189-4200.

Lee, S.K., Cody, G.D., Mysen, B.O., 2005. Structure and the extent of disorder in quaternary (Ca-Mg and Ca-Na) aluminosilicate glasses and melts. *Am. Miner.* 90, 1393-1401.

Lee, S.K., Lee, S.B., Park, S.Y., Yi, Y.S., Ahn, C.W., 2009. Structure of amorphous aluminum oxide. *Phys. Rev. Lett.* 103.

Lee, S.K., Mysen, B.O., Cody, G.D., 2003. Chemical order in mixed-cation silicate glasses and melts. *Phys. Rev. B* 68.

Lee, S.K., Park, S.Y., Yi, Y.S., Moon, J., 2010. Structure and disorder in amorphous alumina thin films: Insights from high-resolution solid-state NMR. *J. Phys. Chem. B*. 114, 13890-13894.

Lee, S.K., Stebbins, J.F., 1999. The degree of aluminum avoidance in aluminosilicate glasses. *Am. Miner.* 84, 937-945.

Lee, S.K., Stebbins, J.F., 2000. The structure of aluminosilicate glasses: High-resolution ^{17}O and ^{27}Al MAS and 3QMAS. *J. Phys. Chem. B.* 104, 4091-4100.

Lee, S.K., Stebbins, J.F., 2002. Extent of intermixing among framework units in silicate glasses and melts. *Geochim. Cosmochim. Acta* 66, 303-309.

Lee, S.K., Stebbins, J.F., 2003. Nature of cation mixing and ordering in Na-Ca silicate glasses and melts. *J. Phys. Chem. B.* 107, 3141-3148.

Lee, S.K., Stebbins, J.F., 2006. Disorder and the extent of polymerization in calcium silicate and aluminosilicate glasses: ^{17}O NMR results and quantum chemical molecular orbital calculations. *Geochim. Cosmochim. Acta* 70, 4275-4286.

Lee, S.K., Stebbins, J.F., 2009. Effects of the degree of polymerization on the structure of sodium silicate and aluminosilicate glasses and melts: An ^{17}O NMR study. *Geochim. Cosmochim. Acta* 73, 1109-1119.

Lee, S.K., Sung, S., 2008. The effect of network-modifying cations on the structure and disorder in peralkaline Ca-Na aluminosilicate glasses: ^{17}O 3QMAS NMR study. *Chem. Geol.* 256, 326-333.

Liu, X., O'Neill, H.S.C., 2004. Partial melting of spinel lherzolite in the system CaO-MgO-Al_2O_3-SiO_2 +/- K_2O at 1 center dot 1 GPa. *J. Petrol.* 45, 1339-1368.

Madhu, P.K., Goldbourt, A., Frydman, L., Vega, S., 1999. Sensitivity enhancement of the MQMAS NMR experiment by fast amplitude modulation of the pulses. *Chem. Phys. Lett.* 307, 41-47.

Maekawa, H., Maekawa, T., Kawamura, K., Yokokawa, T., 1991. The structural groups of alkali silicate-glasses determined from Si-29 MAS-NMR. *J. Non-Cryst. Solids* 127, 53-64.

Mysen, B.O., 1988. Structure and Properties of Silicate Melts. Elsevier, Amsterdam.

Mysen, B.O., Richet, P., 2005. Silicate glasses and melts: Properties and structure. Elsevier, Amsterdam.

Mysen, B.O., Virgo, D., Seifert, F.A., 1982. The structure of silicate melts - implications for chemical and physical-properties of natural magma. *Rev. Geophys.* 20, 353-383.

Navrotsky, A., Zimmermann, H.D., Hervig, R.L., 1983. Thermochemical study of glasses in the system $CaMgSi_2O_6$-$CaAl_2SiO_6$. *Geochim. Cosmochim. Acta* 47, 1535-1538.

Neuville, D.R., 2006. Viscosity, structure and mixing in (Ca, Na) silicate melts. *Chem. Geol.* 229, 28-41.

Neuville, D.R., Cormier, L., Flank, A.M., Briois, V., Massiot, D., 2004a. Al speciation and Ca environment in calcium aluminosilicate glasses and crystals by Al and Ca K-edge X-ray absorption spectroscopy. *Chem. Geol.* 213, 153-163.

Neuville, D.R., Cormier, L., Massiot, D., 2004b. Al environment in tectosilicate and peraluminous glasses: A Al-27 MQ-MAS NMR, Raman, and XANES investigation. Geochimica Et Cosmochimica Acta 68, 5071-5079.

Neuville, D.R., Cormier, L., Massiot, D., 2006. Al coordination and speciation in calcium aluminosilicate glasses: Effects of composition determined by

Al-27 MQ-MAS NMR and Raman spectroscopy. Chemical Geology 229, 173-185.

Neuville, D.R., Cormier, L., Montouillout, V., Florian, P., Millot, F., Rifflet, J.C., Massiot, D., 2008. Structure of Mg- and Mg/Ca aluminosilicate glasses: ^{27}Al NMR and Raman spectroscopy investigations. *Am. Miner.* 93, 1721-1731.

Neuville, D.R., Richet, P., 1991. Viscosity and mixing in molten (Ca, Mg) pyroxenes and garnet. Geochim. Cosmochim. Acta 55, 1011-1019.

Oestrike, R., Kirkpatrick, R.J., 1988. ^{27}Al and ^{29}Si MASS NMR-spectroscopy of glasses in the system anorthite-diopside-forsterite. *Am. Miner.* 73, 534-546.

Ohtani, E., 2009. Melting relations and the equation of state of magmas at high pressure: Application to geodynamics. *Chem. Geol.* 265, 279-288.

Ohtani, E., Kato, T., Sawamoto, H., 1986. Melting of a model chondritic mantle to 20 GPa. Nature 322, 352-353.

Petkov, V., Billinge, S.J.L., Shastri, S.D., Himmel, B., 2000. Polyhedral Units and Network Connectivity in Calcium Aluminosilicate Glasses from High-Energy X-Ray Diffraction. Phys. Rev. Lett. 85, 3436-3439.

Potuzak, M., Dingwell, D.B., 2006. Temperature-dependent thennal. expansivities of multicomponent natural melts between 993 and 1803 K. *Chem. Geol.* 229, 10-27.

Presnall, D.C., Dixon, J.R., Odonnell, T.H., Dixon, S.A., 1979. Generation of mid-ocean ridge tholeiites. *J. Petrol.* 20, 3-35.

Ryerson, F.J., 1985. Oxide solution mechanisms in silicate melts - systematic variations in the activity-coefficient of SiO_2. Geochim. Cosmochim. Acta 49, 637-649.

Schilling, F.R., Hauser, M., Sinogeikin, S.V., Bass, J.D., 2001. Compositional dependence of elastic properties and density of glasses in the system anorthite-diopside-forsterite. *Contrib. Mineral. Petr.* 141, 297-306.

Stebbins, J.F., 1995. Dynamics and structure of silicate and oxide melts: Nuclear magnetic resonance studies, in: Stebbins, J.F., McMillan, P.F.,

Dingwell, D.B. (Eds.), Structure, Dynamics and Properties of Silicate Melts. Mineralogical Society of America, Washington, DC, pp. 191-246.

Stebbins, J.F., Dubinsky, E.V., Kanehashi, K., Kelsey, K.E., 2008. Temperature effects on non-bridging oxygen and aluminum coordination number in calcium aluminosilicate glasses and melts. Geochim. Cosmochim. Acta 72, 910-925.

Stebbins, J.F., Kroeker, S., Lee, S.K., Kiczenski, T.J., 2000. Quantification of five- and six-coordinated aluminum ions in aluminosilicate and fluoride-containing glasses by high-field, high-resolution ^{27}Al NMR. *J. Non-Cryst. Solids* 275, 1-6.

Stebbins, J.F., Oglesby, J.V., Lee, S.K., 2001a. Oxygen sites in silicate glasses: a new view from oxygen-17 NMR. *Chem. Geol.* 174, 63-75.

Stebbins, J.F., Xu, Z., 1997. NMR evidence for excess non-bridging oxygen in an aluminosilicate glass. *Nature* 390, 60-62.

Stebbins, J.F., Zhao, P.D., Lee, S.K., Oglesby, J.V., 2001b. Direct observation of multiple oxygen sites in oxide glasses: recent advances from triple-quantum magic-angle spinning nuclear magnetic resonance. *J. Non-Cryst. Solids* 293, 67-73.

Stixrude, L., Karki, B., 2005. Structure and freezing of $MgSiO_3$ liquid in Earth's lower mantle. *Science* 310, 297-299.

Taniguchi, H., 1989. Densities of melts in the system $CaMgSi_2O_6$-$CaAl_2Si_2O_8$ at low and high-pressures, and their structural significance. *Contrib. Mineral. Petr.* 103, 325-334.

Taniguchi, H., 1992. Entropy dependence of viscosity and the glass-transition temperature of melts in the system diopside-anorthite. *Contrib. Mineral. Petr.* 109, 295-303.

Tauber, P., Arndt, J., 1987. The relationship between viscosity and temperature in the system anorthite diopside. *Chem. Geol.* 62, 71-81.

Tinker, D., Lesher, C.E., Hutcheon, I.D., 2003. Self-diffusion of Si and O in diopside-anorthite melt at high pressures. *Geochim. Cosmochim. Acta* 67, 133-142.

Toplis, M.J., Kohn, S.C., Smith, M.E., Poplett, I.J.F., 2000. Fivefold-coordinated aluminum in tectosilicate glasses observed by triple quantum MAS NMR. *Am. Miner.* 85, 1556-1560.

Vuilleumier, R., Sator, N., Guillot, B., 2009. Computer modeling of natural silicate melts: What can we learn from ab initio simulations. *Geochim. Cosmochim. Acta* 73, 6313-6339.

Walter, M.J., Presnall, D.C., 1994. Melting behavior of simplified lherzolite in the system CaO-MgO-Al_2O_3-SiO_2-Na_2O from 7 to 35 kbar. *J. Petrol.* 35, 329-359.

Winter, J.D., 2009. An Introduction to Igneous and Metamorphic Petrology. Pearson College Div.

Xiao, H.N., Cheng, Y., Yu, L.P., Liu, H.B., 2006. A study on the preparation of CMAS glass-ceramics by in situ crystallization. *Mat. Sci. Eng. -A. -Struct.* 431, 191-195.

Xue, X.Y., Kanzaki, M., 2007. Al coordination and water speciation in hydrous aluminosilicate glasses: Direct evidence from high-resolution heteronuclear ^{1}H-^{27}Al correlation NMR. *Solid State Nucl. Magn. Reson.* 31, 10-27.

Xue, X.Y., Kanzaki, M., 2008. Structure of hydrous aluminosilicate glasses along the diopside-anorthite join: A comprehensive one- and two-dimensional ^{1}H and ^{27}Al NMR study. *Geochim. Cosmochim. Acta* 72, 2331-2348.

Zhao, P., Neuhoff, P.S., Stebbins, J.F., 2001. Comparison of FAM mixing to single-pulse mixing in ^{17}O 3Q-and 5Q-MAS NMR of oxygen sites in zeolites. *Chem. Phys. Lett.* 344, 325-332.

Chapter 3. High-resolution solid-state NMR study of the effect of composition on network connectivity and structural disorder in multi-component glasses in the diopside and jadeite join: implications for structure of andesitic melts

Sun Young Park and Sung Keun Lee

Published in *Geochimica et Cosmochimica Acta*, 2014, v. 147, 26-42

Abstract

The structural evolution of andesitic melts with varying compositions remains one of the unsolved questions in high-temperature geochemistry and petrology. In this article, we report the structural details of model andesitic glasses [CaO–MgO–Na_2O–Al_2O_3–SiO_2 (CMNAS)] in the diopside ($CaMgSi_2O_6$) and jadeite ($NaAlSi_2O_6$) join using high-resolution, multi-nuclear, solid-state nuclear magnetic resonance (NMR). The ^{27}Al NMR spectra of CMNAS glasses confirm that $^{[4]}$Al is dominant. While a minor fraction of $^{[5]}$Al is observed, its presence is only prevalent in the glasses with higher Ca-Mg content. Topological disorder in the glass network also tends to increase with Ca–Mg content as evidenced by the increase in the quadrupolar coupling constant (C_q) of $^{[4]}$Al for glasses with increasing diopside contents ($X_{Diopside}$). Despite the complex nature of the glasses studied here (with five oxide components), the ^{17}O 3QMAS NMR spectra resolve diverse bridging oxygens (BOs) and non-bridging oxygens (NBOs), from which the degree of Al avoidance among framework cations (Si and Al) and preferential proximity among non-network cations (Ca^{2+}, Mg^{2+}, and Na^{+}) and each oxygen site can be estimated: presence of Al–O–Al in jadeite glass implies a violation of the Al-avoidance rule in the glasses and the decrease

in the fraction of NBOs with increasing $X_{Diopside}$ is consistent with a decrease in their viscosity. Analysis of the peak position of {Ca, Mg}-mixed NBOs, along with the absence of Na-NBO peak, and the peak shape of Si–O–Al reveals preferential partitioning of Ca^{2+} and Mg^{2} into NBOs and the proximity of Na^{+} to BOs. The fraction of highly coordinated Al has been linked to thermodynamic and transport properties of the melts. Considering all the experimental Al coordination environments available in the literature, together with the current experimental studies, we attempt to establish the relationship between the fractions of highly coordinated Al and composition, particularly average cationic potential of non-network forming cations ($<c/r>_{ave}$, defined as cationic potential normalized by the mole fraction of each non-network cation). The fraction of highly coordinated Al increases nonlinearly with increasing $<c/r>_{ave}$. The fraction of $^{[5,6]}Al$ is negligible up to $<c/r>_{ave}$ =~ 1.7, then it increases above $<c/r>_{ave}$ > ~1.7 regardless of changes in other compositional variables (e.g., Si/Al, NBO content). This indicates the presence of a threshold $<c/r>_{ave}$ value for the formation of $^{[5,6]}Al$. The current experimental results with the changes in network polymerization, coordination environments, and the degree of disorder in the CMNAS glasses can improve understanding of the structure–property (particularly, configurational thermodynamic properties) relationships of multi-component natural silicate melts, including andesitic melts and glasses.

3.1. Introduction

$CaO–MgO–Na_2O–Al_2O_3–SiO_2$ (CMNAS) glasses in a diopside ($CaMgSi_2O_6$)–jadeite ($NaAlSi_2O_6$) pseudobinary join can be regarded as an important model system for andesitic melts (e.g., Bell and Davis, 1969; Jindal, 2012; Jindal et al., 2011; Schairer and Yoder, 1960). The intermediate

composition of the diopside–jadeite join can also represent high-Mg andesitic melts (defined as having Mg# ≥ 0.45 and SiO_2 = 54~65%) (e.g., Wood and Turner, 2009). Andesite (rock) consists of mineral assemblages including quartz, pyroxene, feldspars, and hornblende. As we are exploring the structure of andesitic *glasses and melts* with typical oxide mole % (e.g., SiO_2: Al_2O_3: CaO: MgO: Na_2O: K_2O: FeO(T)= 62.4: 10.8: 8.3: 6.3: 3.6: 1.1: 6.4 (mol%)] (e.g., Mysen and Richet, 2005), when it comes to its major element composition, diopside-jadeite join with five-oxide components can represent iron free andesitic melts. Andesitic melts are the second most abundant melts in volcanic eruptions next to basaltic melts and several models have been suggested regarding the mechanism of their generation. These includes partial melting at the mantle wedge under hydrous conditions (e.g., Hirose, 1997a; Parman and Grove, 2004), mixing of basaltic melts with felsic crustal components (e.g., Straub et al., 2011; Zhu et al., 2013), and crystallization differentiation of mantle-derived basalt (e.g., Grove and Kinzler, 1986; Mortazavi and Sparks, 2004; Prouteau and Scaillet, 2003) . Changes in the chemical compositions of andesitic melts are accompanied by the above processes of magma generation and differentiation, which lead to changes in the atomic structures and properties of the melts. Thus, understanding the structure and disorder in andesitic melts with varying compositions is essential for comprehending their properties and the complex magmatic processes relevant to andesitic magma in subduction zones. However, despite their importance, details regarding the atomic structure and disorder of these melts, such as the network connectivity and the systematic structure–property relationships, remain unsolved. The objective of this study is to reveal the atomic structure in terms of network connectivity and

disorder in model andesitic melts and glasses with varying compositions, and to unveil systematic structure–property relationships.

The atomic structure (e.g., coordination number, various types of structural disorder, and network connectivity) of *multi-component* silicate glasses and melts including CMNAS glasses has considerable implications for the macroscopic properties of natural silicate melts (e.g., Bauchy et al., 2013; Giordano et al., 2008; Kelsey et al., 2008b; Lee, 2005, 2011b; Mysen and Richet, 2005; Navrotsky et al., 1983; Neuville et al., 2004b, 2006b; Potuzak and Dingwell, 2006, and references therein). However, overlaps among peaks (in any spectroscopic methods) and scattering factors (both x-ray and neutron scattering) of the multi-component silicate glasses become more prominent with increasing numbers of oxide components due to enhanced topological (due to bond angle and bond length distribution and distortion of glass networks around Al and Si) and configurational disorder (due to mixing between different species, e.g., mixing between $^{[4]}$Al and $^{[5]}$Al) in the glasses, making it challenging to probe their detailed atomic structures (Mysen and Toplis, 2007) (see 2.3 below for the definitions used to describe the degree of disorder). In contrast, the macroscopic properties of CMNAS glasses and melts in diopside–jadeite joins have been extensively studied. The configurational entropy of the melts increases with increasing diopside component (Richet, 1984). While the bulk modulus of the glasses decreases in glasses along the diopside–jadeite join, the Poisson's ratio increases with increasing diopside content (Jindal, 2012). The viscosities of silicate melts in diopside–jadeite joins decrease with increasing diopside content (Suzuki et al., 2005).

These changes in the thermo-mechanical and transport properties of CMNAS glasses and melts are obviously linked to changes in the atomic

structure related to changing composition. Despite the aforementioned difficulties in exploring the local structures of multi-component silicate glasses, the cation coordination environments of complex quaternary oxide glasses with geochemical implications have recently been reported. For example of Al coordination environments, recent studies of the model basaltic glasses in diopside–Ca–tschermakite and diopside–anorthite joins show the presence of five coordinated Al ($^{[5]}$Al) (Park and Lee, 2012; Xue and Kanzaki, 2008). A previous study of the shock-compressed model basaltic glasses (diopside–anorthite eutectic composition, $Di_{64}An_{36}$) also showed that the fraction of $^{[5]}$Al in the basaltic glasses increased upon dynamic compression up to peak pressure of ~20 GPa (Lee et al., 2012). Al coordination environments in hydrous andesite glasses have also been studied extensively (Malfait et al., 2012; Mysen and Richet, 2005 for review) (further details in section 2.3).

The intermediate composition of a crystalline diopside–jadeite join (diopside–jadeite = 50:50) shows cation ordering in both octahedral and tetrahedral sites with preference in Ca–Mg and Na–Al pairs (i.e., omphacite). The relevant question is whether there is similar ordering for glass and the precursor liquids in the diopside–jadeite join. Previous studies have shown that the extent of disorder, such as network connectivity and the degree of Al avoidance (Si/Al framework disorder), is important in understanding the configurational thermodynamic properties of the aluminosilicate glasses, such as configurational entropy and heat capacity as well as the Gibbs free energy of mixing (Lee, 2005, 2011; Lee and Stebbins, 1999, 2006, 2009; Mysen and Richet, 2005; Navrotsky et al., 1983; Stebbins, 1995 and references therein). Various types of additional structural disorder also affect configurational properties of melts and glasses. These structural disorders

include bonding preferences between NBOs and the framework cations (e.g., Si–NBO *vs*. Al–NBO) (Allwardt et al., 2003) and partitioning of network modifying cations between non-bridging oxygens (NBOs) and bridging oxygens (BOs) (Lee and Sung, 2008; Park and Lee, 2012). Information regarding these types of disorder can be obtained using various spectroscopic methods, particularly with ^{17}O NMR (see Lee, 2010 and references therein). Additional intrinsic structural disorder also results from bond angle and length distribution (topological disorder). Furthermore, the degree of network connectivity, often represented by the fractions of NBO, offers insights into the viscosity and activity coefficient of SiO_2 (e.g., Giordano and Dingwell, 2003; Lee, 2011, and references therein). Previous efforts and advances to reveal the extent of disorder have often focused on relatively simple model silicate glasses. Relatively few studies have been performed to explore the structure and extent of disorder in other diverse geologically important multi-component glasses and melts, such as andesitic melts. Here, we attempt to reveal the nature of the various aspects of disorder (Si/Al ordering, preference between non-network cations and BOs and NBOs), and the degree of polymerization in five-component andesitic melts in the diopside–jadeite join.

Together with the diverse structural disorder in the glasses, the Al coordination number for silicate melts could provide insight into their macroscopic properties (Allwardt et al., 2005; Neuville et al., 2006; Toplis and Dingwell, 2004; Urbain et al., 1982). The effect of temperature, pressure, and composition on the Al coordination number in diverse model ternary and quaternary aluminosilicate glasses has been reported widely: for example, the fraction of highly coordinated Al increases with increasing quenched temperature [e.g., the $^{[5]}Al$ fraction in anorthite glasses increases with

increasing fictive temperature from 7.2% (1100 K) to 8.9% (1260 K)] (Stebbins et al., 2008) and also increases with increasing pressure (Lee, 2010; Lee et al., 2012, and references therein). The fractions of highly coordinated Al are also affected be the diverse compositional constraints, such as field strength of non-framework cations, (e.g., Allwardt et al., 2005; Florian et al., 2007; Iftekhar et al., 2011; Kelsey et al., 2009; Le Losq et al., 2014; Lee et al., 2005; Thompson and Stebbins, 2011; Thompson and Stebbins, 2012, and references therein), and NBO/T (number of non-bridging oxygens per tetrahedral network cation) (Neuville et al., 2006b; Neuville et al., 2008) [see also section 2.3 for a summary of previous NMR studies of the Al coordination number in aluminosilicate glasses]. With consideration of the available structural studies of Al coordination environments in aluminosilicate glasses, it would be necessary to pursue systematic efforts to provide an integrated view of the effect of composition on $^{[5,6]}$Al with the objective of accounting for (and predicting) the composition-induced coordination environment of Al in multi-component glasses.

In this study, we explore the coordination environments of framework cations, network connectivity, and extent of disorder (i.e., chemical and topological disorder) in multi-component model andesitic glasses in diopside–jadeite joins using multi-nuclear (^{29}Si, ^{27}Al, and ^{17}O) high-resolution solid-state NMR, which has proven effective in revealing detailed degrees of disorder in such glasses (e.g., Lee et al., 2009; Stebbins and Xu, 1997; for a recent reveiw see, Stebbins and Xue, 2014; Stebbins et al., 2001). In conjunction with previous studies of the Al coordination environment of such glasses, we also explore the effect of composition (particularly, the average cationic potential) on the fractions of highly coordinated Al in ternary and quaternary multi-component silicate glasses with the aim of

establishing a model for the prediction of the Al coordination environment in multi-component natural silicate glasses.

3.2. Experimental methods

3.2.1. Sample preparation

A series of CMNAS glasses in diopside ($CaMgSi_2O_6$)–jadeite ($NaAl_2SiO_6$) joins containing 0, 25, 50, 75, and 100 mol% $CaMgSi_2O_6$ were synthesized from carbonates (Na_2CO_3, $CaCO_3$) and oxides (MgO, Al_2O_3, and SiO_2). The Al_2O_3, $CaCO_3$, Na_2CO_3, and SiO_2 powders were dried at 300 °C for ~48 h and the MgO was dried at 1300 °C for 2 h. The weighed powders were mixed and then decarbonated in a Pt crucible at 800 °C for 1 h. The mixed powders were heated above their respective melting temperatures (1600 °C) for 1 h and then quenched into glasses by removal of the crucible from the furnace, which was then lowered manually into water (e.g., Lee and Stebbins, 1999; Mysen et al., 2003; Stebbins et al., 2008). Previous studies with similar synthesis condition showed that quench rate is ~100 °C/s (e.g., Dubinsky and Stebbins, 2006). Approximately 0.2 wt% of cobalt oxide was added to enhance the spin–lattice relaxation. Weight loss of ~1.5–1.7 wt% was observed after decarbonation. ^{17}O-enriched glasses in the diopside–jadeite join were also synthesized from carbonates ($CaCO_3$, Na_2CO_3), oxide agents, and ^{17}O-enriched SiO_2. The mixtures were melted in an Ar environment in a Pt crucible for 1 h at 1600 °C. Iron-free model phonolite glass ($CaO:MgO:Na_2O:K_2O:Al_2O_3:SiO_2:TiO_2:MnO$ =1.4:8.0:9.0:3.8:12.9:64.0: 0.7:0.2 mol%) (see (Mysen and Richet, 2005 and references therein) was synthesized from carbonates (Na_2CO_3, $CaCO_3$, K_2CO_3) and oxides (MgO, Al_2O_3, TiO_2, MnO, and SiO_2). The mixtures were melted at 1400 °C for 1 h. Table 3.1 shows the nominal compositions and chemical compositions of the CMNAS glasses

Table 3.1. Nominal compositions and ICP analyses for CaO–MgO–Na_2O–Al_2O_3–SiO_2 silicate glasses in the diopside–jadeite pseudobinary join. $X_{Diopside}$ is the mole fraction of diopside. NBO/T = $2*\{X_{(CaO+MgO+Na2O)}-X_{Al2O3}\}/[1-\{X_{(CaO+MgO+Na2O)}-X_{Al2O3}\}]$.

Composition		CMNAS mol% (nominal composition)					
		NBO/T[1)]	CaO	MgO	Na_2O	Al_2O_3	SiO_2
$X_{Diopside}$	0	0.0	0.0	0.0	16.7	16.7	66.7
	0.25	0.4	7.7	7.7	11.5	11.5	61.5
	0.50	0.8	14.3	14.3	7.1	7.1	57.1
	0.75	1.3	20.0	20.0	3.3	3.3	53.3
	1	2.0	25.0	25.0	0.0	0.0	50.0

[1)] NBO/T = $2*\{X_{(CaO+MgO+Na2O)}-X_{Al2O3}\}/[1-\{X_{(CaO+MgO+Na2O)}-X_{Al2O3}\}]$

Composition		CMNAS mol% (nominal composition)				CMNAS mol% (ICP analysis)			
		CaO	MgO	Na_2O	Al_2O_3	CaO	MgO	Na_2O	Al_2O_3
$X_{Diopside}$	0			50.0	50.0	0.0	0.0	49.2±0.4	50.8±0.4
	0.25	20.1	20.1	29.9	29.9	19.6±0.3	20.1±0.9	29.7±0.3	30.7±0.8
	0.50	33.4	33.4	16.6	16.6	32.7±0.2	34.2±0.3	16.6±0.4	16.6±0.2
	0.75	42.9	42.9	7.1	7.1	41.8±0.3	43.5±0.4	7.3±0.3	7.5±0.4
	1	50.0	50.0	0.0	0.0	50.0±0.2	49.9±0.1	0.0	0.1

*The ICP analysis was performed for CaO, MgO, Na_2O, and Al_2O_3. SiO_2 was volatilized during pretreatment of the glasses (see text for details).

determined by inductively coupled plasma atomic emission spectroscopy (ICP-AES). SiO_2 in the glasses was removed by reacting with the hydrofluoric acid for the ICP analysis, therefore, we report CaO, MgO, Na_2O, and Al_2O_3 compositions only. Considering the minor to negligible weight loss during glass synthesis and the consistency with ICP analysis for other components, the SiO_2 content and total chemical compositions of the glasses are expected to be close to the nominal compositions.

3.2.2. NMR spectroscopy

The ^{27}Al MAS and triple quantum (3Q) MAS NMR spectra of the CMNAS glasses in the diopside–jadeite join and the synthetic phonolite glasses were collected using a Varian solid-state NMR 400 system (9.4 Tesla) at a Larmor frequency of 104.23 MHz with a 3.2-mm Varian probe (Seoul National University, Korea) with spinning speed of 15 kHz. The relaxation delay for the ^{27}Al MAS NMR was 1 s, and the radio frequency (*rf*) pulse length was 0.3–0.5 μs (~ 30 degree tip angle). A fast-amplitude modulation (FAM)-based shifted-echo pulse sequence was used in the ^{27}Al 3QMAS NMR. This pulse sequence consisted of two hard pulses (3.0 and 0.6–0.8 μs, respectively) and a subsequent soft pulse (~15 μs) with ~500 μs echo time and a relaxation delay of 0.5–0.8 s. The ^{27}Al MAS and 3QMAS spectra for the synthetic phonolite glass are not shown here; however, we do report the $^{[5,6]}Al$ fractions in the glass (see section 3.4).

^{17}O MAS and 3QMAS NMR spectra of CMNAS glasses were collected on the Varian solid-state NMR 400 system (9.4 Tesla) at a Larmor frequency of 54.23 MHz, using a 4-mm Doty double-resonance probe. The relaxation delay for the ^{17}O MAS NMR was 1 s and the *rf* pulse length was 1.0 μs with a spinning speed of 14 kHz. In the ^{17}O 3QMAS NMR experiment,

a FAM-based shifted-echo pulse sequence was used. This consisted of a hard pulse with duration of 4.5 μs for multiple-quantum excitation, two 1.1-μs pulses for single-quantum reconversion, and a soft pulse of approximately 20-μs duration. The spectra of ^{17}O 3QMAS were referenced to external tap water. The *rf* field strengths of the hard pulses for the ^{27}Al 3QMAS and ^{17}O 3QMAS NMR were approximately 125 and 77 kHz, respectively. While the lowest contour lines of the usual 2D NMR spectra have been often ~7 to 10 % in other previous studies (e.g., Lee and Stebbins, 2000), the level of the contour line for the 2D ^{27}Al 3QMAS NMR spectra presented here is as low as 2%, and that for the ^{17}O 3QMAS NMR spectra of the CMNAS glasses in the diopside–jadeite join is as low as 2.5%. To achieve current signal-to-noise ratio in the 2D ^{17}O 3QMAS NMR spectra, approximately 3~4 days of collection time for each spectrum was required. The ^{29}Si MAS NMR spectra were collected at 9.4 Tesla (79.495 MHz), with a recycle delay of 3 s, pulse length of 1.6 μs, and spinning speed of 12 kHz. The ^{29}Si NMR spectra were referenced to an external tetramethylsilane solution.

3.2.3. Previous studies on the fraction of highly coordinated Al in aluminosilicate glasses using high-resolution solid-state NMR

High-resolution solid-state ^{27}Al NMR has been used to yield unambiguous information on Al coordination environment in simple and complex multi-component glasses. Here, we summarize previous high-resolution ^{27}Al NMR studies to reveal the fractions of highly coordinated Al ($^{[5,6]}$Al) in these aluminosilicate glasses (Allwardt et al., 2005; Florian et al., 2007; Iftekhar et al., 2011; Kelsey et al., 2009; Lee, 2010a; Lee et al., 2005; Lee et al., 2012a; Lee et al., 2012b; Malfait et al., 2012; Neuville et al., 2006; Neuville et al., 2008; Stebbins et al., 2008; Thompson and Stebbins, 2011;

Thompson and Stebbins, 2012). The fraction of $^{[5,6]}$Al changes with temperature, pressure, and composition (including the cation field strength of non-network cations, Si/Al ratio, and NBO/T). The $^{[5,6]}$Al fraction slightly increases with increasing glass transition temperature (T_g): the proportion of $^{[5,6]}$Al in fast-quenched glass (higher T_g) is higher than in slow-quenched (lower T_g) aluminosilicate glass (the difference of $^{[5,6]}$Al fraction is from ~0.9% to ~1.7%) (Stebbins et al., 2008). Previous ^{27}Al NMR studies have reported that highly coordinated Al in the aluminosilicate glasses increases with increasing pressure with complex composition dependence (Allwardt et al., 2005a; Allwardt et al., 2005b; Kelsey et al., 2009; Lee, 2004, 2010; Lee et al., 2004; Lee et al., 2012a; Lee et al., 2012b; Yarger et al., 1995). It decreases from ~3.5% to ~1.5%with an increasing Si/Al ratio in Ba-aluminosilicate [(1-X)BaO-(X)Al_2O_3-(0.3)SiO_2, X=0.30, 0.32, 0.35, 0.38] (Thompson and Stebbins, 2012). It has also been well-known that changes in the metal oxide/Al_2O_3 ratio from peralkaline ($M^{n+}O_{n/2}/Al_2O_3$ >1) to peraluminous ($M^{n+}O_{n/2}/Al_2O_3$ <1) composition strongly affect the $^{[5,6]}$Al fraction; the proportion of $^{[5,6]}$Al increases from with decreasing MgO/(MgO+Al_2O_3) and it somewhat increases with decreasing silica content (Neuville et al., 2008; Toplis et al., 2000). The highly coordinated Al in Ca-aluminosilicate glasses [(1-X)CaO-(X)Al_2O_3-(0.5)SiO_2, X=0.25, 0.30, 0.35, 0.40)] also increases from 7% to ~29% with an increasing Al_2O_3/CaO ratio at a constant silica content (Neuville et al., 2006). However, in peralkaline ternary aluminosilicate glasses, it apparently decreases with increasing NBO/T (Neuville et al., 2006; Neuville et al., 2008; Toplis et al., 2000). Additionally, as for more complex, geologically important aluminosilicate glasses, the proportion of $^{[5]}$Al in the glasses in the diopside-Ca-tschermakite join increases from 0% to ~3% with an increasing mole fraction of diopside (Park and Lee, 2012), and ~ 3% of

$^{[5]}$Al is observed for $Di_{64}An_{36}$ glass (Xue and Kanzaki, 2008). Furthermore, the presence of less than 2% highly coordinated Al has been reported in complex rhyolitic and andesitic glasses (Malfait et al., 2012). Note that the detailed discussion on the effect of composition on the quantitative fractions of $^{[5,6]}$Al is provided in the section 3.4 (See Figures 3.1, 3.2, 3.9, 3.11, 3.12, and 13). Because information on the fraction of $^{[5,6]}$Al as a function of composition in silicate glasses and melts has been reported and the trends are provided, further systematic efforts to provide an integrated view of the effect of composition on $^{[5,6]}$Al is necessary. In this study, we explore the relationships among the fractions of $^{[5,6]}$Al and various compositional parameters. Particularly, we introduce the average cationic potential as a descriptor of the fraction of highly coordinated Al in silicate glasses (see section 3.4).

As we pursue to explore the diverse degree of disorder in silicate glasses, we note that there are several ways to define the nature of disorder (Lee, 2005; Richet and Bottinga, 1986 and references therein): particularly, a recent study used geometric (due to bond angle and bond length distribution), topological (due to ring structures, building units, and coordination sequences distribution), and chemical disorder (due to atomic substitutions and compositional variability) to describe the degree of disorder in the oxide glasses (Massiot et al., 2013). The topological disorder in the current study may include both topological and geometrical disorder, accounting for the variation of bond angle and length distribution and network distortion. The configurational disorder refers the disorder resulting from the diversity in distribution of coordinated species. Note that these two are somewhat interdependent.

3.3. Results and discussion

3.3.1. Al coordination environments in model andesitic glasses in the diopside–jadeite join: ^{27}Al MAS and 3QMAS NMR results

Figure 3.1 shows the ^{27}Al MAS NMR spectra for CMNAS silicate glasses in the diopside–jadeite join. The $^{[4]}$Al peak at ~53.0 ± 1.0 ppm is dominant in all the glasses studied here. Only $^{[4]}$Al is observed in jadeite glass, consistent with a previous NMR study (Lee and Stebbins, 2000). The shape of the spectrum is also characterized by long tails extending to lower frequencies (i.e., smaller chemical shift ranges). This trend results from distributions of the quadrupolar coupling constant (C_q) and the isotropic chemical shift (δ_{iso}^{CS}) of Al environments in the glasses, indicating extensive structural disorder in the glasses. The peak widths (full-width at half-maximum, FWHM) of the ^{27}Al MAS NMR spectra for the CMNAS glasses increase systematically with increasing mole fractions of diopside ($X_{Diopside}$) from ~23.0 ± 1.5 ppm for $X_{Diopside}$ = 0 to ~34.5 ± 1.5 ppm for $X_{Diopside}$ = 0.75. The result suggests that the degree of distortion around the Al (e.g., change of bond angle and bond distance) and/or configurational disorder may increase with the diopside component of the glasses. We note that previous 1D ^{27}Al MAS NMR results for glasses in the diopside–jadeite join containing P_2O_5 and CaF_2 indicate that all of the Al is present as $^{[4]}$Al (Abo-Mosallam et al., 2010).

Figure 3.2A shows the 2D ^{27}Al 3QMAS NMR spectra (with much improved site resolution than the 1D MAS) for CMNAS silicate glasses with varying $X_{Diopside}$. While only $^{[4]}$Al is observed in the glasses in the diopside–jadeite join up to $X_{Diopside}$ = 0.5, consistent with the 1D NMR results, a minor but detectable amount of $^{[5]}$Al is also observed for the glass at $X_{Diopside}$ = 0.75

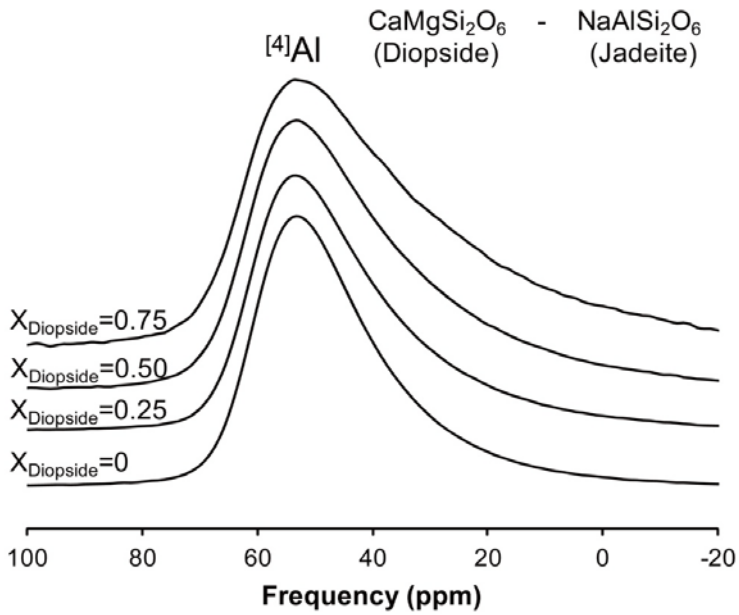

Figure 3.1. ^{27}Al MAS NMR spectra for CaO–MgO–Na_2O–Al_2O_3–SiO_2 glasses in the diopside–jadeite join at 9.4 T with varying mole fractions of diopside ($X_{Diopside}$).

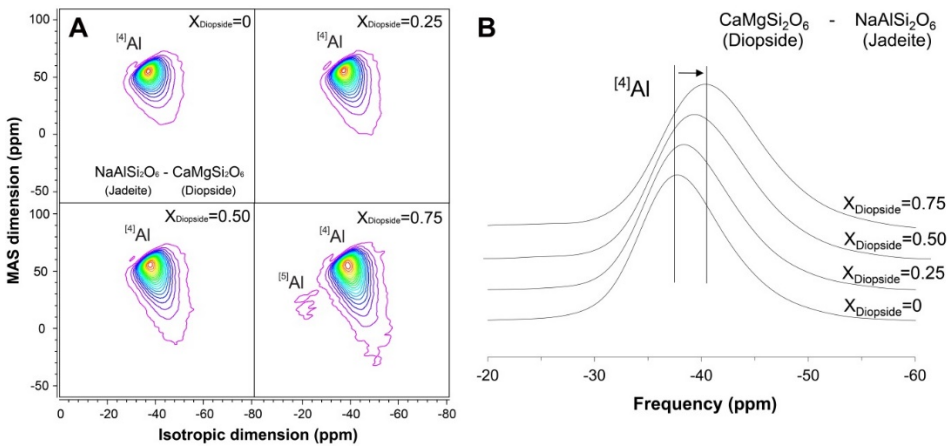

Figure 3.2. (A) ^{27}Al 3QMAS NMR spectra for CaO–MgO–Na_2O–Al_2O_3–SiO_2 glasses in the diopside–jadeite join at 9.4 T with varying mole fractions of diopside ($X_{Diopside}$).Contour lines are drawn at 5% intervals from relative intensities of 12% to 97% with added lines at 2%, 4%, 6%, and 8%. The total NMR collection time for single spectrum is approximately 16~18 h. (B) Total isotropic projection of ^{27}Al 3QMAS NMR spectra for CaO–MgO–Na_2O–Al_2O–SiO_2 glasses in the diopside–jadeite join at 9.4 T. $X_{Diopside}$ is the mole fraction of diopside.

(~–22 ± 1.5 ppm in the isotropic dimension), indicating an increase in the topological and configurational disorder in the glasses with increasing $X_{Diopside}$. The measured peak width (FWHM) of $^{[4]}$Al in the MAS dimension of the 2D spectra increases from 20.7 ± 1.5 ppm ($X_{Diopside}$ = 0) to 22.6 ± 1.5 ppm ($X_{Diopside}$ = 0.75). The peak width in the MAS dimension is directly proportional to the magnitudes of the quadrupolar interactions. Additionally chemical shift distribution in each Al site can also partly contribute to the peak width. Because Al is a quadrupolar nuclide (with a spin-quantum number, $I > 1/2$), non-spherical nuclear charge is interacting with the electric field gradient around Al nuclide. The magnitude of the quadrupolar interactions is parameterized with quadrupolar coupling constant, C_q. This interaction is a measure of the degree of distortion and thus a deviation from perfect cubic symmetry around the Al environments (Baltisberger et al., 1996; Ghose and Tsang, 1973). The deviation from perfect tetrahedral symmetry is relevant to the distortion of $^{[4]}$Al in the silicate glasses. Thus the observed trend of increase in average C_q suggests that the degree of network distortion around the Al (and thus, Q^n species) increase with increasing $X_{Diopside}$ (see Figure 3.3 below for further discussion).

Figure 3.2B shows the total isotropic projections (sum of the spectrum into the isotropic dimension) of the ^{27}Al 3QMAS NMR spectra for CMNAS glasses in the diopside–jadeite join with varying $X_{Diopside}$. The peak maximum of $^{[4]}$Al in the glass shifts from –37.5 ± 1.5 ppm ($X_{Diopside}$ = 0) to –40.3 ± 1.5 ppm ($X_{Diopside}$ = 0.75) in the isotropic dimension. The change of peak maximum suggests a change of Q^4_{Al}(nSi) species [fully polymerized $^{[4]}$Al species with n number of Si as next nearest neighbors; it is often labeled as q^4(nSi)] as Al in the glasses is expected to be fully polymerized forming only Q^4 species (Allwardt et al., 2003). While Q^4_{Al}(nSi) species is dominant in

glasses in anhydrous diopside-jadeite join, previous study shows the evidence for the presence of the depolymerized Q^3_{Al}(nSi) species in Na-aluminosilicate with H_2O (Zeng et al., 2000).

Based on the known relationship between peak position of Q^4(nSi) species with increasing n, the observed changes in the peak position indicates the change of Q^4_{Al}(nSi) species with increasing $X_{Diopside}$ (Lee and Stebbins, 2000). Additionally, the changes could also be due to the presence of cations with higher field strength (e.g., Ca^{2+} and Mg^{2+}): with increasing cation filed strength of non-network forming cations, the peak position in the isotropic dimension moves to more negative shift (Lee and Stebbins, 2000). The estimated peak width (FWHM) for $^{[4]}$Al in the isotropic projection slightly increases from ~9.5 ± 1.5 ppm ($X_{Diopside}$ = 0) to ~11.4 ± 1.5 ppm ($X_{Diopside}$ = 0.75) with increasing $X_{Diopside}$. This result again confirms that the configurational disorder in the glasses increases with increasing $X_{Diopside}$. The relationships among peak position in the 3QMAS in MAS dimensions, and the δ_{iso}^{CS} as well as the second-order quadrupolar shift were shown in appendix.

Figure 3.3 shows the effects of composition on the structurally relevant C_q [= $P_q/(1 + \eta^2/3)^{1/2}$, where P_q and η are the quadrupolar coupling product and the asymmetry parameter, respectively] of $^{[4]}$Al in the CMNAS glasses. Here, P_q was obtained from the center of gravity of the $^{[4]}$Al peak in the ^{27}Al 3QMAS NMR spectra and the asymmetry parameter (η) is assumed to be 0.5 (see appendix): note that the change in η does not lead to noticeable changes in the calculated C_q (Park and Lee, 2012). The C_q of $^{[4]}$Al in the glasses increases slightly with increasing $X_{Diopside}$ from 4.7 ± 0.4 MHz ($X_{Diopside}$ = 0) to 5.3 ± 0.4 MHz ($X_{Diopside}$ = 0.75). Larger C_q indicates a larger deviation from

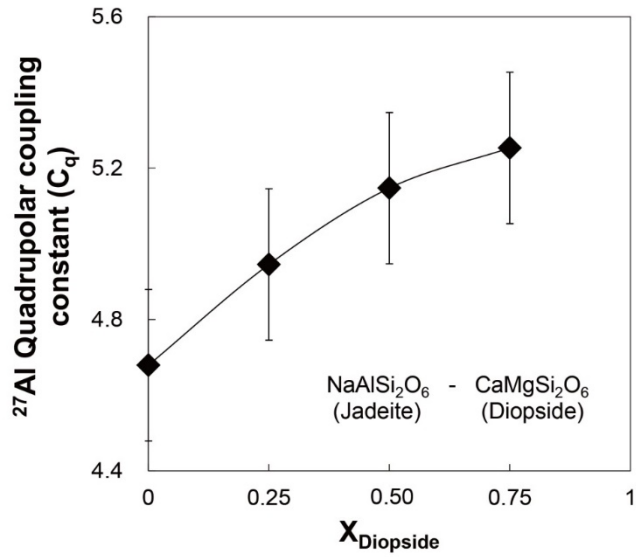

Figure 3.3. Quadrupolar coupling constant (C_q) of [4]Al in CaO–MgO–Na_2O–Al_2O_3–SiO_2 glasses in the diopside–jadeite pseudobinary join with varying $X_{Diopside}$. The asymmetry parameter is assumed to be 0.5. The estimated error bar of ±0.4 MHz for [4]Al was determined based on the uncertainty in the position of the center of gravity of each peak.

the perfect cubic symmetry around Al, which can result from Al–O bond length (as well as bond angle) distribution. The term topological disorder in the current manuscript thus also refers to the degree of deviation from perfect tetrahedral symmetry. The current results indeed indicate that the degree of overall topological disorder around $^{[4]}$Al increases with increasing $X_{Diopside}$ in the diopside–jadeite join. As the Q species in the glasses varies with composition, the observed variation in average C_q of Al sites in the glasses is likely to be affected by the variation in Q^4_{Al}(nSi) species and each Q species have distinct C_q values (see Lee and Stebbins, 2000 and references therein). The degree of distortion of each Q^4_{Al}(nSi) species may also change with Ca^{2+} and Mg^{2+} (those increases with increasing $X_{Diopside}$): presence of higher field strength cations leads to the larger network distortion, contributing to an increase in the average C_q value with increasing $X_{Diopside}$ (Lee and Stebbins, 2006, 2009; Park and Lee, 2012).

The current ^{27}Al NMR results with observed trends for the model andesitic glasses are somewhat different from previous results for the model basaltic glasses in the diopside-Ca-tschermakite join (Park and Lee, 2012). Whereas the predominant Al species is $^{[4]}$Al in both compositional joins, the fraction of $^{[5]}$Al is somewhat larger in the glasses in the model basaltic glasses, potentially due to the abundance in high field strength cations in the latter. Additionally, the peak maximum of the isotropic projection decreases in the diopside–jadeite join with increasing $X_{Diopside}$, whereas it increases in the diopside–Ca–tschermakite join. This difference is mostly due to the difference in peak maximum of $^{[4]}$Al in the isotropic projection of end members [i.e., jadeite glass (–37.5 ± 1.5 ppm) and Ca–tschermakite (–46 ± 1.5 ppm)]. This difference in chemical shift is because the Si/Al ratio of jadeite (2) is higher than that of Ca–tschermakite (0.5), resulting in noticeable

difference in Q^4_{Al}(nSi) species distribution between these endmembers. The fractions of ~84% of Q^4_{Al}(4Si), ~15% of Q^4_{Al}(3Si), and ~1% of Q^4_{Al}(2Si) can be predicted in the jadeite glass (Si/Al = 2) based on a moderate degree of Al avoidance (Q of ~0.95), whereas fractions of ~4% of Q^4_{Al}(4Si), ~20% of Q^4_{Al}(3Si), ~36% of Q^4_{Al}(2Si), ~30% of Q^4_{Al}(1Si), and ~9% of Q^4_{Al}(0Si) are expected in the Ca-tschermakite glass (Si/Al = 0.5), based on the larger degree of Al avoidance (Q of ~0.85) (Lee and Stebbins, 1999). Finally, whereas the C_q of $^{[4]}$Al in the glasses in the diopside–jadeite join increases, that of the diopside–Ca–tschermakite join decreases with increasing $X_{Diopside}$ (Park and Lee, 2012). The difference in trend of C_q is again derived from the difference value of C_q for each end member [i.e., jadeite (~4.7 MHz) and Ca-tschermakite (~6.6 MHz)] and thus, their structural differences associated with the Q^4_{Al}(nSi) distribution and its effect on the network distortion around the Al.

3.3.2. Probing the extent of network connectivity and configurational disorder in the model andesitic glasses and melts in the diopside–jadeite joins ^{17}O MAS and 3QMAS NMR results.

Figure 3.4 shows the ^{17}O MAS NMR spectra for the CMNAS glasses in the diopside–jadeite join. The ^{17}O MAS NMR spectrum of jadeite glasses shows a broad peak that results from overlapping BOs, mostly, Si-O-Al and Si-O-Si. That of diopside glass shows partially resolved Si-O-Si and {Ca, Mg}-NBO (i.e., {Ca, Mg}-O-Si) as labeled. Both the peak shape and width for each BO and NBO site in the intermediate composition change with increasing $X_{Diopside}$. In particular, the {Ca, Mg}–O–Si peak intensity increases systemically with increasing $X_{Diopside}$, indicating that the degree of polymerization (BO fraction) decreases. The overlapped peaks due to the

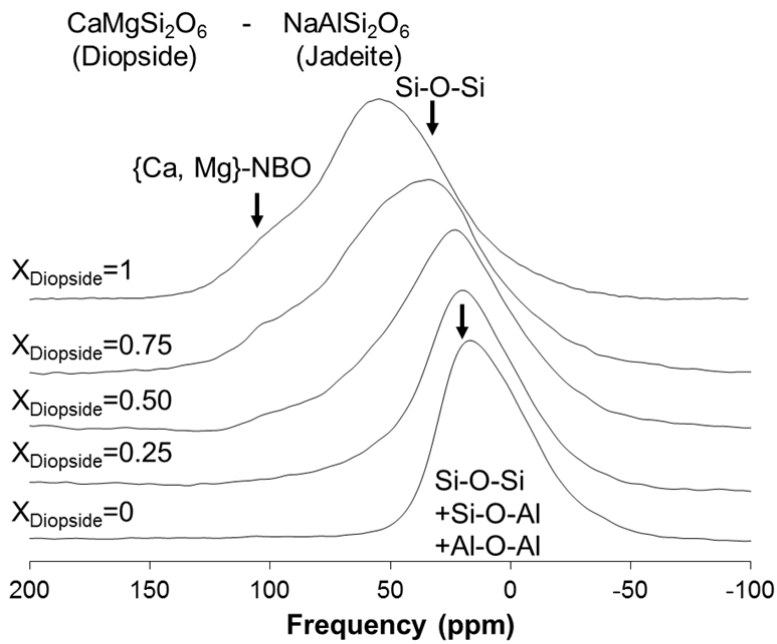

Figure 3.4. ^{17}O MAS NMR spectra for $CaO–MgO–Na_2O–Al_2O_3–SiO_2$ glasses in the diopside–jadeite join at 9.4 T with varying mole fractions of diopside ($X_{Diopside}$).

NBO and BO sites are not fully resolved in the 1D MAS NMR spectra, but better resolution can be achieved by use of ^{17}O 3QMAS NMR.

Figure 3.5 shows the 2D ^{17}O 3QMAS NMR spectra for CMNAS glasses in the diopside–jadeite join with varying $X_{Diopside}$, showing much enhanced resolution among the oxygen peaks compared with the ^{17}O MAS NMR spectra (Figure 3.4). The BOs (Si–O–Si, Al–O–Si, and Al–O–Al) are fully (for jadeite composition) and/or partially resolved (for other glasses in the join). The peaks of the NBOs are not fully resolved yet the peaks due to {Ca, Mg}–O–Si and Ca-O-Si can be seen as labeled; the oxygen clusters from 120 to 0 ppm in the MAS dimension stem from the different types of NBOs such as {Ca, Mg}–O–Si and Ca-O-Si (with peak maximum at ~ 100 ppm). Note that the peak assignments of BOs and NBOs in the ^{17}O NMR spectra are based on previous studies of diverse crystalline and non-crystalline aluminosilicate glasses (e.g., Allwardt et al., 2003; Allwardt and Stebbins, 2004; Dirken et al., 1997; Lee, 2010; Lee et al., 2005; Pingel et al., 1998; Stebbins et al., 2001; Stebbins and Xu, 1997; Stebbins et al., 2001; Van Eck et al., 1999, and references therein). The ^{17}O 3QMAS NMR spectrum of jadeite glasses shows fully resolved Si-O-Al and Si-O-Si. It also shows a non-negligible fraction of Al–O–Al species, indicating a violation of the Al-avoidance rule in the jadeite glass. As expected from the composition, the intensity of Si–O–Al decreases with increasing $X_{Diopside}$. The intensity of Si-O–Si and the mixed NBOs increases with increasing $X_{Diopside}$ up to the end member diopside glass. The presence of an Al–O–Al peak cannot be seen in the other glass compositions except the jadeite glass, partly due to low Al/Si ratio with increasing $X_{Diopside}$.

Figure 3.6 shows the total isotropic projection (sum of the spectral intensity into the isotropic dimension) of the 2D ^{17}O 3QMAS NMR spectra

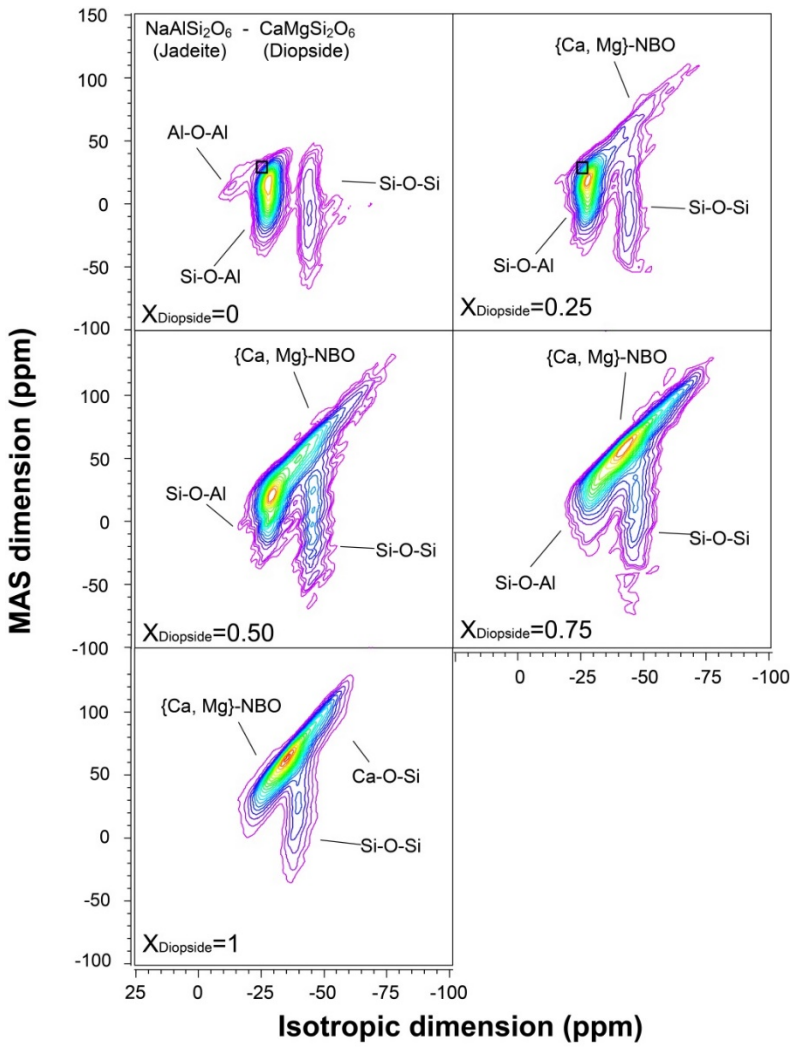

Figure 3.5. ^{17}O 3QMAS NMR spectra for CaO–MgO–Na_2O–Al_2O_3–SiO_2 glasses in the diopside–jadeite join at 9.4 T with varying mole fractions of diopside ($X_{Diopside}$). Contour lines are drawn at 5% intervals from relative intensities of 7% to 92% with added lines at 2.5% and 5%. The total NMR collection time for single spectrum is approximately 3~4 days.

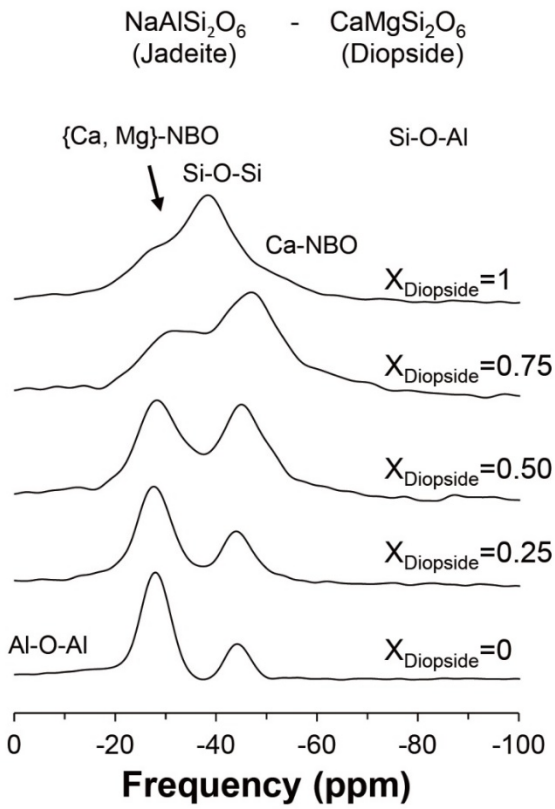

Figure 3.6. Total isotropic projection of ^{17}O 3QMAS NMR spectra for CaO–MgO–Na_2O–Al_2O_3–SiO_2 glasses in the diopside–jadeite join at 9.4 T with varying mole fractions of diopside ($X_{Diopside}$).

for CMNAS glasses in the diopside–jadeite join. Again, a minor fraction of Al-O-Al, and dominant Si–O–Al and Si–O–Si peaks are clearly resolved in the jadeite glass, whereas these peaks are overlapped with the mixed NBO peaks with increasing $X_{Diopside}$. We did not attempt to quantify the fraction of BO and NBO peaks due to the overlap among the peaks in the intermediate composition glasses; while quantitative fractions of these oxygen clusters have been reported for a few quaternary aluminosilicate glasses with relatively small concentration of high field strength cations (Lee, 2011; Lee and Sung, 2008), considerable overlaps among BO and NBO peaks make it difficult to yield quantitative analysis of NBO/BO fractions. Nevertheless, the spectra qualitatively shows that the fraction of NBOs and Si–O–Si apparently increases with increasing $X_{Diopside}$ (increasing network modifying cations such as Mg^{2+}), whereas the Si–O–Al peak intensity decreases.

3.3.3. Preferential partitioning between NBO and non-network cations and the degree of Si/Al disorder.

These ^{17}O NMR results can also help constrain the role of non-framework cations in the glasses, for example, the NBO/T is 0.4 and the X_{NBO} is 0.17 (~16.7%, predicted from the composition, see table caption 1) in the glasses in the diopside-jadeite join at $X_{Diopside}$ = 0.25. In this composition, among the non-framework cations, Na^+ is 75% and Ca^{2+} +Mg^{2+} are 25%. Although Na^+ is the most dominant non-framework cation, the Na–O–Si peak (~-20 ppm in isotropic dimension, see Figure 3.5, open square) is not observed: Na-O-Si peak position is well-defined in the 2D NMR spectra and it does not have strong composition dependence (Lee et al., 2003; Lee and Stebbins, 2003). Additionally Na-O-Si and Si-O-Al peaks are relatively well-resolved in ^{17}O 3QMAS NMR spectrum (Lee and Stebbins, 2009). If more

than 2-3 % of Na-O-Si would exist in jadeite glass, Na-O-Si peak could have been observed. Currently ^{17}O 3QMAS NMR spectra for the glasses do not show any evidence for Na-O-Si.

Nevertheless, a few % of Na-O-Si in diopside-jadeite join, if exist, due to overlaps with Si-O-Al and extremely broad {Ca, Mg}-NBO, may not be detected. The ^{17}O 3QMAS NMR spectrum at $X_{Diopside}$ = 0.25 shows very clear presence of {Ca, Mg}–O–Si peak (Figure 3.5), indicating the strong preference of NBO for Ca^{2+} and Mg^{2+}. These results suggest that Na^{+} plays a preferential role as a charge-balancing cation, whereas Ca^{2+} and Mg^{2+} can act as a network-modifying cation, forming NBOs. The observed non-randomness in the partitioning of those cations (Ca^{2+}, Mg^{2+}, and Na^{+}) into BOs and NBOs can be due to the differences in their field strengths (Maekawa et al., 1991; Mysen, 1988; Mysen et al., 1982); higher field strength cations {e.g., Ca^{2+}, Mg^{2+}} in the glasses studied here are expected to be preferentially partitioned into NBOs, whereas Na^{+} would be expected to have proximity to BOs (e.g., Si-O-Al).

While the NBO preference between Na^{+} and {Ca^{2+}, Mg^{2+}} is clearly demonstrated in the current ^{17}O NMR study, it is not a straightforward matter to probe the preference between Ca^{2+} and Mg^{2+} because of the peak overlap between Ca–O–Si, Mg–O–Si, and {Ca, Mg}–O–Si. Nevertheless, the peak of Ca–O-Si (intensity at ~ 100 ppm in the MAS dimension and ~-64 ppm in the isotropic dimension) is observed at $X_{Diopside}$ = 0.25, indicating the unexpected stability of Ca–O–Si. Similar features with Ca–O–Si have been observed in the glasses in the diopside–Ca–tschermakite join that have been attributed to preferential affinity between Ca^{2+} and the NBOs (over Mg^{2+}) and/or potential clustering of Ca^{2+} and Mg^{2+} around NBOs (Park and Lee, 2012). As Na^{+} plays a preferential role as a charge-balancing cation in

diopside-jadeite glass, Ca^{2+} and Mg^{2+} are primarily network modifying cations, forming NBO. The hypothetical NBO distribution was calculated assuming a random distribution of Ca^{2+} and Mg^{2+} around NBOs with varying $X_{Diopisde}$ (all the glasses have identical Ca/Mg ratio of 1). The random distribution model of Ca^{2+} and Mg^{2+} around NBOs leads to the formation of ^{3}Ca–NBO (i.e., Ca-O-Si, ~-67 ppm in isotropic dimension), ^{2}Ca^{1}Mg–NBO (~-56 ppm), ^{1}Ca^{2}Mg–NBO (~-46 ppm), and ^{3}Mg–NBO (~-36 ppm) (Allwardt and Stebbins, 2004). The predicted NBO fractions at a fixed Ca/(Ca + Mg) ratio are 12.5% (^{3}Ca–NBO), 37.5% (^{2}Ca^{1}Mg–NBO), 37.5% (^{1}Ca^{2}Mg–NBO), and 12.5% (^{3}Mg–NBO), respectively (Kelsey et al., 2008). While the predicted fraction of Ca-O-Si is only 12.5% in diopside-jadeite join with varying $X_{Diopside}$, the intensity of the feature at ~-64 ppm (i.e., Ca-O-Si) remains apparently prevalent regardless of composition. Though qualitative, the result indicates that the observed Ca-O-Si in glasses is likely to be higher (qualitatively) than the expected Ca–NBO based on the random distribution model. Currently due to peak overlap, it is not possible to deduce the origin of the unexpected presence of Ca-O-Si in the glasses quantitatively. Nevertheless, the observed trends in the model andesitic glasses also show that Ca^{2+} and Mg^{2+} in the network both deviate from a random-distribution.

The preferential partitioning of Na^{+}, Ca^{2+}, and Mg^{2+} between NBOs (Na–O–Si and {Ca, Mg}–O–Si) and BOs with charge-balancing cations (i.e., Na---Al–O–Al, {Ca, Mg}---Al–O–Si) in glasses can be described using the following quasi-chemical equations:

Na---Al–O–Si + {Ca, Mg}–O–Si = {Ca, Mg}---Al–O–Si + Na–O–Si (1)

Na---Al–O–Al + {Ca, Mg}–O–Si = {Ca, Mg}---Al–O–Al + Na–O–Si (2)

Na---Si–O–Si + {Ca, Mg}–O–Si = {Ca, Mg}---Si–O–Si + Na–O–Si (3)

In the glasses in the diopside–jadeite join, the current results demonstrate that the formation of Na---Al(Si)–O–Si(Al) and {Ca, Mg}–O–Si species {Ca, Mg}---Al(Si)–O–Si(Al) and Na–O–Si is favored: the result indicates Na^+ may have spatial proximity toward BOs (Si-O-Si, Al-O-Al, Si-O-Al) and Ca^{2+} and Mg^{2+} are used to form NBOs.

The peak width of each BO and NBO species in the isotropic dimension of the 3QMAS NMR spectra also provides complementary information of the configurational disorder in the glasses. For example, the peak width of the BOs in the 2D NMR spectra and their isotropic projections is much narrower than for the NBOs because the chemical dispersion of the BOs is less than that of the NBOs. This indicates that the BOs have weaker interaction with the non-framework cations and thus, that their environments are less sensitive to changes in the types of network as also shown in the previous ^{17}O NMR studies of other silicate glasses with simpler composition (Lee et al., 2005; Lee and Stebbins, 2009; Lee and Sung, 2008). Additionally, the peak width and shape of Si–O–Al change with Ca^{2+} and Na^+ contents; the peak width for Na---(Si–O–Al) in the isotropic dimension is much narrower than for Ca---(Si–O–Al) not to mention the mixed {Ca, Mg}–Si–O–Al (Figure 3.5). The Si–O–Al peak width (though it overlaps other BOs and NBO peaks) apparently increases only slightly from pure jadeite glasses to $X_{Diopside}$ = 0.5. However, that with $X_{Diopside}$ = 0.75 (having more Ca and Mg around Si–O–Al) is much larger. The trend confirms that Na^+ plays a preferential role as a charge-balancing cation around Si–O–Al, even with relatively high Ca–Mg contents of the glasses with $X_{Diopside}$ = 0.5, suggesting that BOs have proximity to Na^+ over Ca^{2+} and Mg^{2+}.

Qualitatively, the fraction of each BO and NBO structural environment changes with $X_{Diopside}$. The fraction of Al–O–Al decreases with

increasing R (Si/Al ratio) in the charge-balanced $NaAlSi_RO_{2+2R}$ glasses (Lee and Stebbins, 2000). It is noted that a small, but non-negligible fraction of Al–O–Al is observed at approximately –10 ppm in the 2D ^{17}O NMR spectrum of the jadeite glass (i.e., R = 2). The presence of Al–O–Al in the glasses again confirms that the distributions of $^{[4]}Si$ and $^{[4]}Al$ in the jadeite melts deviate from the complete Al-avoidance rule. The fraction of Al–O–Al decreases with increasing $X_{Diopside}$ (as the Si/Al ratio increases) and it is below the detection limit (~ 1%) when $X_{Diopside}$ = 0.25.

3.3.4. Si environment in the multi-component aluminosilicate glasses in the diopside–jadeite join: ^{29}Si MAS NMR results

Figure 3.7 shows the ^{29}Si MAS NMR spectra for CMNAS silicate glasses in the diopside–jadeite join, from which a single broad peak due to $^{[4]}Si$ can be seen. The peak maximum increases with $X_{Diopside}$ from –93.4 ± 1.5 ppm for $X_{Diopside}$ = 0 to –81.7 ± 1.5 ppm for $X_{Diopside}$ = 1, variations in the fractions of the $Q^n(m\text{Al})$ species (Si species with zero through m Al next-nearest neighbors with n bridging oxygens) (Kirkpatrick et al., 1986). The observed trends indicate increases of Q^2 and Q^3 with increasing NBOs ($X_{Diopside}$) in the join. Figure 3.8 shows the peak widths (FWHM) and center of gravity of the ^{29}Si MAS NMR spectra for CMNAS glasses in the diopside–jadeite join (red squares). Those for CMAS glasses in the diopside–Ca-tschermakite join are also shown for comparison (closed diamonds) (Kirkpatrick et al., 1986; Park and Lee, 2012). The FWHM of the CMNAS glasses increases from 18.0 ± 1.5 ppm for $X_{Diopside}$ = 0 to 20.6 ± 1.5 ppm for $X_{Diopside}$ = 0.50, and then it decreases to 18.0 ± 1.5 ppm for $X_{Diopside}$ = 1. As the FWHM in these glasses corresponds to the degree of configurational

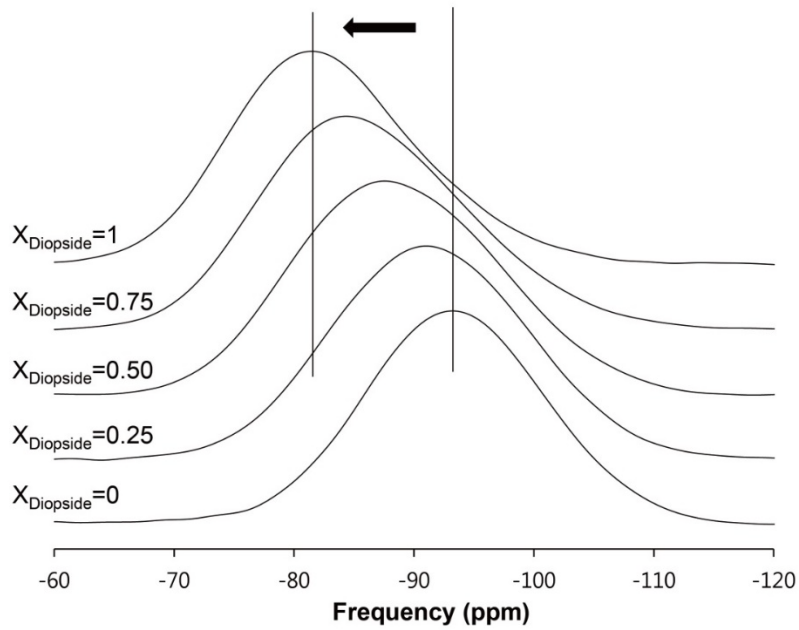

Figure 3.7. ^{29}Si MAS NMR spectra for CaO–MgO–Na_2O–Al_2O_3–SiO_2 glasses in the diopside–jadeite join at 9.4 T with varying mole fractions of diopside ($X_{Diopside}$).

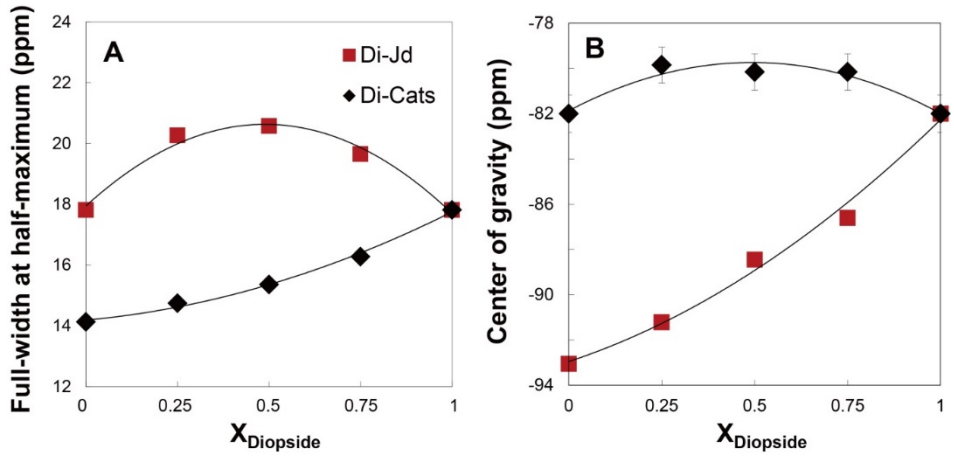

Figure 3.8. Peak widths (FWHM) of $^{[4]}$Si in ^{29}Si MAS NMR spectra for CaO–MgO–Na_2O–Al_2O_3–SiO_2 glasses in the diopside–jadeite pseudobinary join and CaO–MgO–Al_2O_3–SiO_2 glasses in the diopside–Ca–tschermakite pseudobinary join at 9.4 T. $X_{Diopside}$ is the mole fraction of diopside. Error bar of ±0.5 ppm was estimated from the uncertainty in the sample composition, phasing of the NMR spectrum, and the NMR processing conditions. Center of gravity of ^{29}Si MAS NMR spectra for CaO–MgO–Na_2O–Al_2O_3–SiO_2 glasses in the diopside–jadeite pseudobinary join and CaO–MgO–Al_2O_3–SiO_2 glasses in the diopside–Ca–tschermakite pseudobinary join at 9.4 T. $X_{Diopside}$ is the mole fraction of diopside.

disorder around the Si atoms, the results show that that the degree of disorder around $^{[4]}$Si in the intermediate composition glass is higher than those of endmembers. An apparent difference in the trend of peak width between the previous study on a diopside–Ca–tschermakite join and the current study can also be observed. That of the former (CMAS glasses) decreases from 18.0 ± 1.5 ppm for diopside glass to 14.0 ± 1.5 ppm for X_{Diopside} = 0. The centers of gravity for $^{[4]}$Si in the ^{29}Si MAS NMR spectra for glasses in the diopside–jadeite join and those in the diopside–Ca–tschermakite are also shown–. The center of gravity of the glasses in the diopside–jadeite join increases from –93.1 ± 1.5 ppm to –82.0 ± 1.5 ppm with increasing X_{Diopside}.

The observed difference in those trends between the two systems can be explained by differences of the atomic structure around Si (Q^n species) of each end member (i.e., jadeite, Ca–tschermakite) and their mixing for the intermediate composition glasses. While both end members are charge-balanced glasses with primarily Q^4(mAl) species, the fractions of ~60% of Q^4(4Al), ~35% of Q^4(3Al), and ~5% of Q^4(2Al) can be predicted in the Ca–tschermakite glass based on a moderate degree of Al avoidance (Q of ~0.85). Here, we note that there could be ~10% of Q^3 species as expected from the presence of ~ 4~5% NBO in Ca-tschermakite glass [i.e., $2*Q^2+Q^3=4*X_{NBO}/(2-X_{NBO})$] (Lee and Stebbins, 2002a; Stebbins and Xu, 1997). Whereas fractions of ~6% of Q^4(4Al), ~25% of Q^4(3Al), ~38% of Q^4(2Al), ~25% of Q^4(1Al), and ~6% of Q^4(0Al) are expected in the jadeite glass (Si/Al = 2), based on the larger degree of Al avoidance (Q of ~0.95) expected for Na–aluminosilicate glasses (Lee and Stebbins, 1999). The peak position is expected to change from ~80 ppm [for Q^4(4Al)] to ~110 ppm [for Q^4(0Al)] for both Ca- and Na aluminosilicate glasses (Lee and Stebbins, 1999). These differences in Q

species distribution lead to changes in the observed variations in peak widths and positions.

3.3.5. Effects of average cationic potential on Al coordination environments in multi-component aluminosilicate glasses

The observed changes in the Al coordination environments in the glasses with varying composition (Figure 3.2) are compared with previous studies showing the effect of composition on the Al coordination environments. As has been discussed (see section 2.3), the fractions of highly coordinated Al in ternary aluminosilicate glasses at 1 atm are heavily dependent on the cationic potential (here, defined as c/r, where c and r are the charge and ionic radius of the cation) of non-framework cations. While we use cationic potential to provide quantitative relationship between Al coordination number and composition, the similar trend is also expected to be valid with the cation field strength (i.e., c/r^2). In order to quantify this effect in the more complex multi-component silicate glasses, we use the average cationic potential $\langle c/r \rangle_{ave}$ of the non-network cations as a parameter to control the population of $^{[5,6]}$Al. Here, $\langle c/r \rangle_{ave}$ is defined as cationic potential normalized by the mole fraction of each non-network cation. The average cationic potential ($\langle c/r \rangle_{ave}$) can thus be given as

$$\langle c/r \rangle_{ave} = \sum_j x_j \alpha_j \quad (4)$$

where x_j and a_j are the mole fraction and the cationic potential of cation j, respectively. For example, the cationic potential of Na^+ is ~1.0, that of Ca^{2+} is ~2.0, and that of Mg^{2+} is ~2.8. Thus, $\langle c/r \rangle_{ave}$ of $X_{Diopside}$ = 0.25 is ~1.4. The $\langle c/r \rangle_{ave}$ value of glasses in the diopside–jadeite join varies from 1.0 ($X_{Diopside}$ = 0) to 2.4 ($X_{Diopside}$ = 0.75).

Figure 3.9A shows that the population of $^{[5]}$Al for CMNAS glasses in the diopside–jadeite join, CMAS glasses in the diopside–Ca–tschermakite join, and diopside–anorthite eutectic composition glass apparently increases with increasing X_{Diopside}. The dispersion of the $^{[5]}$Al fraction in the studied glasses can be combined into a less-dispersed trend line by utilizing $\langle c/r \rangle_{ave}$. Figure 3.9B shows that the population of $^{[5]}$Al non-linearly increases with the increasing $\langle c/r \rangle_{ave}$ of the glasses in the diopside–Ca–tschermakite join, diopside–anorthite eutectic, phonolite, and diopside–jadeite join. While the population of $^{[5]}$Al does not change with increasing $\langle c/r \rangle_{ave}$ (1.0 to ~1.7) but it increases from 0 to 3.5% with increasing $\langle c/r \rangle_{ave}$ (~1.7 to 2.4).

To further explore the effect of $\langle c/r \rangle_{ave}$ on the fraction of $^{[5,6]}$Al in the diverse aluminosilicate glasses, previously reported $^{[5,6]}$Al populations in other ternary and quaternary aluminosilicate glasses were presented with varying $\langle c/r \rangle_{ave}$. Figure 3.10 shows the ternary composition diagram that marks the compositions of aluminosilicate glasses (used for the presentation), including ternary and quaternary glasses with known $^{[5,6]}$Al fractions (MO–Al_2O_3–SiO_2, M refers to non-framework cations, Ca^{2+}, Mg^{2+}, Na^{+}, K^{+}, and Ba^{2+}). Peralkaline ($M^{n+}O_{n/2} > Al_2O_3$), peraluminous ($M^{n+}O_{n/2} < Al_2O_3$), and charge-balanced ($M^{n+}O_{n/2} = Al_2O_3$) joins are shown. In addition to the glasses shown in Figure 3.9A, those for glasses in other compositions are taken from previous ^{27}Al NMR studies (Allwardt et al., 2005b; Kelsey et al., 2008; Malfait et al., 2012; Neuville et al., 2006; Neuville et al., 2008; Stebbins et al., 2008; Thompson and Stebbins, 2011; Thompson and Stebbins, 2012; Xue and Kanzaki, 2008). These previous efforts, together with the results from the current study, allow us to provide a general view of the effect of composition on Al coordination environments. The shaded area also shows the typical

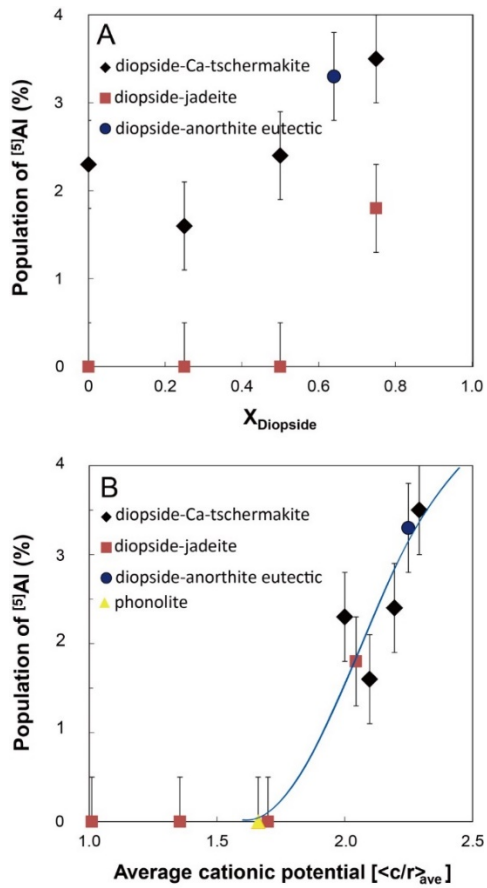

Figure 3.9. (A) Population of [5]Al for CaO–MgO–Al_2O_3–SiO_2 glasses in the diopside–Ca–tschermakite pseudobinary join, diopside–anorthite eutectic glass, and CaO–MgO–Na_2O–Al_2O_3–SiO_2 glasses in the diopside–jadeite pseudobinary join with varying mole fractions of diopside ($X_{Diopside}$). (B) Population of [5]Al for CaO–MgO–Al_2O_3–SiO_2 glasses in the diopside–Ca–tschermakite pseudobinary join, diopside–anorthite eutectic glass, and CaO–MgO–Na_2O–Al_2O_3–SiO_2 glasses in the diopside–jadeite pseudobinary join with $<c/r>_{ave}$ (average cationic potential). The error bar of ±0.5% was estimated based on estimated uncertainty in the peak area and the quadrupolar coupling constant (C_q) that affects peak intensity.

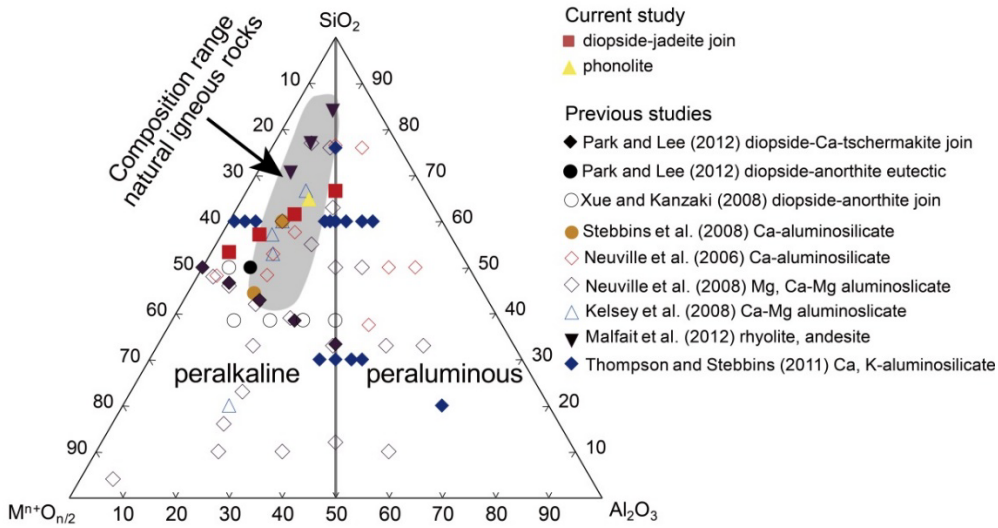

Figure 3.10. Ternary phase diagram showing the glass compositions of the current and previous studies of the Al coordination environments in the diverse ternary and multi-component silicate glasses. M refers to non-framework cation (Ca^{2+}, Mg^{2+}, Na^{+}, K^{+}, Ba^{2+}). Each symbol shows the composition of the glasses (as labeled with references) plotted in the ternary diagram.

composition of natural igneous rocks (Mysen and Richet, 2005). Figure 3.11 shows the relationship between the population of $^{[5,6]}$Al and $\langle c/r \rangle_{ave}$ in all the ternary, quaternary, and five-component aluminosilicate glasses studied so far. Regardless of composition of the glasses the fraction of $^{[5,6]}$Al generally increases with increasing $\langle c/r \rangle_{ave}$ of non-framework cations. Furthermore, the population of $^{[5,6]}$Al only slightly increases with increasing $\langle c/r \rangle_{ave}$ from 1 to ~1.5, and then it increases significantly when $\langle c/r \rangle_{ave}$ is larger than 2. The observed trend demonstrates that there is a threshold value for the $\langle c/r \rangle_{ave}$. Note that we are considering silicate glasses synthesized at 1 atm.

Additionally, the population of $^{[5,6]}$Al (e.g., when $\langle c/r \rangle_{ave}$ is 2) has various values depending on the composition: the population of $^{[5,6]}$Al is apparently scattered when $\langle c/r \rangle_{ave}$ is 2.0 (see Figure 3.11). The dispersion can be explained by the effect of $M^{n+}O_{n/2}/Al_2O_3$ (from peraluminous join to peralkalaine join) and Si/Al on $^{[5,6]}$Al population. The change in the population of $^{[5,6]}$Al caused by each parameter is outlined in the following. First, Figure 3.12A shows the population of $^{[5,6]}$Al in peraluminous silicate glasses ($M^{n+}O_{n/2}/Al_2O_3 < 1$) with $\langle c/r \rangle_{ave}$. The thick dotted curves show the trend lines connecting previous experimental data for $M^{n+}O_{n/2}/Al_2O_3$ ratio at 0.3 and 0.6 (Neuville et al., 2006; Neuville et al., 2008). The two trend lines suggest that the population of $^{[5,6]}$Al may be higher with a low $M^{n+}O_{n/2}/Al_2O_3$ ratio at a constant $\langle c/r \rangle_{ave}$. Second, the population of $^{[5,6]}$Al shows an increasing trend with increasing $\langle c/r \rangle_{ave}$ in the charge-balanced join; however, it appears scattered (see red rectangles in Figure 3.11). The $^{[5,6]}$Al fraction with constant $\langle c/r \rangle_{ave}$ and $M^{n+}O_{n/2}/Al_2O_3$ value is also affected by additional composition constraints such as the Si/Al ratio (Kelsey et al., 2008; Neuville et al., 2006; Neuville et al., 2008; Thompson and Stebbins, 2012). For example, Figure 3.12B shows the relationship between the population of

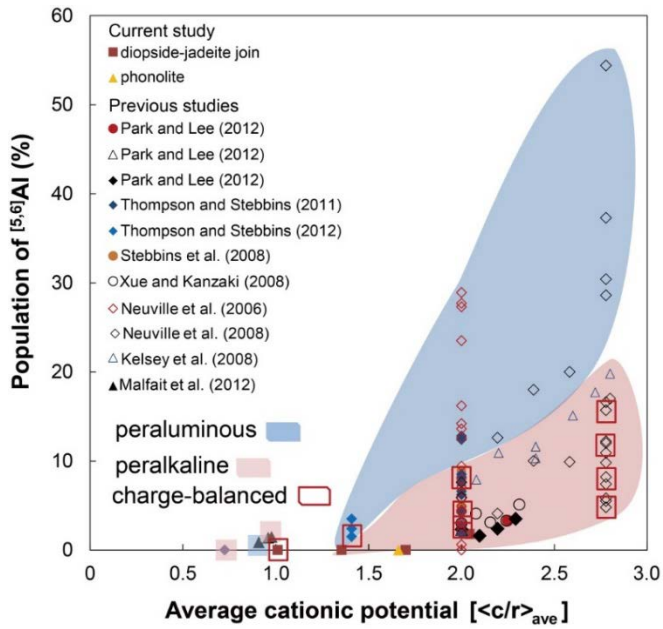

Figure 3.11. The population of $^{[5,6]}$Al in the diverse ternary and multi-component aluminosilicate glasses with varying average cationic potential, $\langle c/r \rangle_{ave}$.

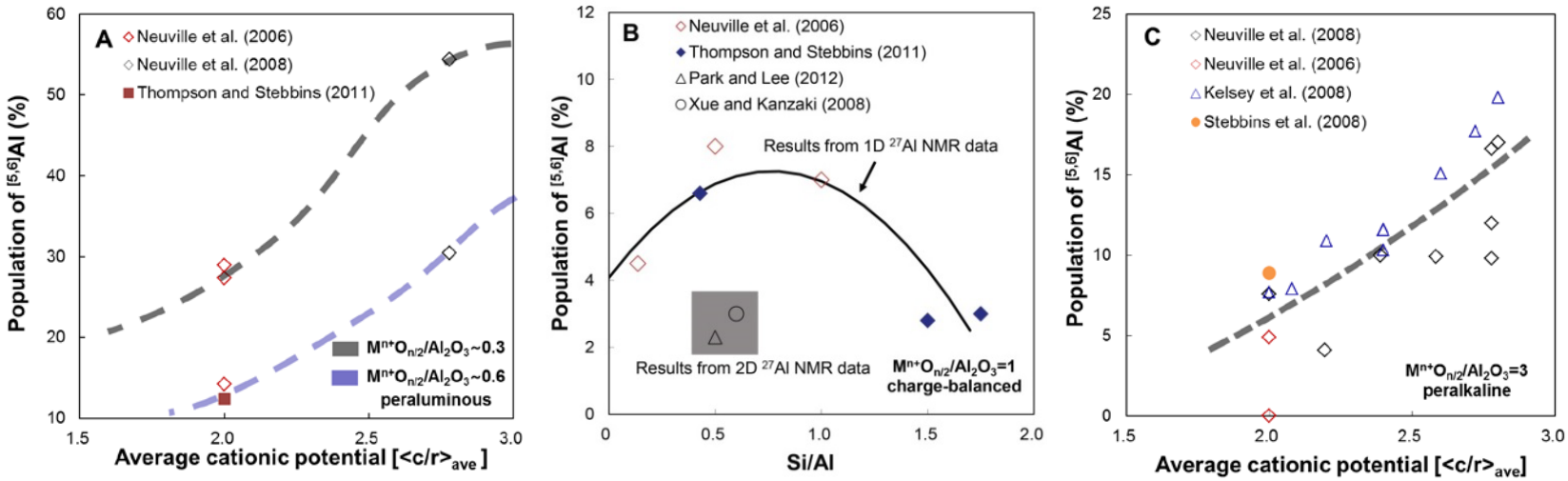

Figure 3.12. (A) The population of $^{[5,6]}$Al in peraluminous aluminosilicate glasses with varying $\langle c/r \rangle_{ave}$. The blue dotted line is for $M^{n+}O_{n/2}/Al_2O_3$ of ~0.3. The red dotted line is for $M^{n+}O_{n/2}/Al_2O_3$ of ~0.6. (B) The population of $^{[5,6]}$Al of metaluminous glasses ($M^{n+}O_{n/2}/Al_2O_3 = 1$) with varying Si/Al ratio. (C) The population of $^{[5,6]}$Al of peralkaline aluminosilicate glass with varying $\langle c/r \rangle_{ave}$.

$^{[5,6]}$Al and the Si/Al ratio at constant $M^{n+}O_{n/2}/Al_2O_3$ ratio of = 1 (i.e., charge-balanced join) and a onstant $<c/r>_{ave}$ of 2.0. The population of $^{[5,6]}$Al obtained from the high-field 1D MAS NMR method increases (when the Si/Al ratio changes from ~0 to ~0.5) and then decreases (when the Si/Al ratio changes from ~1.0 to ~1.7) with increasing Si/Al ratio (Neuville et al., 2006; Park and Lee, 2012; Thompson and Stebbins, 2011; Xue and Kanzaki, 2008). The 2D NMR results however show that the population of $^{[5,6]}$Al may not change significantly when the Si/Al ratio changes from ~0.5 to ~0.6. As the comparison of the fractions of $^{[5,6]}$Al from the different methods (1D *vs.* 2D NMR) have been discussed (Park and Lee, 2012), the apparent discrepancy between the estimated fractions from 1D and 2D NMR is primarily due to the differences in the way to quantify the Al species: briefly, in order to yield quantitative fractions from the 2D 3QMAS NMR technique, additional calibration considering the effect of C_q on the 3QMAS efficiency is necessary, which can often be model-dependent used for the calibration. In the high-field 1D NMR data, the fractions of highly coordinated Al can appear slightly overestimated, whereas the fractions can be rather underestimated in the low-field 2D NMR data (Park and Lee, 2012; Xue and Kanzaki, 2008).

The population of $^{[5,6]}$Al increases with increasing $<c/r>_{ave}$ in peralkaline glasses (i.e., $M^{n+}O_{n/2}/Al_2O_3$ >1). Figure 3.12C shows the relationship between $<c/r>_{ave}$ and the population of $^{[5,6]}$Al at $M^{n+}O_{n/2}/Al_2O_3$ = 3, showing the increasing trend of the population of $^{[5,6]}$Al with increasing $<c/r>_{ave}$. The current and previous results show that temperature, pressure, and composition (e.g., $M^{n+}O_{n/2}/Al_2O_3$, and the Si/Al ratio) are the main factors that affect the population of $^{[5,6]}$Al (Lee, 2010; Lee et al., 2012; Neuville et al., 2006; Neuville et al., 2008; Stebbins et al., 2008); furthermore, $<c/r>_{ave}$, can be useful to account for the formation of highly coordinated Al. Taking

into consideration effect of composition on $^{[5,6]}$Al, Figure 3.13 also shows the predicted population of $^{[5,6]}$Al of natural volcanic glasses that include basalt, rhyolite, andesite, phonolite, and trachyte with varying $\langle c/r \rangle_{ave}$. The current trend with $\langle c/r \rangle_{ave}$ will be useful for predicting the $^{[5,6]}$Al fractions in complex, multi-component natural aluminosilicate glasses.

3.3.6. Implications for macroscopic thermodynamic and transport properties and geochemical processes

Andesitic glasses and melts have other important major (particularly iron), minor, and volatile components that provide important insights into the petrogenesis and properties. Thus, the application of the current results of the model andesitic glasses to real natural andesitic glasses has obvious limitations. In addition, we have studied the structure of the quenched glasses, i.e., that of supercooled liquid frozen below the glass transition temperature that is much lower than the liquidus and thus, the effects of the other **c**omponents and the temperature remain to be explored. Nevertheless, the current results can provide unique information on the microscopic origins of the properties of andesitic melts with varying composition and yields insights into the formation of the melts.

The current ^{17}O NMR results unambiguously show that NBO prefers Ca^{2+} and Mg^{2+} over Na^{+} in an intermediate composition in the diopside–jadeite join ($X_{Diopside}$ = 0.25, 0.5), whereas Na^{+} prefers to have proximity to BOs. The observed bonding preferences among non-network formers and BO and NBOs highlight the non-random distribution of non-network formers in the glass network. Cation-ordering in the crystalline omphacite is characterized by the preference between Ca–Mg and Na–Al (related to local charge balance on the M sites). In contrast, the ordering in glasses in an

intermediate composition is characterized by the non-randomness of the distribution of cations, such as the preferential partitioning of non-framework cations into NBOs and BOs, contributing to the configurational thermodynamic properties.

Additionally, while the potential prevalence of Ca-NBO in the glasses in the intermediate composition and thus a certain degree of unmixing between Ca and Mg around NBO may additionally contribute to the mixing properties (toward a positive deviation), the configuration enthalpy (~ excess Gibbs free energy of mixing) of the CNMAS is expected to show negative deviation due to a strong deviation from the randomness observed in the Si/Al distribution towards chemical ordering and preferential partitioning among network modifying cations and NBOs/BOs. The viscosities of silicate melts in the diopside–jadeite join decrease exponentially with increasing X_{Diopside} (Suzuki et al., 2005), partly due to an increase in NBO content. The current ^{17}O 3QMAS NMR results confirm that NBO content certainly increases with X_{Diopside} (as also expected from the composition), providing atomic-level insights into the strong compositional dependence of melt viscosity. On-going modeling of melt properties utilizing the diverse degree of experimentally observed disorder will certainly be useful in quantifying structural disorder and predicting their macroscopic properties (e.g., Lee, 2011). Future applications of these recent advances and progress (i.e., the network connectivity and the preferential partitioning of non-framework cations into NBOs) in the diopside–jadeite join and other multi-component melts should provide full insights into the atomistic origins of their macroscopic properties.

As the andesitic melts are generated in various tectonic settings, the composition of the mantle and crustal source as well as the formation depth (pressure) affect the generation and composition of high–Mg andesite. It is reported that the SiO_2 content increases as the MgO content in the melts decreases with increasing H_2O content and pressure (Falloon et al., 2008; Hirose, 1997; Kushiro, 1969; Liu et al., 2006; Parman and Grove, 2004; Walter and Presnall, 1994; Wood and Turner, 2009, and references therein). With increasing $X_{Diopside}$ in the diopside–jadeite join, the SiO_2 content decreases and that of MgO increases (Table 1). The change of composition in the diopside–jadeite join with increasing $X_{Diopside}$ can thus provide insights into the change of composition and structure with increasing pressure and H_2O content: while we are not explicitly exploring the detailed effects of pressure and H_2O on the degree of structural disorder, indirectly, changes in the composition of the glasses allow us to see the variations in the NBO and BO fractions due to changes in the composition of the melts with pressure and H_2O content.

Finally, the results for the Al coordination with $<c/r>_{ave}$ offer the possibility of estimating the fraction of highly coordinated Al in melts, including andesitic melts, when the compositions of the melts are known: as shown in Figure 3.13, the current trend would certainly allow us to predict the Al coordination environments in the diverse silicate glasses and melts at 1 atm. Efforts have been made to correlate the highly coordinated Al with configurational and vibrational properties for relatively simple ternary Ca–aluminosilicate glasses and melts (e.g., Richet et al., 2009, and references therein). We expect that similar efforts could be made for more complex, natural silicate melts.

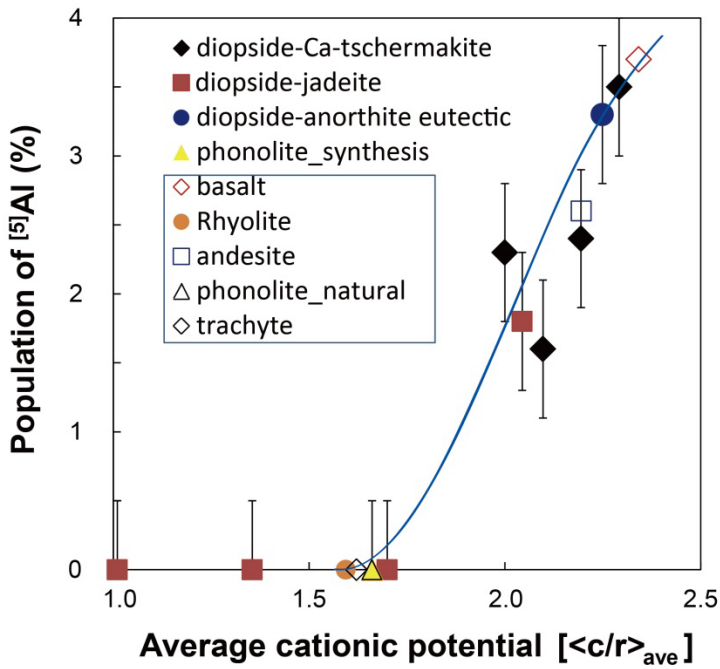

Figure 3.13. The predicted population of $^{[5]}$Al in natural volcanic glass that includes basalt, rhyolite, andesite, phonolite, and trachyte with varying $\langle c/r \rangle_{ave}$.

3.4. Conclusions

The experimental data presented here provide structural details of atomic configurations around Si and Al atoms, their connectivity (through changes in NBO and BO environments), and the extent of chemical and topological disorder in multi-component CMNAS glasses in the diopside–jadeite pseudobinary join. The ^{27}Al MAS and 3QMAS NMR spectra for all the joins show $^{[4]}$Al as well as $^{[5]}$Al. The spectral analysis of $^{[4]}$Al peak suggests that the degree of distortion around the Al coordination environments increases with increasing X_{Diopside}. The 2D ^{17}O 3QMAS NMR spectra revealed previously unknown details of diverse structural disorder in the multi-component glasses. In addition to the clear effects of composition (particularly the effect of the cationic potential of non-network-forming cations: Ca^{2+}, Na^{+}, and Mg^{2+}), the ^{17}O 3QMAS NMR spectra for the model andesitic glasses studied here confirm that the degree of polymerization (BO content) decreases with increasing X_{Diopside}. The significant fraction of Si–O–Al supports extensive mixing between $^{[4]}$Al and $^{[4]}$Si. Furthermore, Al–O–Al is also visible in the jadeite glasses, suggesting a deviation from Al avoidance in these glasses. Based on the analysis of the peak position of {Ca, Mg}–mixed NBOs in the intermediate composition and the peak shape of Si–O–Al, non-random distributions of Na^{2+}, Ca^{2+}, and Mg^{2+} around both NBOs and BOs are manifested by a moderate degree of partitioning of Ca^{2+} and Mg^{2+} into NBOs and by the spatial proximity between Na^{+} and BOs (Al–O–Al and Al–O–Si) in the andesitic glasses studied here. Based on the variations of peak width in the ^{29}Si MAS NMR spectra for the glasses, although it is currently difficult to provide a quantitative description of the extent of topological disorder because of the overlap among each Q species, the topological (peak

widths) and chemical disorders (dispersion in Q species) around the [4]Si are found to be highest in the intermediate compositions.

The relationship between the fraction of highly coordinated Al and composition, particularly, the average cationic potential of non-network cations was proposed and tested. The results in this study show an increasing trend of highly coordinated Al with increasing $<c/r>_{ave}$. The future generalization for the increasing trend of the fraction of highly coordinated Al may be possible for all compositions, including the model and natural compositions, through $<c/r>_{ave}$. The current results provide insights into the structure–property relationship in complex andesitic melts and glasses.

APPENDIX

Center of gravity for each Al peak was obtained from projections in the MAS and isotropic dimension. The estimated center of gravity for [4]Al (δ_{3QMAS} is the center of gravity in the isotropic dimension and δ_{MAS} is that in MAS dimension in 3QMAS NMR spectra) is shown in table A1. NMR parameters were obtained from δ_{3QMAS} and δ_{MAS} from the following relationships (Baltisberger et al., 1996a and references therein):

$$\delta_{3QMAS} = -17/31\delta_{iso}^{CS} + 10/31\delta_{iso}^{2Q} \quad \text{(A1)}$$

$$\delta_{MAS} = \delta_{iso}^{CS} + \delta_{iso}^{2Q} \quad \text{(A2)}$$

Where δ_{iso}^{2Q} is the second-order quadrupolar shift for spin 5/2 nuclei (i.e., ^{27}Al), $6000P_q^{\,2}/\varpi_0^{\,2}$ (ϖ_0 is the Larmor frequency). From the above

relations, mean values of P_q and δ_{iso}^{CS} of Al sites were estimated. Finally, C_q was calculated by assuming that η is 0.5. The results are also shown in Table A1.

Table A1. The center of gravity (obtained from MAS and isotropic dimension) and NMR parameters [the isotropic chemical shift (δ_{iso}^{CS}) and quadrupolar coupling constant (C_q)] for $^{[4]}$Al in CaO–MgO-Na_2O–Al_2O_3–SiO_2 glasses in diopside-jadeite join. $X_{Diopside}$ is the mole fraction of diopside.

$X_{Diopside}$	center of gravity (ppm)		δ_{iso}^{CS} (ppm)	C_q (MHz) (η =0.5)
	MAS dimension	isotropic dimension		
0	49.2 ±1.5	-38.4 ±1.5	62.3 ±0.8	4.7 ±0.2
0.25	48.3 ±1.5	-39.2 ±1.5	62.9 ±0.8	4.9 ±0.2
0.50	47.3 ±1.5	-39.7 ±1.5	63.1 ±0.8	5.1 ±0.2
0.75	48.3 ±1.5	-40.8 ±1.5	64.7 ±0.8	5.3 ±0.2

References

Abo-Mosallam, H.A., Hill, R.G., Karpukhina, N. and Law, R.V. (2010) MAS-NMR studies of glasses and glass-ceramics based on a clinopyroxene-fluorapatite system. *J. Mater. Chem.* 20, 790-797.

Allwardt, J.R., Lee, S.K. and Stebbins, J.F. (2003) Bonding preferences of non-bridging O atoms: Evidence from ^{17}O MAS and 3QMAS NMR on calcium aluminate and low-silica Ca-aluminosilicate glasses. *Am. Miner.* 88, 949-954.

Allwardt, J.R., Poe, B.T. and Stebbins, J.F. (2005a) The effect of fictive temperature on Al coordination in high-pressure (10 GPa) sodium aluminosilicate glasses. *Am. Miner.* 90, 1453-1457.

Allwardt, J.R. and Stebbins, J.F. (2004) Ca-Mg and K-Mg mixing around non-bridging O atoms in silicate glasses: An investigation using ^{17}O MAS and 3QMAS NMR. *Am. Miner.* 89, 777-784.

Allwardt, J.R., Stebbins, J.F., Schmidt, B.C., Frost, D.J., Withers, A.C. and Hirschmann, M.M. (2005b) Aluminum coordination and the densification of high-pressure aluminosilicate glasses. *Am. Miner.* 90, 1218-1222.

Baltisberger, J.H., Xu, Z., Stebbins, J.F., Wang, S.H. and Pines, A. (1996) Triple-quantum two-dimensional ^{27}Al magic-angle spinning nuclear magnetic resonance spectroscopic study of aluminosilicate and aluminate crystals and glasses. *J. Am. Chem. Soc.* 118, 7209-7214.

Bauchy, M., Guillot, B., Micoulaut, M. and Sator, N. (2013) Viscosity and viscosity anomalies of model silicates and magmas: A numerical investigation. *Chem. Geol.* 346, 47-56.

Bell, P.M. and Davis, B.T.C. (1969) Melting relations in the system jadeite-diopside at 30 and 40 kilobars. *Am. J. Sci.* 267-A, 17-32.

Dirken, P.J., Kohn, S.C., Smith, M.E. and vanEck, E.R.H. (1997) Complete resolution of Si-O-Si and Si-O-Al fragments in an aluminosilicate

glass by ^{17}O multiple quantum magic angle spinning NMR spectroscopy. *Chem. Phys. Lett.* 266, 568-574.

Dubinsky, E.V. and Stebbins, J.F. (2006) Quench rate and temperature effects on framework ordering in aluminosilicate melts. *Am. Miner.* 91, 753-761.

Falloon, T.J., Green, D.H., Danyushevsky, L.V. and McNeill, A. (2008) The composition of nearsolidus partial melts of peridotite at 1 and 1.5 GPa: implications for the petrogenesis of MORB. *J. Petrol.* 49, 591-613.

Florian, P., Sadiki, N., Massiot, D. and Coutures, J.P. (2007) Al-27 NMR study of the structure of lanthanum- and yttrium-based aluminosilicate glasses and melts. *J. Phys. Chem. B.* 111, 9747-9757.

Ghose, S. and Tsang, T. (1973) Structural dependence of quadrupole coupling-constant E2QQ/H for ^{27}Al and crystal-field parameter D for Fe^{3+} in aluminosilicate. *Am. Miner.* 58, 748-755.

Giordano, D. and Dingwell, D.B. (2003) Non-Arrhenian multicomponent melt viscosity: a model. *Earth Planet. Sci. Lett.* 208, 337-349.

Giordano, D., Potuzak, M., Romano, C., Dingwell, D.B. and Nowak, M. (2008) Viscosity and glass transition temperature of hydrous melts in the system $CaAl_2Si_2O_8$-$CaMgSi_2O_6$. *Chem. Geol.* 256, 203-215.

Grove, T.L. and Kinzler, R.J. (1986) Petrogenesis of andesites. *Annu. Rev. Earth. Pl. Sc.* 14, 417-454.

Hirose, K. (1997) Melting experiments on Iherzolite KLB-1 under hydrous conditions and generation of high-magnesian andesitic melts. *Geology* 25, 42-44.

Iftekhar, S., Grins, J., Gunawidjaja, P.N. and Eden, M. (2011) Glass Formation and Structure-Property-Composition Relations of the RE_2O_3-Al_2O_3-SiO_2 (RE = La, Y, Lu, Sc) Systems. *J. Am. Ceram. Soc.* 94, 2429-2435.

Jindal, R. (2012) Elastic Properties of Clinopyroxene Based Glasses along Diopside ($CaMgSi_2O_6$)-Jadeite ($NaAlSi_2O_6$) Join. *J. Miner. Mater. Character. Eng.* 11, 267-284.

Jindal, R., Jayaganthan, R., Singh, I.V. and Conradt, R. (2011) Synthesis and characterization of clinopyroxene based glasses and glass-ceramics along diopside ($CaMgSi_2O_6$)-jadeite ($NaAlSi_2O_6$) join. *Ceram. Int.* 37, 741-748.

Kelsey, K.E., Allwardt, J.R. and Stebbins, J.F. (2008) Ca-Mg mixing in aluminosilicate glasses: An investigation using ^{17}O MAS and 3QMAS and ^{27}Al MAS NMR. *J. Non-Cryst. Solids* 354, 4644-4653.

Kelsey, K.E., Stebbins, J.F., Singer, D.M., Brown, G.E., Mosenfelder, J.L. and Asimow, P.D. (2009) Cation field strength effects on high pressure aluminosilicate glass structure: Multinuclear NMR and La XAFS results. *Geochim. Cosmochim. Acta* 73, 3914-3933.

Kirkpatrick, R.J., Oestrike, R., Weiss, C.A., Smith, K.A. and Oldfield, E. (1986) High-resolution ^{27}Al and ^{29}Si NMR-spectroscopy of glasses and crystals along the join $CaMgSi_2O_6$-$CaAl_2SiO_6$. *Am. Miner.* 71, 705-711.

Kushiro, I. (1969) The system forsterite-diopside-silica with and without water at high pressures. *Am. J. Sci.* 267A, 269–294.

Le Losq, C., Neuville, D.R., Florian, P., Henderson, G.S. and Massiot, D. (2014) The role of Al3+ on rheology and structural changes in sodium silicate and aluminosilicate glasses and melts. *Geochim. Cosmochim. Acta* 126, 495-517.

Lee, S.K. (2004) Structure of silicate glasses and melts at high pressure: Quantum chemical calculations and solid-state NMR. *J. Phys. Chem. B.* 108, 5889-5900.

Lee, S.K. (2005) Microscopic origins of macroscopic properties of silicate melts and glasses at ambient and high pressure: Implications for melt generation and dynamics. *Geochim. Cosmochim. Acta* 69, 3695-3710.

Lee, S.K. (2010) Effect of pressure on structure of oxide glasses at high pressure: Insights from solid-state NMR of quadrupolar nuclides. *Solid State Nucl. Magn. Reson.* 38, 45-57.

Lee, S.K. (2011) Simplicity in melt densification in multicomponent magmatic reservoirs in Earth's interior revealed by multinuclear magnetic resonance. *P. Natl. Acad. Sci. USA.* 108, 6847-6852.

Lee, S.K., Cody, G.D., Fei, Y.W. and Mysen, B.O. (2004) Nature of polymerization and properties of silicate melts and glasses at high pressure. *Geochim. Cosmochim. Acta* 68, 4189-4200.

Lee, S.K., Cody, G.D. and Mysen, B.O. (2005) Structure and the extent of disorder in quaternary (Ca-Mg and Ca-Na) aluminosilicate glasses and melts. *Am. Miner.* 90, 1393-1401.

Lee, S.K., Deschamps, M., Hiet, J., Massiot, D. and Park, S.Y. (2009) Connectivity and Proximity between Quadrupolar Nuclides in Oxide Glasses: Insights from through-Bond and through-Space Correlations in Solid-State NMR. *J. Phys. Chem. B.* 113, 5162-5167.

Lee, S.K., Mysen, B.O. and Cody, G.D. (2003) Chemical order in mixed-cation silicate glasses and melts. Physical Review B 68.

Lee, S.K., Park, S.Y., Kim, H.I., Tschauner, O., Asimow, P., Bai, L.G., Xiao, Y.M. and Chow, P. (2012a) Structure of shock compressed model basaltic glass: Insights from O K-edge X-ray Raman scattering and high-resolution Al-27 NMR spectroscopy. *Geophys. Res. Lett.* 39.

Lee, S.K. and Stebbins, J.F. (1999) The degree of aluminum avoidance in aluminosilicate glasses. *Am. Miner.* 84, 937-945.

Lee, S.K. and Stebbins, J.F. (2000) The structure of aluminosilicate glasses: High-resolution ^{17}O and ^{27}Al MAS and 3QMAS. *J. Phys. Chem. B.* 104, 4091-4100.

Lee, S.K. and Stebbins, J.F. (2002) Extent of intermixing among framework units in silicate glasses and melts. *Geochim. Cosmochim. Acta* 66, 303-309.

Lee, S.K. and Stebbins, J.F. (2003) Nature of cation mixing and ordering in Na-Ca silicate glasses and melts. *J. Phys. Chem. B.* 107, 3141-3148.

Lee, S.K. and Stebbins, J.F. (2006) Disorder and the extent of polymerization in calcium silicate and aluminosilicate glasses: O-17 NMR results and quantum chemical molecular orbital calculations. *Geochim. Cosmochim. Acta* 70, 4275-4286.

Lee, S.K. and Stebbins, J.F. (2009) Effects of the degree of polymerization on the structure of sodium silicate and aluminosilicate glasses and melts: An O-17 NMR study. *Geochim. Cosmochim. Acta* 73, 1109-1119.

Lee, S.K. and Sung, S. (2008) The effect of network-modifying cations on the structure and disorder in peralkaline Ca-Na aluminosilicate glasses: O-17 3QMAS NMR study. *Chem. Geol.* 256, 326-333.

Lee, S.K., Yi, Y.S., Cody, G.D., Mibe, K., Fei, Y.W. and Mysen, B.O. (2012b) Effect of Network Polymerization on the Pressure-Induced Structural Changes in Sodium Aluminosilicate Glasses and Melts: Al-27 and O-17 Solid-State NMR Study. *J. Phys. Chem. C.* 116, 2183-2191.

Liu, X., O'Neill, H.S.C. and Berry, A.J. (2006) The effects of small amounts of H_2O, CO_2 and Na_2O on the partial melting of spinel lherzolite in the system CaO–MgO–Al_2O_3–SiO_2± H_2O ± CO_2 ± Na_2O at 1.1 GPa. *J. Petrol.* 47, 409-434.

Maekawa, H., Maekawa, T., Kawamura, K. and Yokokawa, T. (1991) The structural groups of alkali silicate-glasses determined from Si-29 MAS-NMR. *J. Non-Cryst. Solids* 127, 53-64.

Malfait, W.J., Verel, R., Ardia, P. and Sanchez-Valle, C. (2012) Aluminum coordination in rhyolite and andesite glasses and melts: Effect of temperature, pressure, composition and water content. *Geochim. Cosmochim. Acta* 77, 11-26.

Massiot, D., Messinger, R.J., Cadars, S., Deschamps, M., Montouillout, V., Pellerin, N., Veron, E., Allix, M., Florian, P. and Fayon, F. (2013)

Topological, Geometric, and Chemical Order in Materials: Insights from Solid-State NMR. *Acc. Chem. Res.* 46, 1975-1984.

Mortazavi, M. and Sparks, R.S.J. (2004) Origin of rhyolite and rhyodacite lavas and associated mafic inclusions of Cape Akrotiri, Santorini: the role of wet basalt in generating calcalkaline silicic magmas. *Contrib. Mineral. Petr.* 146, 397-413.

Mysen, B.O. (1988) Structure and Properties of Silicate Melts Elsevier Amsterdam.

Mysen, B.O., Lucier, A. and Cody, G.D. (2003) The structural behavior of Al3+ in peralkaline melts and glasses in the system Na_2O-Al_2O_3-SiO_2. *Am. Miner.* 88, 1668-1678.

Mysen, B.O. and Richet, P. (2005) Silicate glasses and melts: Properties and structure. Elsevier, Amsterdam.

Mysen, B.O. and Toplis, M.J. (2007) Structural behavior of Al^{3+} in peralkaline, metaluminous, and peraluminous silicate melts and glasses at ambient pressure. *Am. Miner.* 92, 933-946.

Mysen, B.O., Virgo, D. and Seifert, F.A. (1982) The structure of silicate melts –implications for chemical and physical-properties of natural magam. *Rev. Geophys.* 20, 353-383.

Navrotsky, A., Zimmermann, H.D. and Hervig, R.L. (1983) Thermochemical study of glasses in the system $CaMgSi_2O_6$-$CaAl_2SiO_6$. *Geochim. Cosmochim. Acta* 47, 1535-1538.

Neuville, D.R., Cormier, L. and Massiot, D. (2004) Al environment in tectosilicate and peraluminous glasses: A Al-27 MQ-MAS NMR, Raman, and XANES investigation. *Geochim. Cosmochim. Acta* 68, 5071-5079.

Neuville, D.R., Cormier, L. and Massiot, D. (2006) Al coordination and speciation in calcium aluminosilicate glasses: Effects of composition determined by Al-27 MQ-MAS NMR and Raman spectroscopy. *Chem. Geol.* 229, 173-185.

Neuville, D.R., Cormier, L., Montouillout, V., Florian, P., Millot, F., Rifflet, J.C. and Massiot, D. (2008) Structure of Mg- and Mg/Ca aluminosilicate glasses: ^{27}Al NMR and Raman spectroscopy investigations. *Am. Miner.* 93, 1721-1731.

Park, S.Y. and Lee, S.K. (2012) Structure and disorder in basaltic glasses and melts: Insights from high-resolution solid-state NMR study of glasses in diopside-Ca-tschermakite join and diopside-anorthite eutectic composition. *Geochim. Cosmochim. Acta* 80, 125-142.

Parman, S.W. and Grove, T.L. (2004) Harzburgite melting with and without H_2O: Experimental data and predictive modeling. *J. Geophys. Res. - Solid Earth* 109, B02201.

Pingel, U.T., Amoureux, J.P., Anupold, T., Bauer, F., Ernst, H., Fernandez, C., Freude, D. and Samoson, A. (1998) High-field ^{17}O NMR studies of the SiOAl bond in solids. *Chem. Phys. Lett.* 294, 345-350.

Potuzak, M. and Dingwell, D.B. (2006) Temperature-dependent thennal. expansivities of multicomponent natural melts between 993 and 1803 K. *Chem. Geol.* 229, 10-27.

Prouteau, G. and Scaillet, B. (2003) Experimental constraints on the origin of the 1991 Pinatubo dacite. *J. Petrol.* 44, 2203-2241.

Richet, P. (1984) Viscosity and configurational entropy of silicate melts. *Geochim. Cosmochim. Acta* 48, 471-483.

Richet, P. and Bottinga, Y. (1986) Thermochemical properties of silicate glasses and liquids: A review. *Geochim. Cosmochim. Acta* 24, 1-25.

Richet, P., Nidaira, A. and Neuville, D. (2009) Aluminum speciation, vibrational entropy and short-range order in calcium aluminosilicate glasses. *Geochim. Cosmochim. Acta* 73, 3894-3904.

Schairer, J.F. and Yoder, H.S. (1960) The nature of residual liquids from crystallization, with data on the system nepheline-diopside-silica. *Am. J. Sci.* 258, 273-283.

Stebbins, J.F. (1995) Dynamics and structure of silicate and oxide melts: Nuclear magnetic resonance studies, in: Stebbins, J.F., McMillan, P.F., Dingwell, D.B. (Eds.), Structure, Dynamics and Properties of Silicate Melts. Mineralogical Society of America, Washington, DC, pp. 191-246.

Stebbins, J.F., Dubinsky, E.V., Kanehashi, K. and Kelsey, K.E. (2008) Temperature effects on non-bridging oxygen and aluminum coordination number in calcium aluminosilicate glasses and melts. *Geochim. Cosmochim. Acta* 72, 910-925.

Stebbins, J.F., Oglesby, J.V. and Lee, S.K. (2001a) Oxygen sites in silicate glasses: a new view from oxygen-17 NMR. *Chem. Geol.* 174, 63-75.

Stebbins, J.F. and Xu, Z. (1997) NMR evidence for excess non-bridging oxygen in an aluminosilicate glass. *Nature* 390, 60-62.

Stebbins, J.F. and Xue, X. (2014) NMR Spectroscopy of Inorganic Earth Materials. Elsevier, Amsterdam.

Stebbins, J.F., Zhao, P.D., Lee, S.K. and Oglesby, J.V. (2001b) Direct observation of multiple oxygen sites in oxide glasses: recent advances from triple-quantum magic-angle spinning nuclear magnetic resonance. *J. Non-Cryst. Solids* 293, 67-73.

Straub, S.M., Gomez-Tuena, A., Stuart, F.M., Zellmer, G.F., Espinasa-Perena, R., Cai, Y. and Iizuka, Y. (2011) Formation of hybrid arc andesites beneath thick continental crust. *Earth Planet. Sc. Lett.* 303, 337-347.

Suzuki, A., Ohtani, E., Terasaki, H. and Funakoshi, K. (2005) Viscosity of silicate melts in $CaMgSi_2O_6$-$NaAlSi_2O_6$ system at high pressure. *Phys. Chem. Miner.* 32, 140-145.

Thompson, L.M. and Stebbins, J.F. (2011) Non-bridging oxygen and high-coordinated aluminum in metaluminous and peraluminous calcium and potassium aluminosilicate glasses: High-resolution ^{17}O and ^{27}Al MAS NMR results. *Am. Miner.* 96, 841-853.

Thompson, L.M. and Stebbins, J.F. (2012) Non-stoichiometric non-bridging oxygens and five-coordinated aluminum in alkaline earth aluminosilicate glasses: Effect of modifier cation size. *J. Non.-Cryst. Solids* 358, 1783-1789.

Toplis, M.J. and Dingwell, D.B. (2004) Shear viscosities of CaO-Al_2O_3-SiO_2 and MgO-Al_2O_3-SiO_2 liquids: Implications for the structural role of aluminium and the degree of polymerisation of synthetic and natural aluminosilicate melts. *Geochim. Cosmochim. Acta* 68, 5169-5188.

Toplis, M.J., Kohn, S.C., Smith, M.E. and Poplett, I.J.F. (2000) Fivefold-coordinated aluminum in tectosilicate glasses observed by triple quantum MAS NMR. *Am. Miner.* 85, 1556-1560.

Urbain, G., Bottinga, Y. and Richet, P. (1982) Viscosity of liquid silica, silicates and alumino-silicates. *Geochim. Cosmochim. Acta* 46, 1061-1072.

Van Eck, E.R.H., Smith, M.E. and Kohn, S.C. (1999) Observation of hydroxyl groups by ^{17}O solid-state multiple quantum MAS NMR in sol-gel-produced silica. *Solid State Nucl. Magn. Reson.* 15, 181-188.

Walter, M.J. and Presnall, D.C. (1994) Melting behaviour of simplified lherzolite in the system CaO–MgO–Al_2O_3–SiO_2–Na_2O from 7 to 35 kb. *J. Petrol.* 35, 329–359.

Wood, B.J. and Turner, S.P. (2009) Origin of primitive high-Mg andesite: Constraints from natural examples and experiments. *Earth Planet. Sc. Lett.* 283, 59-66.

Xue, X.Y. and Kanzaki, M. (2008) Structure of hydrous aluminosilicate glasses along the diopside-anorthite join: A comprehensive one- and two-dimensional ^{1}H and ^{27}Al NMR study. *Geochim. Cosmochim. Acta* 72, 2331-2348.

Yarger, J.L., Smith, K.H., Nieman, R.A., Diefenbacher, J., Wolf, G.H., Poe, B.T. and McMillan, P.F. (1995) Al coordination changes in high-pressure aluminosilicate liquids. Science 270, 1964-1967.

Zeng, Q., Nekvasil, H. and Grey, C.P. (2000) In support of a depolymerization model for water in sodium aluminosilicate glasses: Information from NMR spectroscopy. *Geochim. Cosmochim. Acta* 64, 883-896.

Zhu, M.S., Miao, L.C. and Yang, S.H. (2013) Genesis and evolution of subduction-zone andesites: evidence from melt inclusions. *Int. Geol. Rev.* 55, 1179-1190.

Chapter 4. Effects of difference in ionic radii on chemical ordering in mixed-cation silicate glasses: insights from solid-state ^{17}O and ^{7}Li NMR of Li-Ba silicate glasses

Sun Young Park and Sung Keun Lee

Submitted to *Journal of American Ceramic Society*, 2016

Abstract

Understanding of the extent of cation disorder and its effect on the properties in glasses and melts is among the fundamental puzzles in glass sciences, materials sciences, and physical chemistry. Particularly, the nature of chemical ordering in mixed-cation silicate glasses is not fully understood. The Li-Ba silicate glass with significant difference in the ionic radii of network-modifying cations (~0.59 Å) is an ideal system for revealing unknown details of the effect of network modifiers on the extent of mixing and their contribution to the cation mobility. These glasses also find potential application as energy and battery materials. Here, we report the detailed atomic environments and the extent of cation mixing in Li-Ba silicate glasses with varying X_{BaO} [BaO/(Li_2O+BaO)] using high-resolution solid-state nuclear magnetic resonance (NMR) spectroscopy. The first ^{17}O MAS and 3QMAS NMR spectra for Li-Ba silicate glasses reveal the well-resolved peaks due to bridging oxygen (BO, Si-O-Si) and those of the non-bridging oxygens (NBOs) [Li-O-Si, mixed {Li, Ba}-O-Si, and Ba-O-Si]. The fraction of Li-O-Si decreases with an increase in X_{BaO} and is less than that predicted by a random Li-Ba distribution. These results demonstrate a non-random distribution of Li^+ and Ba^+ around NBOs characterized by a prevalence of the dissimilar Li-

Ba pair. Considering the previously reported experimental results on chemical ordering in mixed-cation silicate glasses (e.g., Na-Ba and Ba-Mg silicate glasses), the current results reveal the effect of difference in ionic radius of the cation on a hierarchy in the degree of chemical order for various network modifying cations in the glasses [e.g., K-Mg (~0.66 Å) ≈ Ba-Mg (~0.63 Å) ≈ Li-Ba (~0.59 Å) > Na-Ba (~0.33 Å) > Na-Ca (~0.02 Å)]. The ^{7}Li MAS NMR spectra of the Li-Ba silicate glasses show that the peak maximum increases with increasing X_{BaO}, suggesting that the average Li coordination number and thus Li-O distance decrease slightly with increasing X_{BaO}, potentially leading to an increased activation energy barrier for Li diffusion. Current experimental results confirm that the degree of chemical ordering due to a large difference in ionic radii controls the transport properties of the mixed-cation silicate glasses.

4.1. Introduction

Nature of the extent of structural disorder and its effect on the properties of glasses and the corresponding melts with varying composition are one of the fundamental and unsolved problems in materials sciences of glasses and ceramics, and physical chemistry. In particular, the "mixed-cation effect" in glasses and melts refers to a significant drop (up to several orders of magnitude) in the transport properties (e.g., diffusivity and ionic conductivity) of the glasses and the melts with intermediate compositions compared to those of end members (e.g., Amma et al., 2016; Cormier et al., 2010; Cramer et al., 2003; Day, 1976; Doremus, 1974; Ghosh and Ghosh, 2003; Isard, 1969; Le Losq and Neuville, 2013; Maass et al., 1992; Matusita et al., 1980; Moynihan and Lesikar, 1981; Sen et al., 1996; Swenson and Adams,

2003; Zotov et al., 1995). To elucidate the atomistic origins of the mixed-cation effect in mixed-cation silicate glasses, previous studies employed diverse experimental efforts using neutron and X-ray scattering measurements, X-ray absorption spectroscopy, and theoretical efforts including molecular dynamics simulations (e.g., Cormack and Du, 2001; Cormier et al., 2010; Cormier and Cuello, 2013; Greaves, 1998; Habasaki and Hiwatari, 2003; Konstantinou et al., 2015; Park and Cormack, 1999; Vessal et al., 1992). These studies suggested that the mixed-cation effect can indeed depend on the degree of cation disorder: because activation energy for a cation to hop to a site previously occupied by another type of cation is suggested to be higher than to a site vacated by the same type of cation (e.g., Lengyel and Boksay, 1954; Maass et al., 1992; Matusita et al., 1980; Sen et al., 1996), the degree of cation mixing and thus the fractions of dissimilar pairs (e.g., Na-Ca) is expected to control the overall transport properties.

Together with the aforementioned progress, high-resolution ^{17}O nuclear magnetic resonance (NMR) spectroscopy has been an effective experimental tool for probing the degree of chemical mixing among network modifiers, because it provides unique information on the nature of cation distribution around the non-bridging oxygens (NBOs, e.g., Na-O-Si) as well as the bridging oxygens (BOs, e.g., Si-O-Si) (e.g., Farnan et al., 1992; Florian et al., 1996; Lee et al., 2003; Lee and Stebbins, 2003; Lee and Sung, 2008; Park and Lee, 2012, 2014; Stebbins et al., 1997). Table 4.1 summarizes the results of previous ^{17}O NMR studies on the distribution of cations in various mixed-cation silicate glasses. Briefly, a pioneering ^{17}O dynamic angle spinning (DAS) study on K-Mg silicate glasses demonstrated the deviation from randomness in K-Mg mixing around the NBOs (Farnan et al., 1992).

Table 4.1. Order/disorder of cation distribution in various mixed-cation silicate glasses.

Cation-cation	The difference in ionic radius (Å)	Cation distribution	Method	Ref.
Li-Ba	0.59	preference for Ba-NBO or dissimilar pairs	^{17}O 3QMAS NMR	Current study
Ba-Na	0.33	preference for Ba-NBO	^{17}O 3QMAS NMR	(Lee et al., 2003)
Ba-Mg	0.63	strong preference for Ba-NBO	^{17}O 3QMAS NMR	(Lee et al., 2003)
Na-Ca	0.02	preference for Ca-NBO or dissimilar pairs	^{17}O 3QMAS NMR	(Lee and Stebbins, 2003)
Na-Ca in CNAS	0.02	preference for Ca-NBO or dissimilar pairs	^{17}O 3QMAS NMR	(Lee and Sung, 2008)
K-Mg	0.66	preference for Mg-NBO	^{17}O 3QMAS NMR	(Allwardt and Stebbins, 2004)
Ca-Mg in CMAS	0.28	preferential partitioning of Ca into NBO or unmixing between Ca-NBO and Mg-NBO	^{17}O 3QMAS NMR	(Park and Lee, 2012)
Ca-Mg in CMNAS	0.28	preferential partitioning of Ca into NBO or unmixing between Ca-NBO and Mg-NBO	^{17}O 3QMAS NMR	(Park and Lee, 2014)
Ca-Mg	0.28	random	^{17}O 3QMAS NMR	(Allwardt and Stebbins, 2004)
Na-K	0.36	random	^{17}O DAS NMR	(Florian et al., 1996)
Ca-Ba	0.35	random	^{17}O 3QMAS NMR	(Stebbins et al., 1997)
Li-Na	0.23	random	^{23}Na and ^{7}Li SEDOR NMR	(Gee and Eckert, 1996)

A subsequent ^{17}O DAS NMR study of K-Na silicate glasses suggested that K^+ and Na^+ are likely to be distributed randomly around the NBOs (Florian et al., 1996). A ^{17}O triple-quantum magic angle spinning (3QMAS) NMR study of Ca-Ba silicate glasses suggested a random mixing of Ba^{2+} and Ca^{2+} (Stebbins et al., 1997). In contrast, the NBOs in Ba-Mg silicate glasses revealed the presence of only two dominant types of NBOs, namely, Ba-NBO and the NBO with a Ba^+ and two Mg^{2+}, indicating a certain degree of structural ordering (Lee et al., 2003). Studies on Ba-Na and Ca-Na silicate glasses showed the prevalence of the dissimilar pairs [{Ba, Na}-NBO and {Ca, Na}-NBO], implying extensive mixing between those cations toward a chemical ordering (Lee et al., 2003; Lee and Stebbins, 2003). A ^{17}O 3QMAS study of K-Mg silicate glasses revealed that these glasses contain mostly Mg-NBO while the K^+ has proximity toward the BO (Allwardt and Stebbins, 2004). The non-random distribution of cations around the NBO and the BO has also been observed in complex, multi-component silicate glasses: in Ca-Na, Ca-Mg, and Ca-Mg-Na aluminosilicate glasses, Ca^{2+} and Mg^{2+} tends to be preferentially partitioned into the NBOs with the highlighted proximity of Na^+ to the BOs (Lee and Sung, 2008; Park and Lee, 2012, 2014).

While the preferential proximity between the network-modifying cations and the diverse oxygen species (e.g., BOs and NBOs) is suggested to be controlled by the differences in nature of non-network cations (Lee et al., 2003), the effects of the difference in the ionic radii on chemical ordering in mixed-cation silicate glasses remain to be fully understood. Whereas previous studies on Ba-Mg (~0.63 Å) and K-Mg (~0.66 Å) silicate glasses may address the effect of the ionic radii on the degree of cation mixing, the observed non-randomness in these glasses is attributable to the distinct

nature of Mg^{2+} (i.e., strong affinity between Mg^{2+} and NBOs), rather than the difference in ionic radii on mixing between these cations (Lee et al., 2016). Thus, in order to establish the effects of the difference in the ionic radii on chemical ordering, study of other mixed-cation silicate glasses with a larger difference in ironic radii has been anticipated. In this study, we chose Li-Ba silicate glasses, in which the difference in the ionic radii of network-modifying cations is significant (Li^{+}: 0.76 Å, Ba^{2+}: 1.35 Å, the difference in the ionic radii among cations is ~0.59 Å). Li-Ba silicate glasses also show the significant difference in the isotropic chemical shift (δ_{iso}) (~110 ppm) between Li-NBO [Li-O-$^{[4]}$Si in $Li_2Si_2O_5$ glass with δ_{iso} of ~42 ppm] (Lee et al., 2003; Maekawa et al., 1996; Timken et al., 1987) and Ba-NBO [Ba-O-$^{[4]}$Si with δ_{iso} of ~151 ppm in $BaSi_2O_5$ glass] (Lee et al., 2003; Maekawa et al., 1996; Timken et al., 1987) (see Figure 4.1), and thus the difference in peak positions, enabling robust estimation of the degree of disorder. Furthermore, Li-Ba oxide glasses also find wide application as energy and battery materials: while crystalline Li oxides and silicates have been used as Li-ion conductor materials (e.g., Nytén et al., 2005; Thangadurai and Weppner, 2005), a recent study suggested that amorphous Li-bearing oxides pose a potential promise as a component for high-capacity cathode materials for rechargeable Li-ion batteries (Afyon et al., 2014). Li-bearing glass-ceramics have also been used as solid-state electrolytes in Li batteries with high power densities (Ren et al., 2015; Xu et al., 2007). Glass electrolytes have advantages such as isotropic conductivity and a lack of grain boundaries when compared to crystal electrolytes (Dudney, 2003). Thus, probing the atomic structure of Li-bearing silicate glasses provides atomic insights into the properties of these glasses with potential applications as cathode materials and electrolytes in batteries. Along with the oxygen environments, the atomic environments around Li

can be effective in exploring the mixing behavior of Li-Ba silicate glasses. The ^{7}Li NMR techniques have been used to probe the atomic structures (coordination number) and Li-diffusivity (and/or mobility) of Li-bearing silicate glasses (e.g., Alam et al., 2012; Ali et al., 1995; Dupree et al., 1990; Sen et al., 1996; Stebbins, 1998; Xu and Stebbins, 1995) and batteries (e.g., Bottke et al., 2014; Grey and Lee, 2003; Indris et al., 2012; Lee et al., 2004; Tucker et al., 2002; Wohlmuth et al., 2015). Particularly, ^{7}Li spin-lattice relaxation times (T_1) of a mixed-cation glass ($LiBa_{0.5}Si_2O_5$) and a single alkali glass ($Li_2Si_2O_5$) with variable temperature conditions revealed that the mean barrier height for Li diffusion was higher in the case of the Li-Ba silicate glass than for the pure Li-silicate glass, consistent with the mixed-cation effect (Sen et al., 1996). Whereas such a variation in mobility with composition implies a certain degree of Li-Ba ordering in the glasses, the detailed atomic structures around Li and the extent of Li-Ba disorder in the Li-Ba silicate glasses are not currently available.

In this study, we explore the degree of chemical ordering and thus Li-Ba mixing behaviors, and Li environments in Li-Ba silicate glasses with varying X_{BaO} using high-resolution multi-nuclear (^{17}O and ^{7}Li) solid-state NMR. Particularly, we report the first ^{17}O NMR spectra for the mixed Li-Ba silicate glasses, revealing their detailed NBO and BO environments. Taking into consideration all the available experimental results on the nature of cation distribution in mixed-cation silicate glasses, we discuss the effects of the difference in the ionic radii on the chemical ordering of those cations around NBO.

4.2. Experimental methods

4.2.1. Sample preparation

Mixed-cation Li-Ba disilicate glasses [$(Li_2O)_{1-x}(BaO)_x2SiO_2$] with varying X_{BaO} = BaO/(BaO+Li_2O) were synthesized from ^{17}O-enriched SiO_2 (20%), $BaCO_3$, and Li_2CO_3. ~0.2 wt% paramagnetic cobalt oxide was added to enhance the spin–lattice relaxation, and thus to reduce the total NMR collection time. The mixtures were decarbonated and then melted in a Pt crucible for 1 h at 1600 °C in an Ar atmosphere. The melts were subsequently quenched to form homogenous glasses. Table 4.2 shows the nominal and chemical compositions of the Li-Ba silicate glasses estimated by inductively coupled plasma atomic emission spectroscopy (ICP-AES). Because SiO_2 was removed prior to the ICP analysis (Park and Lee, 2012, 2014), only the Li_2O and BaO compositions were reported. The negligible weight loss during glass synthesis as well as the consistency in Li/Ba contents in the glasses indicates that the overall chemical compositions of the glasses are close to the nominal ones.

4.2.2. NMR spectroscopy

The ^{17}O NMR and ^{7}Li NMR spectra of the Li-Ba silicate glasses were collected using a Varian solid-state NMR 400 system (9.4 T) at Larmor frequencies of 54.23 MHz for ^{17}O and 155.6 MHz for ^{7}Li nuclides, respectively. The ^{17}O MAS and 3QMAS NMR spectra of the Li-Ba silicate glasses were collected using a 4 mm Doty double-resonance probe. The recycle delay for the ^{17}O MAS NMR analysis was 1 s. The radio frequency (*rf*) pulse length of 1.0 μs with the spinning speed of 14 kHz are used. During the ^{17}O 3QMAS NMR experiments, a fast-amplitude modulation (FAM)-based shifted-echo

Table 4.2 Nominal compositions and ICP analysis results for Li-Ba silicate glasses. X_{BaO} is the BaO/(BaO+Li_2O) mole fraction.

X_{BaO}	Nominal composition (mol%)		
	Li_2O	BaO	SiO_2
0	33.3	0.0	66.7
0.25	25.0	8.3	66.7
0.50	16.7	16.7	66.7
0.75	8.3	25.0	66.7

X_{BaO}	Nominal composition (mol%)		ICP analysis (mol%)	
	Li_2O	BaO	Li_2O	BaO
0	100.0	0.0		
0.25	75.0	25.0	74.0	26.0
0.50	50.0	50.0	48.0	52.0
0.75	25.0	75.0	23.0	77.0

pulse sequence was used; it consists of a hard pulse with a duration of 4.5 μs for multiple-quantum excitation, subsequent 1.1 μs pulses for single-quantum reconversion, and a soft pulse of approximately 20 μs for the Li-Ba glasses (Lee and Stebbins, 2006). An echo delay and the recycle delay are 500 μs, and 1 s, respectively. Approximately 60–90 free-induction decay scans were made to construct the two-dimensional (2D) ^{17}O 3QMAS NMR spectra of the Li-Ba silicate glasses. The ^{17}O 3QMAS NMR spectra were referenced to external tap water. The ^{7}Li MAS NMR spectra were collected using a 3.2 mm Varian double-resonance probe, with a recycle delay of 1 s, a pulse length of 0.5 μs. Spinning speed of 12, 15, and 18 kHz are used to explore the effect of spinning speed on ^{7}Li-^{7}Li dipolar coupling. Negligible difference in the spectra with varying spinning speed was observed. All the spectra were referenced to a 1M LiCl solution.

4.3. Results and discussion

4.3.1. The NBO and BO environments in Li-Ba silicate glasses: ^{17}O MAS and 3QMAS NMR results

The structurally relevant NMR parameters [i.e., δ_{iso} and the quadrupolar coupling constant (C_q)] of the NBOs vary with the local atomic configurations, symmetry and thus the extent of structural distortion around target nuclides (Baltisberger et al., 1996; Ghose and Tsang, 1973). For instance, the ^{17}O δ_{iso} of BOs in Na silicate glasses increases with an increase in the Si-O bond length (Angeli et al., 2011). Those of NBOs and BOs in crystalline metasilicate with varying types of network forming cations (i.e., $MgSiO_3$, $CaMgSi_2O_6$, $CaSiO_3$, $SrSiO_3$, and $BaSiO_3$) also increase with increasing cation radius (Timken et al., 1987). The ^{17}O C_q of NBOs in the silicate crystals tends to increase with increasing electronegativity of network modifying cations

(Timken et al., 1987). Particularly, figure 4.1 shows the trend between δ_{iso} and C_q values of diverse NBOs in silicate glasses (Angeli et al., 2011; Lee, 2004b; Lee et al., 2003; Lee and Stebbins, 2003; Maekawa et al., 1996; Xue et al., 1994) where Li-NBO (Li-O-Si) and Ba-NBO (Ba-O-Si) show one of the largest differences in δ_{iso} and C_q values among the diverse NBO configurations in the silicate glasses. This results in a substantial peak separation in both ^{17}O 1D and 2D NMR spectra, enabling robust estimation of the effects of cation radii on the degree of inter-mixing between network modifiers.

Figure 4.2 shows the ^{17}O MAS NMR spectra of the Li-Ba silicate glasses $\{(BaO)_x(Li_2O)_{1-x}2SiO_2$ with X_{BaO} [=BaO/(BaO+Li_2O)]}, revealing partially resolved Si-O-Si (BO) as well as Li-O-Si (~31 ppm), Ba-O-Si (~130 ppm), and {Li, Ba}-O-Si (ranging from ~40 to ~120 ppm). The ^{17}O MAS spectrum of endmember $Li_2Si_2O_5$ glass (X_{BaO} = 0) shows partially resolved Li-O-Si and Si-O-Si peaks. Because of the larger difference in peak positions for Ba-NBO and Li-NBO, the spectra of the Li-Ba silicate glass with X_{BaO} = 0.75, 0.50, and 0.25 show a broad peak that results from the overlapping of Si-O-Si and the NBOs [Li-O-Si, Ba-O-Si, and mixed {Li, Ba}-O-Si], as labeled. While the width of the mixed NBO peaks depends mainly on the multiple configurations of the NBOs with increasing X_{BaO}, Li-O-Si exhibits a much narrower chemical shift distribution (and thus well-defined structural environments) than Ba-O-Si. This indicates a lower degree of Li configurational disorder around NBO. The intensity of the Li-O-Si peak decreases, while that of the mixed NBO peak increases with increasing X_{BaO}.

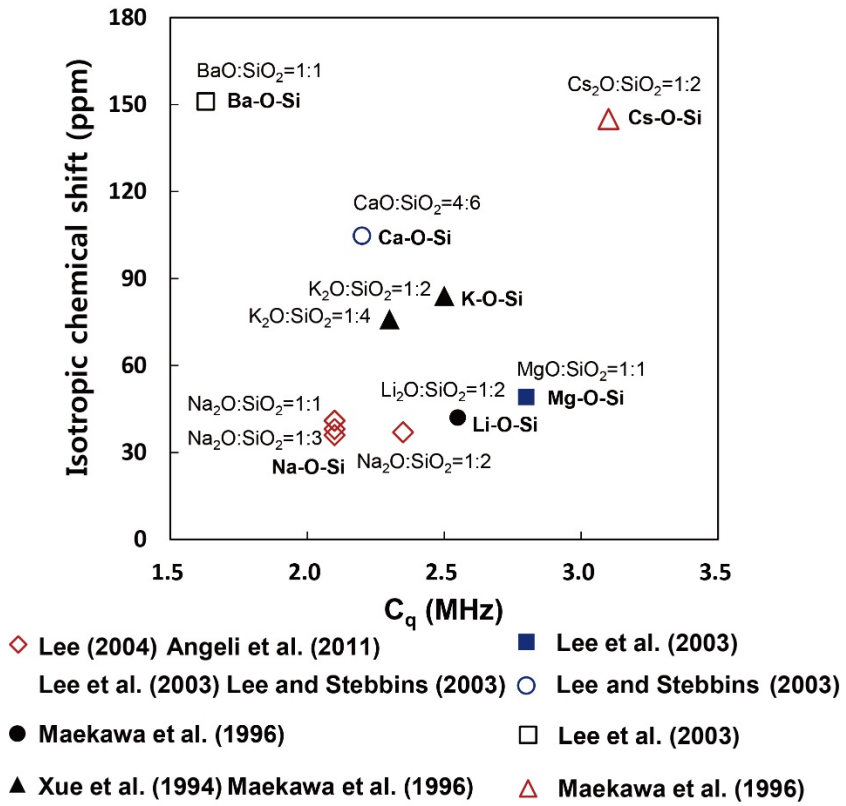

Figure 4.1. Variations in the isotropic chemical shift (δ_{iso}) and quadrupolar coupling constant (C_q) of NBOs in the ^{17}O 3QMAS NMR spectra of silicate glasses (Angeli et al., 2011; Lee, 2004b; Lee et al., 2003; Lee and Stebbins, 2000b, 2003; Maekawa et al., 1996; Timken et al., 1987; Xue et al., 1994).

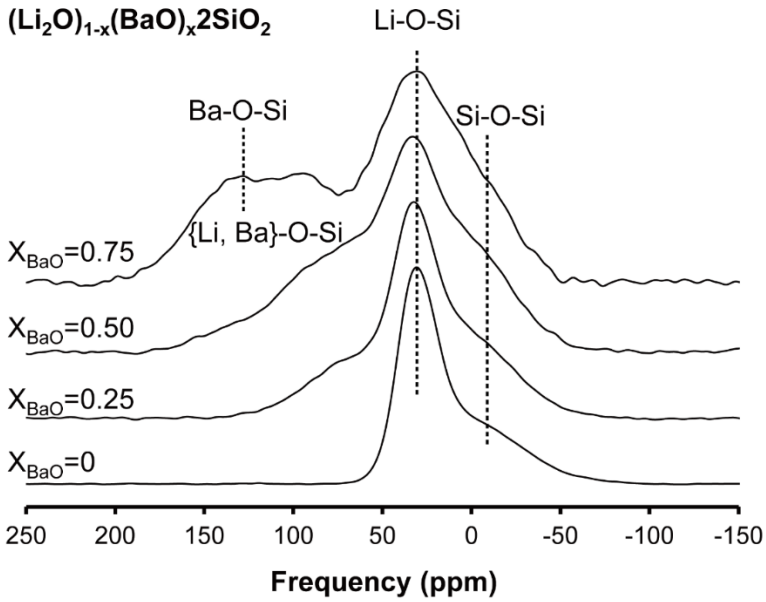

Figure 4.2. ^{17}O MAS NMR spectra of Li-Ba silicate glasses with varying X_{BaO} [BaO/(Li_2O+BaO)] at 9.4 T.

The noticeable intensity of the mixed NBO peaks and their evolution with composition demonstrate an extensive mixing between Li^+ and Ba^{2+} around the NBO.

Figure 4.3 shows the ^{17}O 3QMAS NMR spectra of the Li-Ba silicate glasses; the Li–O–Si, {Li, Ba}-O-Si, Ba-O-Si, and Si–O–Si peaks are better resolved. The peak assignments of the BOs and NBOs in the ^{17}O 3QMAS NMR spectra are based on previous studies on crystalline and amorphous Li and Ba silicates (Lee et al., 2016; Lee and Stebbins, 2000; Maekawa et al., 1996; Timken et al., 1987). In ^{17}O 3QMAS NMR spectrum for $Li_2Si_2O_5$ glass, the Li-O-Si (~-29 ppm in the isotropic dimension, and ~31 ppm in the MAS dimension) and Si-O-Si (~-46 ppm in the isotropic dimension) are completely resolved. The oxygen clusters at ~40–120 ppm in the MAS dimension stem from the mixed NBOs with varying coordination environments (i.e., $^1Li^2Ba$-NBO and $^2Li^1Ba$-NBO) as also expected from the ^{17}O MAS NMR spectra (figure 4.2). These mixed NBO peaks are observed for all the glasses at intermediate compositions (X_{BaO} = 0.25, 0.50, and 0.75). While the Ba-O-Si peaks overlap with those of {Li, Ba}-O-Si yet the peak due to Li-O-Si are fully resolved. The maximum of the mixed NBO peak in the isotropic dimension moves to that of Ba-NBO with X_{BaO}, suggesting that the fractions of $^1Li^2Ba$-NBO and Ba-NBO increase with increasing X_{BaO}. The intensity of the Li-O-Si peak apparently decreases while that of the Ba-O-Si peak increases with increasing X_{BaO}. The current result confirms a preference to form Li-Ba pairs around NBO in the glasses. Figure 4.4 shows the total isotropic projection (the sum of the peaks on the 3QMAS dimension) of the ^{17}O 3QMAS NMR spectra for the Li-Ba silicate glasses. The intensity of the Li-O-Si peak decreases markedly while that of the Ba-O-Si peak increases with increasing X_{BaO}. The presence of mixed NBO peak with varying configuration is also

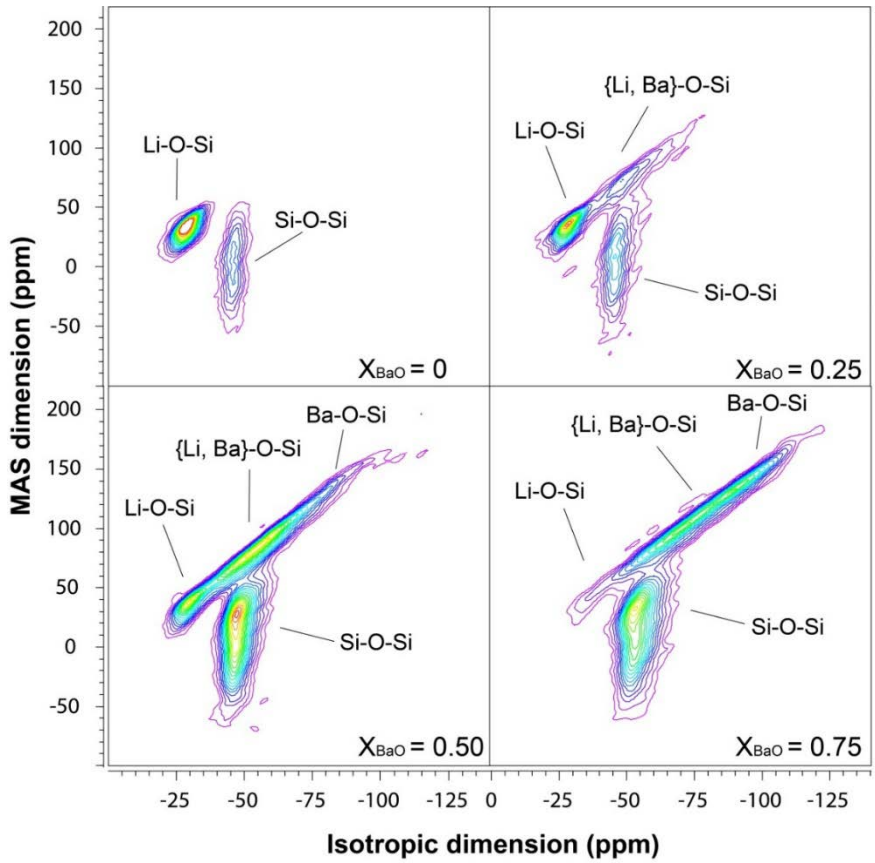

Figure 4.3. ^{17}O 3QMAS NMR spectra of Li-Ba silicate glasses with varying X_{BaO} [BaO/(Li$_2$O+BaO)] at 9.4 T. The contour lines are drawn at 5% intervals for relative intensities of 7–97%, with added lines at 5%.

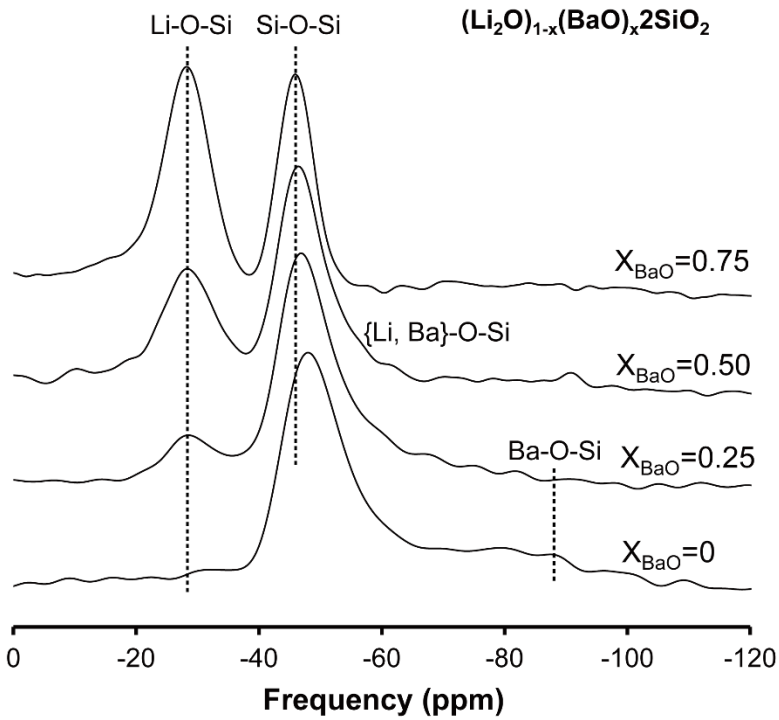

Figure 4.4. Total isotropic projection of the ^{17}O 3QMAS NMR spectra for Li-Ba silicate glasses with varying X_{BaO} [BaO/(Li_2O+BaO)] at 9.4 T.

prevalent, confirming the formation of Li-Ba pair near NBO at the expense of Li-NBO.

Although the narrow Li-O-Si peak is separated from the other mixed peaks, the quantitative information on the population of the NBO peak for these glasses in the 2D 3QMAS spectrum is not trivial because of several well-known uncertainties, particularly, uneven excitation of the oxygen peaks with distinct C_q values (Amoureux et al., 1996; Frydman and Harwood, 1995). For example, the fraction of Si-O-Si (with C_q of ~ 5 MHz) is expected to be underestimated while that of NBO (with C_q of ~ 2.5 MHz) is overestimated. Furthermore, the intensity is also dependent on the *rf* power of the pulses. Figure 4.5A shows ^{17}O 3QMAS NMR spectra for Li-Ba silicate glass at X_{BaO} = 0.25 with varying *rf* strength (~80 kHz and ~35 kHz) where the changes in the peak intensity of each oxygen site with *rf* strength is demonstrated: the fraction of Si-O-Si peak is larger at high *rf* strength (~80 kHz) than is at low *rf* strength (~35 kHz) while that of NBOs (Li-O-Si and {Li, Ba}-NBO) is smaller at high *rf* strength. With decreasing *rf* field strength, the overall signal intensity also decreases. The larger C_q sites (e.g., 5 MHz for Si-O-Si) are also selectively suppressed at low *rf* field strength. Figure 4.5B shows the total isotropic projections of the ^{17}O 3QMAS NMR spectra for Li-Ba silicate glass at X_{BaO} = 0.25. The green area shows Li-O-Si, the red area shows Si-O-Si, and the blue area shows {Li, Ba}-O-Si. These spectra confirm that the Si-O-Si peak is more effected excited at higher *rf* fields power (~80 kHz).

Taking into consideration the non-quantitative representation of the peak intensity in the 2D NMR spectra with *rf* field strength and C_q, the quantitative fractions of oxygen sites were obtained from the simulation of

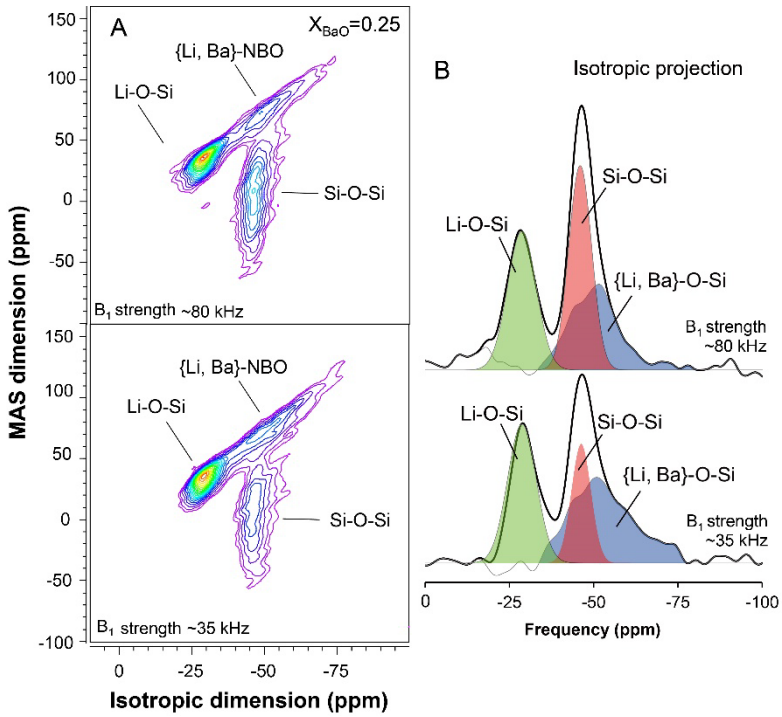

Figure 4.5. (A) ^{17}O 3QMAS NMR spectra of Li-Ba silicate glass at X_{BaO} = 0.25 with varying *rf* field strength (B_1 strength). (B) Total isotropic projection of the ^{17}O 3QMAS NMR spectra for Li-Ba silicate glass at X_{BaO} = 0.25 with varying *rf* field strength. The green area shows Li-O-Si, the red area shows Si-O-Si, and the blue area shows {Li, Ba}-O-Si.

^{17}O MAS NMR spectra that provide quantitative information. However, the information of peak positions and widths were obtained from 2D NMR spectra. The ^{17}O MAS NMR spectra with varying Ba/Li ratio were simulated using a Si-O-Si and four NBO sites (^{4}Li, ^{2}Li^{1}Ba, ^{1}Li^{2}Ba, and ^{3}Ba) (Lee et al., 2003; Lee and Stebbins, 2003). Because coordination numbers of the NBO and Li^+ and Ba^{2+} are not fully understood, the choice of the four NBO peaks with distinct Li^+ and Ba^{2+} coordination environment can be somewhat arbitrary [e.g., 4 Li atoms around NBO for the Li-end member, ^{4}Li-O-Si vs. 3 Ba atoms around the NBO for the Ba-end member, ^{3}Ba-O-Si]. Despite the uncertainty, the purpose of the current simulation is to determine the relative intensity of the Li-O-Si peak from the 1D NMR spectra and compare its fraction with predicted peak intensities based on either a random mixing or chemical order. We used four Gaussian functions to represent the four NBO environments and two Gaussian functions to represent the Si-O-Si. Because the position of the ^{4}Li-O-Si peak in the MAS dimension (i.e., the position in the ^{17}O MAS NMR spectrum) in the 2D spectrum is well constrained (Figure 4.2) and does not change with varying X_{BaO}, and thus its peak position is fixed at 31 ppm. The initial peak position of ^{3}Ba-O-Si is obtained from previous ^{17}O MAS NMR study for $BaSi_2O_5$ glass (130 ppm) (Lee et al., 2003) and is also based on results of several trial simulations. The peak positions of ^{3}Ba-O-Si move toward higher frequency (larger chemical shift, ~136 ppm) with increasing X_{BaO}. The FWHM of ^{3}Ba-O-Si (45 ppm) are obtained from previous ^{17}O MAS NMR study for $BaSi_2O_5$ glass with small ranges of variation (4 ppm) allowed for compositional effects (Lee et al., 2003). Initial peak positions of the mixed NBO peaks were assumed to be the statistical average of the endmember peaks ^{4}Li-O-Si (31 ppm) and ^{3}Ba-O-Si (130 ppm) peak, and thus ^{2}Li^{1}Ba-NBO: ~64 ppm [=31+(1/3)*(130-31)], ^{1}Li^{2}Ba-NBO: ~97

ppm [=31+(2/3)*(130-31)]. These are allowed to vary during simulations. The FWHM of ^{2}Li^{1}Ba-NBO and ^{1}Li^{2}Ba-NBO peaks are set to be 30 ppm, again based on results of several trial simulations. The quadrupolar peak shape of Si-O-Si peak is simulated with two Gaussian functions. The initial Si-O-Si peak positions are obtained from 2D 3QMAS NMR spectrum of $Li_2Si_2O_5$ and move toward higher frequency with increasing X_{BaO}, consistent with variation of Si-O-Si peak positions in the MAS projection of the 2D ^{17}O 3QMAS NMR spectra (which is similar to 1D MAS NMR spectra). The FWHM of two Gaussian peaks for Si-O-Si are set to be 65 and 30 ppm, respectively, which reproduces the major quadrupolar patterns for BO site (Lee et al., 2003; Lee and Stebbins, 2003). Table 4.3 lists the final simulation parameters for each NBO and BO sites for ^{17}O MAS NMR spectra of Li-Ba silicate glasses. Due to the aforementioned uncertainty, the simulation results for these peaks are not unique. Nevertheless, it should also be noted that, during the simulation, the ratio of the BOs and NBOs [NBO/(NBO+BO)] is fixed to be 0.4, consistent with the nominal composition of the glasses studied here. It also provides a quantitative fraction of Li-O-Si peak among the NBOs. Figure 4.6 shows the simulation results for the ^{17}O MAS NMR spectra of the Li-Ba silicate glasses with varying X_{BaO} where the decrease in Li-NBO with increasing X_{BaO} is demonstrated.

Figure 4.7 shows the estimated fraction of Li-O-Si with varying X_{Ba} [=Ba/(Li+Ba)]. The extent of Li-Ba disorder is expected to vary from one extreme case of clustering of similar pairs (i.e., formation of Ba-rich and Li-rich domains) through random distributions to the other extreme of chemical ordering where the formation of dissimilar pairs are prevalent. The black solid line indicates the fraction of Li-O-Si based on a random distribution of

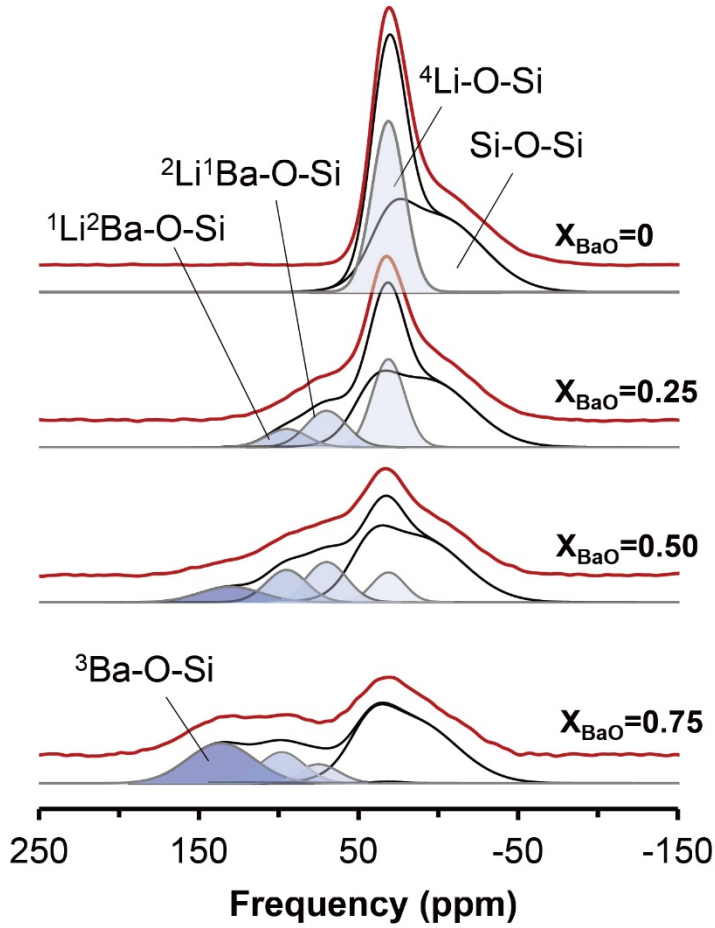

Figure 4.6. Simulation results of the ^{17}O MAS NMR spectra of Li-Ba silicate glasses with varying X_{BaO} [BaO/(Li$_2$O+BaO)]. The red and black lines represent the experimental and simulation results, respectively.

Table 4.3. Simulation parameters and results for ^{17}O MAS NMR spectra for Li-Ba silicate glasses.

Composition	Oxygen species		Peak position (ppm)	FWHM (ppm)	Intensity
X_{BaO}=0	‡NBO	^{4}Li-O-Si	31	24	0.66
	†BO	Si-O-Si	0	65	0.29
			30	30	0.18
X_{BaO}=0.25	‡NBO	^{4}Li-O-Si	31	24	0.34
		^{2}Li^{1}Ba-NBO	70	30	0.14
		^{1}Li^{2}Ba-NBO	95	30	0.07
	†BO	Si-O-Si	7	65	0.26
			40	30	0.15
X_{BaO}=0.50	‡NBO	^{4}Li-O-Si	31	24	0.12
		^{2}Li^{1}Ba-NBO	70	30	0.16
		^{1}Li^{2}Ba-NBO	95	30	0.13
		^{3}Ba-O-Si	130	45	0.06
	†BO	Si-O-Si	12	65	0.25
			42	30	0.14
X_{BaO}=0.75	‡NBO	^{4}Li-O-Si	31	24	0.0006
		^{2}Li^{1}Ba-NBO	75	30	0.073
		^{1}Li^{2}Ba-NBO	98	33	0.12
		^{3}Ba-O-Si	136	49	0.16
	†BO	Si-O-Si	17	65	0.25
			42	30	0.12

‡ NBO are simulated with four Gaussian functions assumed that there are four NBO sites (^{4}Li, ^{2}Li^{1}Ba, ^{1}Li^{2}Ba, and ^{3}Ba). The choice of types of NBO peaks is somewhat arbitrary.

† BO is simulated with two Gaussian functions due to second-order quadrupolar broadening.

Notes: The position and width of the Li-O-Si (NBO) peak are relatively well constrained by the spectrum for $Li_2Si_2O_5$. The peak position and FWHM of mixed NBO peaks are set based on results of several trial simulations.

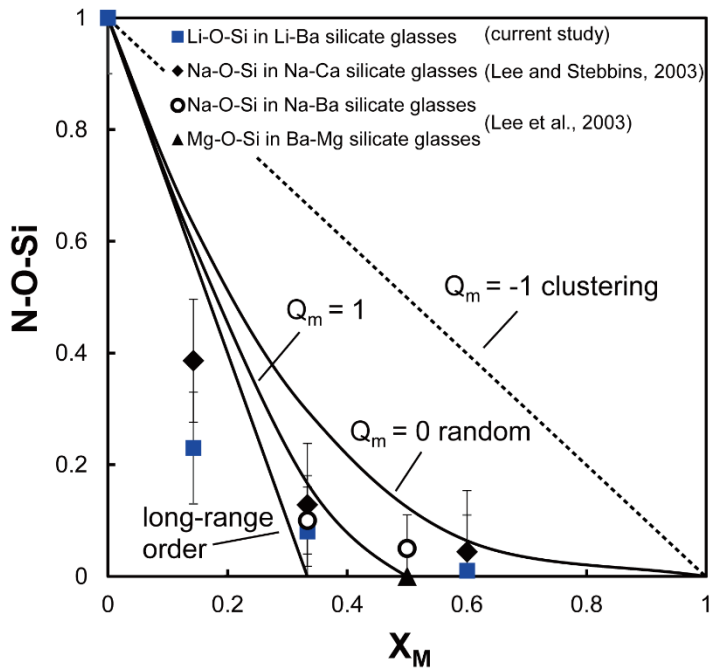

Figure 4.7. Fraction of *N*-O-Si (N = Li^+, Na^+, and Mg^+) as determined from the simulation results by varying X_M [X_M=M/(M+N), M = Ba^{2+} and Ca^{2+}]. The black diamonds indicate the Na-O-Si fractions for Na-Ca silicate glasses (Lee and Stebbins, 2003); the open circles present the fractions of Na-O-Si for Ba-Na silicate glasses; the black triangle indicates the Mg-O-Si fraction for a Ba-Mg silicate glass (Lee et al., 2003); and the blue squares indicate the Li-O-Si fractions for Li-Ba silicate glasses (current study).

Li^+ and Ba^{2+} around the NBOs: the estimated fractions of each NBO environment at X_{Ba} = 0.33 are 30% [^{4}Li-NBO, $(1-x)^3$], 44% [^{2}Li^{1}Ba-NBO, $3x(1-x)^2$], 22% [^{1}Li^{2}Ba-NBO $3x^2(1-x)$], and 4%[^{3}Ba-NBO, x^3] (Kelsey et al., 2008). The dashed black line indicates the fraction of Li-O-Si when the Li^+ and Ba^{2+} are phase separated. The simulation results show that the fraction of Li-O-Si decreases with increasing X_{BaO} and is less than that predicted by the random distribution of Li^+ and Ba^{2+}. This indicates a prevalence of the dissimilar Li-Ba pair around the NBO. Figure 4.7 also shows the predicted fraction of NBO with varying extent of cation distribution (Q_m) in diverse mixed-cation (*M-N*) silicate glasses. Q_m was defined previously and varies from chemical short-range order with preference to form *M-N* pairs around NBO (Q_m=1), random distributions of *M-N* (Q_m=0), to phase separation among cations (Q_m=-1) (Lee et al., 2003). Additional long-range order (LRO) in the cation distribution refers to the situation where the *N-M* pair extends beyond nearest-neighbor interactions and *N*-O-Si fraction can be expressed as $1-3X_M$ (Lee et al., 2003). The fractions of Li-O-Si (in Li-Ba silicate glasses) and Na-O-Si (in Na-Ba silicate glasses) are much less than would be predicted by a random distribution of mixed cations. Furthermore, these fractions are less than those predicted from LRO partly due to the NBO preference to Ba over Li. It should be note that the fractions of Li-NBO in the Li-Ba silicate glasses are somewhat less than those of Na-NBO in Na-Ba silicate glasses. This indicates a larger chemical alkali-Ba ordering in the former, revealing the effect of difference in ionic radius of the cation on a hierarchy in the degree of chemical order for various network modifying cations in the glasses (see below for further discussion).

4.3.2. Li environments in Li-Ba silicate glasses: ^{7}Li MAS NMR results

Figure 4.8A shows the ^{7}Li MAS NMR spectra for the Li-Ba silicate glasses with varying X_{BaO}. The NMR peak is characterized with the Lorentzian broadening (and thus the life-time broadening), suggesting the substantial mobility of the Li^{+} in the glasses at room temperature. The peak position and width of ^{7}Li MAS NMR spectra vary with X_{BaO}. While a previous ^{7}Li MAS NMR study for Li-Na disilicate glasses with varying Li contents does not show the changes in peak position with varying Li/Na contents (at constant peak maximum of ~0.4 ppm) (Ali et al., 1995), the peak maximum in the Li-Ba disilicate glasses increases with increasing X_{BaO} from 0 ppm (for X_{BaO} = 0) to 0.3 ppm (for X_{BaO} = 0.75) (Figure 4.8B). Because ^{7}Li δ_{iso} of Li site tends to decrease with increasing coordination number (and thus Li-O distance) (Alam et al., 2012; Stebbins, 1998; Xu and Stebbins, 1995), the trend shown in the ^{7}Li MAS NMR spectra for Li-Ba silicate glasses suggests that the average Li coordination number in the mixed-cation silicate glasses may decrease slightly with increasing X_{BaO}. The result also indicates a minor decrease in Li-O distance with increasing X_{BaO}, potentially leading to an increased activation energy barrier for Li diffusion. Figure 4.8C shows the ^{7}Li MAS NMR spectra for Li disilicate glasses with varying spinning speed (12, 15, and 18 kHz) where a slight (though minor) change in peak width was observed. Therefore, the peak broadening in the ^{7}Li MAS NMR spectra in Li-Ba silicate glasses is also controlled by the ^{7}Li-^{7}Li dipolar interaction as well as the Li mobility while both mechanisms may prevail. Taking into consideration the pronounced Li mobility at room temperature and the sample spinning-induced increases in temperature, the peak width could be partly affected by changes in the dynamics due to the frictional

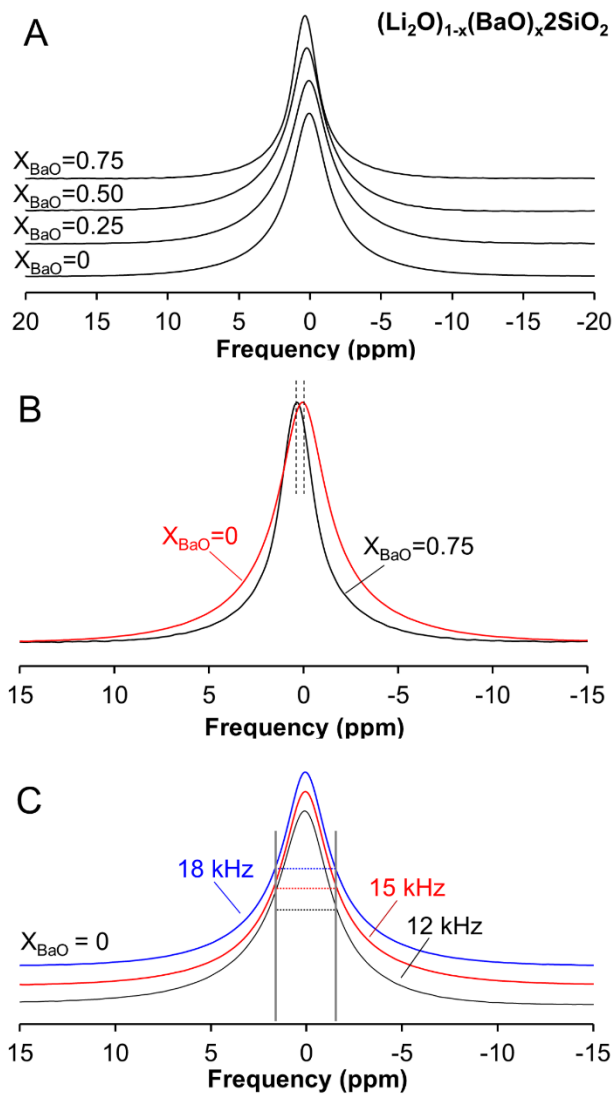

Figure 4.8. (A) ^{7}Li MAS NMR spectra for of Li-Ba silicate glasses with varying X_{BaO} [BaO/(Li_2O+BaO)] at 9.4 T. (B) Variation of the peak maximums and peak widths of the ^{7}Li MAS NMR spectra of Li-Ba silicate glasses (X_{BaO} = 0 and 0.75). (C) ^{7}Li MAS NMR spectra for $Li_2Si_2O_5$ glasses with varying spinning speed (12, 15, and 18 kHz).

heating during magic angle spinning (Doty et al., 1998; Elbayed et al., 2005; Kim and Lee, 2013). Despite the complexity, the systematic variation of peak position in the Li-Ba glasses with composition also confirms a substantial mixing between Li^+ and Ba^{2+}, consistent with ^{17}O NMR results and further suggests that Li mobility may vary with increasing Ba content.

Figure 4.9 shows that the FWHM of the ^7Li MAS NMR spectra for the Li-Ba silicate glasses show positive deviation from linearity: the FWHM increases from 3.3 ppm (X_{BaO} = 0) to 3.6 ppm (X_{BaO} = 0.25). However, it decreases with a further increase in X_{BaO} to 2.2 ppm (X_{BaO} = 0.75). Note that the FWHM of ^7Li MAS NMR spectra for Li-Na silicate glasses linearly decreases with decreasing Li contents mainly due to an expected decrease in the dipolar coupling by an increase in distance between ^7Li's (Ali et al., 1995). The observed non-linear trend in Li-Ba silicate glasses indicates a complex effect of both Li mobility and magnitude of the dipolar coupling between ^7Li's in the Li-Ba glasses that are distinct from those of Li-Na silicate glasses. A slight increase in the peak with at intermediate composition in the Li-Ba silicate glasses implies a larger drop in the Li mobility than that in the Li-Na silicate glasses (see below for further discussion).

4.3.3. The extent of cation order, difference in cation radii, and transport properties

The observed atomic structures of the Li-Ba silicate glasses yield insights into the effect of difference ionic radii on the extent of mixing among network modifiers. The ^{17}O NMR results confirm a non-random distribution of Li^+ and Ba^{2+} around the NBOs characterized by the prevalence of the Li-

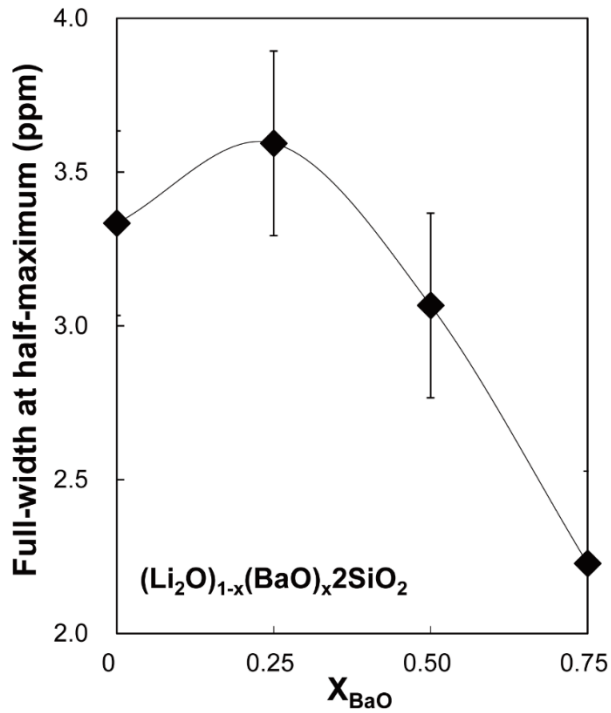

Figure 4.9. Full-width at half-maximum of the ^{7}Li MAS NMR spectra of Li-Ba silicate glasses with varying X_{BaO} [BaO/(Li_2O+BaO)] at 9.4 T. The error bars of ±0.3 ppm were estimated from the uncertainty in the sample composition, phasing of the NMR spectrum, and NMR processing conditions.

Ba pair due mainly to the substantial difference in their ionic radii (Δr = ~0.59 Å). This corroborates previous proposal where a chemical ordering becomes prevalent with a potential threshold Δr value of ~0.3 Å (e.g., Ba-Na and Ba-Mg) (Lee et al., 2003). As also shown in Table I, the mixing of two alkalis or two alkaline-earth elements with relatively similar cation field strength (c/r^2, where c and r are the charge and ionic radius of the cation) [e.g., Na (~0.96)-K (~0.53) and Ca (~2.00)-Ba (~1.10)] is likely to be random (Allwardt and Stebbins, 2004; Florian et al., 1996; Stebbins et al., 1997). Furthermore, when the mixing involves an alkali and an alkaline earth element (e.g., K-Mg and Ca-Na), chemical ordering between network modifiers seems to occur (Allwardt and Stebbins, 2004; Lee and Stebbins, 2003). The current results with Li-Ba silicate glasses allow us to conclude that the *greater* difference in the cation radii leads to an increased degree of chemical ordering. For instance, as shown in figure 4.7, the estimated Li-NBO fraction in the Li-Ba silicate glasses (Δr of ~0.59 Å) is less than Na-NBO in Na-Ba silicate glasses (Δr of ~0.33 Å), suggesting an increased Li-Ba ordering over Na-Ba in Na-Ba silicate glasses. While the origins of enhanced chemical ordering in Ba-Mg and K-Mg in the Mg-bearing silicate glasses have been somewhat obscured due to ambiguous structural role of Mg^{2+}, based on the current results, the difference in the ionic radii is the primary factor affecting the degree of chemical ordering in mixed-cation silicate glasses. A greater difference in the ionic radii may result in greater chemical ordering [e.g., K-Mg (~0.66 Å) ≈ Ba-Mg (~0.63 Å) ≈ Li-Ba (~0.59 Å) > Na-Ba (~0.33 Å) > Na-Ca (~0.02 Å)]. While the observed prevalence of Li-Ba pair is also stemming from the difference in charges of the cations, the degree of Li-Ba order is apparently larger than those of Na-Ca in the Na-Ca silicate glasses, indicating that the

steric effect appears to be dominant and thus the mixing behavior can be predicted mainly from the difference in the ionic radii.

The observed atomic structures of the Li-Ba silicate glasses also yielded atomistic insights into the Li-mobility. As demonstrated previously, the diffusivity of mixed-cation silicate glasses that shows a non-random distribution (towards a chemical order favoring dissimilar pair) of the network-modifying cation is lower than that of glasses with a random distribution (Lee et al., 2003). For example, a previous ^{17}O NMR studies on Na-K and Na-Ca silicate glasses suggested that the diffusivity of Na^+ in Na-Ca silicate glasses is lower than that in Na-K silicate glasses, because of the chemical ordering of the Na-Ca silicate glasses (Lee and Stebbins, 2003). It is also expected that the diffusivity of Li^+ in Li-Ba silicate glasses is smaller, owing to the enhanced chemical ordering, than that in Li-Na silicate glasses, in which the cations are randomly distributed around the NBOs (Gee and Eckert, 1996). This prediction is consistent with trend observed in ionic conductivity in Li-bearing silicate glasses: the ionic conductivity of the Li-Ba silicate glasses is smaller than that of Li-Na silicate glasses (Mazurin and Borisovskii, 1957).

4.4. Conclusions

We elucidated the structural details of the atomic configurations around O and Li atoms in Li-Ba silicate glasses and the nature of distribution of alkali-alkaline earth pairs, in which ionic radii are significantly different. The ^{17}O NMR spectra of the Li-Ba silicate glasses show that the fraction of Li-O-Si decreases with increasing X_{BaO} and is less than that predicted by a random distribution of Li^+ and Ba^{2+} around NBOs. These results

demonstrate a non-random distribution of Li^+ and Ba^+ into NBOs characterized by a prevalence of the dissimilar pair. The ^7Li MAS NMR spectra of the Li-Ba silicate glasses imply that the average Li coordination number and/or Li-O distance may decrease slightly with increasing X_{BaO}, leading to an increased activation energy barrier for Li diffusion. The current results allow us to propose the relationship between the chemical ordering and the difference in the ionic radii in mixed-cation silicate glasses. The larger difference in the ionic radii of the cations in mixed-cation silicate glasses leads to an increase in the degree of chemical ordering [e.g., K-Mg (~0.66 Å) ≈ Ba-Mg (~0.63 Å) ≈ Li-Ba (~0.59 Å) > Na-Ba (~0.33 Å) > Na-Ca (~0.02 Å)] and thus the degree of inter-mixing between network modifiers can be predicted mainly from the difference in the ionic radii. The results highlight the atomistic origins of transport properties of archetypal Li-Ba silicate glasses and can be potentially utilized to account for the complex Li-bearing oxide glasses with noble applications in amorphous ionic conductors, battery and related materials.

APPENDIX

3.A.1 Si environments in Li-Ba silicate glasses: ^{29}Si MAS NMR results

^{29}Si MAS NMR spectroscopy has been used to probe the Si environments in silicate glasses, such as the degree of polymerization (i.e., the abundance of Q^n species in silicate glasses; Q^n refers to a Si species with n bridging oxygens) (e.g., Grimmer et al., 1984; Maekawa et al., 1991; Martin et al., 1992; Stebbins, 1987). For example, the ^{29}Si MAS NMR spectra of lithium, sodium, and potassium silicate glasses have shown that the abundance of Q^3 decreases, whereas that of Q^2 and Q^4 increases with an increase in the cation field strength (charge/r^2; r is the ionic radius) of the

alkali metal for the same alkali oxide concentration. (Maekawa et al., 1991) That study reported that ~22% of Q^4, ~63% of Q^3, and ~15% of Q^2 were observed in $Li_2Si_2O_5$ while another ^{29}Si MAS NMR study of $Li_2Si_2O_5$ glass reported that ~11 % of Q^4, ~81% of Q^3, and ~8% of Q^2 were observed. (Grimmer et al., 1984) The differences in the fractions of the Q^n species observed in these studies stem from differences in the experimental conditions during the NMR experiments and/or the fitting parameters used. The former was performed at 4.7 T, while the latter was performed at 8.5 T. Further, the peak positions of Q^2, Q^3, and Q^4 in the former study were -102.7, -91.0, and -81.1 ppm, respectively, while those in latter study were -105.0, -90.5, and -78.5 ppm, respectively. In this study, we perform high-resolution ^{29}Si MAS NMR experiment for $Li_2Si_2O_5$ glass in order to determine the fractions of the Q^n species in the glass using high-resolution solid-state NMR and to elucidate the effects of the network-modifying cations on network polymerization in Li-Ba silicate glasses with varying compositions.

Figure 4.A1 shows the ^{29}Si MAS NMR spectra and fitting results for the Li-Ba silicate glasses. A single overlapped broad peak is observed for all the Li-Ba silicate glasses. The peak maximum decreases with increasing X_{BaO} from -90.6 ± 1.0 ppm for X_{BaO} = 0 to -92.1 ± 1.0 ppm for X_{BaO} = 0.25 and 0.50. It increases further to -90.6 ± 1.0 ppm for X_{BaO} = 0.75. The ^{29}Si MAS NMR spectra for the Li-Ba silicate glasses with varying X_{BaO} are simulated with three Gaussian functions corresponding to the Q^4, Q^3, and Q^2 species, respectively. The peak positions are set to -102.4 ± 1.0, -91.4 ± 1.0, and -82.1 ± 1.0 ppm for Q^4, Q^3, and Q^2 species, respectively. The FWHM is set to 13.3 ± 0.2, 12.2 ± 0.5, and 10.4 ± 0.5 for the Q^4, Q^3, and Q^2 species, respectively. The predicted fractions of Q^4, Q^3, and Q^2 for $Li_2Si_2O_5$ are 18 ± 1%, 64 ± 1%, and 18 ± 1%, respectively.

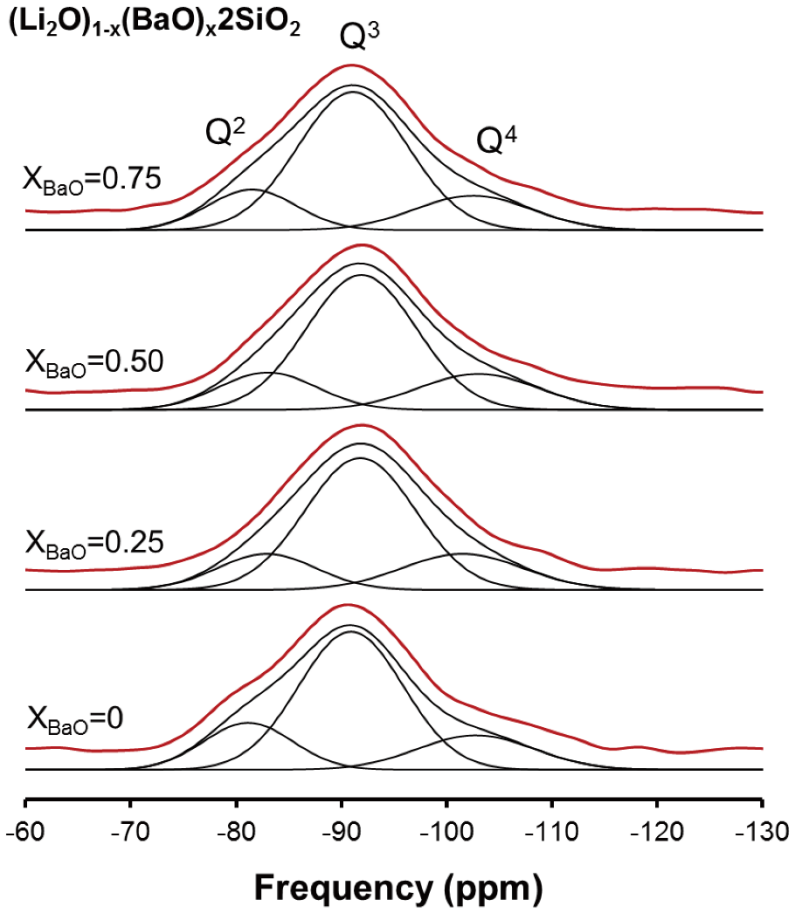

Figure 4.A1. ^{29}Si MAS NMR spectra and simulation results for Li-Ba silicate glasses with varying X_{BaO} [BaO/(Li_2O+BaO)] at 9.4 T.

Figure 4.A2 shows the fractions of the Q^n species with varying mole fractions of the network-modifying cations in the silicate glasses. The fractions of Q^2 and Q^3 increase with increasing M_2O (M=K, Na, Li) while that of Q^4 decreases; a previous ^{29}Si MAS NMR study on $Li_2Si_2O_5$ reported Q^4, Q^3, and Q^2 fractions of ~22%, 63%, and 15%, respectively. (Maekawa et al., 1991) While the predicted fraction of Q^4 (~22%) is higher than that of Q^2 (~15%) in the aforementioned study, (Maekawa et al., 1991) another ^{29}Si MAS NMR study on $Li_2Si_2O_5$ glass reported Q^4, Q^3, Q^2 fractions of 11%, 81%, and 8%, respectively. (Grimmer et al., 1984) The results of the simulation perform in this study show that the fraction of Q^4 (~18%) is similar to that of Q^2 (~18%). The differences in the fractions of the Q^n species in the aforementioned previous studies are probably owing to differences in the experimental conditions for the NMR analysis and/or the fitting parameters used, as mentioned above. The fitting results for the fractions of Q^n species may have significant uncertainties in the latter case. However, in spite of these uncertainties, the predicted fractions of the Q^n species suggest that the Q^n species in Li-Ba silicate glasses do not change significantly with X_{BaO}, suggesting that a change in X_{BaO} would not affect the environments of BO and thus the role of Li^+ and Ba^{2+}, the network-modifying cations.

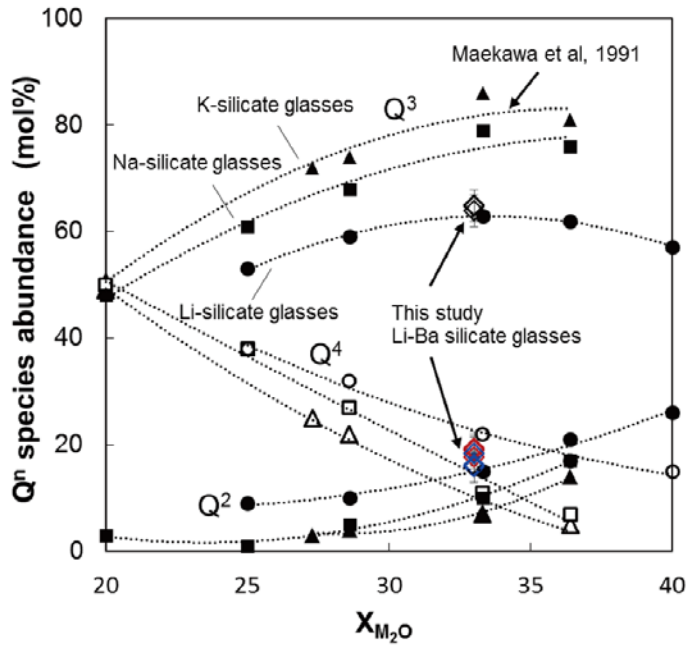

Figure 4.A2. Q^n distribution in Li, Na, K, and Li-Ba silicate glasses with varying M_2O (M refers to non-framework cation, Li^+, Na^+, K^+, and Li^++Ba^{2+}). Diamonds indicate the results in this study (black one is Q^3, blue one is Q^2 and red one is Q^4) and circles, squares, and triangles denote the results for previous study (Maekawa et al., 1991).

References

Afyon, S., Krumeich, F., Mensing, C., Borgschulte, A. and Nesper, R. (2014) New High Capacity Cathode Materials for Rechargeable Li-Ion Batteries: Vanadate-Borate Glasses. *Sci. Rep.* 4, 7113.

Alam, T.M., Jenkins, J.E., Bolintineanu, D.S., Stevens, M.J., Frischknecht, A.L., Buitrago, C.F., Winey, K.I., Opper, K.L. and Wagener, K.B. (2012) Heterogeneous Coordination Environments in Lithium-Neutralized Ionomers Identified Using ^{1}H and ^{7}Li MAS NMR. Materials 5, 1508.

Ali, F., Chadwick, A.V., Greaves, G.N., Jermy, M.C., Ngai, K.L. and Smith, M.E. (1995) Examination of the Mixed-Alkali Effect in (Li,Na) Disilicate Glasses by Nuclear Magnetic Resonance and Conductivity Measurements. *Solid State Nucl. Magn. Reson.* 5, 133-143.

Allwardt, J.R. and Stebbins, J.F. (2004) Ca-Mg and K-Mg Mixing around Non-Bridging O Atoms in Silicate Glasses: An Investigation Using ^{17}O MAS and 3QMAS NMR. *Am. Miner.* 89, 777-784.

Amma, S.-i., Lanagan, M.T., Kim, S.H. and Pantano, C.G. (2016) Ionic Conductivity in Sodium–Alkaline Earth–Aluminosilicate Glasses. *J. Amer. Ceram. Soc.*, n/a-n/a.

Amoureux, J.-P., Fernandez, C. and Frydman, L. (1996) Optimized multiple-quantum magic-angle spinning NMR experiments on half-integer quadrupoles. *Chem. Phys. Lett.* 259, 347-355.

Angeli, F., Villain, O., Schuller, S., Ispas, S. and Charpentier, T. (2011) Insight into Sodium Silicate Glass Structural Organization by Multinuclear NMR Combined with First-Principles Calculations. *Geochim. Cosmochim. Acta* 75, 2453-2469.

Baltisberger, J.H., Xu, Z., Stebbins, J.F., Wang, S.H. and Pines, A. (1996) Triple-Quantum Two-Dimensional ^{27}Al Magic-Angle Spinning Nuclear Magnetic Resonance Spectroscopic Study of Aluminosilicate and Aluminate Crystals and Glasses. *J. Am. Chem. Soc.* 118, 7209-7214.

Bottke, P., Ren, Y., Hanzu, I., Bruce, P.G. and Wilkening, M. (2014) Li ion dynamics in TiO_2 anode materials with an ordered hierarchical pore structure - insights from ex situ NMR. *Phys. Chem. Chem. Phys.* 16, 1894-1901.

Cormack, A.N. and Du, J. (2001) Molecular Dynamics Simulations of Soda–Lime–Silicate Glasses. *J. Non-Cryst. Solids* 293–295, 283-289.

Cormier, L., Calas, G. and Cuello, G.J. (2010) Structural Study of Ca–Mg and K–Mg Mixing in Silicate Glasses by Neutron Diffraction. *J. Non-Cryst. Solids* 356, 2327-2331.

Cormier, L. and Cuello, G.J. (2013) Structural Investigation of Glasses along the $MgSiO_3$–$CaSiO_3$ Join: Diffraction Studies. *Geochim. Cosmochim. Acta* 122, 498-510.

Cramer, C., Brunklaus, S., Ratai, E. and Gao, Y. (2003) New Mixed Alkali Effect in the Ac Conductivity of Ion-Conducting Glasses. *Phys. Rev. lett.* 91, 266601.

Day, D.E. (1976) Mixed Alkali Glasses — Their Properties and Uses. *J. Non-Cryst. Solids* 21, 343-372.

Doremus, R.H. (1974) Mixed-Alkali Effect and Interdiffusion of Na and K Ions in Glass. *J. Amer. Ceram. Soc.* 57, 478-480.

Doty, F.D., Entzminger, G. and Yang, Y.A. (1998) Magnetism in High-Resolution NMR Probe Design. II: HR MAS. *Concepts Magn. Reson.* 10, 239-260.

Dudney, N.J. (2003) Glass and Ceramic Electrolytes for Lithium and Lithium-Ion Batteries, in: Nazri, G.-A., Pistoia, G. (Eds.), *Lithium Batteries*. Springer US, pp. 624-642.

Dupree, R., Holland, D. and Mortuza, M.G. (1990) A MAS-NMR Investigation of Lithium Silicate Glasses and Glass Ceramics. *J. Non-Cryst. Solids* 116, 148-160.

Elbayed, K., Dillmann, B., Raya, J., Piotto, M. and Engelke, F. (2005) Field Modulation Effects Induced by Sample Spinning: Application to

High-Resolution Magic Angle Spinning NMR. *J. Magn. Reson.* 174, 2-26.

Farnan, I., Grandinetti, P.J., Baltisberger, J.H., Stebbins, J.F., Werner, U., Eastman, M.A. and Pines, A. (1992) Quantification of the Disorder in Network-Modified Silicate Glasses. *Nature* 358, 31-35.

Florian, P., Vermillion, K.E., Grandinetti, P.J., Farnan, I. and Stebbins, J.F. (1996) Cation Distribution in Mixed Alkali Disilicate Glasses. *J. Am. Chem. Soc.* 118, 3493-3497.

Frydman, L. and Harwood, J.S. (1995) Isotropic Spectra of Half-Integer Quadrupolar Spins from Bidimensional Magic-Angle Spinning NMR. *J. Am. Chem. Soc.* 117, 5367-5368.

Gee, B. and Eckert, H. (1996) Cation Distribution in Mixed-Alkali Silicate Glasses. NMR Studies by Na-23-{Li-7} and Na-23-{Li-6} Spin Echo Double Resonance. *J. Phys. Chem.* 100, 3705-3712.

Ghose, S. and Tsang, T. (1973) Structural Dependence of Quadrupole Coupling-Constant E2QQ/H for ^{27}Al and Crystal-Field Parameter D for Fe^{3+} in Aluminosilicate. *Am. Miner.* 58, 748-755.

Ghosh, S. and Ghosh, A. (2003) Relaxation Dynamics of Charge Carriers in Mixed Alkali Fluoride Glasses. *J. Chem. Phys.* 119, 9106-9110.

Greaves, G.N. (1998) Structural Studies of the Mixed Alkali Effect in Disilicate Glasses. *Solid State Ionics* 105, 243-248.

Grey, C.P. and Lee, Y.J. (2003) Lithium MAS NMR studies of cathode materials for lithium-ion batteries. Solid State Sciences 5, 883-894.

Habasaki, J. and Hiwatari, Y. (2003) Fast and slow dynamics in single and mixed alkali silicate glasses. *J. Non-Cryst. Solids* 320, 281-290.

Indris, S., Heitjans, P., Uecker, R. and Roling, B. (2012) Li Ion Dynamics in a $LiAlO_2$ Single Crystal Studied by ^{7}Li NMR Spectroscopy and Conductivity Measurements. *J. Phys. Chem. C* 116, 14243-14247.

Isard, J.O. (1969) The Mixed Alkali Effect in Glass. *J. Non-Cryst. Solids* 1, 235-261.

Kelsey, K.E., Allwardt, J.R. and Stebbins, J.F. (2008) Ca-Mg mixing in aluminosilicate glasses: An investigation using ^{17}O MAS and 3QMAS and ^{27}Al MAS NMR. *J. Non-Cryst. Solids* 354, 4644-4653.

Kim, H.N. and Lee, S.K. (2013) Atomic Structure and Dehydration Mechanism of Amorphous Silica: Insights from ^{29}Si and ^{1}H Solid-State MAS NMR Study of SiO_2 Nanoparticles *Geochim. Cosmochim. Acta*.

Konstantinou, K., Sushko, P.V. and Duffy, D.M. (2015) Structure and Ionic Diffusion of Alkaline-Earth Ions in Mixed Cation Glasses A_2O–2MO–$4SiO_2$ with Molecular Dynamics Simulations. *J. Non-Cryst. Solids* 422, 57-63.

Le Losq, C. and Neuville, D.R. (2013) Effect of the Na/K Mixing on the Structure and the Rheology of Tectosilicate Silica-Rich Melts. *Chem. Geol.* 346, 57-71.

Lee, S.K. (2004) Structure of Silicate Glasses and Melts at High Pressure: Quantum Chemical Calculations and Solid-State NMR. *J. Phys. Chem. B* 108, 5889-5900.

Lee, S.K., Kim, H.-I., Kim, E.J., Mun, K.Y. and Ryu, S. (2016) Extent of Disorder in Magnesium Aluminosilicate Glasses: Insights from ^{27}Al and ^{17}O NMR. *J. Phys. Chem. C* 120, 737-749.

Lee, S.K., Mysen, B.O. and Cody, G.D. (2003) Chemical Order in Mixed-Cation Silicate Glasses and Melts. *Phys. Rev. B* 68, 214206.

Lee, S.K. and Stebbins, J.F. (2000) The Structure of Aluminosilicate Glasses: High-Resolution O-17 and Al-27 MAS and 3QMAS. *J. Phys. Chem. B* 104, 4091-4100.

Lee, S.K. and Stebbins, J.F. (2003) Nature of Cation Mixing and Ordering in Na-Ca silicate Glasses and Melts. *J. Phys. Chem. B* 107, 3141-3148.

Lee, S.K. and Stebbins, J.F. (2006) Disorder and the extent of polymerization in calcium silicate and aluminosilicate glasses: O-17 NMR results and

quantum chemical molecular orbital calculations. *Geochim. Cosmochim. Acta* 70, 4275-4286.

Lee, S.K. and Sung, S. (2008) The Effect of Network-Modifying Cations on the Structure and Disorder in Peralkaline Ca-Na Aluminosilicate Glasses: O-17 3QMAS NMR Study. *Chem. Geol.* 256, 326-333.

Lee, Y., Woo, A., Ryu, K.S., Park, Y.J., Jung, B.Y., Lee, J.H. and Han, K.S. (2004) Li-7 MAS NMR studies of layered LixCoO2 prepared using eutectic self-mixing technique for a cathode material. Solid State Ionics 175, 311-314.

Lengyel, B. and Boksay, Z. (1954) On the Electrical Conductivity of Glasses. I. The Conductivity of Mixed Glasse. *Phys. Chem. Chem. Phys.* 203, 93.

Maass, P., Bunde, A. and Ingram, M.D. (1992) Ion-Transport Anomalies in Glasses. *Phys. Rev. lett.* 68, 3064-3067.

Maekawa, H., Florian, P., Massiot, D., Kiyono, H. and Nakamura, M. (1996) Effect of Alkali-Metal Oxide on O-17 NMR Parameters and Si-O-Si Angles of Alkali-Metal Disilicate Glasses. *J. Phys. Chem.* 100, 5525-5532.

Matusita, K., Takayama, S. and Sakka, S. (1980) Electrical Conductivities of Mixed Cation Glasses. *J. Non-Cryst. Solids* 40, 149-158.

Mazurin, O.V. and Borisovskii, E.S. (1957) Neutralization reduction of electrical conductivity in silica glasses. *Soy. Phys.-Tech. Phys.* 2, 243-254.

Moynihan, C.T. and Lesikar, A.V. (1981) Weak-Electrolyte Models for the Mixed-Alkali Effect in Glass. *J. Amer. Ceram. Soc.* 64, 40-46.

Nytén, A., Abouimrane, A., Armand, M., Gustafsson, T. and Thomas, J.O. (2005) Electrochemical Performance of Li_2FeSiO_4 as a New Li-Battery Cathode Material. *Electro. Commun.* 7, 156-160.

Park, B. and Cormack, A.N. (1999) Molecular Dynamics Simulations of Structural Changes in Mixed Alkali (Li–K) Silicate Glasses. *J. Non-Cryst. Solids* 255, 112-121.

Park, S.Y. and Lee, S.K. (2012) Structure and Disorder in Basaltic Glasses and Melts: Insights from High-Resolution Solid-State NMR Study of Glasses in Diopside-Ca-Tschermakite Join and Diopside-Anorthite Eutectic Composition. *Geochim. Cosmochim. Acta* 80, 125-142.

Park, S.Y. and Lee, S.K. (2014) High-Resolution Solid-State NMR Study of the Effect of Composition on Network Connectivity and Structural Disorder in Multi-Component Glasses in the Diopside and Jadeite Join: Implications for Structure of Andesitic Melts. *Geochim. Cosmochim. Acta* 147, 26-42.

Ren, Y., Chen, K., Chen, R., Liu, T., Zhang, Y. and Nan, C.-W. (2015) Oxide Electrolytes for Lithium Batteries. *J. Am. Chem. Soc.* 98, 3603-3623.

Sen, S., George, A.M. and Stebbins, J.F. (1996) Ionic Conduction and Mixed Cation Effect in Silicate Glasses and Liquids: ^{23}Na and ^{7}Li NMR Spin-Lattice Relaxation and a Multiple-Barrier Model of Percolation. *J. Non-Cryst. Solids* 197, 53-64.

Stebbins, J.F. (1998) Cation Sites in Mixed-Alkali Oxide Glasses: Correlations of NMR Chemical Shift Data with Site Size and Bond Distance. *Solid State Ionics* 112, 137-141.

Stebbins, J.F., Oglesby, J.V. and Xu, Z. (1997) Disorder among Network-Modifier Cations in Silicate Glasses; New Constraints from Triple-Quantum ^{17}O NMR. *Am. Miner.* 82, 1116-1124.

Swenson, J. and Adams, S. (2003) Mixed Alkali Effect in Glasses. *Phys. Rev. lett.* 90, 155507.

Thangadurai, V. and Weppner, W. (2005) $Li_6ALa_2Nb_2O_{12}$ (A=Ca, Sr, Ba): A New Class of Fast Lithium Ion Conductors with Garnet-Like Structure. *J. Amer. Ceram. Soc.* 88, 411-418.

Timken, H.K.C., Schramm, S.E., Kirkpatrick, R.J. and Oldfield, E. (1987) Solid-State Oxygen-17 Nuclear Magnetic Resonance Spectroscopic Studies of Alkaline Earth Metasilicates. *J. Phys. Chem.* 91, 1054-1058.

Tucker, M.C., Reimer, J.A., Cairns, E.J., Choi, S. and Manthiram, A. (2002) Li-7 NMR studies of chemically-delithiated $Li_{1-x}CoO_2$. *J. Phys. Chem. B* 106, 3842-3847.

Vessal, B., Greaves, G.N., Marten, P.T., Chadwick, A.V., Mole, R. and Houde-Walter, S. (1992) Cation Microsegregation and Ionic Mobility in Mixed Alkali Glasses. *Nature* 356, 504-506.

Wohlmuth, D., Epp, V. and Wilkening, M. (2015) Fast Li Ion Dynamics in the Solid Electrolyte $Li_7P_3S_{11}$ as Probed by $^{6,7}Li$ NMR Spin-Lattice Relaxation. *ChemPhysChem* 16, 2582-2593.

Xu, X., Wen, Z., Wu, X., Yang, X. and Gu, Z. (2007) Lithium Ion-Conducting Glass–Ceramics of $Li_{1.5}Al_{0.5}Ge_{1.5}(PO_4)_3$–$xLi_2O$ (x=0.0–0.20) with Good Electrical and Electrochemical Properties. *J. Amer. Ceram. Soc.* 90, 2802-2806.

Xu, Z. and Stebbins, J.F. (1995) Cation Dynamics and Diffusion in Lithium Orthosilicate: Two-Dimensional Lithium-6 NMR. Science 270, 1332-1334.

Xue, X.Y., Stebbins, J.F. and Kanzaki, M. (1994) Correlations between ^{17}O NMR Parameters and Local-Structure around Oxygen in High-Pressure Silicates - Implications for the Structure of Silicate Melts at High-Pressure. *Am. Miner.* 79, 31-42.

Zotov, N., Boysen, H., Romano, C., Dingwell, D. and Yanev, Y. (1995) Neutron Diffraction Study of Feldspar Glasses. Mixed Alkali Effect. *J. Non-Cryst. Solids* 191, 124-131.

Chapter 5. Probing the structural disorder of natural basaltic glasses and melts: high-resolution solid-state ^{27}Al and ^{17}O NMR study of glasses in nepheline-forsterite-quartz eutectic composition and KLB-1 basaltic glasses

Abstract

The structural evolution of natural basaltic melts with varying compositions remains one of the unsolved problems in high-temperature geochemistry and petrology. Here, we report experimental results on the effects of composition on the structure of multi-component NaO-MgO-Al_2O_3-SiO_2 (NMAS) glasses in nepheline ($NaAlSiO_4$)-forsterite (Mg_2SiO_4)-quartz (SiO_2) eutectic composition and basaltic glasses generated by partial melting of upper mantle peridotite (KLB-1) using high-resolution, multi-nuclear solid-state nuclear magnetic resonance (NMR). While the ^{27}Al MAS and 3QMAS NMR spectra for NMAS glasses in nepheline-forsterite-quartz eutectic composition show only $^{[4]}$Al, those for KLB-1 basaltic glasses show $^{[5]}$Al as well as $^{[4]}$Al. The fraction of $^{[5]}$Al in KLB-1 basaltic glasses increase upto ~2.6% with increasing X_{MgO}. The spectral analysis of $^{[4]}$Al peak in NMAS glasses in nepheline-forsterite-quartz eutectic composition suggests that the degree of distortion around the Al coordination environments increases with increasing X_{MgO} [MgO/(MgO+Al_2O_3)]. Despite the complex nature of the glasses studied here (with six oxide components), the ^{17}O 3QMAS NMR spectra resolve diverse bridging oxygens (BOs) and non-bridging oxygens (NBOs). The first 2D ^{17}O 3QMAS NMR spectra revealed previously unknown details of diverse structural disorder in the multi-component NMAS glasses in nepheline-forsterite-quartz join and KLB-1 basaltic glasses. The ^{17}O

3QMAS NMR spectra for the KLB-1 basaltic glasses studied here confirm that the degree of polymerization (BO content) decreases with increasing X_{MgO}. The significant fraction of Si-O-Al supports extensive mixing between $^{[4]}$Al and $^{[4]}$Si. Furthermore, Al-O-Al is observed in NMAS glasses in nepheline-forsterite quartz eutectic composition and KLB-1 basaltic glasses, suggesting a deviation from Al avoidance in these glasses. Based on the analysis of the peak position of {Ca, Mg}-mixed NBOs, non-random distributions of Na^+, Ca^{2+}, and Mg^{2+} around both NBOs and BOs are manifested by a moderate degree of partitioning of Ca^{2+} and Mg^{2+} into NBOs and by the spatial proximity between Na^+ and BOs (Al-O-Al and Al-O-Si) in the KLB-1 basaltic glasses studied here. The current experimental results with the changes in network polymerization, coordination environments, and the degree of disorder in the NMAS glasses and KLB-1 basaltic glasses can improve understanding of the structure-property relationships of natural silicate melts, including basaltic melts and glasses.

5.1. Introduction

The compositions of multi-component basaltic melts vary with temperature, pressure, and melt fraction (Kushiro, 2001). Especially, the eutectic point (the composition of first melt) of nepheline ($NaAlSiO_4$)-forsterite (Mg_2SiO_4)-quartz (SiO_2) moves with pressure from silica-saturated to highly undersaturated and alkaline melts (Gupta et al., 1987; Kushiro, 1968) and these composition can be regarded as a simplest model system for basaltic melts (Eggler, 1978; Windom and Boettcher, 1981; Yoder and Tilley, 1962). Nepheline-forsterite-quartz eutectic composition could be model system for alkali rich basaltic melts (e.g., Humphreys and Niu, 2009; Niu, 2008). The compositions of basaltic melts generated by partial melting of

upper mantle peridotite (KLB-1, the olivine xenolith from Kilbourne Hole) also vary with pressure (Hirose and Kushiro, 1993; Takahashi, 1986; Zhang, 1994). While previous ^{27}Al NMR study for diopside-anorthite eutectic composition suggested the effects of pressure on the atomic structure of model basaltic glasses, the effects of composition on the atomic structure of natural glasses and melts remain unsolved (Lee et al., 2012).

KLB-1 has been used to represent the composition of mantle in many high-pressure experimental studies (Agee and Walker, 1993; Herzberg et al., 1990; Herzberg and Zhang, 1996; Hirose, 1997a, b, 2002; Hirose and Fei, 2002; Hirose and Kawamoto, 1995; Hirose and Kushiro, 1993; Konzett and Fei, 2000; Matsukage and Kubo, 2003; McFarlane et al., 1994; Takahashi, 1986; Takahashi et al., 1993; Wang and Takahashi, 2000; Yoshino et al., 2004; Zhang, 1994) and theoretical studies (Arndt et al., 1997; Dobretsov et al., 2006; Iwamori et al., 1995; Katz et al., 2003; Komiya, 2004; Moore et al., 1998; Ogawa and Nakamura, 1998). Previous experimental and theoretical studies depend on the KLB-1 bulk composition because it is among very few natural peridotite samples that may approximate the composition of the source of the typical mid-ocean ridge basalt (MORB). While compositions of MORB indicate that the upper mantle is fertile with respect to major elements such as CaO, Al_2O_3, and Na_2O, but depleted K_2O, all natural peridotite samples are depleted in those elements relative to the MORB source and have non-negligible K_2O (Salters and Stracke, 2004; Workman and Hart, 2005).

The atomic structure (e.g., coordination number, various types of structural disorder, and network connectivity) of multi-component silicate glasses and melts including Na_2O-MgO-Al_2O_3-SiO_2 (NMAS) glasses in nepheline-forsterite-quartz eutectic composition and KLB-1 basaltic glasses and melts has considerable implications for the macroscopic properties of

natural silicate melts (Bajgain et al., 2015; Bauchy et al., 2013; Giordano et al., 2008; Kelsey et al., 2008; Lee, 2005, 2011; Moulton et al., 2016; Mysen and Richet, 2005; Navrotsky et al., 1983; Neuville et al., 2004, 2006; Potuzak and Dingwell, 2006). However, overlaps among peaks (in any spectroscopic methods) and scattering factors (X-ray and neutron scattering) of the multi-component silicate glasses become more prominent with increasing numbers of oxide components due to enhanced topological (due to bond angle and bond length distribution and distortion of glass networks around Al and Si) and configurational disorder (due to mixing between different species, e.g., mixing between $^{[4]}$Al and $^{[5]}$Al) in the glasses, making it challenging to probe their detailed atomic structures (Mysen and Toplis, 2007). As a results, the structure of basaltic glasses and melts has been studied on relatively simple model system, thus the structural behavior of the natural basaltic glasses and melts remains unsolved question. In contrast, melting experiments at high pressure and temperature and macroscopic properties of multi-component silicate glasses including NMAS glasses in nepheline-forsterite-quartz and KLB-1 basaltic glasses and melts have been extensively studied. The previous study for the viscosity of olivine tholeiite and calc-alkaline andesite melts showed that the viscosity decreases with increasing pressure and the viscosity of tholeiitic magma is larger than that of calc-alkaline magma (Kushiro, 1976). Previous study for the partial melting of KLB-1 peridotite showed that the partial melting of KLB-1 peridotite occurs fast. Thus the melting rate may be faster than the seismic time scale and may be a dominant factor in defining the seismic velocity and attenuation of partially molten regions (Du et al., 2014). V_P and V_S were measured for synthetic KLB-1 peridotite and bulk modulus was calculated from those measurement. The results showed that the velocities for an aggregate with the pyrolitic

composition of KLB-1 are in close agreement with seismic data at the depths of the Earth's upper mantle (Wang et al., 2015). While the element partitioning coefficient changes with NBO/T in silicate, there is no simple universal structural relationship that relates mineral/melt partitioning behavior to NBO/T of the melt. Those results suggest that the composition of silicate melt affect mineral/melt element partitioning (Kushiro and Mysen, 2002; Mysen, 2004; Mysen and Dubinsky, 2004).

These changes in the thermo-mechanical and transport properties of NMAS glasses in nepheline-forsterite-quartz eutectic composition and KLB-1 basaltic glasses and melts are obviously linked to changes in the atomic structure related to changing composition. Despite the aforementioned difficulties in exploring the local structures of multi-component silicate glasses, the cation coordination environments of complex quaternary oxide glasses with geochemical implications have recently been reported. For example of Al coordination environments, recent studies of the model basaltic glasses in diopside–Ca–tschermakite join and diopside–anorthite eutectic composition showed the presence of five coordinated Al ($^{[5]}$Al) (Park and Lee, 2012; Xue and Kanzaki, 2008). A previous study of the shock-compressed model basaltic glasses (diopside–anorthite eutectic composition, $Di_{64}An_{36}$) also showed that the fraction of $^{[5]}$Al in the basaltic glasses increased upon dynamic compression up to peak pressure of ~20 GPa (Lee et al., 2012). Al coordination environments in hydrous andesite glasses have also been studied extensively (Malfait et al., 2012). A previous study of the model andesitic glasses in diopside–jadeite join showed only $^{[4]}$Al is observed in those glasses (Park and Lee, 2014).

Previous studies have shown that the extent of disorder, such as network connectivity and the degree of Al avoidance (Si/Al framework

disorder), is important in understanding the configurational thermodynamic properties of the aluminosilicate glasses, such as configurational entropy and heat capacity as well as the Gibbs free energy of mixing (Lee, 2005, 2011; Mysen and Richet, 2005; Navrotsky et al., 1983). Various types of additional structural disorder also affect configurational properties of glasses and melts. These structural disorders include bonding preferences between NBOs and the framework cations (e.g., Si–NBO vs. Al–NBO) (Allwardt et al., 2003) and partitioning of network modifying cations between non-bridging oxygens (NBOs) and bridging oxygens (BOs) (Lee and Sung, 2008; Park and Lee, 2012, 2014). Information regarding these types of disorder can be obtained using various spectroscopic methods, particularly with ^{17}O NMR (Lee, 2010). Additional intrinsic structural disorder also results from bond angle and length distribution (topological disorder). Furthermore, the degree of network connectivity, often represented by the fractions of NBO, offers insights into the viscosity and activity coefficient of SiO_2 (Giordano and Dingwell, 2003; Lee, 2011). Previous efforts and advances to reveal the extent of disorder have often focused on relatively simple model silicate glasses. Relatively few studies have been performed to explore the structure and the extent of disorder in other diverse geologically important multi-component glasses and melts (Park and Lee, 2012, 2014). Here, we attempt to reveal the nature of the various aspects of disorder (Si/Al ordering, preference between non-network cations and BOs and NBOs), and the degree of polymerization in the simplest basaltic glasses and melts (NMAS glasses in nepheline-forsterite-quartz eutectic composition) and multi-component KLB-1 basaltic glasses and melts.

In this study, we explore the coordination environments of framework cations, network connectivity, and the extent of disorder (i.e.,

chemical and topological disorder) in NMAS glasses in nepheline ($NaAlSiO_4$)-forsterite (Mg_2SiO_4)-quartz (SiO_2) eutectic composition and basaltic glasses generated by partial melting of upper mantle peridotite (KLB-1) using multi-nuclear (^{27}Al and ^{17}O) high-resolution solid-state NMR, which has proven effective in revealing detailed degrees of disorder in such glasses (Lee et al., 2009; Stebbins et al., 2001a; Stebbins and Xu, 1997; Stebbins and Xue, 2014). While natural basaltic glasses have additional essential components (FeO and Fe_2O_3), NMR has shown limited utility in resolving atomic structures of iron bearing glasses. Thus the focus of the current study is on the iron-free basaltic glasses.

5.2. Experimental methods

5.2.1. Sample preparation

Na-Mg silicate glasses, NMAS glasses in nepheline-forsterite-quartz eutectic composition, and KLB-1 basaltic glasses were synthesized from oxide (Al_2O_3, SiO_2, MgO, and TiO_2) and carbonate ($CaCO_3$, Na_2CO_3, and K_2CO_3). Small weight loss (~0.9~2.1 wt%) was observed after decarbonation. Approximately 0.2 wt% of cobalt oxide was added to reduce the spin–lattice relaxation time. The mixtures were then melted in a Pt crucible for 1 h at 1450~1600 °C (above their respective melting temperatures) and then quenched by removing the crucible from the furnace and manually lowering it into water. ^{17}O-enriched Na-Mg silicate glasses, Na_2O-MgO-Al_2O_3-SiO_2 glasses in nepheline-forsterite-quartz eutectic composition, and KLB-1 basaltic glasses were synthesized from oxide (Al_2O_3, MgO, and TiO_2), carbonate ($CaCO_3$, Na_2CO_3, and K_2CO_3), and ^{17}O-enriched SiO_2. Negligible weight loss (~1.2~2.4 wt% for NMAS glasses and ~0.8–1.4 wt% for KLB-1 basaltic glasses) was observed after decarbonation. The mole fraction of FeO

and Fe_2O_3 were removed from the composition of KLB-1 basaltic glasses using previous results of the oxidation state of Fe in basalt (Fe^{3+}:Fe^{2+} = 0.16 : 0.84) (Cottrell and Kelley, 2011). The oxidation state of Fe in subduction zone basalts is higher than basalts from other tectonic settings (Fe^{3+}:Fe^{2+} = 0.25:0.75), thus the composition of basaltic glasses and melts generated from KLB-1 could have variation due to the difference of oxidation state (Kelley and Cottrell, 2012). The composition of KLB-1 basaltic glasses are recalculated by the mole fraction of FeO are replaced MgO fraction and that of Fe_2O_3 are replaced by Al_2O_3 fraction. The effects of composition on natural basaltic glasses and melts including iron remain to be explored. Table 5.1, 5.2, and 5.3 show the nominal and chemical compositions of the Na-Mg silicate glasses, NMAS glasses in nepheline-forsterite-quartz eutectic composition, and KLB-1 basaltic glasses estimated by inductively coupled plasma atomic emission spectroscopy (ICP-AES).

5.2.2. NMR spectroscopy

^{17}O NMR, ^{29}Si NMR, and ^{27}Al NMR spectra of Na-Mg silicate glasses and nepheline-forsterite-quartz eutectic glass were collected on the Varian solid-state NMR 400 system (9.4 T) at Larmor frequency of 54.23 MHz, 79.50 MHz, and 104.23 MHz respectively. ^{17}O MAS and 3QMAS NMR spectra Na-Mg silicate glasses were collected using a 4 mm Doty double-resonance probe. The relaxation delay for the ^{17}O MAS NMR was 1 s, the radio frequency pulse length was 1.0 μs, and the spinning speed was 14 kHz for Na-Mg silicate glasses. A 0.4 μs radio frequency (rf) pulse was used with a relaxation delay of 1 s and 1920 scans of free-induction decay (FID) were averaged for Na-Mg silicate glasses. In the ^{17}O 3QMAS NMR experiment at 9.4 T, a FAM-based shifted-echo pulse sequence was used, which consisted

Table 5.1. Nominal composition and ICP analysis of Na-Mg disilicate glasses.

X_{MgO}	Nominal composition (mol%)		
	Na_2O	MgO	SiO_2
0.025	32.5	0.8	66.7
0.05	31.7	1.7	66.7
0.1	30.0	3.3	66.7
0.25	25.0	8.3	66.7
0.5	16.7	16.7	66.7
0.75	8.3	25.0	66.7

X_{MgO}	Nominal composition (mol%)		ICP analysis (mol%)	
	Na_2O	MgO	Na_2O	MgO
0.025	97.5	2.5	95.8	4.2
0.05	95.0	5.0	93.5	6.5
0.1	90.0	10.0	87.8	12.2
0.25	75.0	25.0	70.8	29.2
0.5	50.0	5.0	44.9	55.1
0.75	25.0	75.0	21.7	78.3

Table 5.2. Nominal composition and ICP analysis of Na_2O-MgO-Al_2O_3-SiO_2 (NMAS) glasses in nepheline-forsterite-quartz eutectic composition.

X_{MgO}	NMAS mol% (nominal composition)				
	Na_2O	MgO	Al_2O_3	SiO_2	NBO/T
0.13	10.4	1.6	10.4	77.6	0.03
0.24	13.2	4.1	13.2	69.5	0.09
0.30	14.5	6.2	14.5	64.8	0.13
0.39	16.4	10.3	16.4	56.9	0.23

X_{MgO}	NMAS mol% (nominal composition)			NMAS mol% (ICP analysis)		
	Na_2O	MgO	Al_2O_3	Na_2O	MgO	Al_2O_3
0.13	46.4	7.1	46.4	45.0	12.2	42.8
0.24	43.3	13.4	43.3	42.1	16.6	41.3
0.30	41.2	17.6	41.2	39.7	20.9	39.4
0.39	38.1	23.9	38.1	36.1	27.4	36.5

Table 5.3. Nominal composition and ICP analysis of KLB-1 basaltic glasses.

composition (mol%)	X_{MgO}		
	0.55	0.70	0.79
SiO_2	54.3	49.8	46.2
TiO_2	0.7	0.4	0.3
Al_2O_3	12.3	9.5	8.1
MgO	15.2	22.5	29.6
CaO	12.4	16	14.7
Na_2O	4.7	1.6	0.8
K_2O	0.2	0.1	0.1
NBO/T	0.51	0.89	1.18

composition (mol%)	nominal composition			ICP analysis		
	X_{MgO}			X_{MgO}		
	0.55	0.70	0.79	0.55	0.70	0.79
TiO_2	1.5	0.8	0.6	1.6	1.0	1.0
Al_2O_3	27.0	19.0	15.1	23.5	16.7	13.3
MgO	33.4	44.9	55.2	34.9	47.0	57.9
CaO	27.3	31.9	27.4	28.9	31.9	26.2
Na_2O	10.3	3.2	1.5	10.6	3.2	1.4
K_2O	0.4	0.2	0.2	0.5	0.3	0.2

of a hard pulse with a duration of 4.5 μs for multiple-quantum excitation, two 1.1 μs pulses for single-quantum reconversion, and a soft pulse of approximately 20 μs duration for Li-Ba and Na-Mg silicate glasses. A 500 μs echo time was used with a relaxation delay of 1 s.

The ^{27}Al MAS and 3QMAS NMR spectra of glasses in nepheline-forsterite-quartz eutectic composition and KLB-1 glasses were collected using a Varian solid-state NMR 400 system (9.4 T) at a Larmor frequency of 104.23 MHz with a 3.2-mm Varian probe (Seoul National University, Korea) with spinning speed of 17 kHz. The relaxation delay for the ^{27}Al MAS NMR was 1.0 s for glasses in nepheline-forsterite-quartz eutectic composition and that was 0.5 s for KLB-1 basaltic glasses. The *rf* pulse length was 0.3 μs (~ 30 degree tip angle). A fast-amplitude modulation (FAM)-based shifted-echo pulse sequence was used in the ^{27}Al 3QMAS NMR. This pulse sequence consisted of two hard pulses (3.0 and 0.6 μs) and a subsequent soft pulse (~15 μs) with ~500 μs echo time and a relaxation delay of 0.5–1.0 s. Approximately 768–864 scans were averaged to achieve the signal-to-noise ratio shown in the 3QMAS NMR spectra for glasses in nepheline-forsterite-quartz eutectic composition and 3168–4032 scans were averaged for KLB-1 basaltic glasses.

The ^{17}O MAS and 3QMAS NMR spectra of glasses in nepheline-forsterite-quartz eutectic composition are performed with Varian solid-state NMR 400 system (9.4 T) at a Larmor frequency of 54.23 MHz with a 4 mm Doty probe (Seoul National University, Korea) with spinning speed of 14 kHz. The relaxation delay for the ^{17}O MAS NMR was 1.0 s for glasses in nepheline-forsterite-quartz eutectic composition and that was 0.5 s for KLB-1 basaltic glasses. The rf pulse length was 0.3 μs. A FAM-based shifted-echo pulse sequence was used in the ^{17}O 3QMAS NMR. This pulse sequence consisted of two hard pulses (3.0 and 0.6 μs) and a subsequent soft pulse (~15 μs) with ~500 μs echo time and a relaxation delay of 0.5–1.0 s. Approximately

768–864 scans were averaged to achieve the signal-to-noise ratio shown in the 3QMAS NMR spectra for glasses in nepheline-forsterite-quartz eutectic composition and 3168–4032 scans were averaged for KLB-1 basaltic glasses.

5.3. Results and discussion

5.3.1. Al environments of NMAS glasses in nepheline-forsterite-quartz eutectic composition and KLB-1 basaltic glasses: ^{27}Al MAS and 3QMAS NMR results

Figure 5.1A shows ^{27}Al MAS NMR spectra of NMAS glasses in nepheline-forsterite-quartz eutectic composition with varying X_{MgO}, revealing predominant $^{[4]}$Al (here, X_{MgO} is mole fraction of MgO). The peak maximum of $^{[4]}$Al increases from 51.1 ± 1.5 ppm at X_{MgO} = 0.13 to 54.3 ± 1.5 ppm at X_{MgO} = 0.39, suggesting that the fraction of Q^4_{Al}(nSi) species around Al change with X_{MgO}. Additionally, the changes could also be due to the presence of cations with higher field strength (e.g., Mg^{2+}): with increasing cation field strength of non-network forming cations, the peak position in the isotropic dimension moves to more negative shift (Lee and Stebbins, 2000). The peak width of $^{[4]}$Al (i.e., full-width at half-maximum, FWHM) is consistent (~24 ppm) from X_{MgO} = 0.13 to X_{MgO} = 0.30, suggesting that the topological disorder (including atomic configuration) around Al is consistent. However, it increases with a further increase in X_{MgO} to 25.8 ± 1.5 ppm (X_{MgO} = 0.39).

Figure 5.1B shows ^{27}Al 3QMAS NMR spectra of NMAS glasses in nepheline-forsterite-quartz eutectic composition with varying X_{MgO}. The $^{[4]}$Al is only observed at ~-37 ppm in isotropic dimension in NMAS glasses in nepheline-forsterite-quartz eutectic composition, consistent with the 1D ^{27}Al MAS NMR results. The peak position of $^{[4]}$Al in the glasses shifts from -36.6.

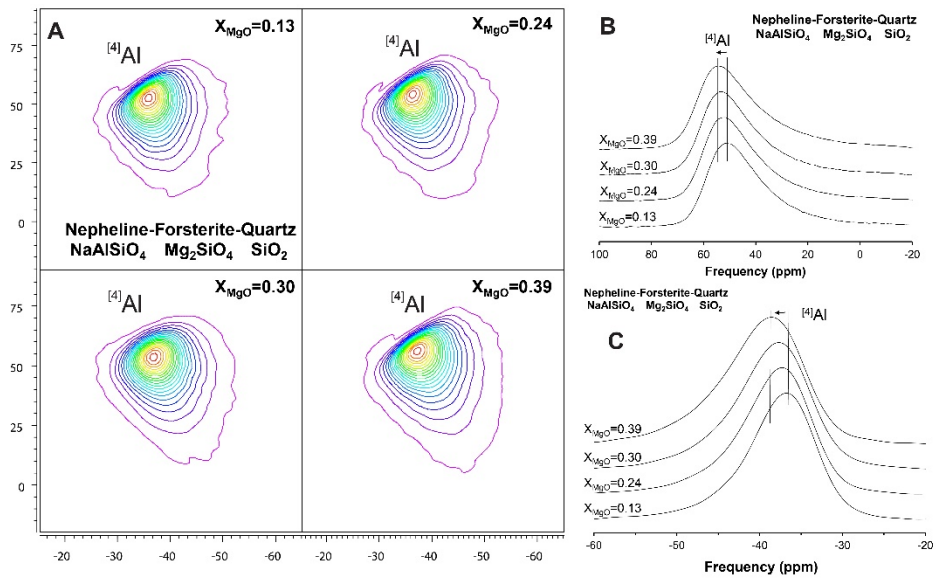

Figure 5.1. (A) ^{27}Al MAS NMR spectra for $Na_2O–MgO–Al_2O_3–SiO_2$ glasses in nepheline-forsterite-quartz eutectic composition at 9.4 T with varying X_{MgO} [$MgO/(MgO+Al_2O_3)$]. (B) ^{27}Al 3QMAS NMR spectra for $Na_2O–MgO–Al_2O_3–SiO_2$ glasses in nepheline-forsterite-quartz eutectic composition with varying X_{MgO}. Contour lines are drawn at 5% intervals from relative intensities of 2% to 97%. (C) Total isotropic projection of ^{27}Al 3QMAS NMR spectra for $Na_2O–MgO–Al_2O_3–SiO_2$ glasses in nepheline-forsterite-quartz eutectic composition with varying X_{MgO}.

± 1.5 ppm at X_{MgO} = 0.13 to -38.6 ± 1.5 ppm at X_{MgO} = 0.39 in the isotropic dimension. The measured peak width (FWHM) of $^{[4]}$Al in the MAS dimension of the 2D spectra increases from 21.5 ± 1.5 ppm (X_{MgO} = 0) to 22.5 ± 1.5 ppm (X_{MgO} = 0.75). The peak width in the MAS dimension is directly proportional to the magnitudes of the quadrupolar interactions. Additionally chemical shift distribution in each Al site can also partly contribute to the peak width. Because Al is a quadrupolar nuclide, non-spherical nuclear charge is interacting with the electric field gradient around Al nuclide. The magnitude of the quadrupolar interactions is parameterized with quadrupolar coupling constant, C_q. This interaction is a measure of the degree of distortion and thus a deviation from perfect cubic symmetry around the Al environments (Baltisberger et al., 1996; Ghose and Tsang, 1973). The deviation from perfect tetrahedral symmetry is relevant to the distortion of $^{[4]}$Al in the silicate glasses. Thus the observed trend of increase in average C_q suggests that the degree of network distortion around the Al (and thus, Q^n species) increases with increasing X_{MgO}.

Figure 1C shows the total isotropic projections (sum of the spectrum into the isotropic dimension) of the ^{27}Al 3QMAS NMR spectra for NMAS glasses in the nepheline-forsterite-quartz eutectic composition with varying X_{MgO}. The peak maximum of $^{[4]}$Al in the glass shifts from -36.6 ± 1.5 ppm (X_{MgO} = 0.13) to -38.6 ± 1.5 ppm (X_{MgO} = 0.39) in the isotropic dimension. The change of peak maximum suggests a change of $Q^4{}_{Al}$(nSi) species (fully polymerized $^{[4]}$Al species with n number of Si as next nearest neighbors) as Al in the glasses is expected to be fully polymerized forming only Q^4 species (Allwardt et al., 2003). Based on the known relationship between peak position of Q^4(nSi) species with increasing n, the observed changes in the peak position indicate the change of $Q^4{}_{Al}$(nSi) species with increasing X_{MgO}

(Lee and Stebbins, 2000). Additionally, the changes could also be due to the presence of cations with higher field strength (e.g., Mg^{2+}): with increasing cation field strength of non-network forming cations, the peak position in the isotropic dimension moves to more negative shift (Lee and Stebbins, 2000). The estimated peak width (FWHM) for $^{[4]}$Al in the isotropic projection slightly increases from 8.9 ± 1.5 ppm (X_{MgO} = 0.13) to 10.9 ± 1.5 ppm (X_{MgO} = 0.39) with increasing X_{MgO}. Those results again confirm that the configurational disorder around Al in the glasses increases with increasing X_{MgO}.

Figure 5.2A shows the ^{27}Al MAS NMR spectra for KLB-1 basaltic glasses with varying X_{MgO}. The $^{[4]}$Al peak at ~52.7 ± 1.0 ppm is dominant in all the glasses studied here. While only $^{[4]}$Al is observed in glass at X_{MgO} = 0.55, non-negligible fraction of $^{[5]}$Al are observed in glass at X_{MgO} = 0.79. The shape of the spectrum is also characterized by long tails extending to lower frequencies (i.e., smaller chemical shift ranges). This trend results from distributions of the quadrupolar coupling constant (C_q) and the isotropic chemical shift (δ_{iso}) of Al environments in the glasses, indicating extensive structural disorder in the glasses. The peak widths (FWHM) of the ^{27}Al MAS NMR spectra for KLB-1 basaltic glasses increase systematically with increasing X_{MgO} from ~36.3 ± 1.5 ppm for X_{MgO} = 0.55 to ~45.7 ± 1.5 ppm for X_{MgO} = 0.79. Those results suggest that the degree of distortion around the Al (e.g., change of bond angle and bond distance) and/or configurational disorder may increase with the MgO component of the glasses. 3QMAS NMR provides a much improved resolution in 2D spectra over 1D MAS NMR and thus can yield detailed information on the network connectivity in oxide glasses (e.g., Frydman and Harwood, 1995).

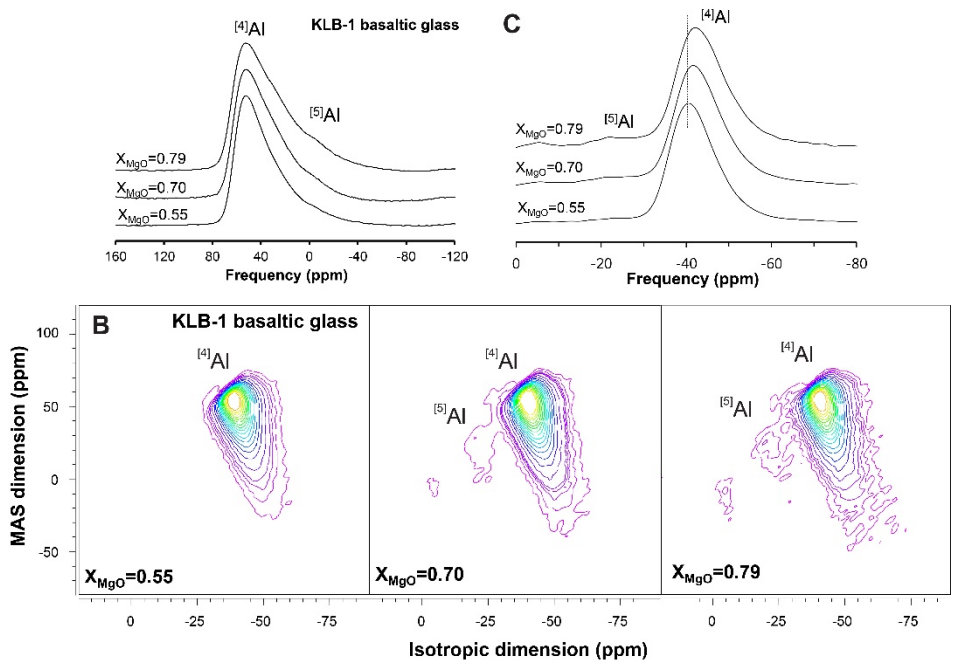

Figure 5.2. (A) ^{27}Al MAS NMR spectra for KLB-1 basaltic glasses at 9.4 T with varying X_{MgO} [MgO/(MgO+Al_2O_3)]. (B) ^{27}Al 3QMAS NMR spectra for KLB-1 basaltic glasses at 9.4 T with varying X_{MgO} [MgO/(MgO+Al_2O_3)]. Contour lines are drawn at 5% intervals from relative intensities of 12% to 82% with added lines at 4%, 6% and 8%. (C) Total isotropic projection of ^{27}Al 3QMAS NMR spectra for KLB-1 basaltic glasses with varying X_{MgO}.

Figure 5.2B shows the 2D ^{27}Al 3QMAS NMR spectra (with much improved site resolution than the 1D MAS) for KLB-1 basaltic glasses with varying X_{MgO}. While only $^{[4]}$Al is observed in the glass at X_{MgO} = 0.55, consistent with the 1D NMR results, a minor but detectable amount of $^{[5]}$Al is also observed for the glasses at X_{MgO} = 0.70 and 0.79 (~–20 ± 1.5 ppm in the isotropic dimension), indicating an increase in the topological and configurational disorder in the glasses with X_{MgO} = 0.70 and 0.79. The measured peak width (FWHM) of $^{[4]}$Al in the MAS dimension of the 2D 3QMAS NMR spectra increases from 29.5 ± 1.5 ppm (X_{MgO} = 0.55) to 35.1 ± 1.5 ppm (X_{MgO} = 0.79). The peak width in the MAS dimension is directly proportional to the magnitudes of the quadrupolar interactions originating from the electric field gradient around the Al nuclide and the nuclear quadrupolar moment (i.e., quadrupolar coupling constant, C_q). This interaction is a measure of the degree of distortion and thus a deviation from perfect cubic symmetry around the Al environments (Baltisberger et al., 1996; Ghose and Tsang, 1973). Thus the trend indicates that the degree of network distortion around the Al increases with increasing X_{MgO}. Figure 5.2C shows the total isotropic projections of the ^{27}Al 3QMAS NMR spectra for KLB-1 basaltic glasses with varying X_{MgO}. The peak maximum of $^{[4]}$Al in the glass shifts from –40.6 ± 1.5 ppm (X_{MgO} = 0.55) to –42.1 ± 1.5 ppm (X_{MgO} = 0.79) in the isotropic dimension. The change of peak maximum suggests a change of Q^4(nSi) species (fully polymerized $^{[4]}$Al species with n number of Si as next nearest neighbors) as Al in the glasses is expected to be fully polymerized forming only Q^4 species (Allwardt et al., 2003). Based on the known relationship between peak position of Q^4(nSi) species with increasing n, the observed changes in the peak position indicates that the proportions of

Q^4(4Si) and Q^4(3Si) species increase with increasing X_{Mgo} (Lee and Stebbins, 2000).

Figure 5.3 shows that the relative population of $^{[5]}$Al, which is calibrated taking into consideration the 3QMAS efficiency (excitation of triple-quantum coherence and its reconversion to single-quantum coherence) of each Al site (Lee et al., 2010). Note that the 3QMAS efficiency is affected by quadrupolar interactions between nuclear quadrupole moment and electric field gradient around Al nuclide (Bak et al., 2000; Baltisberger et al., 1996). The calibrated fraction of $^{[5]}$Al slightly increases upto ~2.6% (X_{MgO} = 0.79) with increasing X_{MgO}, while the variation is within error range. This trend is to some extent consistent with previous NMR studies ternary and quaternary aluminosilicate glasses where the fraction of $^{[5]}$Al increases with increasing cation field strength (Allwardt et al., 2005; Bunker et al., 1991; Kelsey et al., 2008; Lee et al., 2005; Park and Lee, 2014). We note that estimation of the fraction of a small amount of $^{[5]}$Al and $^{[6]}$Al (~1-10%) is intrinsically difficult because the measurement and analysis of 1D ^{27}Al MAS NMR at high (and low) field often depends on the model for the parameter (C_q and isotropic chemical shift) distributions and assumptions used to fit the 1D experimental data and 2D ^{27}Al 3QMAS technique is not quantitative and the larger C_q sites are often underestimated. It should be noted that the $^{[5]}$Al fraction in the current study may not be regarded as unique value but rather represents one of the possible solutions.

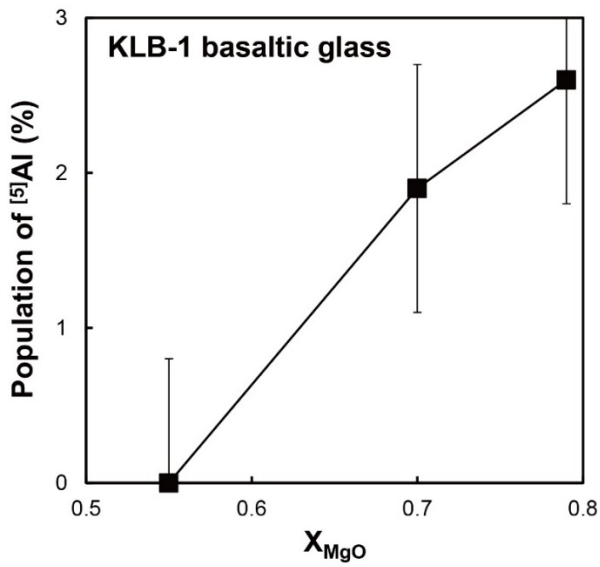

Figure 5.3. Population of [5]Al for KLB-1 basaltic glasses with varying X_{MgO}. The error bar of $\pm$0.5% was estimated based on estimated uncertainty in peak area and quadrupolar coupling constant (C_q) that affects peak intensity.

5.3.2. Variation in NMR parameters in NMAS glasses in nepheline-forsterite-quartz eutectic composition and KLB-1 basaltic glasses

Figure 5.4 shows the effects of composition on the structurally relevant C_q [=$P_q/(1 + \eta^2/3)^{1/2}$, where P_q and η are the quadrupolar coupling product and the asymmetry parameter, respectively] of $^{[4]}$Al in the NMAS glasses and $^{[4]}$Al and $^{[5]}$Al in KLB-1 basaltic glasses. Here, P_q was obtained from the center of gravity of the $^{[4]}$Al and $^{[5]}$Al peak in the ^{27}Al 3QMAS NMR spectra and the asymmetry parameter (η) is assumed to be 0.5: note that the change in η does not lead to noticeable changes in the calculated C_q (Park and Lee, 2012). The C_q of $^{[4]}$Al in NMAS glasses in nepheline-forsterite-quartz eutectic composition increases with increasing X_{MgO} from 5.0 ± 0.4 MHz (X_{MgO} = 0) to 5.4 ± 0.4 MHz (X_{MgO} = 0.75). Larger C_q indicates a larger deviation from the perfect cubic symmetry around Al, which can result from Al–O bond length (as well as bond angle) distribution. The current results indeed indicate that the degree of overall topological disorder around $^{[4]}$Al increases with increasing X_{MgO} in the NMAS glasses in nepheline-forsterite-quartz eutectic composition. As the Q species in the glasses varies with composition, the observed variation in average C_q of Al sites in the glasses is likely to be affected by the variation in Q^4_{Al}(nSi) species and each Q species have distinct C_q values (Lee and Stebbins, 2000 and references therein). The degree of distortion of each Q^4_{Al}(nSi) species may also change with Mg^{2+} (those increases with increasing X_{MgO}): presence of higher field strength cations leads to the larger network distortion, contributing to an increase in the average C_q value with increasing X_{MgO} (Lee and Stebbins, 2006, 2009; Park and Lee, 2012, 2014). The C_q of $^{[4]}$Al in KLB-1 basaltic glasses increases slightly with increasing X_{MgO} from 6.5 ± 0.4 MHz (X_{MgO} = 0.55) to 6.8 ± 0.4 MHz (X_{MgO} = 0.79). The current results indeed indicate that the degree of

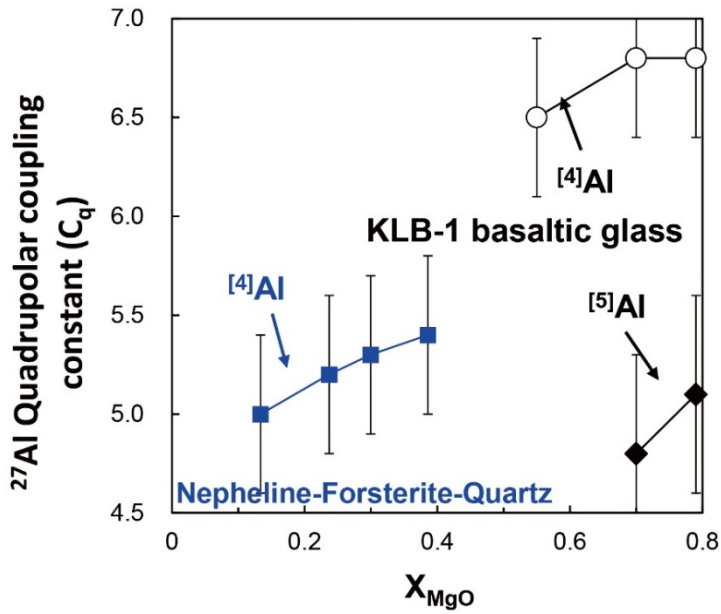

Figure 5.4. Quadrupolar coupling constant (C_q) of [4]Al in Na_2O–MgO–Al_2O_3–SiO_2 glasses in nepheline-forsterite-quartz eutectic composition and those of [4]Al and [5]Al in KLB-1 basaltic glasses at 9.4 T with varying X_{MgO} [MgO/(MgO+Al_2O_3)]. The asymmetry parameter is assumed to be 0.5. The estimated error bar of ±0.4 MHz for [4]Al and that of ±0.5 MHz for [5]Al were determined based on the uncertainty in the position of the center of gravity of each peak.

overall topological disorder around $^{[4]}$Al (due to Al–O bond length and angle distribution) slightly increases with increasing X_{MgO} in the KLB-1 basaltic glasses, accompanied with enhanced variations in Q species in the glasses with an increase in X_{MgO}. The C_q of $^{[5]}$Al seems to increase slightly from 4.8 ± 0.5 MHz (for X_{MgO} = 0.70) to 5.1 ± 0.5 MHz (for X_{MgO} = 0.79) with increasing X_{MgO}. This result demonstrates that the presence of Mg^{2+} leads to the formation of $^{[5]}$Al and increases the degree of network distortion and thus Al-O bond length and angle distribution around $^{[5]}$Al. Note that due to relatively low $^{[5]}$Al intensity there is uncertainty in the absolute C_q value of $^{[5]}$Al. Furthermore, the C_q value for the site can be larger at higher magnetic field. The current results thus show the observed trend for C_q's for both $^{[4,5]}$Al with increasing X_{MgO} at 9.4 T.

5.3.3. Probing the extent of network connectivity and configurational disorder: ^{17}O 3QMAS NMR results of Na-Mg silicate glasses

Figure 5.5 shows ^{17}O 3QMAS NMR spectra for Na-Mg silicate glasses with varying X_{MgO}. The current peak assignment is based on previous reports on binary and ternary silicate glasses (Lee and Stebbins, 2009). The peak intensity, position, and width for each NBO and BO peak varies with composition, suggesting changes in structurally relevant NMR parameters and the degree of disorder with the degree of polymerization. While the peak position of Na-O-Si is ~-22 ppm in isotropic dimension in Na-disilicate glass (Lee and Stebbins, 2003), the NBO peaks [Na-O-Si + {Na, Mg}-NBO + Mg-O-Si] are observed around ~-24 ppm in isotropic dimension at X_{MgO} = 0.025, 0.05, 0.10, 0.25, and 0.50. The NBO peak shifts to lower frequency (~-26 ppm) with a further increase in X_{MgO} (X_{MgO} = 0.75). The Si–O–Si peaks are completely resolved at ~-45 ppm in isotropic dimension as labeled. The peak

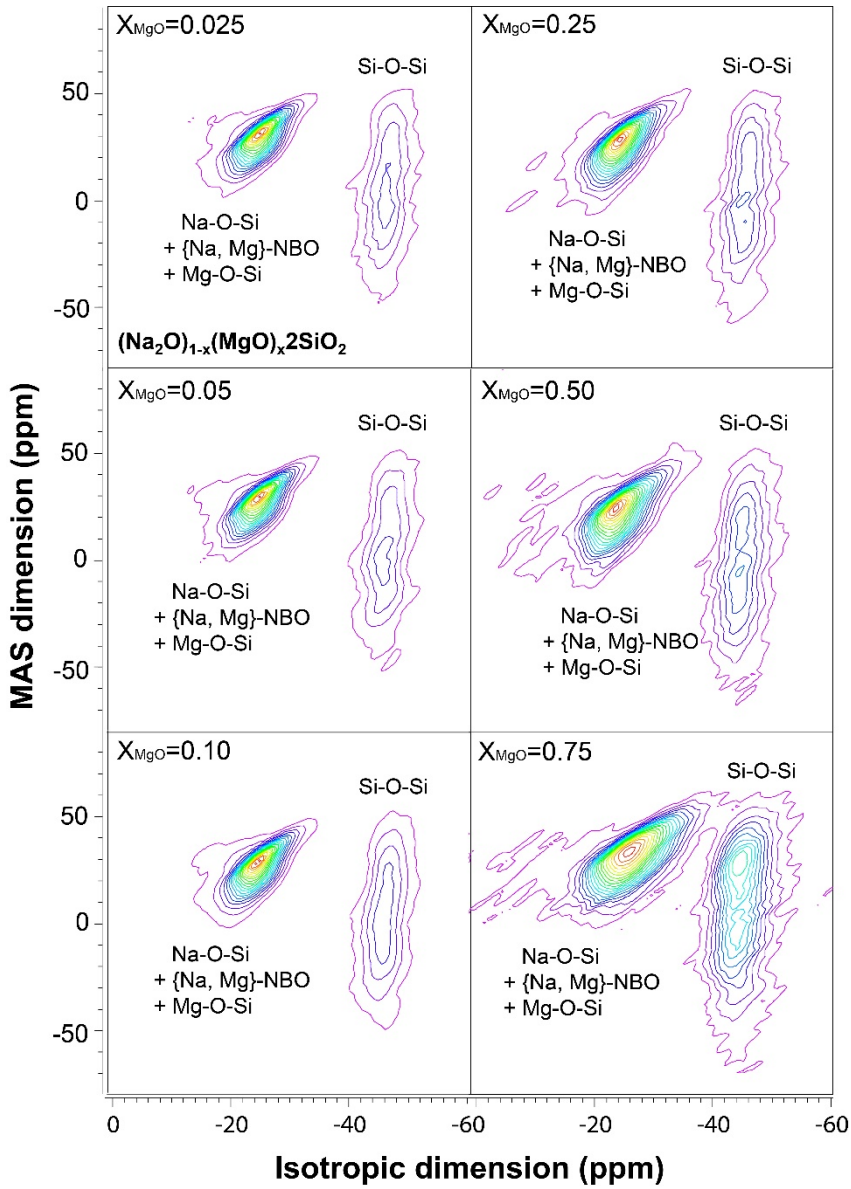

Figure 5.5. ^{17}O 3QMAS NMR spectra for Na-Mg silicate glasses with varying X_{MgO} [MgO/(MgO+Al_2O_3)]. Contour lines are drawn at 5% intervals from relative intensities of 3% to 98%.

maximum of Si-O-Si changes with increasing X_{MgO}. The peak maximum of Si-O-Si shifts toward higher frequency in isotropic dimension with increasing X_{MgO}, suggesting that the topological disorder (i.e., Si-O-Si bond angle and length) changes with increasing X_{MgO}. The peak width (full width at half maximum) of Si-O-Si increases with increasing X_{MgO}. The peak shape of glass at X_{MgO}=0.025 is similar with Na-disilicate glass (Lee and Stebbins, 2003, 2009). The peaks of Na-O-Si, {Na, Mg}-O-Si, and Mg-O-Si are expected in Na-Mg silicate glasses at X_{MgO} = 0.025. Nevertheless, if a few % of Mg-O-Si exist in Na-Mg silicate glasses at X_{MgO} = 0.025, due to the overlap with Si-O-Si and Na-O-Si may not be detected. The peak width of {Na, Mg}-O-Si increases with increasing X_{MgO} because of the increased NBO configurations and structural perturbation caused by Mg^{2+} (higher cation field strength). The peak width of Si-O-Si slightly increases from ~6.4 ppm at at X_{MgO} = 0.025 to ~7.5 ppm at X_{MgO} = 0.75 with increasing X_{MgO}, suggesting that Mg^{2+} interacts with Si-O-Si.

Figure 5.6 shows total isotropic projection of ^{17}O 3QMAS NMR spectra for Na-Mg silicate glasses with varying X_{MgO}. The Si-O-Si peak is well resolved in Na-Mg silicate glasses. The peak maximum of Si-O-Si increases from -46.4 $\pm$ 0.5 ppm at X_{MgO} = 0.025 to -44.5 $\pm$ 0.5 ppm at X_{MgO}=0.75. The peak maximum of NBOs [Na-O-Si + {Na, Mg}-NBO + Mg-O-Si] increases from -24.5 $\pm$ 0.5 ppm at X_{MgO} = 0.025 to -23.8 $\pm$ 0.5 ppm at X_{MgO}=0.05. It further decreases to -25.7 $\pm$ 0.5 ppm at X_{MgO} = 0.75. It should be noted that both NBO and BO peak positions change with composition, suggesting a relatively homogenous distribution of Mg^{2+}. In other word, Mg^{2+} interacts with BO and NBO. Similar observations have been reported for Ca-silicate glasses and Na-silicate glasses, where both the NBO and BO peak positions are strongly dependent on composition (Lee and Stebbins, 2006, 2009). The

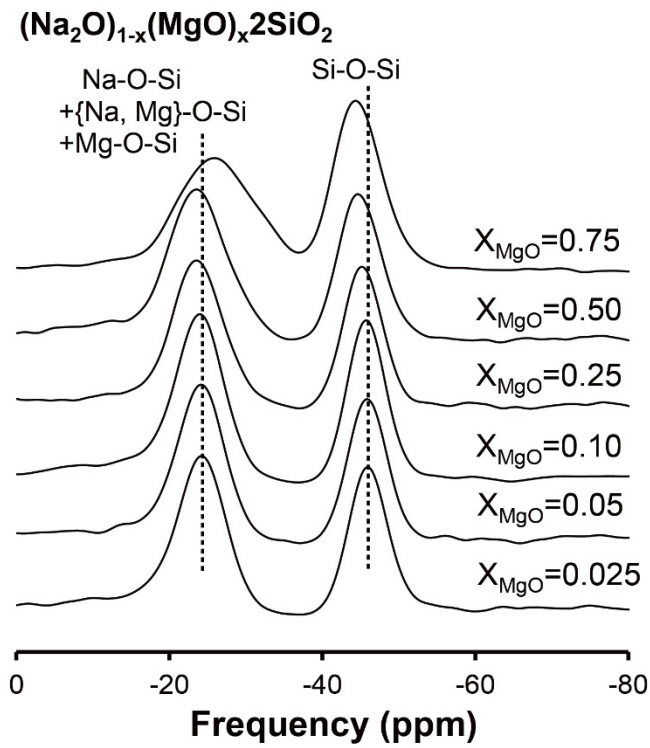

Figure 5.6. Total isotropic projection of ^{17}O 3QMAS NMR spectra for Na-Mg silicate glasses with varying at 9.4 T with varying X_{MgO} [MgO/(MgO+Al_2O_3)].

peak width of Si-O-Si increases from 6.3 ± 0.5 ppm at X_{MgO} = 0.025 to 7.5 ± 0.5 ppm at X_{MgO}=0.75. The peak width of {Na, Mg}-O-Si increases from 8.5 ± 0.5 ppm at X_{MgO}=0.025 to 13.5 ± 0.5 ppm at X_{MgO}=0.75 in isotropic dimension.

5.3.4. Probing the extent of network connectivity and configurational disorder in NMAS glasses and melts in nepheline-forsterite-quartz eutectic composition: ^{17}O MAS and 3QMAS NMR results

Figure 5.7 shows the 2D ^{17}O 3QMAS NMR spectra for NMAS glasses in the nepheline-forsterite-quartz eutectic composition with varying X_{MgO}, showing much enhanced resolution among the oxygen peaks compared with the ^{17}O MAS NMR spectra (data not shown here). The peak of Si-O-Si is completely resolved and those of Si–O–Al, and Al–O–Al are partially resolved. While the peaks of the NBOs [Na-O-Si, {Na, Mg}-O-Si, and Mg-O-Si] are not fully resolved due to peak overlapped with BOs, the peak shape of overlapped peak (Si-O-Al + NBOs) change with increasing X_{MgO}, suggesting an increase of NBOs. The NBO peaks are partially resolved at -35 ppm in isotropic dimension at X_{MgO} = 0.39. Note that the peak assignments of BOs and NBOs in the ^{17}O NMR spectra are based on previous studies of diverse crystalline and non-crystalline aluminosilicate and silicate glasses (Allwardt et al., 2003; Allwardt and Stebbins, 2004; Dirken et al., 1997; Lee, 2010; Lee et al., 2005; Lee et al., 2016; Maekawa et al., 1996; Pingel et al., 1998; Stebbins et al., 2001a; Stebbins and Xu, 1997; Stebbins et al., 2001b; Timken et al., 1987; Van Eck et al., 1999). The intensity of Si–O–Si decreases with increasing X_{MgO}. While the mixed NBOs peaks are overlapped with Si-O-Al, ^{17}O 3QMAS spectra show that the intensity of mixed NBOs peaks increases

with increasing X_{MgO}, consistent with expected fraction from composition. A non-negligible fraction of Al-O-Al species are observed in all of composition, indicating a violation of the Al-avoidance rule in the NMAS glasses in nepheline-forsterite-quartz eutectic composition. The fraction of Al-O-Al increases with increasing X_{MgO}.

Figure 5.8 shows the total isotropic projection of the 2D ^{17}O 3QMAS NMR spectra for NMAS glasses in nepheline-forsterite-quartz eutectic composition. While Si–O–Al are overlapped with NBOs, the Si-O-Si are clearly resolved and the fraction of Si-O-Si decreases with increasing X_{MgO}. The peak position of Si-O-Si decreases from ~-42.7 ppm at X_{MgO} = 0.13 to ~-44.5 ppm at X_{MgO} = 0.39. The peak position of Si-O-Al + NBOs [Na-O-Si + {Na, Mg}-O-Si + Mg-O-Si] increase from ~-26.3 ppm at X_{MgO} = 0.13 to ~-28.9 ppm at X_{MgO} = 0.39. A non-negligible fraction of Al–O–Al (~-12 ppm at X_{MgO} = 0.13) are partially resolved and it increases with increasing X_{MgO}.

Figure 5.9 shows the ^{17}O MAS NMR spectra for KLB-1 basaltic glasses with varying X_{MgO}, which a single broad peak due to the overlap among BOs and NBOs can be seen. The peak maximum of ^{17}O MAS NMR spectra for KLB-1 basaltic glasses increases from ~13 ppm (X_{MgO} = 0.55) to ~19 ppm (X_{MgO} = 0.79), suggesting the fraction of BOs and NBOs change with X_{MgO}. The overlapped peaks due to the NBO and BO sites are not resolved in the 1D MAS NMR spectra, but better resolution can be achieved by use of ^{17}O 3QMAS NMR. While the 1D MAS NMR spectra provide quantitative information for each BO and NBO, it is difficult to quantitative analysis due to peak overlap, the following discussion is thus qualitative.

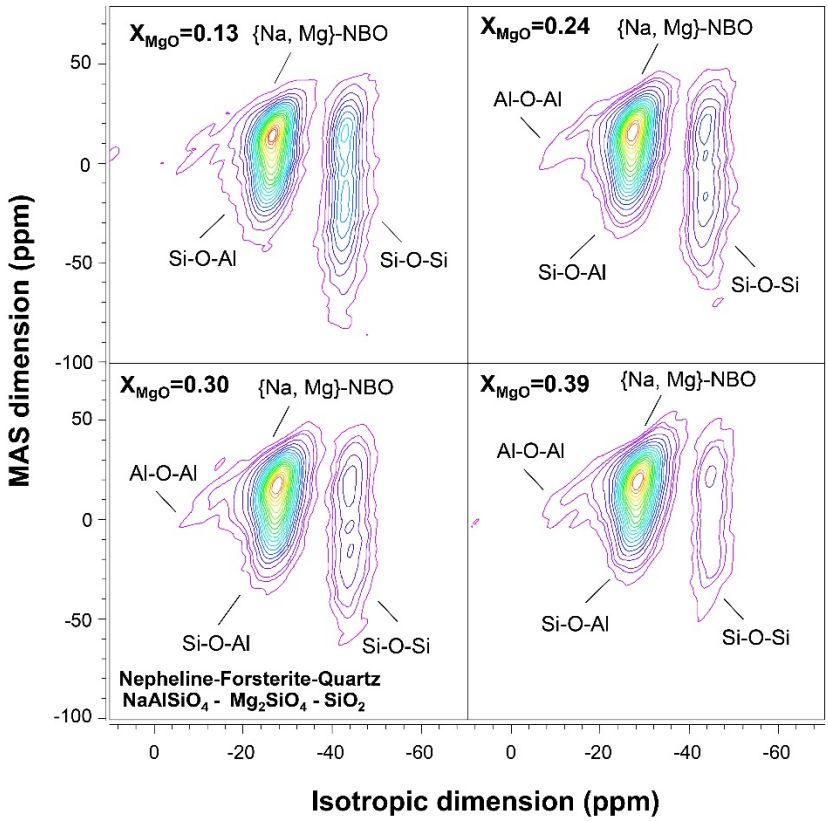

Figure 5.7. ^{17}O 3QMAS NMR spectra for Na_2O–MgO–Al_2O_3–SiO_2 glasses in nepheline-forsterite-quartz eutectic composition at 9.4 T with varying X_{MgO} [MgO/(MgO+Al_2O_3)]. Contour lines is drawn at 5% intervals from relative intensities of 8% to 98% with added lines at 3% and 5%.

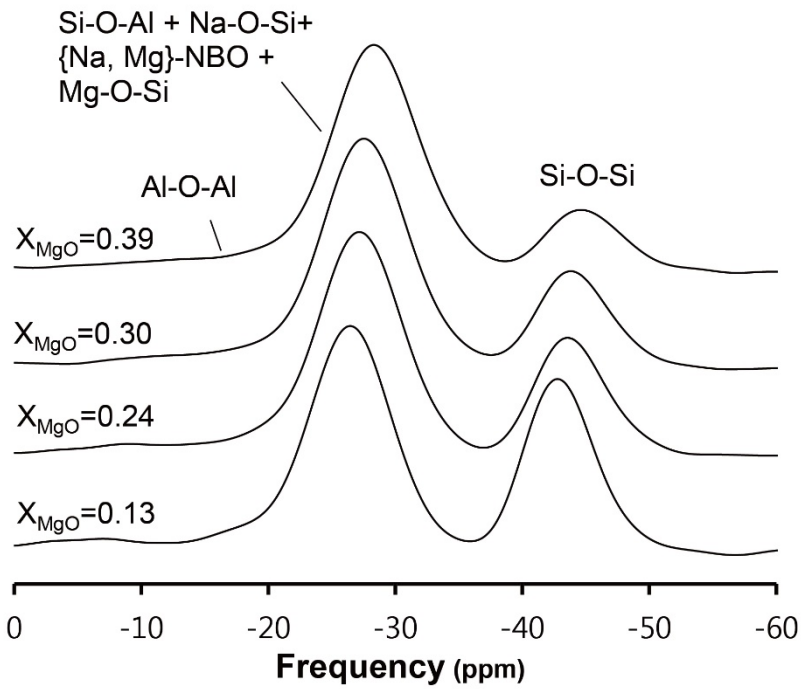

Figure 5.8. Total isotropic projection of ^{17}O 3QMAS NMR spectra for Na_2O–MgO–Al_2O_3–SiO_2 glasses in nepheline-forsterite-quartz eutectic composition at 9.4 T with varying X_{MgO} [MgO/(MgO+Al_2O_3)].

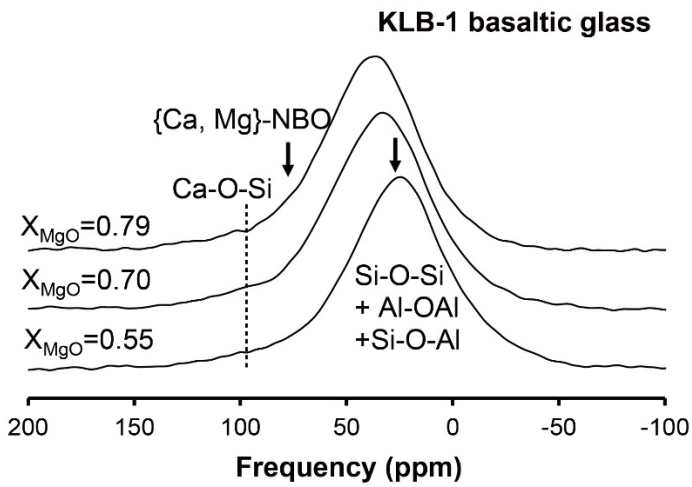

Figure 5.9. ^{17}O MAS NMR spectra for KLB-1 basaltic glasses at 9.4 T with varying X_{MgO} [$MgO/(MgO+Al_2O_3)$].

Figure 5.10 shows the 2D ^{17}O 3QMAS NMR spectra for KLB-1 basaltic glasses with varying X_{MgO}, showing much enhanced resolution among the oxygen peaks compared with the ^{17}O MAS NMR spectra (Figure 9). The peaks of BOs (Si–O–Si, Si–O–Al, and Al–O–Al) are partially resolved. The peaks of the NBOs are not fully resolved yet the peaks due to {Ca, Mg}–O–Si and Ca-O-Si can be seen as labeled; the oxygen clusters from 120 to 0 ppm in the MAS dimension stem from the different types of NBOs such as {Ca, Mg}–O–Si and Ca-O-Si (with peak maximum at ~ 100 ppm in MAS dimension). Note that the peak assignments of BOs and NBOs in the ^{17}O 3QMAS NMR spectra are based on previous studies of diverse crystalline and non-crystalline aluminosilicate glasses (e.g., Allwardt et al., 2003; Allwardt and Stebbins, 2004; Dirken et al., 1997; Lee, 2010; Lee et al., 2005; Pingel et al., 1998; Stebbins et al., 2001a; Stebbins and Xu, 1997; Stebbins et al., 2001b; Van Eck et al., 1999, and references therein). It also shows a non-negligible fraction of Al–O–Al species (~-12 ppm in isotropic dimension), indicating a violation of the Al-avoidance rule in KLB-1 basaltic glass at X_{MgO} = 0.55. As expected from the composition, the intensity of Si–O–Al increases and that of Al-O-Si decrease with increasing X_{Mgo}. The intensity of Si-O–Si and the mixed NBOs increases with increasing X_{MgO}.

5.3.5. Preferential partitioning between NBO and non-network cations and the degree of Si/Al disorder.

The ^{17}O MAS and 3QMAS NMR results can also help constrain the role of non-framework cations in the glasses, for example, the NBO/T is 0.51 and the X_{NBO} is 0.22 (~22%) in the KLB-1 basaltic glass at X_{MgO} = 0.55. Na–O–Si peak position is well-defined in the 2D NMR spectra and it does not

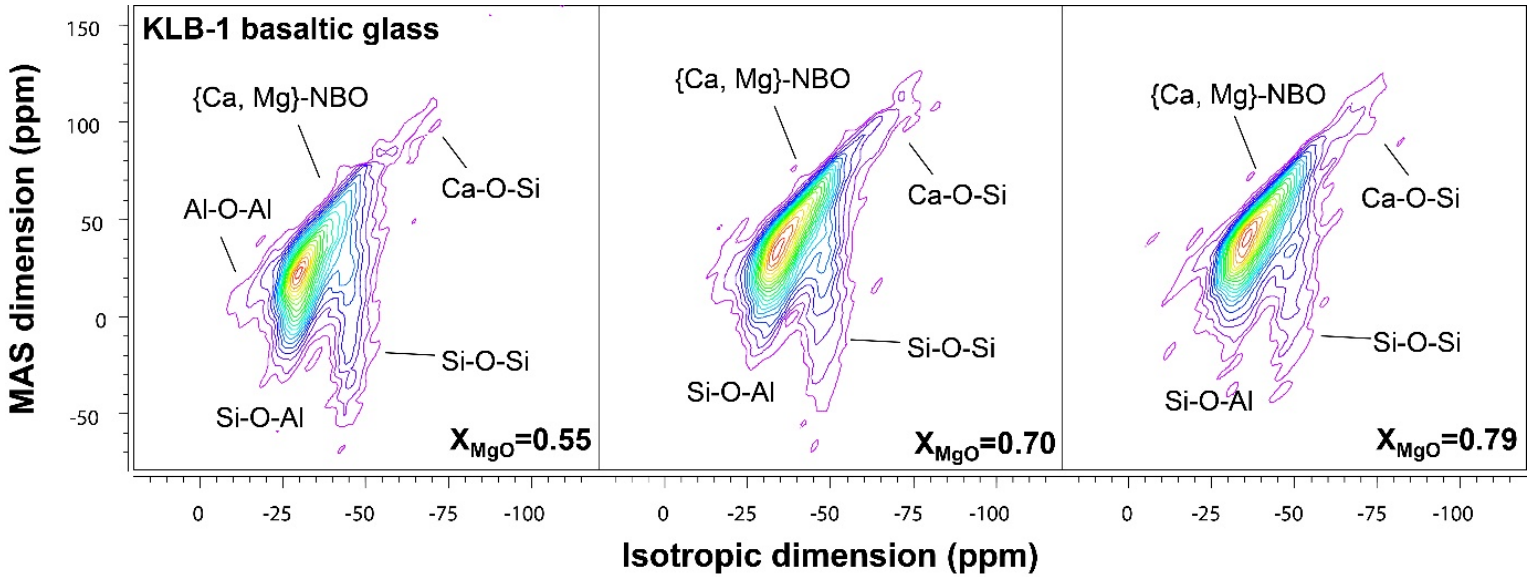

Figure 5.10. ^{17}O 3QMAS NMR spectra for KLB-1 basaltic glasses at 9.4 T with varying X_{MgO} [$MgO/(MgO+Al_2O_3)$].Contour lines are drawn at 5% intervals from relative intensities of 8% to 98% with added lines at 4%.

have strong composition dependence (Lee et al., 2003; Lee and Stebbins, 2003). Additionally Na–O–Si and Si–O–Al peaks are relatively well-resolved in ^{17}O 3QMAS NMR spectrum (Lee and Stebbins, 2009). If more than 2–3% of Na–O–Si would exist in KLB-1 basaltic glass at X_{MgO} = 0.55, Na–O–Si peak could be observed. Currently ^{17}O 3QMAS NMR spectra for KLB-1 basaltic glasses do not show any evidence for Na–O–Si. Nevertheless, a few % of Na–O–Si in KLB-1 basaltic glass, if exist, due to overlaps with Si–O–Al and extremely broad {Ca, Mg}-NBO, may not be detected. The ^{17}O 3QMAS NMR spectrum for KLB-1 basaltic glass at X_{MgO} = 0.55 shows very clear presence of {Ca, Mg}–O–Si peak, indicating the strong preference of NBO for Ca^{2+} and Mg^{2+}. These results suggest that Na^{+} plays a preferential role as a charge-balancing cation, whereas Ca^{2+} and Mg^{2+} can act as a network-modifying cation, forming NBOs. The observed non-randomness in the partitioning of those cations (Ca^{2+}, Mg^{2+}, and Na^{+}) into BOs and NBOs can be due to the differences in their field strengths (Maekawa et al., 1991; Mysen, 1988; Mysen et al., 1982; Park and Lee, 2014); higher field strength cations {e.g., Ca^{2+}, Mg^{2+}} in the glasses studied here are expected to be preferentially partitioned into NBOs, whereas Na^{+} would be expected to have proximity to BOs (e.g., Si–O–Al).

While the NBO preference between Na^{+} and {Ca^{2+}, Mg^{2+}} is clearly demonstrated in the current ^{17}O NMR study, it is not a straightforward matter to probe the preference between Ca^{2+} and Mg^{2+} because of the peak overlap between Ca–O–Si, Mg–O–Si, and {Ca, Mg}–O–Si. Nevertheless, the peak of Ca–O-Si (intensity at ~100 ppm in the MAS dimension and ~-64 ppm in the isotropic dimension) is observed at X_{MgO} = 0.79, indicating the unexpected stability of Ca–O–Si. Similar features with Ca–O–Si have been observed in the glasses in the diopside ($CaMgSi_2O_6$)–Ca–tschermakite

($CaAl_2SiO_6$) and diopside-jadeite ($NaAlSi_2O_6$) join that have been attributed to preferential affinity between Ca^{2+} and the NBOs (over Mg^{2+}) and/or potential clustering of Ca^{2+} and Mg^{2+} around NBOs (Park and Lee, 2012, 2014). As Na^+ plays a preferential role as a charge-balancing cation in KLB-1 basaltic glasses, Ca^{2+} and Mg^{2+} are primarily network modifying cations, forming NBOs.

The hypothetical NBO distribution was calculated assuming a random distribution of Ca^{2+} and Mg^{2+} around NBOs with varying X_{MgO}. The random distribution model of Ca^{2+} and Mg^{2+} around NBOs leads to the formation of ^{3}Ca–NBO (i.e., Ca–O–Si, ~-64 ppm in isotropic dimension), ^{2}Ca^{1}Mg–NBO (~-56 ppm), ^{1}Ca^{2}Mg–NBO (~-46 ppm), and ^{3}Mg–NBO (~-36 ppm) (Allwardt and Stebbins, 2004). The predicted NBO fractions at Ca/(Ca+Mg) = 0.33 (X_{MgO} = 0.79) are 4% (^{3}Ca–NBO), 22% (^{2}Ca^{1}Mg–NBO), 44% (^{1}Ca^{2}Mg–NBO), and 30% (^{3}Mg–NBO), respectively (Kelsey et al., 2008). While the predicted fraction of Ca–O–Si is only 4% in KLB-1 basaltic glass at X_{MgO} = 0.79, the intensity of the feature at ~-64 ppm (i.e., Ca–O–Si) remains apparently prevalent regardless of composition. Though qualitative, the result indicates that the observed Ca–O–Si in glasses is likely to be higher than the expected Ca–NBO based on the random distribution model. Currently due to peak overlap, it is not possible to deduce the origin of the unexpected presence of Ca-O-Si in the glasses. Nevertheless, the observed trends in KLB-1 basaltic glasses also show that Ca^{2+} and Mg^{2+} in the network both deviate from a random-distribution. The preferential partitioning of Na^+, Ca^{2+}, and Mg^{2+} between NBOs [Na–O–Si and {Ca, Mg}–O–Si] and BOs with charge-balancing cations (i.e., Na---Al–O–Al, {Ca, Mg}---Al–O–Si) in glasses can be described using the following quasi-chemical equations:

$$Na\text{---}Al\text{–}O\text{–}Si + \{Ca, Mg\}\text{–}O\text{–}Si = \{Ca, Mg\}\text{---}Al\text{–}O\text{–}Si + Na\text{–}O\text{–}Si \quad (1)$$

$$Na\text{---}Al\text{–}O\text{–}Al + \{Ca, Mg\}\text{–}O\text{–}Si = \{Ca, Mg\}\text{---}Al\text{–}O\text{–}Al + Na\text{–}O\text{–}Si \quad (2)$$

$$Na\text{---}Si\text{–}O\text{–}Si + \{Ca, Mg\}\text{–}O\text{–}Si = \{Ca, Mg\}\text{---}Si\text{–}O\text{–}Si + Na\text{–}O\text{–}Si \quad (3)$$

In the KLB-1 basaltic glasses, the current results demonstrate that the formation of Na---Al(Si)–O–Si(Al) and {Ca, Mg}–O–Si species over {Ca, Mg}---Al(Si)–O–Si(Al) + Na–O–Si is favored. Qualitatively, the fraction of each BO and NBO structural environments changes with X_{MgO}. The fraction of Al–O–Al decreases with increasing R (Si/Al ratio) in the charge-balanced $NaAlSi_RO_{2+2R}$ glasses (Lee and Stebbins, 2000). It is noted that a small, but non-negligible fraction of Al–O–Al is observed at ~–15 ppm in isotropic dimension in the 2D ^{17}O 3QMAS NMR spectra of the KLB-1 basaltic glasses. The presence of Al–O–Al in the glasses again confirms that the distributions of $^{[4]}Si$ and $^{[4]}Al$ in the KLB-1 basaltic glasses and melts deviate from the complete Al-avoidance rule. The fraction of Al–O–Al decreases with increasing X_{MgO} (as the Si/Al ratio increases upto 5.7) and it is below the detection limit (~ 1%) when $X_{MgO} = 0.79$.

5.3.6. Implications for macroscopic thermodynamic and transport properties and geochemical processes

Natural basaltic glasses and melts have other important major (particularly iron), minor, and volatile components that provide important insights into the petrogenesis and properties. Thus, the application of the current results of the model basaltic glasses to real natural basaltic glasses has obvious limitations. In addition, we have studied the structure of the

quenched glasses, i.e., that of supercooled liquid frozen below the glass transition temperature that is much lower than the liquidus and thus, the effects of the other components and the temperature remain to be explored. Nevertheless, the current results can provide unique information on the microscopic origins of the properties of basaltic glasses and melts with varying composition and yields insights into the formation of the melts. Due to overlap among peaks in the glass system studied here, the information of quantitative fraction of each oxygen cluster is missing. The following discussion is thus qualitative.

The negative experimental enthalpy of mixing in NMAS glasses in nepheline-forsterite-quartz eutectic composition and KLB-1 basaltic glasses can be expected from the predominance of $^{[4]}$Al and its extensive mixing with Si, as evidenced by the significant fractions of $^{[4]}$Si–O–$^{[4]}$Al. The extensive Si–Al mixing in the glasses studied here is similar to the results from previous studies of ternary and quaternary aluminosilicate glasses where mixing between different framework cations are often preferred (Lee et al., 2005; Park and Lee, 2012). The presence of Al–O–Al is also apparent for the glasses studied here. While it is difficult to quantify the fractions of those bridging oxygens due to overlap among peaks, it is likely that the degree of intermixing between Al and Si (degree of Al avoidance, Q) may range between a random distribution, (Q = 0) and chemical order (Q = 1). Due to considerable mixing between Si and Al in the melts, activity coefficient of silica is thus expected to be less than 1 (predicted value for a random distribution of Al–Si), increasing the tendency to form a silica-rich melt in contact with mantle rocks (Ryerson, 1985).

The current ^{17}O NMR results unambiguously show that NBO prefers Ca^{2+} and Mg^{2+} over Na^{+} in the KLB-1 basaltic glasses, whereas Na^{+} prefers to have proximity to BOs. The observed bonding preferences among non-network formers and BOs and NBOs highlight the non-random distribution of non-network formers in the glass network. Additionally, while the potential prevalence of Ca-NBO in the glasses in the intermediate composition and thus a certain degree of unmixing between Ca^{2+} and Mg^{2+} around NBO may additionally contribute to the mixing properties (toward a positive deviation), the configuration enthalpy of the KLB-1 basaltic glasses is expected to show negative deviation due to a strong deviation from the randomness observed in the Si/Al distribution towards chemical ordering and preferential partitioning among network modifying cations and NBOs/BOs. It is certainly a weak correlation, however previous study for the model basaltic glasses and melts suggested that NBO preference could affect the chemical composition of groundwater on volcanic islands where Mg^{2+} concentration is higher than expected from the composition of basalts considering the stronger bond between network-modifying cations (Ca^{2+}) and NBOs, Mg^{2+} (with proximity to BO) (Hurwitz et al., 2003; Jeong and Sohn, 2011; Park and Lee, 2012). This correlation also could apply for KLB-1 basaltic glasses, where Mg^{2+} is likely to be dissolved easily due to NBO preference of Ca^{2+} while Na^{+} is likely to be dissolved easily due to NBO preference of Ca^{2+} and Mg^{2+} in andesitic glasses (Park and Lee, 2014). Nevertheless, natural basalts have significant minerals, thus the application of dissolution mechanisms in KLB-1 basaltic glasses to real natural basalts has limitations. The dissolution mechanisms in minerals are different from those process in glasses. For, example, the dissolution in crystalline diopside is determined by the weaker bonding of Ca^{2+} (which is in M_2 sites) than Mg^{2+} (which is in more

strongly bonded M_1 sites). Thus Ca^{2+} is dissolved easily than Mg^{2+} in crystalline diopside (e.g., Schott et al., 1981). In contrast, the dissolution in basaltic glasses is determined by NBO preference between cations. Thus Mg^{2+} is likely to be dissolved easily than Ca^{2+}.

The viscosities of silicate melts are strongly affected by the volatiles (i.e., H_2O and CO_2) in natural magma. For example, the fraction of H_2O affects melt polymerization, thus the viscosity that depends on silicate polymerization decreases with increasing the fraction of H_2O (e.g., Richet et al., 1996). The viscosity also depends on the CO_2 content because the formation of CO_3^{2-} species requires that the silicate melt becomes more polymerized (e.g., Bourgue and Richet, 2001). Thus the viscosities of silicate melts decrease with increasing NBO fraction {e.g., $\eta \propto \exp[A/(B + X_{NBO})]$}, where A and B are constant) (Giordano and Dingwell, 2003; Lee et al., 2004). The estimated NBO fraction from the composition of glasses in nepheline-forsterite-quartz eutectic composition increases with increasing X_{MgO} from ~1.6% (X_{MgO} = 0.13) to ~10.9% (X_{MgO} = 0.39). The current ^{17}O 3QMAS NMR spectra for NMAS glasses in nepheline-forsterite-quartz eutectic composition also confirm that NBO content certainly increases with an increase of X_{MgO}. Although the experimental melt viscosity data for NMAS glasses in nepheline-forsterite-quartz eutectic composition are not available, a decrease in the degree of polymerization due to an increase of NBO fraction implies that the melt viscosity at constant temperature is expected to increase (e.g., Giordano and Dingwell, 2003; Mazurin, 1983).

Although the viscosities of silicate melts are affected by melt polymerization, it is also affected by highly coordinated Al because that property is proportional to $\exp(1/S_{config})$, which is related to the fraction of highly coordinate Al (Adam and Gibbs, 1965; Neuville and Richet, 1991;

Richet, 1984). Previous ^{17}O NMR study for Ca-aluminosilicate glasses suggested that the highly-coordinated Al could affect an increase of viscosity because it could have a role of highly-coordinated Si (Stebbins and Xu, 1997). Current ^{27}Al NMR results for KLB-1 basaltic glasses show that the fraction of $^{[5]}Al$ increases upto ~2.6% with increasing X_{MgO}. Those results suggest that the viscosity of KLB-1 basaltic glasses and melts are expected to decrease due to $^{[5]}Al$ as well as NBOs. Because the iron contents are removed from the original composition of KLB-1 and thus the viscosity of KLB-1 basaltic glasses studied here are expected to be different from natural basaltic glasses and melts generated by partial melting of KLB-1. For example, the viscosity of model basaltic melts (diopside:anorthite = 50 : 50) is higher than that of natural basaltic melts (Hofmeister et al., 2009; Villeneuve et al., 2008). Thus the application of viscosity for current results have limitations. The viscosities of silicate melts affect melt mobility. For example, the mobility of carbonate-rich melt is higher than that of basaltic melts due to the difference of viscosity between carbonate and basaltic melts (e.g., Kono et al., 2014). While the viscosity of basaltic melts slightly increases due to highly-coordinated Al with increasing X_{MgO}, it could affect the melt mobility and thus it yield the effective melt extraction.

Previous ^{27}Al MAS and 3QMAS NMR study for diopside-anorthite eutectic composition (model basaltic glasses) at high pressure showed that highly coordinated Al increases with increasing pressure (Lee et al., 2012). Current ^{27}Al 3QMAS NMR results for KLB-1 basaltic glasses show that the fraction of $^{[5]}Al$ increases with increasing X_{MgO}, suggesting that the depth where the highly coordinated Al are generated is shallower than expected one. The highly coordinated Al could affect the transport properties such as viscosity.

On-going modeling of melt properties utilizing the diverse degree of experimentally observed disorder will certainly be useful in quantifying structural disorder and predicting their macroscopic properties (e.g., Lee, 2011). Future applications of these recent advances and progress (i.e., the network connectivity and the preferential partitioning of non-framework cations into NBOs) in the KLB-1 basaltic glasses and other multi-component melts should provide full insights into the atomistic origins of their macroscopic properties.

5.4. Conclusions

The experimental data presented here provide structural details of atomic configurations around Al atoms and their connectivity (through changes in NBO and BO environments), and the extent of chemical and topological disorder in multi-component NMAS glasses in nepheline-forsterite-quartz eutectic composition and KLB-1 basaltic glasses. While the ^{27}Al MAS and 3QMAS NMR spectra for NMAS glasses in nepheline-forsterite-quartz eutectic composition show only $^{[4]}$Al, those for KLB-1 basaltic glasses show $^{[5]}$Al as well as $^{[4]}$Al. The fraction of $^{[5]}$Al in KLB-1 basaltic glasses increase upto ~2.6% with increasing X_{MgO}. The spectral analysis of $^{[4]}$Al peak in NMAS glasses in nepheline-forsterite-quartz eutectic composition suggests that the degree of distortion around the Al coordination environments increases with increasing X_{MgO}. The 2D ^{17}O 3QMAS NMR spectra revealed previously unknown details of diverse structural disorder in the multi-component NMAS glasses in nepheline-forsterite-quartz eutectic composition and KLB-1 basaltic glasses. In addition to the clear effects of composition, the ^{17}O 3QMAS NMR spectra for the KLB-1 basaltic glasses studied here confirm that the degree of polymerization (BO

content) decreases with increasing X_{MgO}. The significant fraction of Si-O-Al supports extensive mixing between $^{[4]}$Al and $^{[4]}$Si. Furthermore, Al-O-Al is observed in NMAS glasses in nepheline-forsterite quartz eutectic composition and KLB-1 basaltic glasses, suggesting a deviation from Al avoidance in these glasses. Based on the analysis of the peak position of {Ca, Mg}-mixed NBOs, non-random distributions of Na^+, Ca^{2+}, and Mg^{2+} around both NBOs and BOs are manifested by a moderate degree of partitioning of Ca^{2+} and Mg^{2+} into NBOs and by the spatial proximity between Na^+ and BOs (Al-O-Al and Al-O–Si) in the KLB-1 basaltic glasses studied here.

APPENDIX

5.A.1. Effect of composition on structural disorder

5.A.1.1. Effect of composition on network connectivity for Na-Mg silicate glasses with varying X_{MgO}.

Figure 5.A1 shows the ^{17}O MAS NMR spectra for Na-Mg silicate glasses with varying X_{MgO} [MgO/(MgO+ Na_2O)] at 9.4 T. The peak shape of ^{17}O MAS spectrum of Na-Mg silicate glasses at X_{MgO} = 0.025 is similar with that of previous study for $Na_2O{\cdot}2SiO_2$ glass (Lee and Stebbins, 2009). The NBO peaks [Na-O-Si (~35 ppm)+ {Na, Mg}−O−Si + Mg-O-Si (~30 ppm)] and a BO peak (Si−O−Si) are partially resolved in the ^{17}O MAS NMR spectra for Na-Mg silicate glasses. Because of the smaller difference in the peak positions for Na-NBO and Mg-NBO, the spectra of the Na-Mg silicate glasses show a broad peak that results from the overlapping of Si-O-Si and the NBOs [Na-O-Si, Mg-O-Si, and mixed {Na, Mg}-O-Si], as labeled. The peak maximum of ^{17}O MAS spectra for Na-Mg silicate glasses decreases from 29.7

± 0.5 ppm at X_{MgO} = 0.025 to 24.3 ± 0.5 ppm at X_{MgO} = 0.25 with increasing X_{MgO}. It increases with a further increase in X_{MgO} to 27.0 ±0.5 ppm at X_{MgO} = 0.75. Those results suggest that the oxygen environments change with increasing X_{MgO}. The noticeable intensity of the mixed NBO peaks and their evolution with composition demonstrate an extensive mixing between Na^{+} and Mg^{2+} around the NBO.

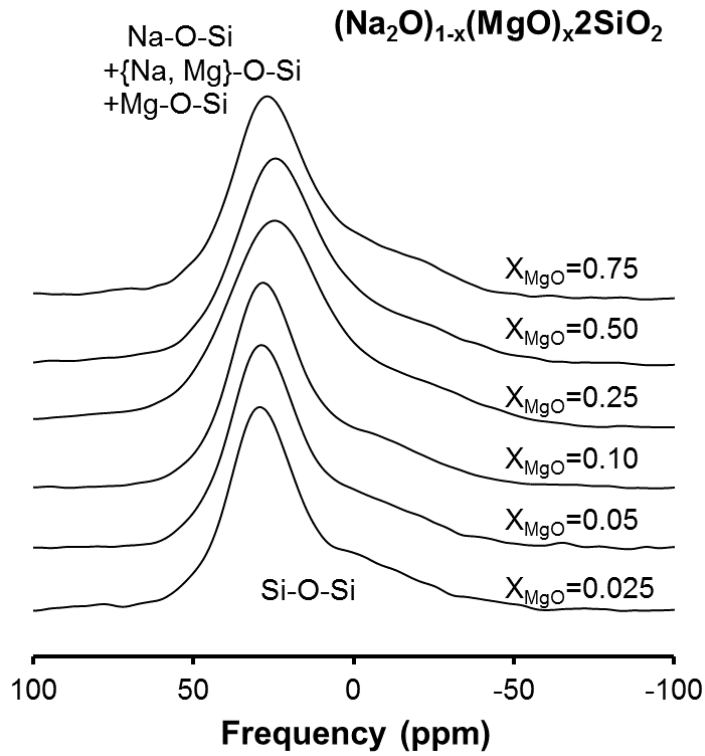

Figure 5.A1. ^{17}O MAS NMR spectra for Na-Mg silicate glasses with varying X_{MgO} [$MgO/(MgO+Al_2O_3)$].

5.A.1.2. Effect of composition on Si environments of Na-Mg silicate glasses

Figure 5.A2 shows the ^{29}Si MAS NMR spectra and fitting results for the Na-Mg silicate glasses. A single overlapped broad peak is observed for all the Na-Mg silicate glasses. The chemical shift of ^{29}Si MAS NMR spectra is sensitive to variations in bond angles and length as well as second and third neighbor environments around the Si atom. So the wider variety of the atomic arrangements around Si atoms will result in broader linewidth (FWHM) in its ^{29}Si MAS NMR spectrum. The peak maximum is consistent (~-89 ppm) at X_{MgO} = 0.025, 0.50, and 0.10 and then it decreases to ~-93 ppm for X_{MgO} = 0.50. The ^{29}Si MAS NMR spectra for the Na-Mg silicate glasses with varying X_{MgO} are simulated with three Gaussian functions corresponding to the Q^4, Q^3, and Q^2 species, respectively. The peak positions are set to -98.5, -89.0, and -78.5 ppm for Q^4, Q^3, and Q^2 species, respectively. The FWHM is set to 13, 9.8, and 8.5 ppm for the Q^4, Q^3, and Q^2 species, respectively. Previous ^{29}Si MAS NMR study for $Na_2Si_2O_5$ glass reported that the fractions of Q^4, Q^3, and Q^2 for $Na_2Si_2O_5$ are 11%, 79%, and 10%, respectively (Maekawa et al., 1991). The predicted fractions of Q^4, Q^3, and Q^2 for glass at X_{MgO} = 0.025 are ~10%, ~17%, and 74%, respectively. The predicted fractions of Q^4, Q^3, and Q^2 for glass at X_{MgO} = 0.05 are ~10%, ~18%, and 72%, respectively. Those results indicate that the variation of Q^n species (i.e., degree of disorder around Si) is not significant with varying X_{MgO}.

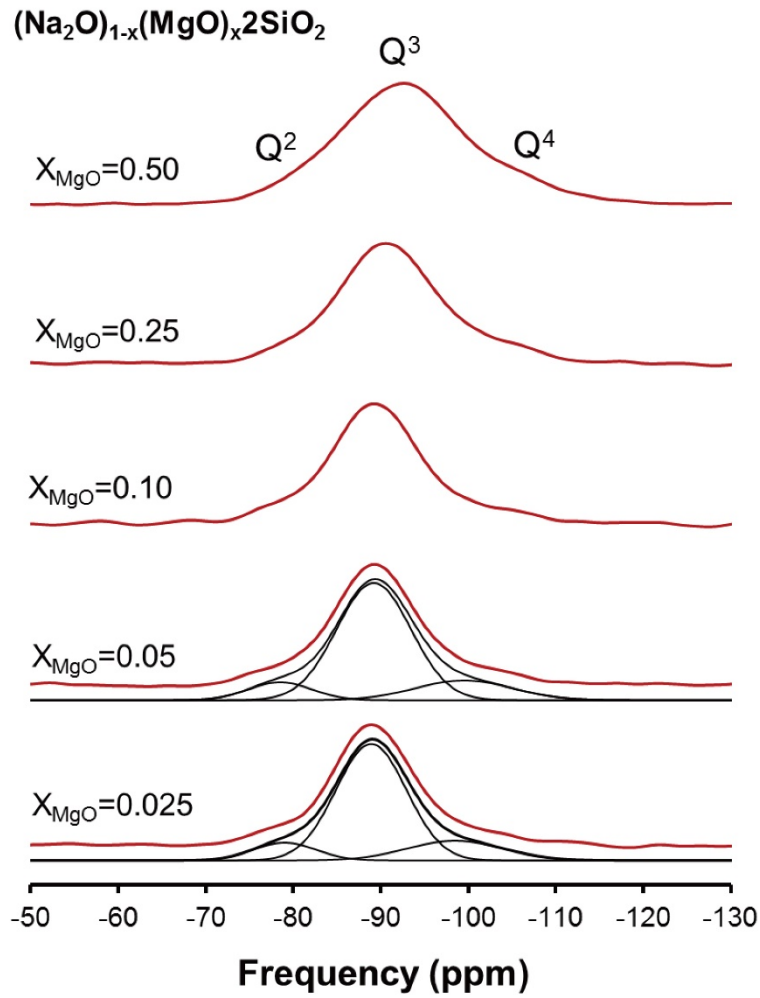

Figure 5.A2. ^{29}Si MAS NMR spectra for Na-Mg silicate glasses with varying X_{MgO} [MgO/(MgO+Al_2O_3)] and simulation results of the ^{29}Si MAS NMR spectra for Na-Mg silicate glasses at X_{MgO}=0.025 and 0.05. The red and black lines represent the experimental and simulation results, respectively.

5.A.1.3. Effect of composition on Al environments of NMAS glasses in nepheline-forsterite-quartz eutectic composition

Figure 5.A3 shows that the estimated peak width (FWHM) for $^{[4]}$Al in the isotropic projection slightly increases from 8.9 ± 1.5 ppm (X_{MgO} = 0.13) to 10.9 ± 1.5 ppm (X_{MgO} = 0.39) with increasing X_{MgO}. Those results again confirm that the configurational disorder around Al in the glasses increases with increasing X_{MgO}.

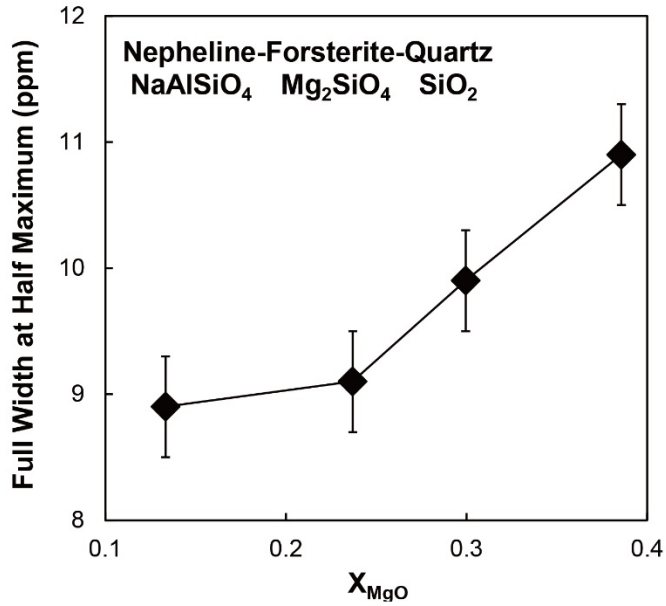

Figure 5.A3. Peak widths (full-width at half-maximum) of $^{[4]}$Al in total isotropic projection of ^{27}Al 3QMAS NMR spectra for Na_2O–MgO–Al_2O_3–SiO_2 glasses in nepheline-forsterite-quartz eutectic composition with varying X_{MgO} [MgO/(MgO+Al_2O_3)] at 9.4 T.

5.A.1.4. Effect of composition on network connectivity of NMAS glasses in nepheline-forsterite-quartz eutectic composition

Figure 5.A4 shows the ^{17}O MAS NMR spectra for the NMAS glasses in nepheline-forsterite-quartz eutectic composition with varying X_{MgO}, which shows a single broad peak that results from overlapping BOs and NBOs. The peak maximum of ^{17}O MAS NMR spectra increases from 14.4 ± 1.5 ppm at X_{MgO} = 0.13 to 19.8 ± 1.5 ppm at X_{MgO} = 0.39, suggesting the change of BOs and NBOs fraction. Figure 10 shows the ^{17}O MAS NMR spectra for the KLB-1 basaltic glasses with varying X_{MgO}. Those spectra also show a single broad peak that results from overlapping BOs and NBOs. The peak shape, position, and width for each BO and NBO site change with increasing X_{MgO}. The peak position of ^{17}O MAS NMR spectra increases from 12.6 ± 1.5 ppm at X_{MgO} = 0.55 to 18.9 ± 1.5 ppm at X_{MgO} = 0.79, suggesting the change of BOs and NBOs fraction. The overlapped peaks due to the NBO and BO sites are not fully resolved in the 1D MAS ^{17}ONMR spectra, but better resolution can be achieved by use of ^{17}O 3QMAS NMR.

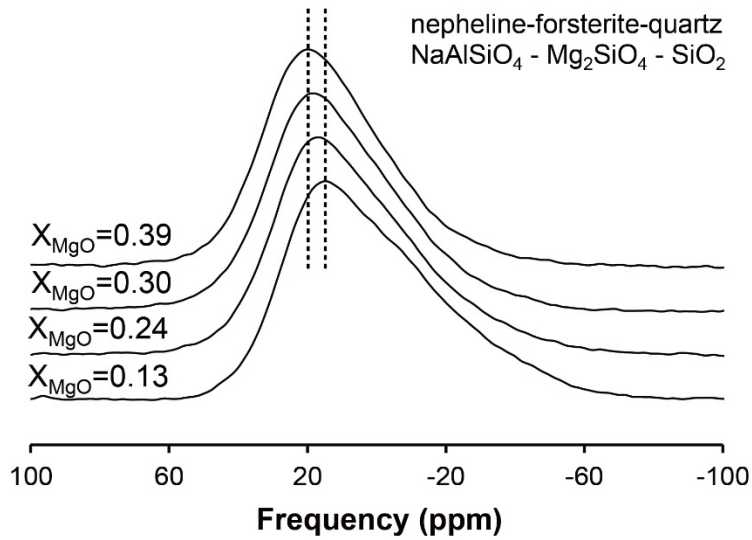

Figure 5.A4. ^{17}O MAS NMR spectra for Na_2O–MgO–Al_2O_3–SiO_2 glasses in nepheline-forsterite-quartz eutectic composition at 9.4 T with varying X_{MgO} [MgO/(MgO+Al_2O_3)].

5.A.1.5. Effect of composition on network connectivity of KLB-1 basaltic glasses

Figure 5.A5 shows the total isotropic projection (sum of the spectral intensity into the isotropic dimension) of the 2D ^{17}O 3QMAS NMR spectra for KLB-1 basaltic glasses. We did not attempt to quantify the fraction of BO and NBO peaks due to the overlap among the peaks in these glasses. Nevertheless, the spectra clear shows that the fraction of NBOs and Si–O–Si apparently increases with increasing X_{MgO}, whereas the Si–O–Al peak intensity decreases.

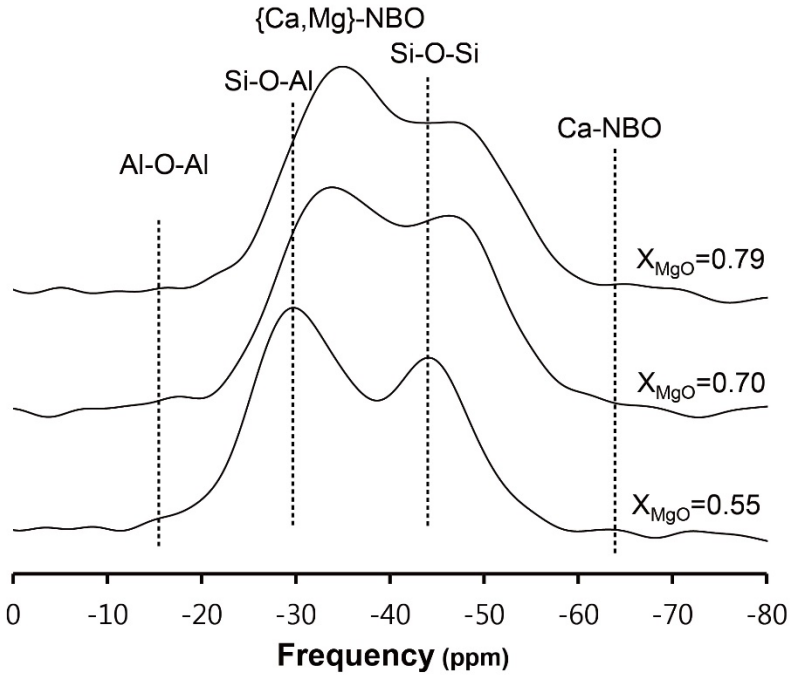

Figure 5.A5. Total isotropic projection of ^{17}O 3QMAS NMR spectra for KLB-1 basaltic glasses at 9.4 T with varying X_{MgO} [MgO/(MgO+Al_2O_3)].

References

Adam, G. and Gibbs, J.H. (1965) On temperature dependence of cooperative relaxation properties in glass-forming liquids. *J. Chem. Phys.* 43, 139-&.

Agee, C.B. and Walker, D. (1993) Olivine flotation in mantle melt. *Earth Planet. Sci. Lett.* 114, 315-324.

Allwardt, J.R., Lee, S.K. and Stebbins, J.F. (2003) Bonding preferences of non-bridging O atoms: Evidence from ^{17}O MAS and 3QMAS NMR on calcium aluminate and low-silica Ca-aluminosilicate glasses. *Am. Miner.* 88, 949-954.

Allwardt, J.R. and Stebbins, J.F. (2004) Ca-Mg and K-Mg mixing around non-bridging O atoms in silicate glasses: An investigation using ^{17}O MAS and 3QMAS NMR. *Am. Miner.* 89, 777-784.

Allwardt, J.R., Stebbins, J.F., Schmidt, B.C., Frost, D.J., Withers, A.C. and Hirschmann, M.M. (2005) Aluminum coordination and the densification of high-pressure aluminosilicate glasses. *Am. Miner.* 90, 1218-1222.

Arndt, N.T., Kerr, A.C. and Tarney, J. (1997) Dynamic melting in plume heads: The formation of Gorgona komatiites and basalts. *Earth Planet. Sci. Lett.* 146, 289-301.

Bajgain, S., Ghosh, D.B. and Karki, B.B. (2015) Structure and density of basaltic melts at mantle conditions from first-principles simulations. *Nat. Commun.* 6, 8578.

Bak, M., Rasmussen, J.T. and Nielsen, N.C. (2000) SIMPSON: A general simulation program for solid-state NMR spectroscopy. *J. Magn. Reson.* 147, 296-330.

Baltisberger, J.H., Xu, Z., Stebbins, J.F., Wang, S.H. and Pines, A. (1996) Triple-quantum two-dimensional ^{27}Al magic-angle spinning

nuclear magnetic resonance spectroscopic study of aluminosilicate and aluminate crystals and glasses. *J. Am. Chem. Soc.* 118, 7209-7214.

Bauchy, M., Guillot, B., Micoulaut, M. and Sator, N. (2013) Viscosity and viscosity anomalies of model silicates and magmas: A numerical investigation. *Chem. Geol.* 346, 47-56.

Bechgaard, T.K., Goel, A., Youngman, R.E., Mauro, J.C., Rzoska, S.J., Bockowski, M., Jensen, L.R. and Smedskjaer, M.M. (2016) Structure and mechanical properties of compressed sodium aluminosilicate glasses: Role of non-bridging oxygens. *J. Non-Cryst. Solids* 441, 49-57.

Bourgue, E. and Richet, P. (2001) The effects of dissolved CO_2 on the density and viscosity of silicate melts: a preliminary study. *Earth Planet. Sci. Lett.* 193, 57-68.

Bunker, B.C., Kirkpatrick, R.J. and Brow, R.K. (1991) Local-structure of alkaline-earth boroaluminate crystals and glasses .1., crystal chemical concepts structural predictions and comparisons to known crystal-structures. *J. Amer. Ceram. Soc.* 74, 1425-1429.

Cottrell, E. and Kelley, K.A. (2011) The oxidation state of Fe in MORB glasses and the oxygen fugacity of the upper mantle. *Earth Planet. Sci. Lett.* 305, 270-282.

Dirken, P.J., Kohn, S.C., Smith, M.E. and vanEck, E.R.H. (1997) Complete resolution of Si-O-Si and Si-O-Al fragments in an aluminosilicate glass by ^{17}O multiple quantum magic angle spinning NMR spectroscopy. *Chem. Phys. Lett.* 266, 568-574.

Dobretsov, N.L., Kirdyashkin, A.A., Kirdyashkin, A.G., Gladkov, I.N. and Surkov, N.V. (2006) Parameters of hotspots and thermochemical plumes during their ascent and eruption. *Petrology* 14, 477-491.

Du, W., Li, L. and Weidner, D.J. (2014) Experimental observation on grain boundaries affected by partial melting and garnet forming phase

transition in KLB-1 peridotite. *Phys. Earth and Planet. In.* 228, 287-293.

Eggler, D.H. (1978) Effect of CO_2 upon partial melting of peridotite in system Na_2O-CaO-Al_2O_3-MgO-SiO_2-CO_2 to 35 kb, with an analysis of melting in a peridotite-H_2O-CO_2 system. *Am. J. Sci.* 278, 305-343.

Frydman, L. and Harwood, J.S. (1995) Isotropic spectra of half-integer quadrupolar spins from bidimensional magic-angle spinning NMR. *J. Am. Chem. Soc.* 117, 5367-5368.

Ghose, S. and Tsang, T. (1973) Structural dependence of quadrupole coupling-constant E2QQ/H for ^{27}Al and crystal-field parameter D for Fe^{3+} in aluminosilicate. *Am. Miner.* 58, 748-755.

Giordano, D. and Dingwell, D.B. (2003) Non-Arrhenian multicomponent melt viscosity: a model. *Earth Planet. Sci. Lett.* 208, 337-349.

Giordano, D., Potuzak, M., Romano, C., Dingwell, D.B. and Nowak, M. (2008) Viscosity and glass transition temperature of hydrous melts in the system $CaAl_2Si_2O_8$-$CaMgSi_2O_6$. *Chem. Geol.* 256, 203-215.

Gupta, A.K., Green, D.H. and Taylor, W.R. (1987) The liquidus surface of the system forsterite-nepheline-silica at 28 kb. *Am. J. Sci.* 287, 560-565.

Herzberg, C., Gasparik, T. and Sawamoto, H. (1990) Origin of mantle peridotite - constraints from melting experiments to 16.5 GPa. *J. Geophys. Res.-Solid Earth* 95, 15779-15803.

Herzberg, C. and Zhang, J.Z. (1996) Melting experiments on anhydrous peridotite KLB-1: Compositions of magmas in the upper mantle and transition zone. *J. Geophys. Res.-Solid Earth* 101, 8271-8295.

Hirose, K. (1997a) Melting experiments on Iherzolite KLB-1 under hydrous conditions and generation of high-magnesian andesitic melts. *Geology* 25, 42-44.

Hirose, K. (1997b) Partial melt compositions of carbonated peridotite at 3 GPa and role of CO_2 in alkali-basalt magma generation. *Geophys. Res. Lett.* 24, 2837-2840.

Hirose, K. (2002) Phase transitions in pyrolitic mantle around 670-km depth: Implications for upwelling of plumes from the lower mantle. *J. Geophys. Res.-Solid Earth* 107.

Hirose, K. and Fei, Y.W. (2002) Subsolidus and melting phase relations of basaltic composition in the uppermost lower mantle. *Geochim. Cosmochim. Acta* 66, 2099-2108.

Hirose, K. and Kawamoto, T. (1995) Hydrous partial melting of lherzolite at 1 GPa - the effect of H_2O on the genesis of basaltic magmas. *Earth Planet. Sci. Lett.* 133, 463-473.

Hirose, K. and Kushiro, I. (1993) Partial melting of dry peridotites at high pressures: Determination of compositions of melts segregated from peridotite using aggregates of diamond. *Earth Planet. Sci. Lett.* 114, 477-489.

Hofmeister, A.M., Whittington, A.G. and Pertermann, M. (2009) Transport properties of high albite crystals, near-endmember feldspar and pyroxene glasses, and their melts to high temperature. *Contrib. Mineral. Petr.* 158, 381-400.

Humphreys, E.R. and Niu, Y. (2009) On the composition of ocean island basalts (OIB): The effects of lithospheric thickness variation and mantle metasomatism. *Lithos* 112, 118-136.

Hurwitz, S., Goff, F., Janik, C.J., Evans, W.C., Counce, D.A., Sorey, M.L. and Ingebritsen, S.E. (2003) Mixing of magmatic volatiles with groundwater and interaction with basalt on the summit of Kilauea Volcano, Hawaii. *J. Geophys. Res.-Solid Earth* 108.

Iwamori, H., McKenzie, D. and Takahashi, E. (1995) Melt generation by isentropic mantle upwelling. *Earth Planet. Sci. Lett.* 134, 253-266.

Jeong, G.Y. and Sohn, Y.K. (2011) Microtextures, microchemistry, and mineralogy of basaltic glass alteration, Jeju Island, Korea, with implications for elemental behavior. American Mineralogist 96, 1129-1147.

Katz, R.F., Spiegelman, M. and Langmuir, C.H. (2003) A new parameterization of hydrous mantle melting. *Geochem. Geophy. Geosy.* 4.

Kelley, K.A. and Cottrell, E. (2012) The influence of magmatic differentiation on the oxidation state of Fe in a basaltic arc magma. *Earth Planet. Sci. Lett.* 329–330, 109-121.

Kelsey, K.E., Allwardt, J.R. and Stebbins, J.F. (2008) Ca-Mg mixing in aluminosilicate glasses: An investigation using ^{17}O MAS and 3QMAS and ^{27}Al MAS NMR. *J. Non-Cryst. Solids* 354, 4644-4653.

Komiya, T. (2004) Material circulation model including chemical differentiation within the mantle and secular variation of temperature and composition of the mantle. *Phys. Earth and Planet. In.* 146, 333-367.

Kono, Y., Kenney-Benson, C., Hummer, D., Ohfuji, H., Park, C., Shen, G., Wang, Y., Kavner, A. and Manning, C.E. (2014) Ultralow viscosity of carbonate melts at high pressures. *Nat. Commun.* 5.

Konzett, J. and Fei, Y.W. (2000) Transport and storage of potassium in the Earth's upper mantle and transition zone: an experimental study to 23 GPa in simplified and natural bulk compositions. *J. Petrol.* 41, 583-603.

Kushiro, I. (1968) Compositions of magmas formed by partial zone melting of Earths upper mantle *J. Geophys. Res.* 73, 619-&.

Kushiro, I. (1976) Changes in viscosity and structure of melt of $NaAlSi_2O_6$ composition at high pressures. *J. Geophys. Res.* 81, 6347-6350.

Kushiro, I. (2001) Partial melting experiments on peridotite and origin of mid-ocean ridge basalt. *Annu. Rev. Earth and Pl. Sc.* 29, 71-107.

Kushiro, I. and Mysen, B.O. (2002) A possible effect of melt structure on the Mg-Fe^{2+} partitioning between olivine and melt. *Geochim. Cosmochim. Acta* 66, 2267-2272.

Lee, S.K. (2005) Microscopic origins of macroscopic properties of silicate melts and glasses at ambient and high pressure: Implications for melt generation and dynamics. *Geochim. Cosmochim. Acta* 69, 3695-3710.

Lee, S.K. (2010) Effect of pressure on structure of oxide glasses at high pressure: Insights from solid-state NMR of quadrupolar nuclides. *Solid State Nucl. Magn. Reson.* 38, 45-57.

Lee, S.K. (2011) Simplicity in melt densification in multicomponent magmatic reservoirs in Earth's interior revealed by multinuclear magnetic resonance. *P. Natl. Acad. Sci. USA.* 108, 6847-6852.

Lee, S.K., Cody, G.D., Fei, Y.W. and Mysen, B.O. (2004) Nature of polymerization and properties of silicate melts and glasses at high pressure. *Geochim. Cosmochim. Acta* 68, 4189-4200.

Lee, S.K., Cody, G.D. and Mysen, B.O. (2005) Structure and the extent of disorder in quaternary (Ca-Mg and Ca-Na) aluminosilicate glasses and melts. *Am. Miner.* 90, 1393-1401.

Lee, S.K., Deschamps, M., Hiet, J., Massiot, D. and Park, S.Y. (2009) Connectivity and Proximity between Quadrupolar Nuclides in Oxide Glasses: Insights from through-Bond and through-Space Correlations in Solid-State NMR. *J. Phys. Chem. B.* 113, 5162-5167.

Lee, S.K., Kim, H.-I., Kim, E.J., Mun, K.Y. and Ryu, S. (2016) Extent of Disorder in Magnesium Aluminosilicate Glasses: Insights from ^{27}Al and ^{17}O NMR. *J. Phys. Chem. C* 120, 737-749.

Lee, S.K., Mysen, B.O. and Cody, G.D. (2003) Chemical order in mixed-cation silicate glasses and melts. *Phys. Rev. B* 68.

Lee, S.K., Park, S.Y., Kim, H.I., Tschauner, O., Asimow, P., Bai, L.G., Xiao, Y.M. and Chow, P. (2012) Structure of shock compressed model basaltic glass: Insights from O K-edge X-ray Raman scattering and high-resolution Al-27 NMR spectroscopy. *Geophys. Res. Lett.* 39.

Lee, S.K., Park, S.Y., Yi, Y.S. and Moon, J. (2010) Structure and Disorder in Amorphous Alumina Thin Films: Insights from High-Resolution Solid-State NMR. *J. Phys. Chem. C.* 114, 13890-13894.

Lee, S.K. and Stebbins, J.F. (2000) The structure of aluminosilicate glasses: High-resolution ^{17}O and ^{27}Al MAS and 3QMAS. *J. Phys. Chem. B.* 104, 4091-4100.

Lee, S.K. and Stebbins, J.F. (2003) Nature of cation mixing and ordering in Na-Ca silicate glasses and melts. *J. Phys. Chem. B.* 107, 3141-3148.

Lee, S.K. and Stebbins, J.F. (2006) Disorder and the extent of polymerization in calcium silicate and aluminosilicate glasses: O-17 NMR results and quantum chemical molecular orbital calculations. *Geochim. Cosmochim. Acta* 70, 4275-4286.

Lee, S.K. and Stebbins, J.F. (2009) Effects of the degree of polymerization on the structure of sodium silicate and aluminosilicate glasses and melts: An O-17 NMR study. *Geochim. Cosmochim. Acta* 73, 1109-1119.

Lee, S.K. and Sung, S. (2008) The effect of network-modifying cations on the structure and disorder in peralkaline Ca-Na aluminosilicate glasses: O-17 3QMAS NMR study. *Chem. Geol.* 256, 326-333.

Maekawa, H., Florian, P., Massiot, D., Kiyono, H. and Nakamura, M. (1996) Effect of Alkali-Metal Oxide on O-17 NMR Parameters and Si-O-Si Angles of Alkali-Metal Disilicate Glasses. *J. Phys. Chem.* 100, 5525-5532.

Maekawa, H., Maekawa, T., Kawamura, K. and Yokokawa, T. (1991) The structural groups of alkali silicate-glasses determined from Si-29 MAS-NMR. *J. Non-Cryst. Solids* 127, 53-64.

Malfait, W.J., Verel, R., Ardia, P. and Sanchez-Valle, C. (2012) Aluminum coordination in rhyolite and andesite glasses and melts: Effect of temperature, pressure, composition and water content. *Geochim. Cosmochim. Acta* 77, 11-26.

Matsukage, K.N. and Kubo, K. (2003) Chromian spinel during melting experiments of dry peridotite (KLB-1) at 1.0-2.5 GPa. *Am. Miner.* 88, 1271-1278.

Mazurin, O.V. (1983) *Handbook of Glass Data: Silica Glass and Binary Silicate Glasses*. Elsevier Science.

McFarlane, E.A., Drake, M.J. and Rubie, D.C. (1994) Element partitioning between mg-perovskite, magnesiowustite, and silicate melt at conditions of the Earths mantle. *Geochim. Cosmochim. Acta* 58, 5161-5172.

Moore, W.B., Schubert, G. and Tackley, P. (1998) Three-dimensional simulations of plume-lithosphere interaction at the Hawaiian swell. *Science* 279, 1008-1011.

Moulton, B.J.A., Henderson, G.S., Sonneville, C., O'Shaughnessy, C., Zuin, L., Regier, T. and de Ligny, D. (2016) The structure of haplobasaltic glasses investigated using X-ray absorption near edge structure (XANES) spectroscopy at the Si, Al, Mg, and O K-edges and Ca, Si, and Al L2,3-edges. *Chem. Geol.* 420, 213-230.

Mysen, B.O. (1988) Structure and Properties of Silicate Melts Elsevier Amsterdam.

Mysen, B.O. (2004) Element partitioning between minerals and melt, melt composition, and melt structure. *Chem. Geol.* 213, 1-16.

Mysen, B.O. and Dubinsky, E.V. (2004) Melt structural control on olivine/melt element partitioning of Ca and Mn. *Geochim. Cosmochim. Acta* 68, 1617-1633.

Mysen, B.O. and Richet, P. (2005) Silicate glasses and melts: Properties and structure. Elsevier, Amsterdam.

Mysen, B.O. and Toplis, M.J. (2007) Structural behavior of Al^{3+} in peralkaline, metaluminous, and peraluminous silicate melts and glasses at ambient pressure. *Am. Miner.* 92, 933-946.

Mysen, B.O., Virgo, D. and Seifert, F.A. (1982) The structure of silicate melts –implications for chemical and physical-properties of natural magam. *Rev. Geophys.* 20, 353-383.

Navrotsky, A., Zimmermann, H.D. and Hervig, R.L. (1983) Thermochemical study of glasses in the system $CaMgSi_2O_6$-$CaAl_2SiO_6$. *Geochim. Cosmochim. Acta* 47, 1535-1538.

Neuville, D.R., Cormier, L. and Massiot, D. (2004) Al environment in tectosilicate and peraluminous glasses: A Al-27 MQ-MAS NMR, Raman, and XANES investigation. *Geochim. Cosmochim. Acta* 68, 5071-5079.

Neuville, D.R., Cormier, L. and Massiot, D. (2006) Al coordination and speciation in calcium aluminosilicate glasses: Effects of composition determined by Al-27 MQ-MAS NMR and Raman spectroscopy. *Chem. Geol.* 229, 173-185.

Neuville, D.R. and Richet, P. (1991) Viscosity and mixing in molten (Ca, Mg) pyroxenes and garnets. *Geochim. Cosmochim. Acta* 55, 1011-1019.

Niu, Y. (2008) Geochemistry - The origin of alkaline lavas. Science 320, 883-884.

Ogawa, M. and Nakamura, H. (1998) Thermochemical regime of the early mantle inferred from numerical models of the coupled magmatism-mantle convection system with the solid-solid phase transitions at depths around 660 km. *J. Geophys. Res.-Solid Earth* 103, 12161-12180.

Park, S.Y. and Lee, S.K. (2012) Structure and disorder in basaltic glasses and melts: Insights from high-Resolution solid-state NMR study of glasses in diopside-Ca-tschermakite join and diopside-anorthite eutectic composition. *Geochim. Cosmochim. Acta* 80, 125-142.

Park, S.Y. and Lee, S.K. (2014) High-resolution solid-state NMR study of the effect of composition on network connectivity and structural disorder in multi-component glasses in the diopside and jadeite join:

Implications for structure of andesitic melts. *Geochim. Cosmochim. Acta* 147, 26-42.

Pingel, U.T., Amoureux, J.P., Anupold, T., Bauer, F., Ernst, H., Fernandez, C., Freude, D. and Samoson, A. (1998) High-field ^{17}O NMR studies of the SiOAl bond in solids. *Chem. Phys. Lett.* 294, 345-350.

Potuzak, M. and Dingwell, D.B. (2006) Temperature-dependent thermal expansivities of multicomponent natural melts between 993 and 1803 K. *Chem. Geol.* 229, 10-27.

Richet, P. (1984) Viscosity and configurational entropy of silicate melts. *Geochim. Cosmochim. Acta* 48, 471-483.

Richet, P., Lejeune, A.M., Holtz, F. and Roux, J. (1996) Water and the viscosity of andesite melts. *Chem. Geol.* 128, 185-197.

Ryerson, F.J. (1985) Oxide solution mechanisms in silicate melts - systematic variations in the activity-coefficient of SiO_2. *Geochim. Cosmochim. Acta* 49, 637-649.

Salters, V.J.M. and Stracke, A. (2004) Composition of the depleted mantle. *Geochem. Geophy. Geosy.* 5, Q05004.

Schott, J., Berner, R.A. and Sjöberg, E.L. (1981) Mechanism of pyroxene and amphibole weathering—I. Experimental studies of iron-free minerals. *Geochim. Cosmochim. Acta* 45, 2123-2135.

Stebbins, J.F., Oglesby, J.V. and Lee, S.K. (2001a) Oxygen sites in silicate glasses: a new view from oxygen-17 NMR. *Chem. Geol.* 174, 63-75.

Stebbins, J.F. and Xu, Z. (1997) NMR evidence for excess non-bridging oxygen in an aluminosilicate glass. *Nature* 390, 60-62.

Stebbins, J.F. and Xue, X.Y. (2014) NMR Spectroscopy of Inorganic Earth Materials, in: Henderson, G.S., Neuville, D.R., Downs, R.T. (Eds.), Spectroscopic Methods in Mineralology and Materials Sciences, pp. 605-653.

Stebbins, J.F., Zhao, P.D., Lee, S.K. and Oglesby, J.V. (2001b) Direct observation of multiple oxygen sites in oxide glasses: Recent

advances from triple-quantum magic-angle spinning nuclear magnetic resonance. *J. Non-Cryst. Solids* 293, 67-73.

Takahashi, E. (1986) Melting of a Dry Peridotite KLB-1 up to 14 GPa: Implications on the Origin of Peridotitic Upper Mantle. *J. Geophys. Res.* 91, 9367-9382.

Takahashi, E., Shimazaki, T., Tsuzaki, Y. and Yoshida, H. (1993) Melting Study of a Peridotite KLB-1 to 6.5 GPa, and the Origin of Basaltic Magmas. *Philos. T. Roy. Soc. A* 342, 105-120.

Timken, H.K.C., Schramm, S.E., Kirkpatrick, R.J. and Oldfield, E. (1987) Solid-state oxygen-17 nuclear magnetic resonance spectroscopic studies of alkaline earth metasilicates. *J. Phys. Chem.* 91, 1054-1058.

Van Eck, E.R.H., Smith, M.E. and Kohn, S.C. (1999) Observation of hydroxyl groups by ^{17}O solid-state multiple quantum MAS NMR in sol-gel-produced silica. *Solid State Nucl. Magn. Reson.* 15, 181-188.

Villeneuve, N., Neuville, D.R., Boivin, P., Bachelery, P. and Richet, P. (2008) Magma crystallization and viscosity: A study of molten basalts from the Piton de la Fournaise volcano (La Reunion island). *Chem. Geol.* 256, 242-251.

Wang, W.Y. and Takahashi, E. (2000) Subsolidus and melting experiments of K-doped peridotite KLB-1 to 27 GPa: Its geophysical and geochemical implications. *J. Geophys. Res.-Solid Earth* 105, 2855-2868.

Wang, X., Chen, T., Zou, Y., Liebermann, R.C. and Li, B. (2015) Elastic wave velocities of peridotite KLB-1 at mantle pressures and implications for mantle velocity modeling. *Geophys. Res. Lett.* 42, 3289-3297.

Windom, K.E. and Boettcher, A.L. (1981) Phase-relations for the joins jadeite-enstatite and jadeite-forsterite at 28-kb and their bearing on basalt genesis. *Am. J. Sci.* 281, 335-351.

Workman, R. and Hart, S.R. (2005) Major and trace element composition of the depleted MORB mantle (DMM). *Earth Planet. Sci. Lett.* 231, 53-72.

Xue, X.Y. and Kanzaki, M. (2008) Structure of hydrous aluminosilicate glasses along the diopside-anorthite join: A comprehensive one- and two-dimensional ^{1}H and ^{27}Al NMR study. *Geochim. Cosmochim. Acta* 72, 2331-2348.

Yoder, H.S. and Tilley, C.E. (1962) Origin of basalt magmas - an experimental study of natural and synthetic rock systems. *J. Petrol.* 3, 342-&.

Yoshino, T., Walter, M.J. and Katsura, T. (2004) Connectivity of molten Fe alloy in peridotite based on in situ electrical conductivity measurements: implications for core formation in terrestrial planets. *Earth Planet. Sci. Lett.* 222, 625-643.

Zhang, J., and C. Herzberg (1994) Melting experiments on an anhydrous peridotite KLB-1 from 5.0 to 22.5 GPa. *J. Geophys. Res.* 99, 17729-17742.

APPENDIX

A1. Abstracts published in Korean journal

A1.1. A solid-state ^{27}Al MAS and 3QMAS NMR study of basaltic and phonolitic silicate glasses

Sun Young Park and Sung Keun Lee

Published in Journal of Mineralogical society of Korea, 28, 61-69 (2015)

Abstract

While the macroscopic properties and eruption style of basaltic and phonolitic melts are different, the microscopic origins including atomic structures are not well understood. Here we report the atomic structure differences of glass in diopside-anorthite eutectic composition (basaltic glass) and phonolitic glass using high-resolution 1D and 2D solid-state Nuclear Magnetic Resonance (NMR). The ^{27}Al MAS NMR spectra for basaltic glass and phonolitic glass show that the full width at half maximum (FWHM) of $^{[4]}$Al for basaltic glass is about twice than phonolitic glass, suggesting the topological disorder of basaltic magma is larger than that of phonolitic magma. The ^{27}Al 3QMAS NMR spectra for basaltic glass and phonolite glass show much improved resolution than the 1D MAS NMR, resolving $^{[4]}$Al and $^{[5]}$Al. Approximately 3.3% of $^{[5]}$Al is observed for basaltic glass, demonstrating the configurational disorder of basaltic magma is larger than phonolitic magma. This result confirms that the topological disorder of $^{[4]}$Al in basaltic glass is larger than that of phonolitic glass. The observed structural differences between basaltic glass and phonolitic glass can provide an atomistic origin for change of the macroscopic properties with composition including viscosity.

A2. Publication list

Journal Articles

International Journals

Park, S. Y. and Lee, S. K., Probing the structural disorder of natural basaltic glasses and melts: high-resolution solid-state ^{27}Al and ^{17}O NMR study of glasses in nepheline-forsterite-quartz eutectic composition and KLB-1 basaltic glasses– to be submitted to Geochimica et Cosmochimca Acta (2016)

Park, S. Y. and Lee, S. K., Effects of difference in ionic radii on chemical ordering in mixed-cation silicate glasses: insights from solid-state ^{17}O and ^{7}Li NMR of Li-Ba silicate glasses– submitted to Journal of America Ceramic Society (2016)

Park, S. Y. and Lee, S. K., High-resolution solid-state NMR study of the effect of composition on network connectivity and structural disorder in multi-component glasses in the diopside and jadeite join: implications for structure of andesitic melts, Geochimica et Cosmochim Acta, 147, 26-42 (2014)

Lee, S. K., **Park, S. Y.**, Kim, H.-I., Tschauner, O., Asimow, P., Bai, L., Xiao, Y., and Chow, P., Structure of shock compressed model basaltic glass: Insights from O K-edge X-ray Raman scattering and high-resolution ^{27}Al NMR spectroscopy, Geophysical Review Letters, 39 5306 (2012)

Park, S. Y. and Lee, S. K., Structure and disorder in basaltic glasses and melts: Insights from high-resolution solid-state NMR study of glasses in diopside-Ca-tschermakite join and diopside-anorthite eutectic composition, Geochimica et Cosmochimica Acta, 80, 125-142 (2012)

Lee, S. K., **Park, S. Y.**, Yi, Y. S., and Moon, J. H., Structures and disorder in amorphous alumina thin films: Insights from high-resolution solid-state NMR, Journal of Physical Chemistry C, 114 13890-13894 (2010)

Lee, S. K., Lee, S. B., **Park, S. Y.**, Yi, Y. S., and Ahn, C. W., Structure of amorphous aluminum oxide, Physical Review Letters, 103 095501 (2009)

Lee, S. K., Deschamps, M., Hiet, J., Massiot, D., and **Park, S. Y.**, Connectivity and proximity between quadrupolar nuclides in oxide glasses: Insights from through-bond and through-space correlations in solid-state NMR, Journal of Physical Chemistry B, 113 5162-5167 (2009)

Domestic Journals (Korean)

Park, S. Y., and Lee, S. K., A solid-state ^{27}Al MAS and 3QMAS NMR study of basaltic and phonolitic silicate glasses, 28, 61-69 (2015)

Park, S. Y., and Lee, S. K., Probing atomic structure of quarternary aluminosilicate glasses using solid-state NMR, Journal of the Mineralogical Society of Korea, 22, 343-352 (2009)

Conference Abstracts

International Conferences

Park, S.Y. and Lee, S.K., Probing the structure and the disorder of multi-component silicate glasses and melts: Insights from high-resolution solid-state NMR, SNU – PDU Workshop, Seoul (2016) (oral)

Park, S.Y. and Lee, S.K., Probing the atomic structure of basaltic melts generated by partial melting of upper mantle peridotite (KLB-1): Insights from high-resolution solid-state NMR study, American Geophysical Union fall meeting, San Francisco (2015) (poster)

Park, S.Y. and Lee, S.K., Probing the structure and the disorder of multi-component silicate glasses and melts: Insights from high-resolution solid-state NMR, SNU – PDU Workshop, Paris (2015) (oral)

Lee, S.K., **Park, S.Y.,** Tschauner, O., Asimow, P., Bai, L. G., Xiao, Y. M., and Chow, P., Probing the structural disorder of basalts and slab-driven andesite melts: Insights from high-resolution solid-state NMR study, American Geophysical Union fall meeting, San Francisco (2012) (poster)

Park, S.Y. and Lee, S.K., Probing the structural disorder of basalts and slab-driven andesite melts: Insights from high-resolution solid-state NMR study, American Geophysical Union fall meeting, San Francisco (2012) (oral)

Ryu, S.B., Lee, S.K, **Park, S.Y.**, and Yi, Y.S., Structure of alumina glass: A view from Al-27 NMR, 9th silicate melt workshop, La Petite Pierre, (2011) (poster)

Park, S.Y. and Lee, S.K., Structure and disorder in basaltic glasses and melts: Insights from high-resolution ^{27}Al, ^{17}O, and ^{29}Si solid-state NMR study, 9th silicate melt workshop, La Petite Pierre, (2011) (poster)

Park, S.Y. and Lee, S.K., Probing the effect of composition on structural disorder of basaltic and slab-driven melts using solid state NMR, Japan Geosceince Union meeting, Chiba (2010) (oral)

Park, S.Y. and Lee, S.K., Effect of composition on the extent of disorder and structure of quaternary (CaO-MgO-Al_2O_3-SiO_2) silicate melts: A view from high-resolution solid state NMR, Western Pacific Geophysics Meeting, Taipei (2010) (poster)

Park, S.Y. and Lee, S.K., The extent of disorder in amorphous alumina and magnesium aluminosilicate glasses, SNU Earth Material Science

Laboratory, OSAKA Univ. Research Center for Material Science and Extreme Condition, Seoul (2008) (oral)

Domestic Conferences

Park, S.Y. and Lee, S.K., Effects of difference in ionic radii on chemical ordering in mixed-cation silicate glasses: insights from solid-state ^{17}O and ^{7}Li NMR of Li-Ba silicate glasses, Petrological Society of Korea and Mineralogical Society of Korea, Pusan (2016) (oral)

Park, S.Y. and Lee, S.K., Effect of composition on the atomic structure of basaltic glasses and melts: insights from solid-state NMR study of basaltic glasses generated by partial melting of upper mantle peridotite (KLB-1), 2015 fall joint Conference of Geology•Mineral and Energy Resources, Jeju (2015) (oral)

Park, S.Y. and Lee, S.K., The 1atomic structure of basaltic melt from upper mantle peridotite (KLB-1): Microscopic study on the origin of basaltic magma, Annual Joint Conference, Petrological Society of Korea and Mineralogical Society of Korea, Andong (2015) (oral)

Lee, A-Chim, **Park, S.Y.**, Lim, C.W., Lee, I.S., and Lee, S.K., Probing the effect of composition on structural disorder of basaltic and slab-driven melts, Annual Joint Conference, Petrological Society of Korea and Mineralogical Society of Korea, Seoul (2014) (poster)

Park, S.Y. and Lee, S.K., Probing the effect of composition on structural disorder of basaltic and slab-driven melts, Annual Joint Conference, Petrological Society of Korea and Mineralogical Society of Korea, Seoul (2012) (oral)

Park, S.Y. and Lee, S.K., Probing atomic structure of multi-component basaltic glasses using solid-state NMR, Annual Joint Conference, Petrological Society of Korea and Mineralogical Society of Korea, Jeonju (2010) (oral)

Park, S.Y. and Lee, S.K., Probing the atomic structure of quaternary (CaO-MgO-Al_2O_3-SiO_2) silicate glasses using high resolution solid state NMR: microscopic origins of macroscopic properties of mantle melts, Annual Joint Conference, Petrological Society of Korea and Mineralogical Society of Korea, Jeju (2009) (oral)

Park, S.Y. and Lee, S.K., Probing the atomic structure of multi-component silicate glasses using high resolution solid state NMR: microscopic origins of macroscopic properties of natural melts, Annual Joint Conference, Petrological Society of Korea and Mineralogical Society of Korea, Chun Cheon (2009) (oral)

Park, S.Y. and Lee, S.K., The extent of disorder and Al site distortion in crystalline alumina and amorphous at 1 atm: Al-27 3QMAS NMR Study, Annual Joint Conference, Petrological Society of Korea and Mineralogical Society of Korea, Busan (2008) (oral)

요약 (국문초록)

다성분계 비정질 규산염의 원자구조와 물리 화학적 특성을 밝히는 것은 지구 내부의 마그마의 이동, 지구 시스템의 분화 등의 설명에 실마리를 제공해 준다. 자연계 용융체의 조성을 가지는 다성분계 비정질 규산염의 거시적 성질에 대해서는 많은 이론적-실험적 연구들이 수행되었으나 시스템을 근본적으로 설명해 줄 수 있는 원자 구조에 대한 연구는 대부분 이성분계나 삼성분계에 대해서만 이루어져 왔고 비정질 자체가 가지고 있는 고유의 무질서도와 성분이 많아지면서 여러 원자 환경을 지시하는 분광 스펙트럼이 겹치는 것을 극복할 수 있는 적절한 분광 분석 장치의 부재로 다성분계 비정질 규산염에 대한 명확한 구조 분석은 지금까지 풀어야 할 난제로 남아있었다. 고상 핵자기공명(nuclear magnetic resonance, NMR) 분광분석은 특정 원자 중심의 정보를 제공하며 정량적인 정보를 제공하므로 다성분계 비정질 규산염의 구조를 분석하기에 적합하다. 본 학위논문에서는 NMR 분광분석을 이용하여 자연계 용융체를 나타내는 다성분계 비정질 규산염의 조성에 따른 원자구조의 변화에 대해 연구하여 자연계 용융체의 구조와 물성 간의 관계를 체계적으로 정립하고자 하였다.

현무암질 용융체의 모델 조성인 투휘석($CaMgSi_2O_6$)과 Ca-처마카이트($CaAl_2SiO_6$) 유사이원계와 투휘석과 아노르다이트($CaAl_2Si_2O_8$) 유사이원계의 조성을 가지는 다성분계 비정질 규산염의 조성에 따른 원자 구조가 NMR 분광분석을 통해 연구되었다. 본 연구에서 규명된 원자구조를 통해 현무암질 용융체 내에서의 혼합 엔탈피의 값의 변화가 설명 되었으며 투휘석의 양이 증가할수록 점성도가 감소하는 것이 설명되었다. 본 연구에서 밝혀진 Ca^{2+}과 Mg^{2+}의 선호적인 분배 혹은 비연결산소(non-bridging oxygen, NBO)와 연결산소(bridging oxygen, BO) 사이에서 양이온들이 섞이지 않는 현상은 중앙해령에서 생성되는 현무암질 용융체의

조성에 영향을 미칠 수 있다.

안산암질 용융체의 모델 조성인 투휘석과 제이다이트($NaAlSi_2O_6$) 유사이원계의 조성을 가지는 다성분계 비정질 규산염의 원자구조가 고분해능 2D ^{17}O, ^{27}Al 3Q(triple quantum) MAS(magic angle spinning) NMR 분광분석과 ^{29}Si MAS NMR 분광분석을 통해 연구되었다. 본 연구의 결과를 통해 제이다이트 비정질 규산염 내에 Al-O-Al의 존재가 확인되었으며 이는 안산암질 용융체 내에서 Al-avoidance rule이 적용되지 않는 것을 의미한다. 투휘석의 증가에 따른 NBO의 증가는 안산암질 용융체 내에서 투휘석의 양이 증가할수록 점성도가 감소한다는 것을 의미한다. 이전 연구와 본 연구의 결과의 종합을 통해 평균 양이온세기(average cationic potential, $<c/r>_{ave}$)라는 새로운 변수가 제시되었으며 이를 통해 고배위수 Al의 양과 조성과의 관계가 정립되었고 용융체 내의 고배위수 Al은 $<c/r>_{ave}$이 증가할수록 비선형적으로 증가하는 것이 확인되었다.

Li-Ba 비정질 규산염의 조성에 따른 원자구조의 변화가 NMR 분광분석을 통해 규명되었다. 본 연구의 결과를 통해 NBO 주변에 Li^+과 Ba^{2+} 이온이 랜덤하지 않게 분포하는 것이 확인되었다. 본 연구의 결과와 이전 연구 결과의 종합을 통해 이온 반경의 차이가 클수록 비정질 규산염 내에서의 화학적 질서도가 증가하는 것이 밝혀졌다.

가장 복잡하지만 실제 자연계에 존재하는 용융체의 조성과 가장 유사한 시스템인 상부맨틀 암석인 “KLB-1”으로부터 생성되는 현무암질 용융체의 생성되는 깊이의 변화에 따른 조성의 변화가 원자구조에 미치는 영향이 NMR 분광분석을 통해 연구되었다. 연구결과 KLB-1으로부터 생성되는 현무암질 용융체 내에 $X_{MgO}[MgO/(MgO+Al_2O_3)]$가 증가할수록 $^{[5]}Al$이 증가하는 것이 관찰되었고 이는 용융체 내의 배열 엔트로피의 증가로 인해 점성도가 감소할 수 있다는 것을 의미한다. 또한 이전 모델 조성에서도 관찰되었던 Ca^{2+}, Mg^{2+}, Na^+의 NBO와 BO 사이의 랜덤 하지 않은 분포가 실제 자연계 용융체의 조성과 유사한

KLB-1으로부터 생성되는 현무암질 용융체 내에서도 일어나는 것이 확인되었다.

본 학위논문의 결과와 같이 용융체 내의 조성의 변화는 용융체 내의 원자 구조의 변화를 가져오는 것이 확인되었으며 이를 통해 조성의 변화에 따른 물성의 변화의 근본적인 원인이 밝혀졌다. 본 학위 논문의 결과를 통해 현무암질 용융체와 안산암질 용융체를 포함하는 자연계 용융체 내의 구조와 물성의 관계에 대한 체계적인 이해가 증진될 것이 기대된다.

주요어: 다성분계 비정질 규산염, 현무암질 안산암질 용융체, 고상 핵자기공명 분광분석, 구조와 무질서도

학번: 2010-30103